Alternatives to Steel Grid Decks

DRAFT FINAL REPORT

FDOT Contract No. BD015 RPWO #22

Submitted by

Amir Mirmiran , Muhammad Azhar Saleem
Department of Civil and Environmental Engineering
Florida International University
Miami, Florida

and

Kevin Mackie, Jun Xia
Department of Civil and Environmental Engineering
University of Central Florida
Orlando, Florida

Submitted to:

Mr. Marc Ansley
Project Manager
Florida Department of Transportation
Research Center

December 2009

DISCLAIMER

The opinions, findings and conclusions expressed in this publication are those of the authors and not necessarily those of the State of Florida Department of Transportation.

APPROXIMATE CONVERSIONS TO SI UNITS

SYMBOL	WHEN YOU KNOW	MULTIPLY BY	TO FIND	SYMBOL
LENGTH				
in	inches	25.4	millimeters	mm
ft	feet	0.305	meters	m
yd	yards	0.914	meters	m
mi	miles	1.61	kilometers	km

SYMBOL	WHEN YOU KNOW	MULTIPLY BY	TO FIND	SYMBOL
AREA				
in²	squareinches	645.2	square millimeters	mm²
ft²	squarefeet	0.093	square meters	m²
yd²	square yard	0.836	square meters	m²
ac	acres	0.405	hectares	ha
mi²	square miles	2.59	square kilometers	km²

SYMBOL	WHEN YOU KNOW	MULTIPLY BY	TO FIND	SYMBOL
VOLUME				
fl oz	fluid ounces	29.57	milliliters	mL
gal	gallons	3.785	liters	L
ft³	cubic feet	0.028	cubic meters	m³
yd³	cubic yards	0.765	cubic meters	m³
NOTE: volumes greater than 1000 L shall be shown in m³				

SYMBOL	WHEN YOU KNOW	MULTIPLY BY	TO FIND	SYMBOL
MASS				
oz	ounces	28.35	grams	g
lb	pounds	0.454	kilograms	kg
T	short tons (2000 lb)	0.907	megagrams (or "metric ton")	Mg (or "t")

SYMBOL	WHEN YOU KNOW	MULTIPLY BY	TO FIND	SYMBOL
TEMPERATURE (exact degrees)				
°F	Fahrenheit	5 (F-32)/9 or (F-32)/1.8	Celsius	°C

SYMBOL	WHEN YOU KNOW	MULTIPLY BY	TO FIND	SYMBOL
ILLUMINATION				
fc	foot-candles	10.76	lux	lx
fl	foot-Lamberts	3.426	candela/m^2	cd/m^2

SYMBOL	WHEN YOU KNOW	MULTIPLY BY	TO FIND	SYMBOL
FORCE and PRESSURE or STRESS				
lbf	poundforce	4.45	newtons	N
lbf/in^2	poundforce per square inch	6.89	kilopascals	kPa

APPROXIMATE CONVERSIONS TO SI UNITS

SYMBOL	WHEN YOU KNOW	MULTIPLY BY	TO FIND	SYMBOL
LENGTH				
mm	millimeters	0.039	inches	in
m	meters	3.28	feet	ft
m	meters	1.09	yards	yd
km	kilometers	0.621	miles	mi

SYMBOL	WHEN YOU KNOW	MULTIPLY BY	TO FIND	SYMBOL
AREA				
mm^2	square millimeters	0.0016	square inches	in^2
m^2	square meters	10.764	square feet	ft^2
m^2	square meters	1.195	square yards	yd^2
ha	hectares	2.47	acres	ac
km^2	square kilometers	0.386	square miles	mi^2

SYMBOL	WHEN YOU KNOW	MULTIPLY BY	TO FIND	SYMBOL
VOLUME				
mL	milliliters	0.034	fluid ounces	fl oz
L	liters	0.264	gallons	gal
m^3	cubic meters	35.314	cubic feet	ft^3
m^3	cubic meters	1.307	cubic yards	yd^3

SYMBOL	WHEN YOU KNOW	MULTIPLY BY	TO FIND	SYMBOL
MASS				
g	grams	0.035	ounces	oz
kg	kilograms	2.202	pounds	lb
Mg (or "t")	megagrams (or "metric ton")	1.103	short tons (2000 lb)	T

SYMBOL	WHEN YOU KNOW	MULTIPLY BY	TO FIND	SYMBOL
TEMPERATURE (exact degrees)				
^{o}C	Celsius	1.8C+32	Fahrenheit	^{o}F

SYMBOL	WHEN YOU KNOW	MULTIPLY BY	TO FIND	SYMBOL
ILLUMINATION				
lx	lux	0.0929	foot-candles	fc
cd/m^2	candela/m^2	0.2919	foot-Lamberts	fl

SYMBOL	WHEN YOU KNOW	MULTIPLY BY	TO FIND	SYMBOL
FORCE and PRESSURE or STRESS				
N	newtons	0.225	poundforce	lbf
kPa	kilopascals	0.145	poundforce per square inch	lbf/in^2

1. Report No.	2. Government Accession No.	3. Recipient's Catalog No.
4. Title and Subtitle **Alternatives to Steel Grid Decks**		5. Report Date December 2009
		6. Performing Organization Code
7. Author(s) **Amir Mirmiran, Muhammad Azhar Saleem, Kevin Mackie, Jun Xia**		8. Performing Organization Report No.
9. Performing Organization Name and Address FIU, Department of Civil Engineering, 10555 W. Flagler Street, EC 3600, Miami, FL 33174 UCF, Department of Civil and Environmental Engineering, 402 Engineering Building 2, Orlando, FL 32816		10. Work Unit No. (TRAIS)
		11. Contract or Grant No. BD015 RPWO #22
12. Sponsoring Agency Name and Address The Florida Department of Transportation Research Center 605 Suwannee Street, MS 30 Tallahassee, FL 32399		13. Type of Report and Period Covered Draft Final Feb. 2007 – Dec. 2009
		14. Sponsoring Agency Code
15. Supplementary Notes		

16. Abstract

Most of the moveable bridges in Florida use open grid steel decks, because these are factory assembled, light-weight, and easy to install. Open grid steel decks, however, are not as skid resistant as solid decks. Costly maintenance, high noise levels, poor riding comfort and susceptibility to vibrations are among the other disadvantages of these decks. The major objective of this project was to develop three alternative deck systems which weigh no more than 25 lb/ft², have solid riding surface, are no more than 4-5 in. thick and are able to withstand AASHTO LRFD loading. Three deck systems were considered in this study: SAPA aluminum deck by SAPA Group of Sweden, Ductal®-MMFX steel deck and Ductal®-fiber reinforced polymer (FRP) tube deck.

SAPA aluminum deck panels have been used in Europe, mainly Sweden, for the last 15 years. A detailed experimental and analytical evaluation of the system has been carried out. The experimental work included static and dynamic testing on the deck panels. Analytical work included elastic and simple plastic analysis and detailed finite element analysis. Based on the in-depth experimental and analytical evaluation, it was concluded that SAPA aluminum deck is a feasible alternative to open grid steel deck and ready for implementation.

Ductal®-MMFX steel deck is the second alternative system developed as a part of this project. Ductal® is a type of ultra high performance concrete (UHPC). Due to its ultra high strength, Ductal® results in thinner sections, which helps satisfy the strict self-weight limit. A comprehensive experimental and analytical evaluation of the system has been carried out to establish its suitability. Both single and multi-unit specimens with one or two spans have been tested for static loading. Finite element models have been developed to predict the deck behavior. The study leads to the conclusion that the Ductal®-MMFX steel deck has a great potential to serve as an alternative system. The deck requires development of only a few additional components before it is ready to be implemented.

Ductal®-FRP tube deck is the third system that was studied in this project. Prestressed hollow core decks are commonly used but this type of steel-free deck is new. Preliminary experimental and analytical evaluations of two simple-span specimens, one with uniform section and the other with tapered section, were carried out. The system has shown good promise to replace the conventional open grid decks. A detailed experimental and analytical work is, however, needed before the system is recommended for field application.

17. Key Word	18. Distribution Statement
Moveable Bridges, Light-Weight Decks, Aluminum, Ductal®, FRP.	Document is available to the US public through, The NTIS, Springfield, VA 22161

19. Security Classif. (of this report)	20. Security Classif. (of this page)	21. No. of Pages	22. Price
Unclassified	Unclassified	168	

Technical Report Documentation Page Form DOT F 1700.7 (8-72) Reproduction of completed page authorized

ACKNOWLEDGEMENTS

The authors would like to thank Florida Department of Transportation (FDOT) Structures Lab in Tallahassee and FDOT State Materials Office for their support in fatigue test and material testing. Special thanks are also due to the Project Manager, Mr. Marc Ansley.

The authors would also like to acknowledge MMFX Technologies of Irvine, CA. and Lafarge North America for providing materials for this project.

EXECUTIVE SUMMARY

Most of the moveable bridges in Florida use open grid steel decks, because these are factory assembled, light-weight, and easy to install. Open grid steel decks, however, are not as skid resistant as solid decks, which causes accidents especially during rains. Costly maintenance, high noise levels, poor riding comfort and susceptibility to vibrations are among the other disadvantages of these decks. The major objective of this project is to develop three alternative deck systems which weigh no more than 25 lb/ft^2, have a solid riding surface, no more than 4-5 in. thick and be able to withstand AASHTO LRFD loading. Three deck systems were considered in this study: SAPA aluminum deck by SAPA Group of Sweden, Ductal®-MMFX steel deck and Ductal®-fiber reinforced polymer (FRP) tube deck.

SAPA aluminum deck panels have been used in Europe, mainly Sweden, for the last 15 years. The deck panels weigh around 14 lb/ft^2 which satisfies the self-weight limit. The cost of the system is approximately $45 per ft^2, excluding the connections, wearing surface and shipping cost. A detailed experimental and analytical evaluation of the system has been carried out. The experimental work included static and dynamic testing on the deck panels and some ancillary tests on the connections. Analytical work included elastic and simple plastic analysis and detailed finite element analysis. Based on the in-depth experimental and analytical evaluation, it is concluded that SAPA aluminum deck is a feasible alternative to open grid steel deck and ready for implementation.

Ductal®-MMFX steel deck is the second alternative system developed as a part of this project. Ductal® is a type of ultra high performance concrete (UHPC) developed from the joint research of three French companies Bouygues, Lafarge, and Rhodia. Ultra high strength properties of Ductal® make it a favorable material for this project. Due to ultra high strength, Ductal® results in thinner sections, which helps satisfying the strict self-weight limit. MMFX steel bars have high strength and high corrosion resistance which make it suitable to be used with an ultra high strength material and in a marine environment. A comprehensive experimental and analytical evaluation of the system has been carried out to establish its suitability as an alternative to open grid steel decks. Both single and multi-unit specimens with simple and two spans have been tested for static loading. Finite element models have been developed to predict the deck behavior. The study leads to the conclusion that the Ductal®-MMFX steel deck has a great potential to serve as an alternative system. The deck requires development of only a few additional components e.g., deck-to-girder connection, and joint between adjacent deck panels etc., before it is ready to be implemented.

Ductal®-FRP tube deck is the third system that was studied in this project. This is for the first time that UHPC has been combined with FRP tubes to develop a hollow core deck. Prestressed hollow core decks are commonly used but this type of steel-free deck has never been developed before. FRP tubes serve as tensile reinforcement both in the positive and negative moment regions. Preliminary experimental and analytical evaluations of two simple-span specimens, one with uniform section and other with tapered section, have been carried out. System has shown good promise to replace the conventional open grid decks. A detailed experimental and analytical work is, however, needed before the system is recommended for field application.

TABLE OF CONTENTS

LIST OF TABLES

LIST OF FIGURES

Chapter-1

Introduction

1.1 Problem Statement

Florida has the largest stock of moveable bridges, with a total of 148, of which 91% are bascule, 7% swing and 2% lift bridges (National Bridge Inventory 2008). More than half of these bridges are located along the Intracoastal Waterway in Miami and Fort Lauderdale. Most of the moveable bridges use open grid steel decks (Figure 1.1), which are typically supported by steel stringers with 4 ft spacing. On average, these decks weigh less than 25 lb/ft^2; while some can weigh as little as 14 lb/ft^2. They are factory assembled and quite easy to install. Also, deck crowning, scuppers, and drains are not required, since rain water drains through the openings in the deck.

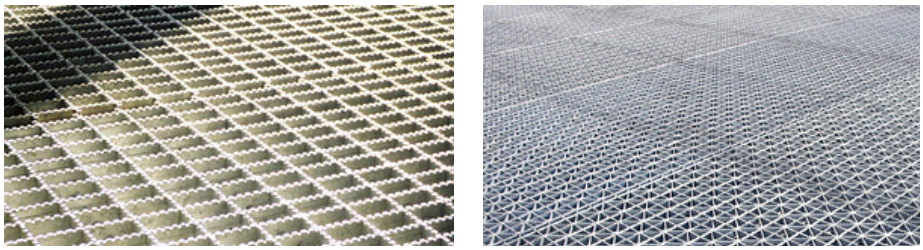

Figure 1.1 Open Rectangular and Diagonal Steel Grating for Bridge Decks
Source: www.idsi.org

The open grid steel decks, however, have the following disadvantages:

- Rideability: not as skid resistant as decks with a solid riding surface;
- Damage prone and costly to maintain and repair;
- High noise levels;
- Susceptible to vibrations and poor riding comfort

Since these bridge decks can polish over time, their skid resistance can further deteriorate to unacceptable levels without an active maintenance program, leading to poor rideability. Noise is another potential concern in some urban areas. Baseline acoustic testing by Florida Atlantic University (Takkasila and Reddy 1996) measured noise levels radiating from these bridge decks at levels that may cause public concern.

In addition, open grid steel decks may also develop fatigue problems, leading to breakage of the deck welds. Experience at FDOT District 6 indicates that at times part or the entire panel may come loose (see Figure 1.2), and often requires welding at least once a year (communications with Mr. Ryan Fisher, Moveable Structures Project Manager, D6).

Figure 1.2 Re-Welding of Joints Broken due to Fatigue

Due to the safety, maintenance, and environmental concerns pertaining to open grid steel decks, research is needed into alternative deck systems that address the rideability concerns while meeting strict self-weight limits (25 lb/ft^2) on these types of bridges.

1.2 Research Objectives

The main objective of this research is to investigate three promising alternatives to open grid steel decks. The alternative decks should have the following attributes:

1. Solid riding surface;
2. Weigh no more than 25 lb/ft^2;
3. Have no more than 4-5 in. thickness to fit within current structures;
4. Have a capacity to withstand AASHTO LRFD HS 20 truck loading;
5. Ability to span at least 4 ft between supporting stringers

1.3 Research Approach

Three deck Systems were considered in this study:

1. Aluminum deck panel made by SAPA Group of Sweden;
2. Ductal®-MMFX steel deck;
3. Ductal®-fiber reinforced polymer (FRP) tube deck

This project included flexural tests on the above three deck systems to establish their suitability for moveable bridges. Some ancillary tests on the connections of SAPA aluminum deck panels, and Ductal® prisms were also performed. Analytical models were also developed to predict the behavior of the above deck systems. The predicted responses were then compared with the experimental results.

1.4 Report Organization

This report is comprised of four chapters. This first chapter serves as an introduction, mainly describing the problem statement, research objectives, and research approach. The following three chapters present the literature review, experimental and analytical work and recommendations for the three alternative decks considered: SAPA aluminum deck, Ductal®-MMFX steel deck, and Ductal®-FRP tube deck, respectively. Chapter 5 provides summary and conclusions for the project, as well as recommendations for future research.

Chapter-2

SYSTEM 1-SAPA Aluminum Deck

2.1 Introduction

Several aluminum systems were found in the literature. After contacting five different suppliers in five different countries, the research team concluded that only the one by SAPA Group of Sweden has off-the-shelf profiles that were suitable for this study, and could be obtained and tested within the scope of this project.

SAPA Group has developed a light-weight aluminum bridge deck system that can be mechanically fastened to steel girders. SAPA aluminum deck is made up of five voided extrusions connected to each other by tongue and groove connection. These deck panels are available in two sizes, 11 in. and 11.8 in. wide; both 4 in. deep. These extrusions weigh around 14 lb/ft^2, which satisfies the self-weight limit (25 lb/ft^2) required as a replacement for open grid steel deck systems. This system has been used in Europe, mainly Sweden, for more than 15 years. An acrylic-based material (Acrydur) and hot asphalt mix have been the most commonly used wearing surfaces with the SAPA decks. The cost of this system is approximately $45 per ft^2, excluding the connectors, wearing surface, and shipping. Figure 2.1 shows the shape and size of a single deck panel and its connections with the steel girders.

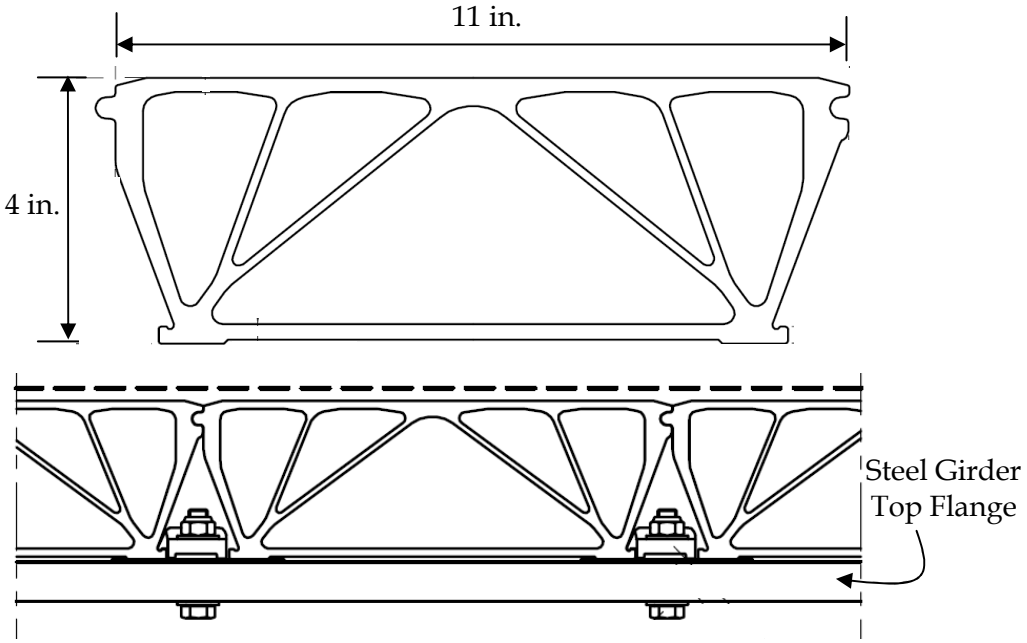

Figure 2.1 SAPA Aluminum Bridge Deck Panel

2.2 Use of Aluminum for Bridge Decks

During the past few decades there has been a considerable growth in the structural application of aluminum alloys. High strength-to-weight ratio makes aluminum a favorable material for high-speed trains, aircrafts, and ferries. In civil engineering applications, when self-weight is the deciding factor, aluminum is a very good choice. Furthermore, aluminum has good corrosion and fatigue resistance. Moreover, extrusions make aluminum profiles quite versatile (see www.aluminium.matter.org.uk).

Practical applications of aluminum in bridges can be traced back to 1933, when the timber and steel floor system in the Smithfield Street Bridge (Figure 2.2) in Pittsburg, PA was replaced by an aluminum deck. The first all-aluminum railway bridge in the U.S. was constructed near Massena, New York in 1946. The first all-aluminum highway bridge in North America was erected in Arvida, Canada, over the Saguenay River in 1950 (Das and Kaufman 2007). In Europe, the first aluminum bridge dates back to 1949 in Sutherland, U.K. Another 35 aluminum bridges were built between 1949 and 1985, most of them between 1950 and 1970 (see www.aluminium.matter.org.uk).

Figure 2.2 Smithfield Street Bridge in Pittsburg, PA
(Source: www.glasssteelandstone.com)

A typical concern for using metals such as aluminum in bridges is often related to potential for corrosion. Many researchers have worked on this issue and reported that aluminum has an excellent corrosion resistance, and that it does not need any protection in this regard. Siwowski (2003) and Hoglund and Nilsson (2006) have reported that the 6000 series aluminum alloy exhibits optimal mechanical and anti-corrosive properties, which could be of great benefit for bridge applications.

Fatigue is another issue that needs to be addressed for aluminum bridge decks. In a detailed study, Wright (1997) reported that the aluminum bridge deck of Smithfield Street Bridge showed very little degradation due to fatigue and corrosion after 27 years of service. Soetens

and Straalen (2003), and Siwowski (2003) on the other hand reported that welded connections in aluminum bridge decks are susceptible to fatigue. Strength in the heat-affected zones is significantly reduced by the heat of welding, and fatigue fracture may occur even at service load levels. Epoxy-based or bolted connections are potential solutions to mitigate such fatigue concerns.

Galvanic corrosion is another concern in bridges with dissimilar metals. Aluminum decks, when used with steel girders, can experience galvanic corrosion due to material dissimilarity between steel and aluminum. Therefore, aluminum deck must be kept separate from steel girders. A layer of stainless steel, if attached to the top flanges of steel girders, can prevent galvanic corrosion. This solution was adopted for the Aselva Bridge in 1958 (Siwowski 2003). Aluminum haunches constructed on girder's top flange is another solution to this problem.

Decision on the type of wearing surface is also important, because aluminum decks have a very smooth surface that may cause delamination of the wearing surface. Various types of wearing surface have been suggested in the literature, including asphalt, polyester and sand, and acrylic-based wearing courses. In 1933, the Smithfield Street Bridge was rehabilitated using aluminum deck with an asphalt wearing course. In 1967, a new lighter-weight aluminum orthotropic deck with a polyester and sand wearing course was assembled on the existing aluminum deck. In the U.K. and Germany, aluminum plates have been used as decks with an asphalt wearing course (Siwowski 2003). Hoglund and Nilsson (2006) reported that an acrylic-based material called Acrydur has been applied to bridges for many years and has shown very high resistance to wear in existing bridges. The Federal Highway Administration (FHWA) has funded research on a variety of polymer-sand aggregate surface materials that are designed to bond with aluminum and to prevent skidding (Wright 1997).

Aluminum guardrails are also available for use with aluminum bridge decks. According to the FHWA, aluminum guardrails have been used in Virginia, Georgia, and North Carolina. Aluminum tube bridge rail is 32-33 in. high, and costs $75-$110 per linear foot (Bridge Rail Guide, 2005).

In short, aluminum bridge decks are light-weight and corrosion resistant, and have a short installation time, predictable behavior, and low maintenance cost. Therefore, aluminum bridge deck panels were selected as one of the three systems that would be studied in this project.

2.3 Material and Geometric Properties

SAPA aluminum bridge deck panels are fabricated from 6063F25-T6 aluminum alloy, with the following geometric and material properties:

- Area of cross section, A = 10.56 in^2 per unit
- Area for resisting shear, A_v = 5.71 in^2 per unit
- Moment of inertia, I_x = 24.09 in^4 per unit
- Distance from top fiber to the neutral axis (N.A.) = 1.834 in.
- Unit weight = 169 lb/ft^3
- Yield strength in tension = 29,000 psi
- Yield strength in shear = 16,675 psi

- Ultimate strength in tension = 35,525 psi
- Ultimate strength in shear = 20,445 psi
- Young's modulus of elasticity = 10.15 x 10^6 psi
- Modulus of rigidity = 3.92 x 10^6 psi
- Yield strain = 0.004857
- Piosson's ratio = 0.33

2.4 Loading Requirements

2.4.1 Live Load Requirements

Live load calculations are based on the recommendations of AASHTO LRFD Highway Bridge Design Specifications (2005). The LRFD design philosophy is based on the following relationship:

$$\varphi R_n \geq \sum \eta_i \gamma_i Q_i \tag{2.1}$$

where φ is strength reduction factor, R_n is the nominal resistance, η_i is the i^{th} modification factor, γ_i is the i^{th} load factor, and Q_i is the i^{th} load in the load combination. From AASHTO LRFD (2005), one can infer that $\gamma = 1.75$, $\varphi = 0.9$, and $\eta = 1.0$. Also, typically, the impact factor is 1.33. For the wheel load of an HS 20 truck, which is 16 kips, one can then derive the ultimate load as:

$$P_u = 1.75\ (16 \times 1.33) = 37.24 \text{ kips} \tag{2.2}$$

The nominal load will then be derived as:

$$P_n = \frac{P_u}{\varphi} = \frac{37.24}{0.9} = 41.38 \text{ kips} \tag{2.3}$$

The target load for the experiment should however be 37.24 kips, because the experiment directly provides the ultimate load.

2.4.2 Braking Force Requirements

The AASHTO LRFD (2005) defines the braking force F_B as:

$$F_B = bW \tag{2.4}$$

where

$$b = \frac{V^2}{2gs} \tag{2.5}$$

and W is the weight of the design truck load or design tandem load, vehicle speed V is assumed as $55mph$ or $80 ft/s$, the braking distance s is assumed as 400 ft, and therefore, the resulting weight coefficient b is 0.25.

The calculations are based on the following assumptions:

1. Braking force is assumed to act horizontally at 6 ft above the roadway surface;
2. Dynamic allowance is not included in the analysis;
3. Only one lane exists for each direction on the bridge. Therefore, the multiple presence factor *m* is taken as 1.2. This is a more critical case than those with multiple lanes;
4. The maximum weight of axle of the design truck (HS 20) is 32 kips (only one axle could be placed on one deck strip);
5. The load factor for Strength I design combination is 1.75 for the braking force;
6. The width of one lane is 10 ft, and therefore, the number of stringers within one lane is three;
7. The clamps on the stringer are placed as shown in Figure 2.3, with each deck strip having two clamps

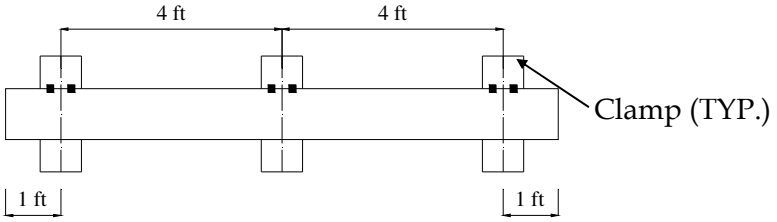

Figure 2.3 Arrangement of Clamps

Since the braking force is resisted by the clamps on the stringers, one can write:

$$\frac{32 \text{ kips} \times 1.2 \times 0.25 \times 1.75}{3} = 2n\phi R_n \tag{2.6}$$

where n is the number of deck strips to resist the braking force. The results based on the number of deck strips participating in resisting the braking force are presented in Table 2.1.

Table 2.1 Braking Force

No. of Clamps	**Required Nominal Shear Resistance of Each Clamp (lbs)**
1	2,800
2	1,400
3	935
4	700

2.4.3 Uplift Force Requirements Due to Wind

According to AASHTO LRFD (2005) Article 3.8.2, a vertical upward wind pressure of 20 lb/ft^2 should be applied over the width of the deck, including parapet and sidewalks, as a longitudinal line load. This force shall be applied only for the Strength III and Service IV limit states that do not involve wind on live load, and only when the direction of the wind is taken to be perpendicular to the longitudinal axis of the bridge. This line load shall be applied at the windward quarter-point of the deck, as shown in Figure 2.4, where B is the total width of the bridge.

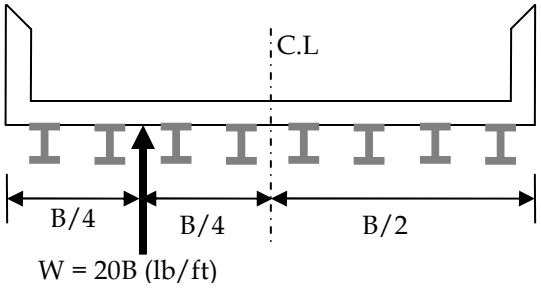

Figure 2.4 Uplift Force due to Wind

For a four-lane bridge, B is assumed to be 60 ft (based on a lane width of 12 ft and 6 ft wide shoulders on both sides), the wind load can be as high as 1,200 lb/ft. Because the deck panel is 11 in. wide, one deck needs to resist 1,100 lbs service uplift force due to wind. The uplift force can act somewhere between the two stringers depending on the stringer spacing. Two mechanisms help resist this uplift force: the clamps (total of four clamps, two on top flange of each stringer, as shown in Figure 2.3) and the lip joint between the adjacent deck panels. For the worst case scenario, the contribution of the lip joint is ignored, and the uplift force is assumed to act very close to the stringer. In such cases, only two clamps will be resisting the upward force. Therefore, one clamp should at least be able to resist a service uplift force of 550 lbs. The load factor for Strength III limit state is 1.4, which makes the required capacity from each clamp as 770 lbs.

2.5 Experimental Work

Most of the tests for this project were performed at the Titan America Structures and Construction Testing Laboratory at Florida International University (FIU), except for the fatigue and residual strength tests, which were performed at the FDOT Structures Lab in Tallahassee. In all, six deck panels were purchased, and were then cut to size to perform various tests.

Two types of configurations were used for flexural tests; simple span and two-span continuous decks. The simple-span specimens were subjected to a single load, whereas the two-span specimens were loaded with one load at the middle of each span. Both flexural and fatigue tests were conducted with the AASHTO prescribed footprint of an HS 20 truck dual tire wheel (20 in. x 10 in.). Both the panel and beam actions were examined at service and ultimate load levels. The panels were oriented with extrusions perpendicular to the supporting stringers and the direction of traffic. Actuator and hydraulic jack were used for the load application. Strain gauges, linear potentiometer, and string potentiometers were installed at strategic locations to acquire the strain and deflection data. All instruments were connected to data acquisition system which recorded the data at a frequency of 1 Hz.

The main objective of testing SAPA aluminum bridge deck panels was to establish their ultimate load capacity, mode of failure, and long-term fatigue behavior. To fulfill these objectives the following test matrix was developed:

1. Flexural Tests
    a. Simple-Span Test
    b. Two-Span Continuous Test
    c. Simple-Span Inverted Panel Test
2. Connector Shear Test
3. Connector Uplift Test
4. Lip Test (Tongue and Groove Test)
5. Fatigue and Residual Strength Tests

2.5.1 Flexural Tests

The displacement control procedure was adopted for the flexural tests with a displacement rate of 0.015 in./min. Deck panels were loaded up to yielding level, and were then fully unloaded and finally reloaded up to the failure. Excessive deflection of deck panel or local buckling of plate elements was considered as the failure point and an indicator to stop the test.

For the simple-span and the simple-span inverted panel tests, a 6 ft and an 8 ft long piece, respectively, were cut from two full panels. The left-over pieces were used later on for the ancillary tests. For the two-span continuous beam, a complete deck panel was used. Figures 2.5 and 2.6 show the schematic diagrams of the simple-span and two-span continuous panel tests, respectively. To simulate the wheel of an HS 20 truck, a neoprene pad with a steel plate on top, each of the size 20 in. x 10 in. were used for loading.

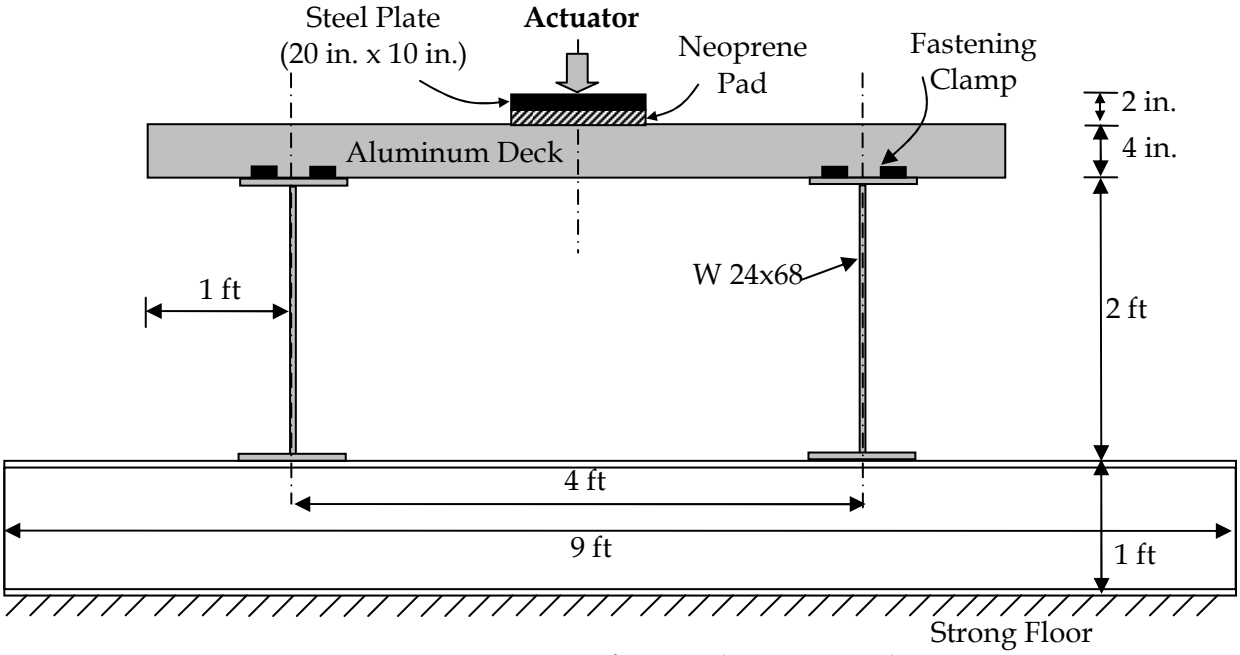

Figure 2.5 Test Setup for Simple-Span Panel

For the simple-span and inverted panel tests, three strain gauges were installed at the mid-span on the tension side (bottom face) of the section. One of three strain gauges was installed at the middle of the section, while the remaining two were placed at the two edges. For the two-span continuous deck, strain gauges were applied at the bottom in the mid-span and on the top face

at the interior support. String potentiometers with 12 in. range were used to monitor deflections. Three string potentiometers were used in each of the three flexural tests, one at the middle of the section and one at each edge.

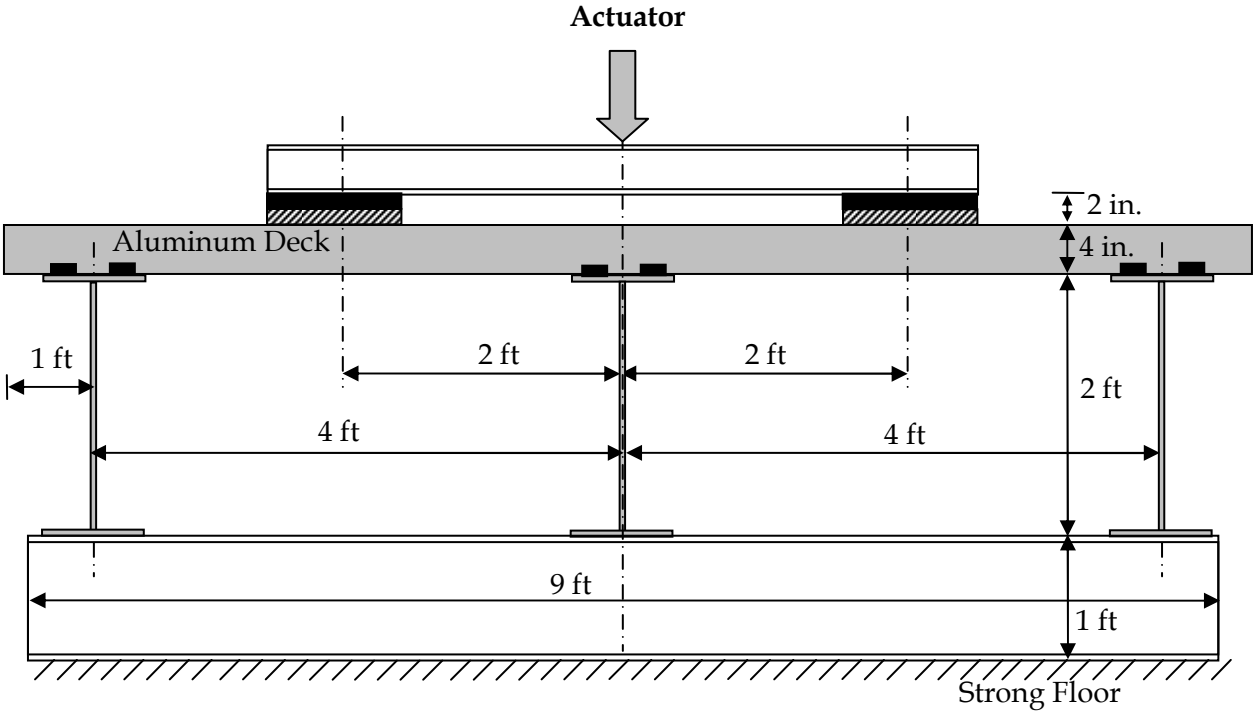

Figure 2.6 Test Setup for Two-Span Continuous Panel

Figures 2.7 and 2.8 show the test setup and deflected shape of the simple-span deck panel, respectively. Load-deflection and load-strain responses are presented in Figures 2.9 and 2.10, respectively. The simple-span deck panel exhibited a stiffness of 90 kip/in. up to a load of 45 kips, and then began softening gradually. The unloading was started at a load of 63 kips originally planned at the outset of yielding. As this was the first test, the yielding point could not be judged accurately and the unloading was started beyond the first yield point but before the development of the full plastic hinge. The deck panel had a residual tensile strain of around 0.009 at mid-span when completely unloaded. This first test showed very promising results with an ultimate load of 70 kips, which is 87% higher than the required ultimate load of 37.24 kips, as discussed in Section 2.4.1.

Figure 2.7 Test Setup for Simple-Span Panel

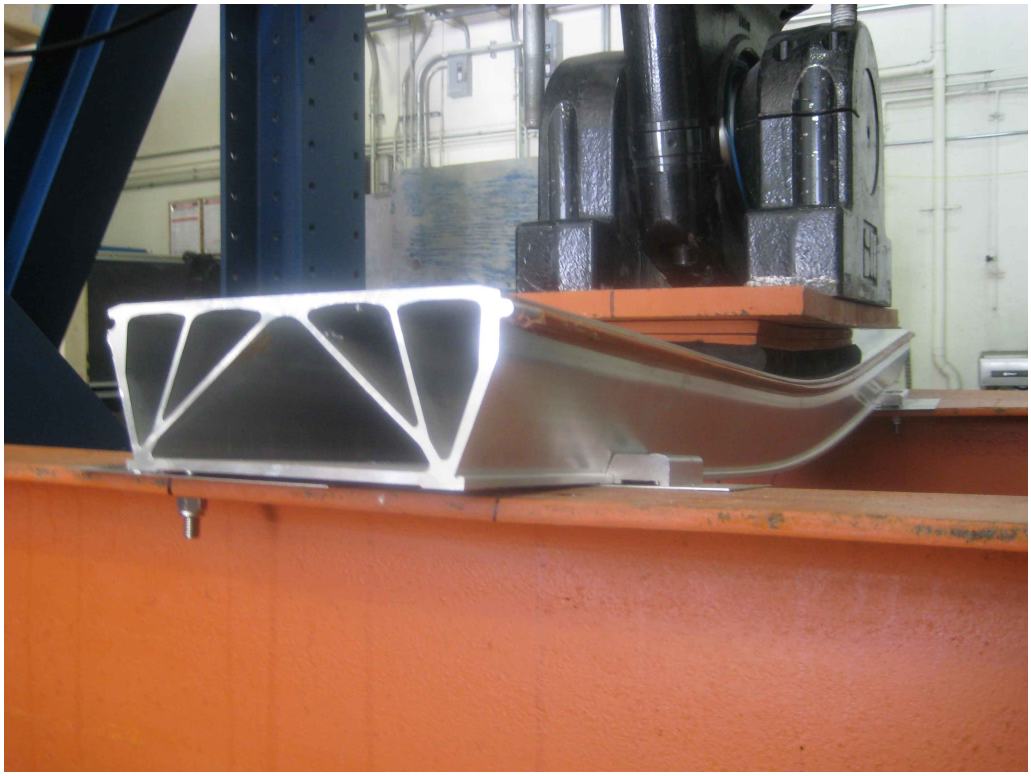
Figure 2.8 Deformed Shape of Simple-Span Panel at Ultimate Load

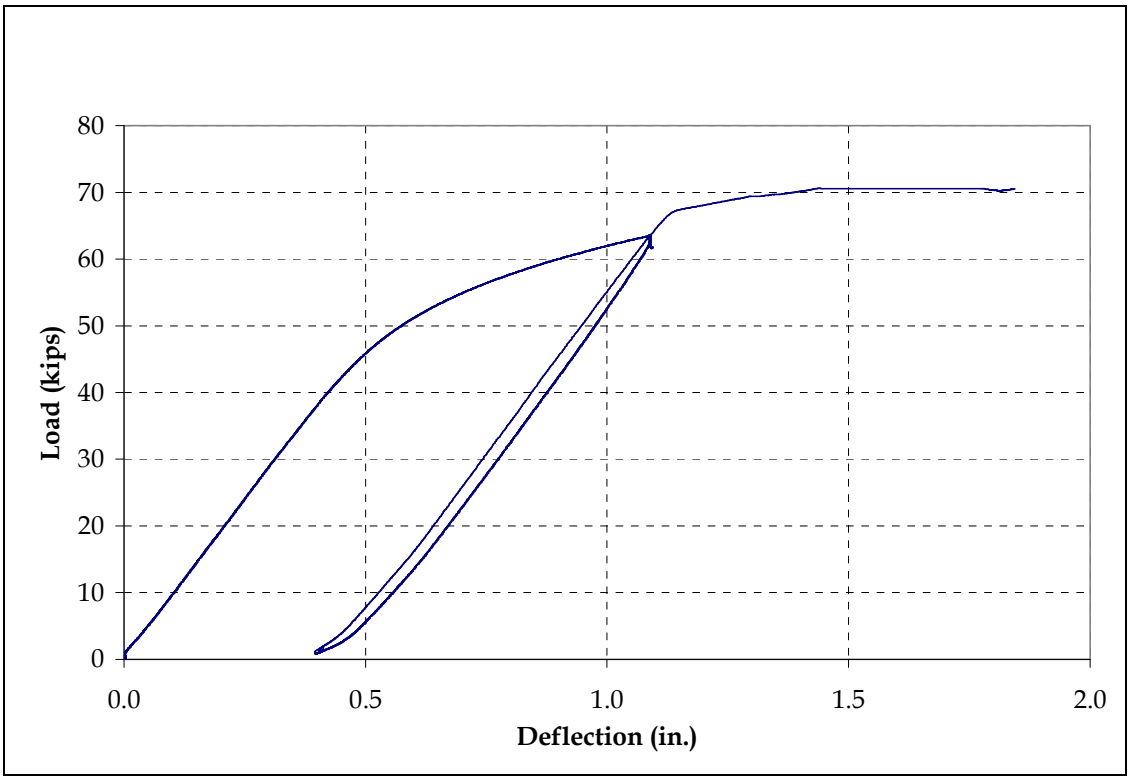

Figure 2.9 Load-Deflection Response for the Simple-Span Panel at Mid-Span

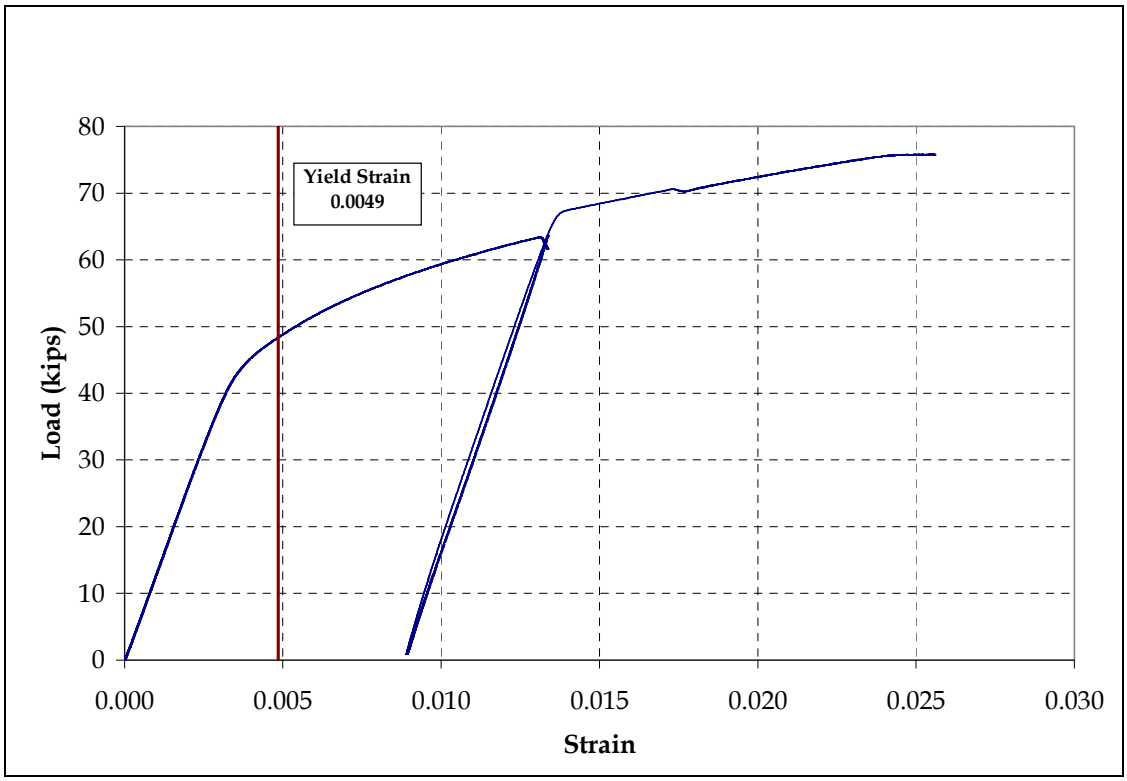

Figure 2.10 Tensile Strain at Mid-Span of Simple-Span Panel

The two-span continuous beam was tested to observe the behavior of the deck under a negative moment. Because the cross section of the deck is unsymmetrical about its bending axis, it behaved quite differently in the positive and negative moment regions. Figures 2.11 and 2.12 show the test setup and the deformed shape of the deck, respectively. Load-deflection and load-strain responses are presented in Figures 2.13 to 2.15. The loading, unloading and reloading curves are almost parallel indicating minimal stiffness degradation. The initial stiffness was 205 kips/in., which was 128% higher than that of the simple-span beam. The total ultimate load is 168 kips or 84 kips for each span, approximately 20% higher than that in the simple-span beam. The major difference between the simple-span and the two-span beams is in the stiffness, due to the redundancy of the system.

Figure 2.11 Test Setup for Two-Span Continuous Panel


Figure 2.12 Deformed Shape of Two-Span Continuous Panel at Ultimate Load

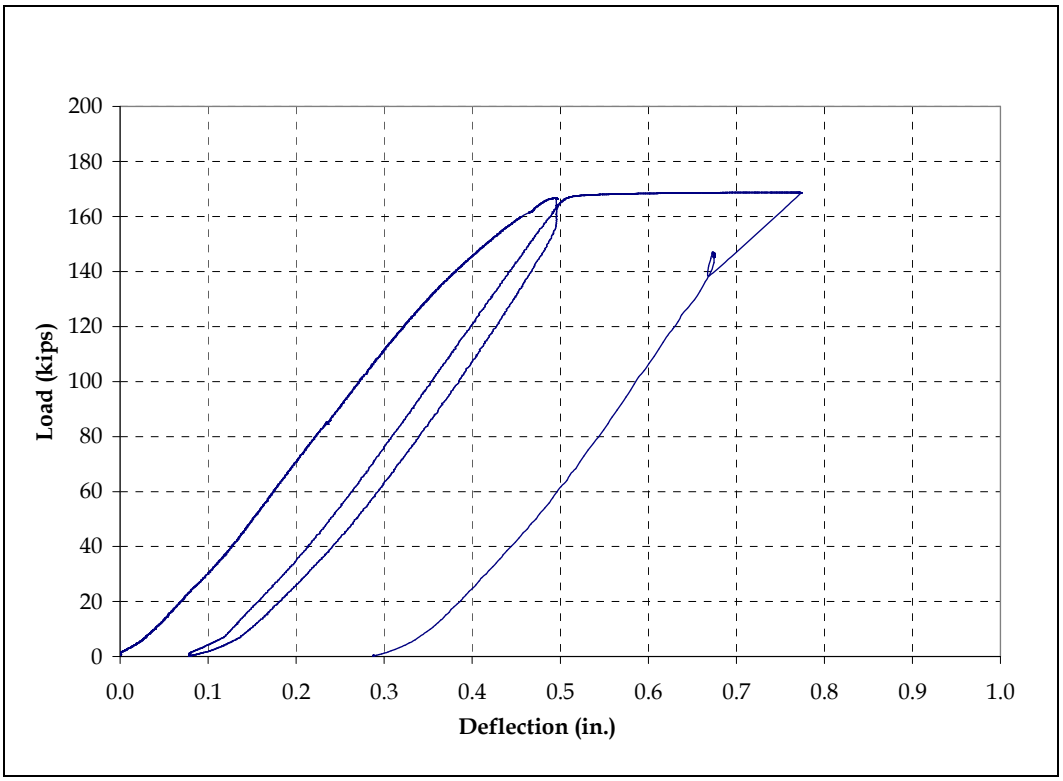

Figure 2.13 Load-Deflection Response for the Two-Span Continuous Panel at Mid-Span

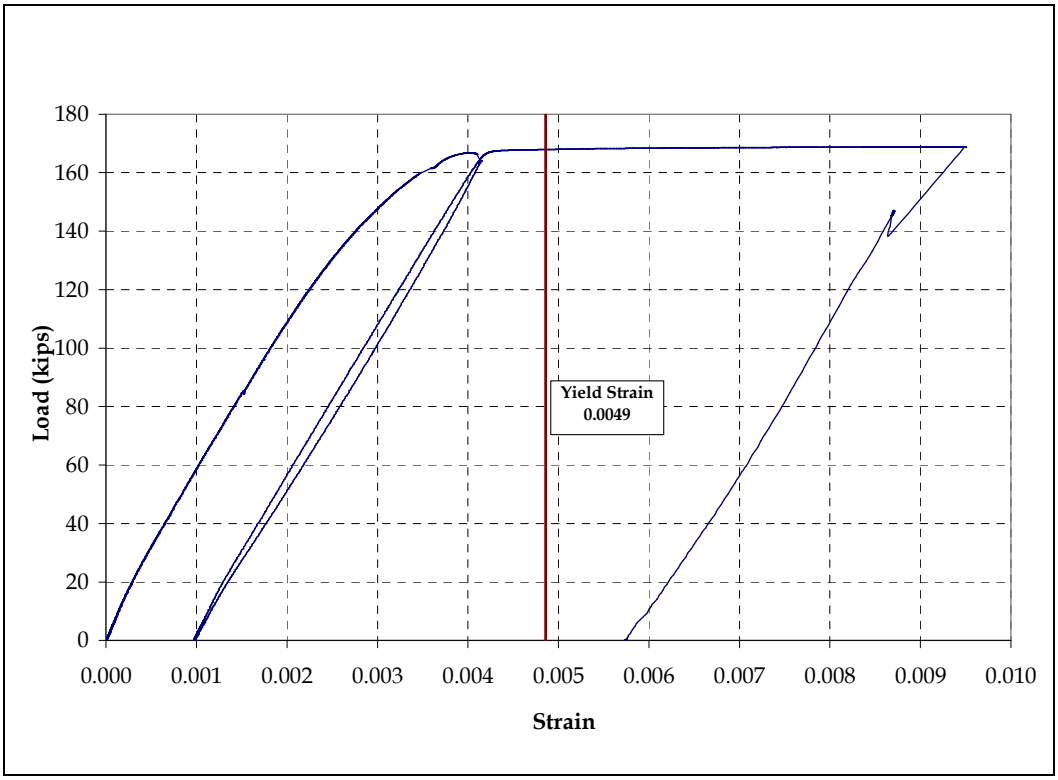

Figure 2.14 Tensile Strain at Mid-Span of Two-Span Continuous Panel

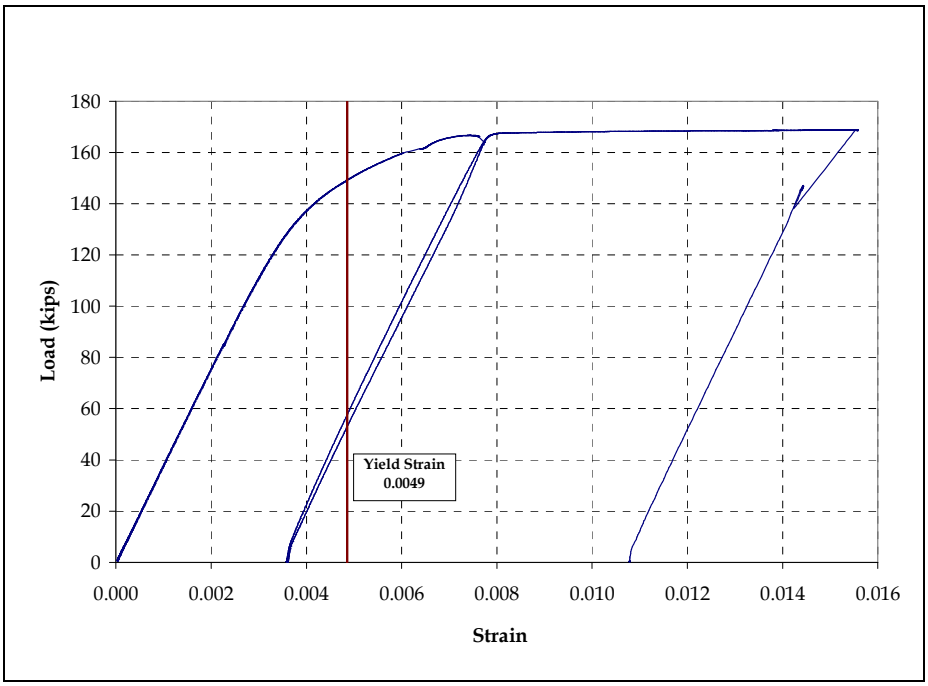

Figure 2.15 Tensile Strain at Interior Support of Two-Span Continuous Panel

The inverted panel test simulated the overhang portion of the deck, which is subjected to a hogging moment. The load was applied at the third point of a 6-ft simply supported span to simulate an overhang length of 4 ft. Figures 2.16 to 2.18 present the test setup and deformed shape. Load-deflection and load-strain responses are shown in Figures 2.19 and 2.20, respectively. The deck failed at an ultimate load of 35 kips with a stiffness of 37.7 kips/in. Near the ultimate load, the top plate (bottom plate in regular configuration) and the side plates showed sings of local buckling.

Figure 2.16 Test Setup for Simple-Span Inverted Panel

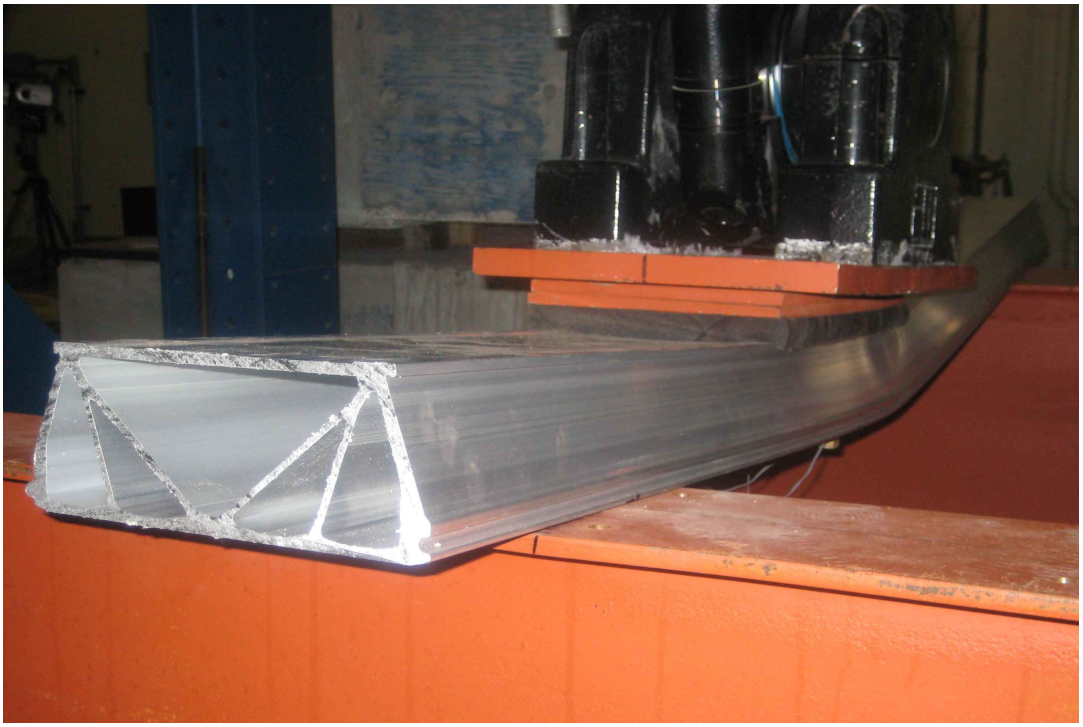

Figure 2.17 Deformed Shape of Simple-Span Inverted Panel

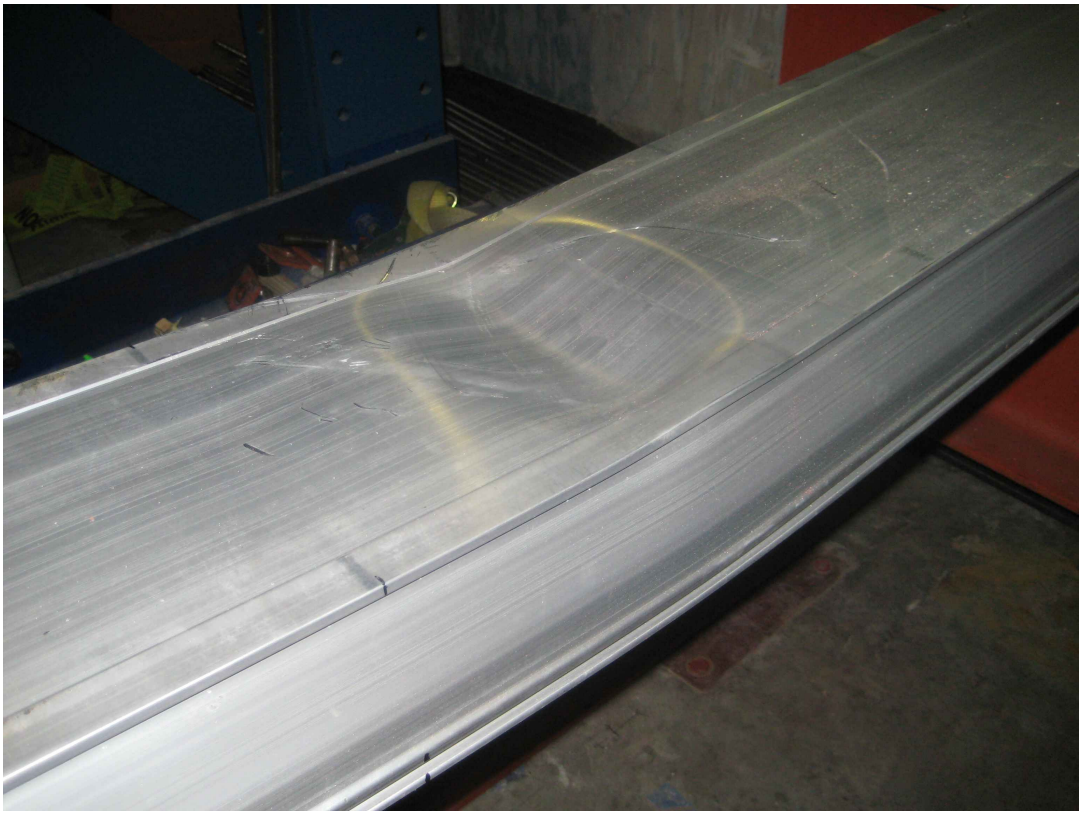

Figure 2.18 Local Flange Buckling of Inverted Panel at Failure

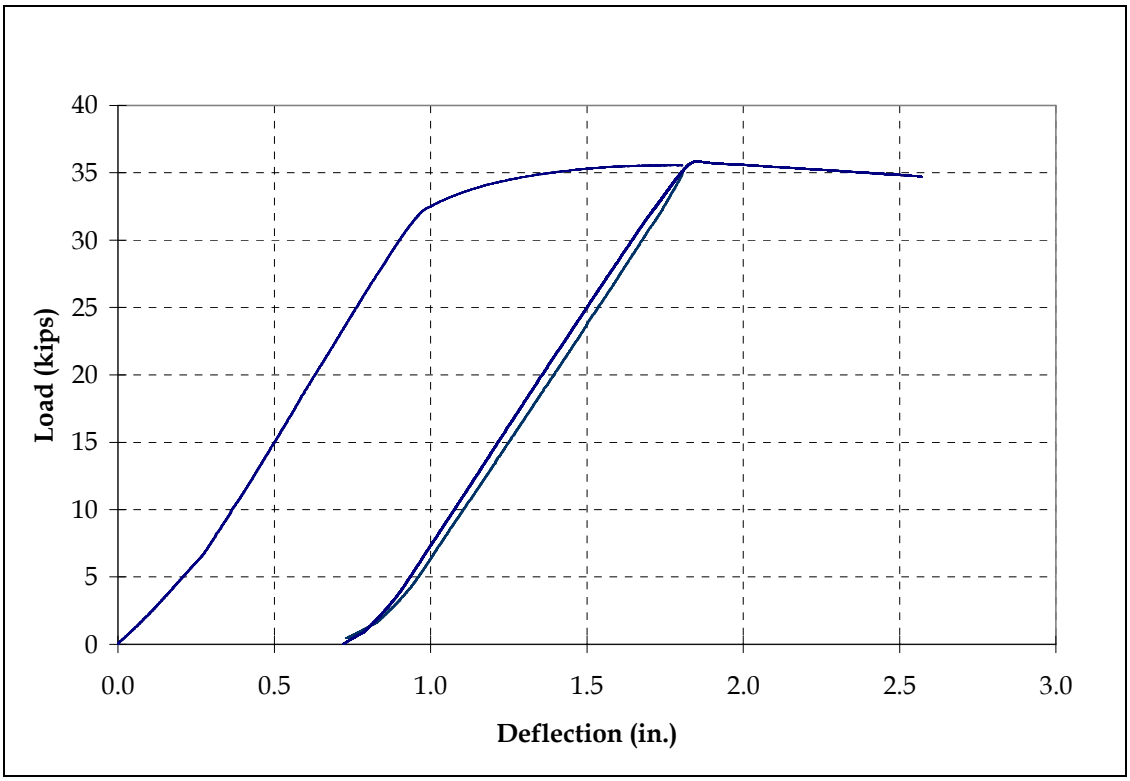

Figure 2.19 Load-Deflection Response of Simple-Span Inverted Panel under the Loading Point

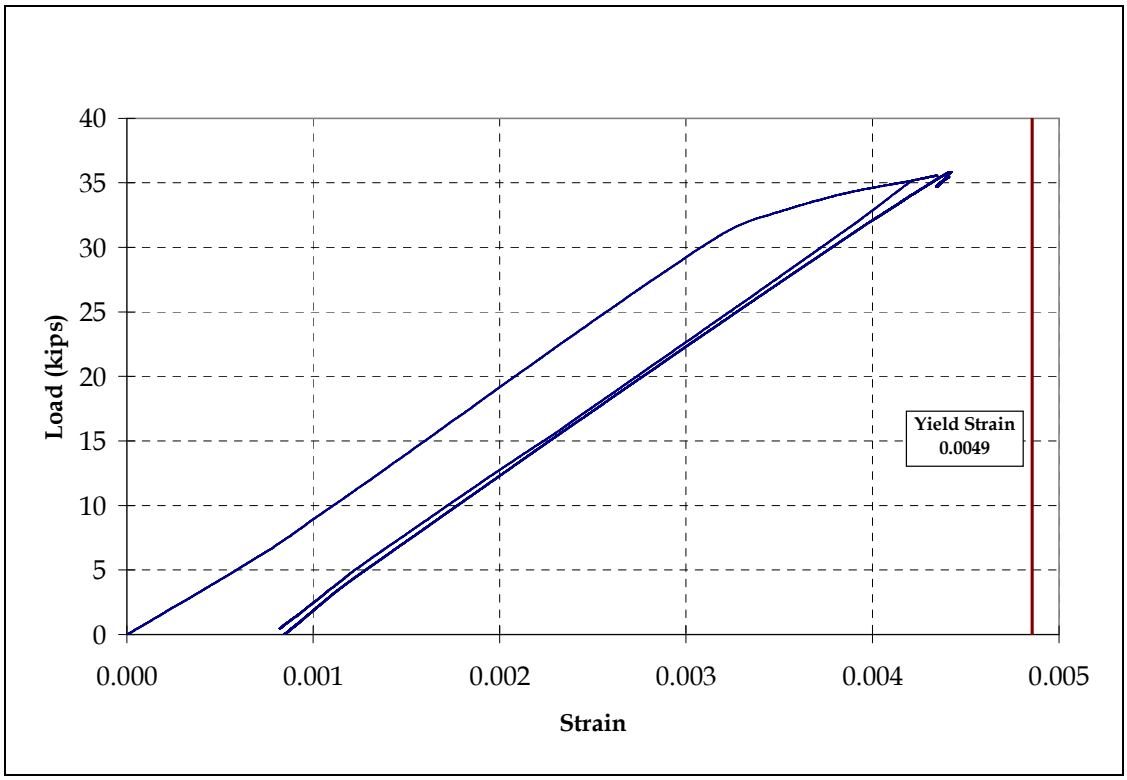

Figure 2.20 Tensile Strain of Simple-Span Inverted Panel under the Loading Point

2.5.2 Shear Test for Connectors

The shear test was performed to establish the ultimate shear capacity of the deck-to-girder connection. This mechanical connection consists of a clamp, which holds down the deck with the help of 2.36 in. long stainless steel screws. Figure 2.21 shows the connection accessories. This clamped connection will be subjected to a horizontal shear force in the event that brakes are applied to the vehicles moving over the bridge. In the case of an interior panel, the braking force will be resisted in two ways, first by the tongue and groove connection, which will transfer the force to the adjacent panel, and second by the clamped connection, which will transfer the force to the girder. For the last panel on the bridge deck, the braking force will be resisted by the clamped connections only. Therefore, it is imperative to establish the shear capacity of the clamped connection alone. Figure 2.22 shows the schematic diagram of the test setup showing two clamps per panel to resist the shear force. As discussed earlier, each clamp has to resist a minimum of 700 lbs of shear force (Table 2.1), if four clamps are resisting the force. Figures 2.23 to 2.25 show the mode of failure and load-displacement response of the deck under the shear force applied through a hydraulic jack. Displacement was measured at the top of the panel using a linear potentiometer, and the load was measured using a load cell.

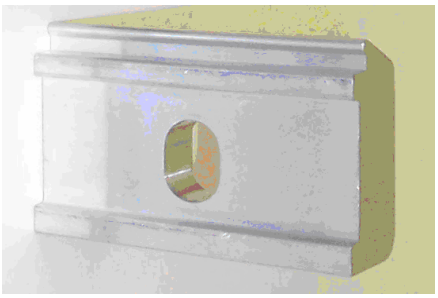

Fastening Clamp

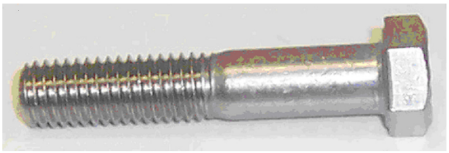

Bolt

Locking Nut

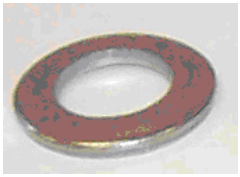

Washer

Distance Shim

Figure 2.21 Connection Accessories

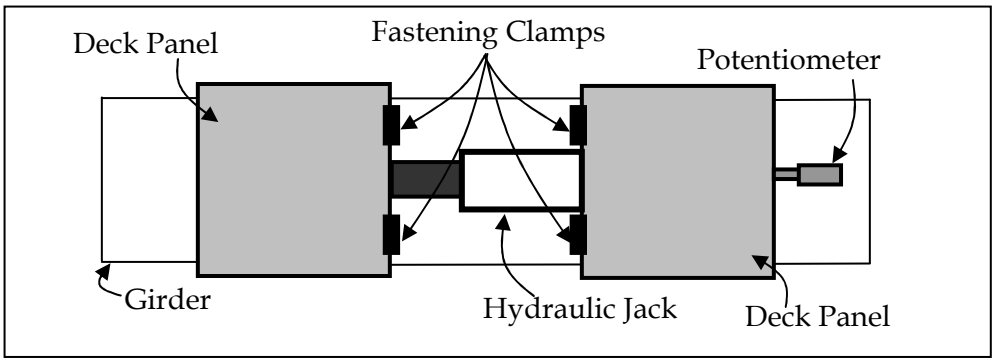

Figure 2.22 Schematic Plan View of Test Setup

Figure 2.23 Test Setup for the Clamps Shear Test

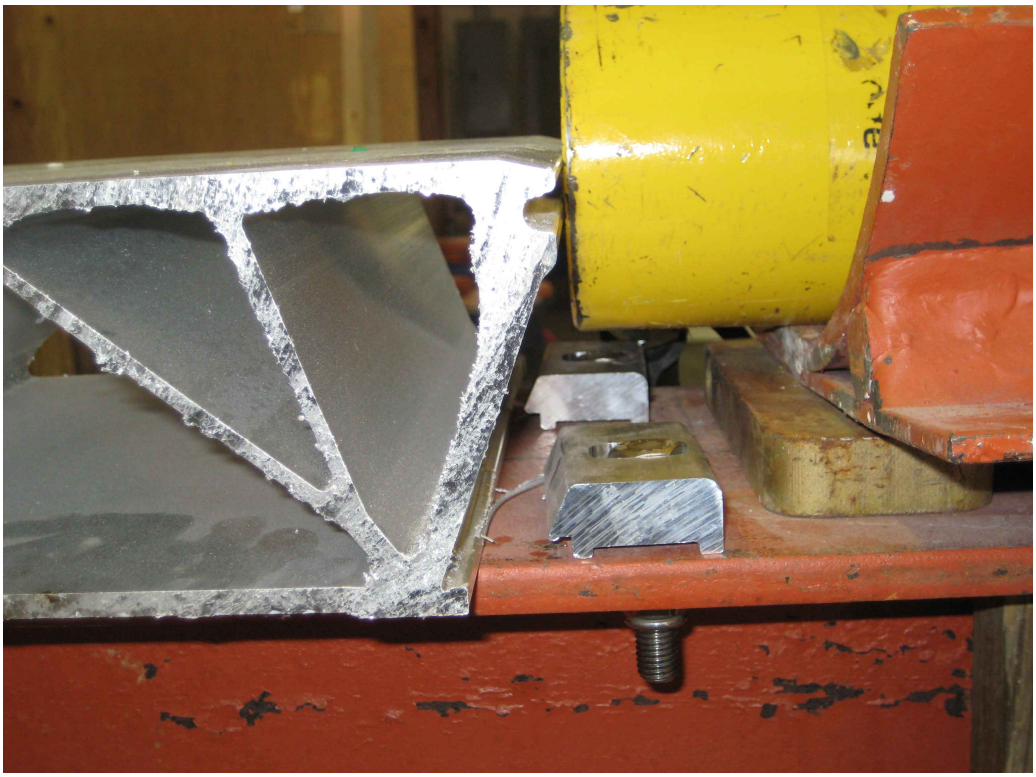
Figure 2.24 Failure of Aluminum Deck Edge

The ultimate shear strength of the connections proved to be more than 1.6 times the required strength. The load-displacement curve (Figure 2.25) shows two peaks. The sudden load drop after the first peak represents the failure of the first clamp along with a portion of the deck edge, which was chipped off the deck. After the failure of the first clamp, the entire load was taken by the second clamp, which also failed suddenly at a later stage. In case a clamp of an in-service deck fails due to unexpected loading, it can be easily replaced. However, if the deck edge is also chipped off then the entire panel needs to be replaced. Failure of one clamp on a deck will not be catastrophic as there will always be other clamps to take the load. A routine inspection of the deck is recommended to check whether all clamps are in good shape.

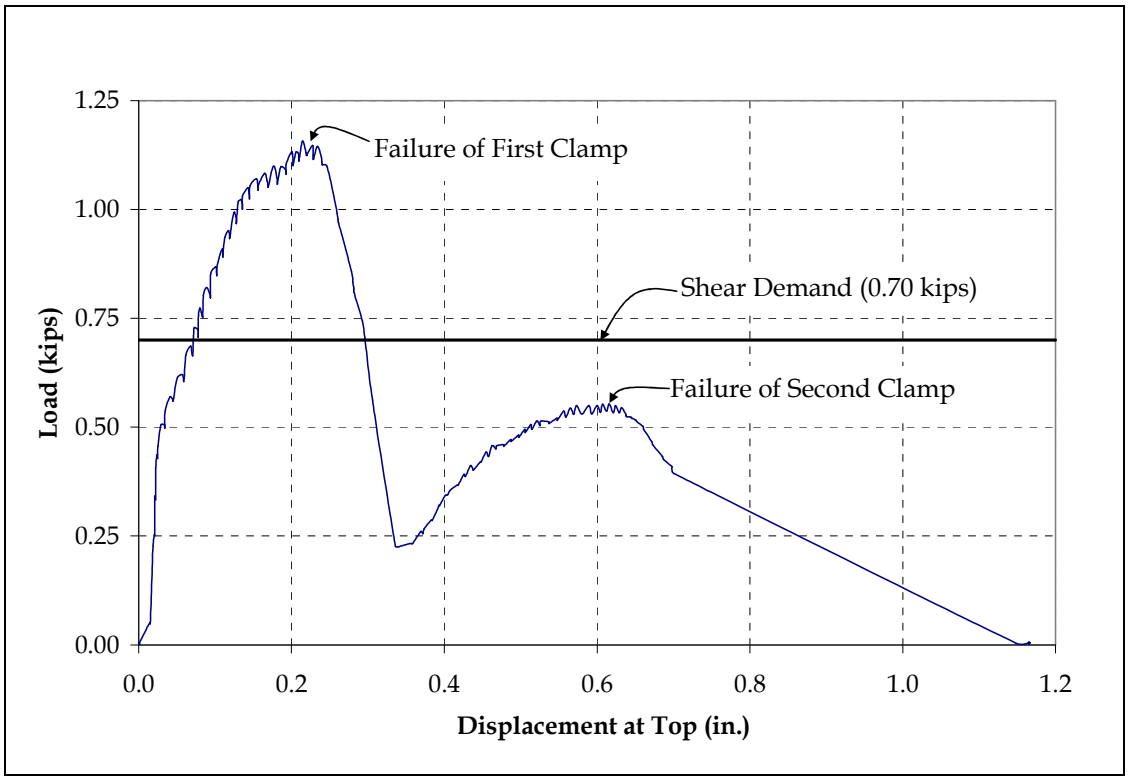

Figure 2.25 Load-Displacement Response in Shear Test

2.5.3 Uplift Test for Connectors

The uplift test characterizes the resistance of the clamped connection against the wind pressure acting upwards from the bottom of the deck. Two 12 in. wide deck specimens were used for the test. They were placed side by side and connected to the girder with four clamps, two on each deck panel. Load was applied from two hydraulic jacks one on each side. Deflection was measured at the joint and at the middle of each panel. Figures 2.26 to 2.29 show the test setup and mode of failure for the uplift test.

The clamps proved to be very strong against the uplift pressure. The peak load was more than four times the required ultimate load. The failure took place at the deck edge, while all clamps remained intact. Two solid pieces of deck edge, each of a length equal to that of the clamp were removed from the deck. Failure was sudden, as indicated by the sudden load drop in Figures 2.30 and 2.31.

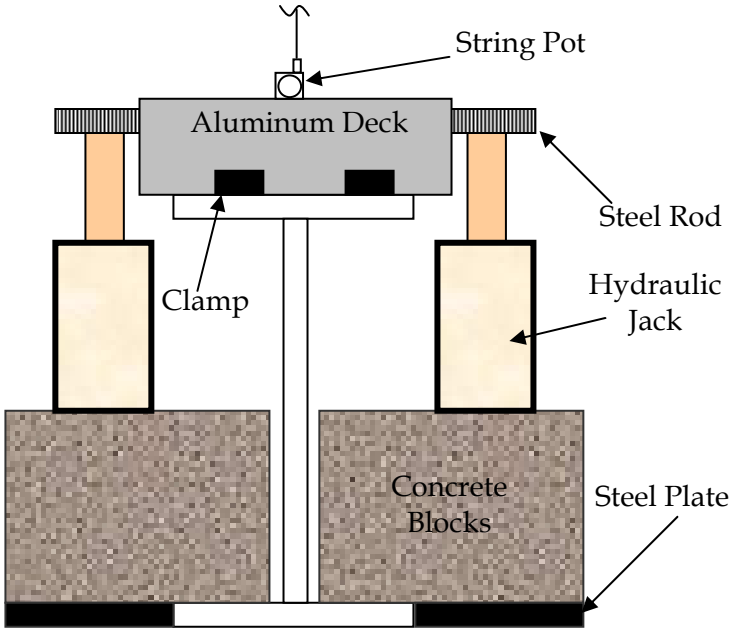

Figure 2.26 Schematic Diagram for Uplift Test

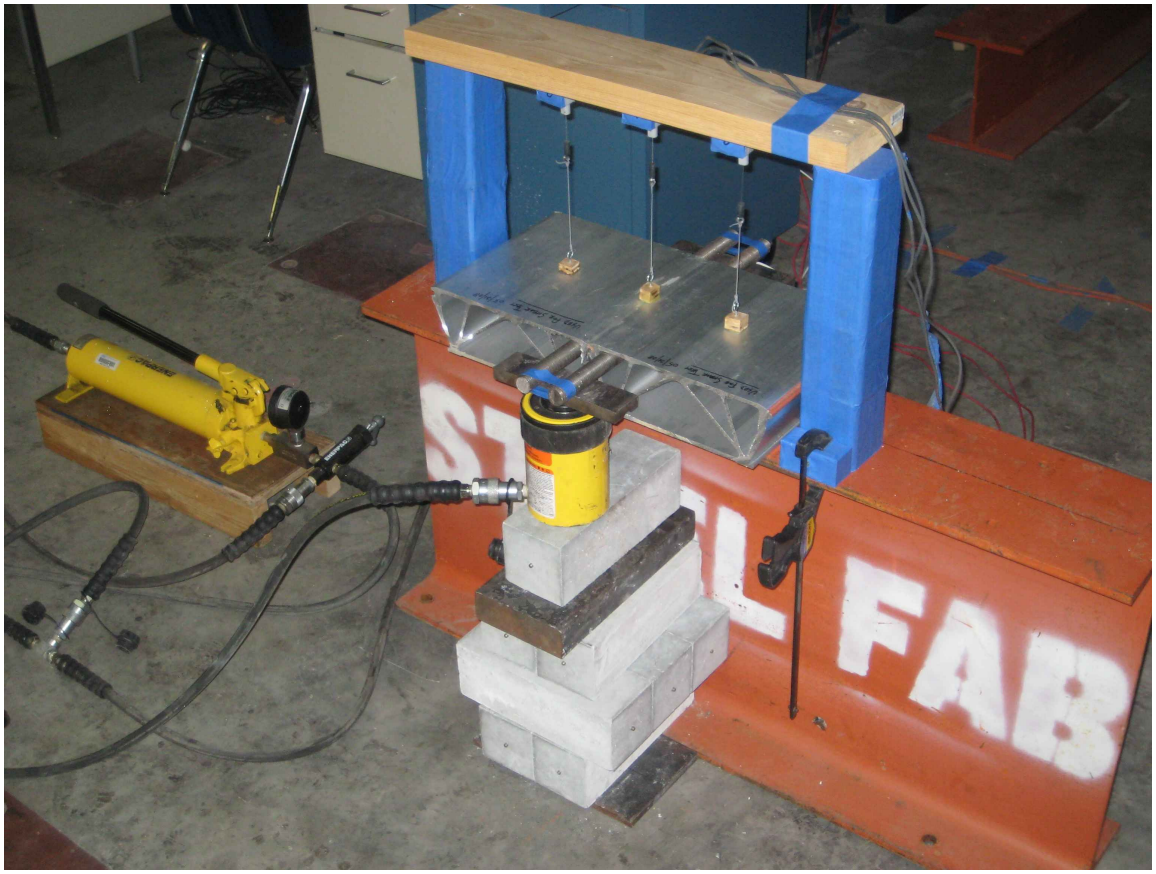
Figure 2.27 Setup for Uplift Test

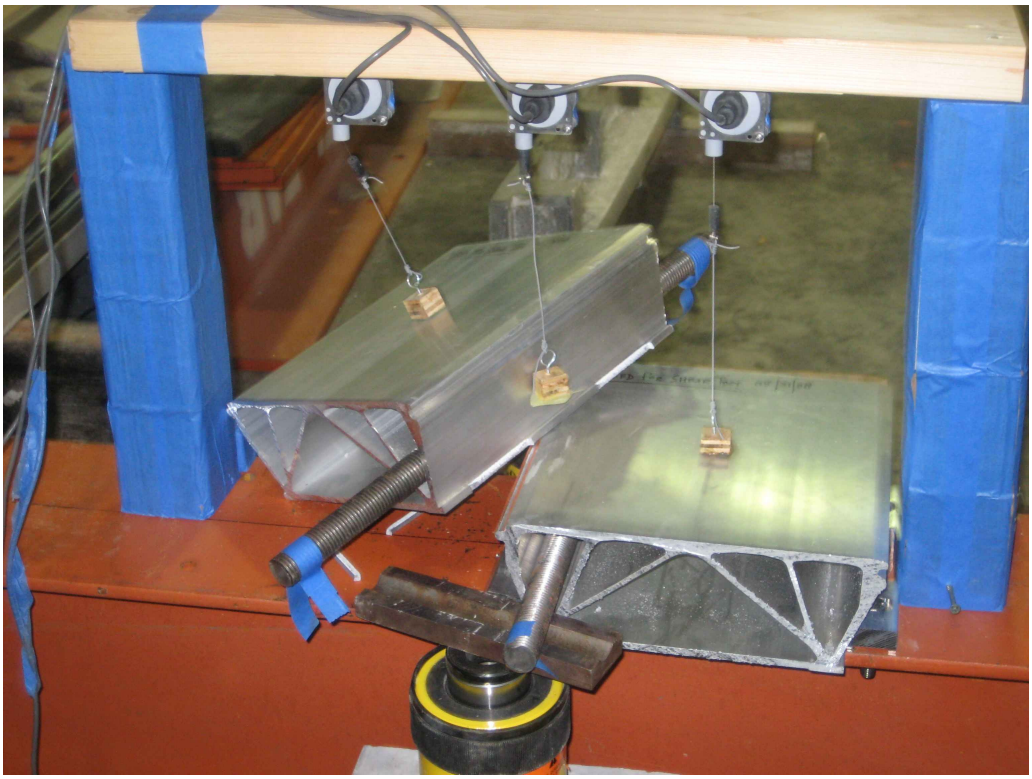

Figure 2.28 Failure of Deck Edge in Uplift Test

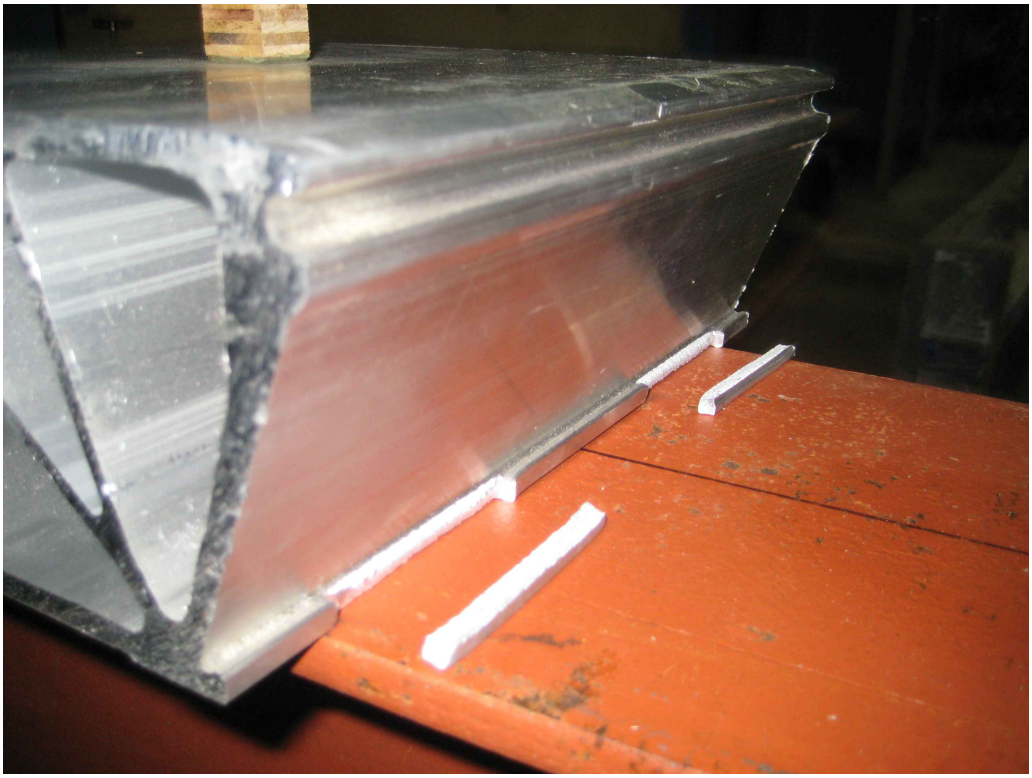

Figure 2.29 Broken Pieces of Deck Edge

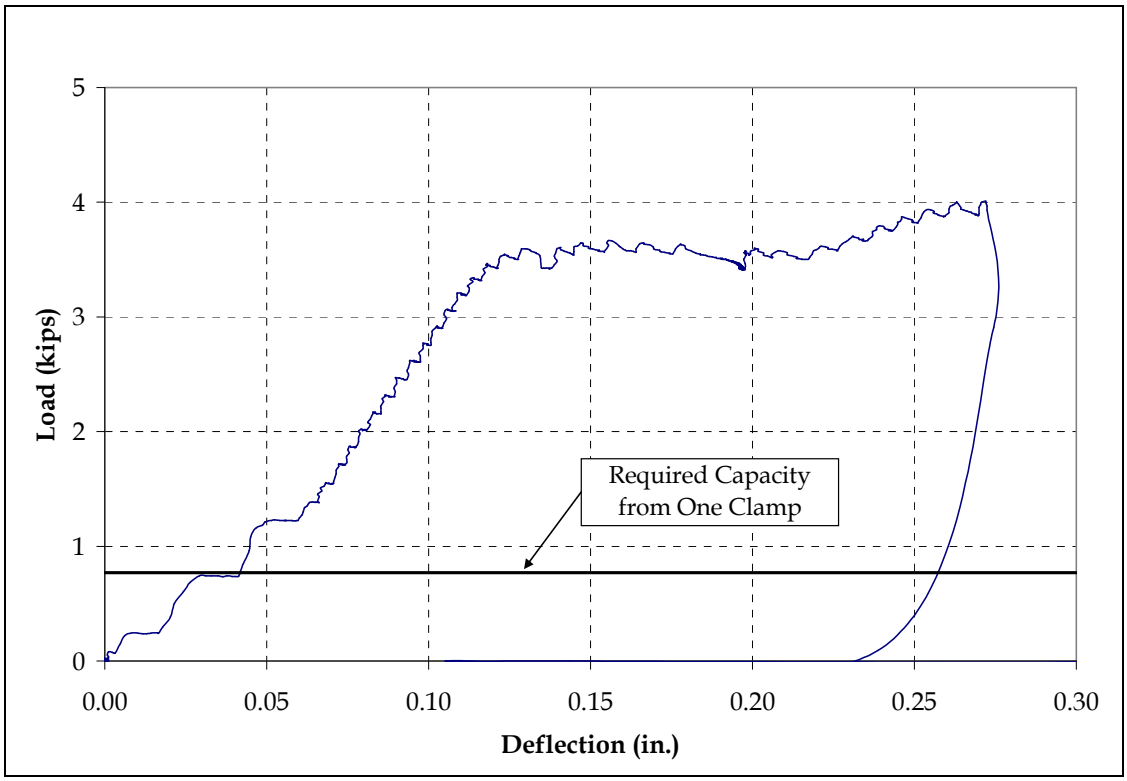

Figure 2.30 Upward Deflection at the Lip Joint

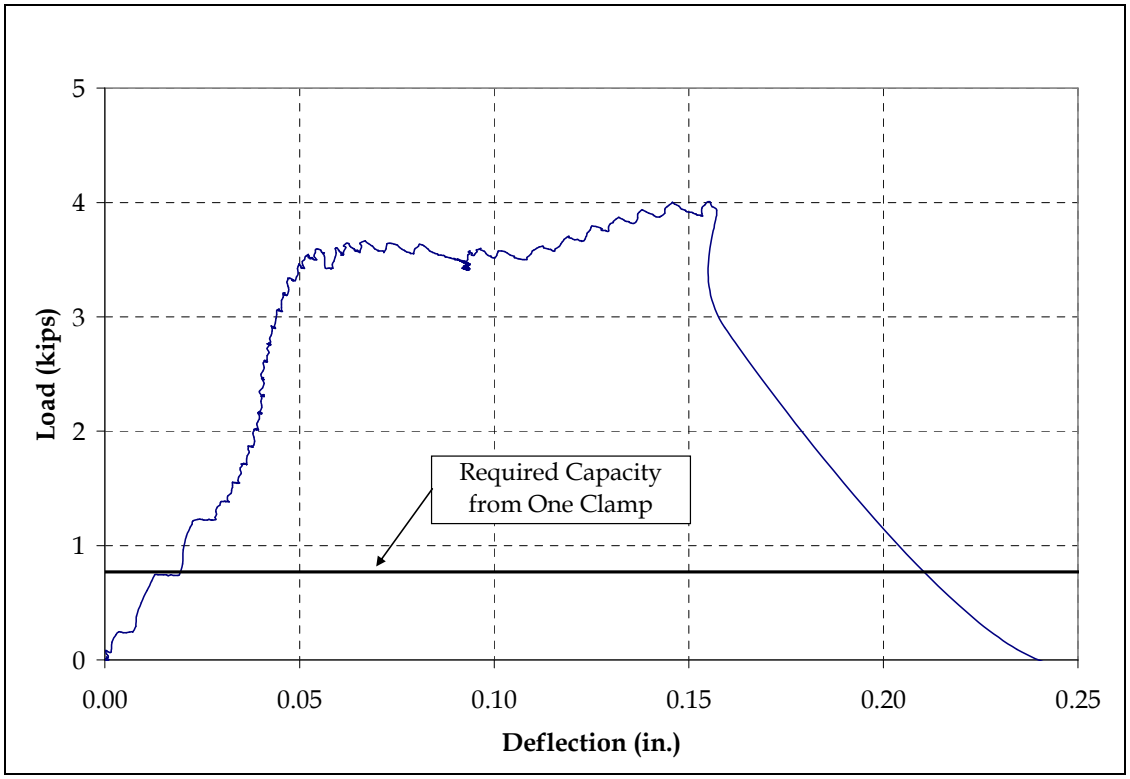

Figure 2.31 Average Upward Deflection at the Center of the Top Plate

2.5.4 Lip Test (Tongue and Groove Test)

Strength of the tongue and groove connection is important for the transfer of load from one panel to the other. Failure of the tongue and groove connection may lead to excessive deflection and perhaps delamination of wearing surface. Hence, it is imperative to establish the strength of this connection. A 12 in. long piece of deck panel along with two 4 ft long panels was used to perform the test. One string potentiometer was installed under the loading point at the middle of the section to monitor deflection. Figures 2.32 and 2.33 show the test setup and the mode of failure, respectively.

Figure 2.34 shows the load-deflection response. The 12 in. wide lip failed at 75.14 kips, which is twice the target load of 37.24 kips. In an actual bridge deck the lip failure is unlikely to happen because the lip will be present along the entire length of the panels. This high strength of the lips will ensure the development of panel action to distribute the load in the lateral direction.

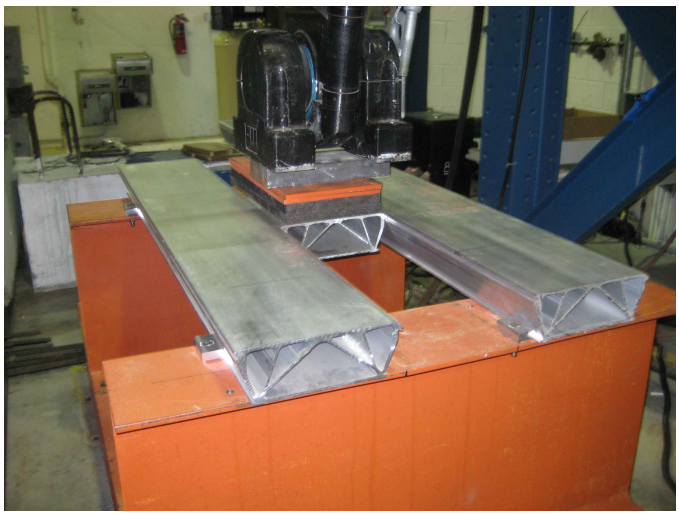

Figure 2.32 Test Setup for the Lip Test

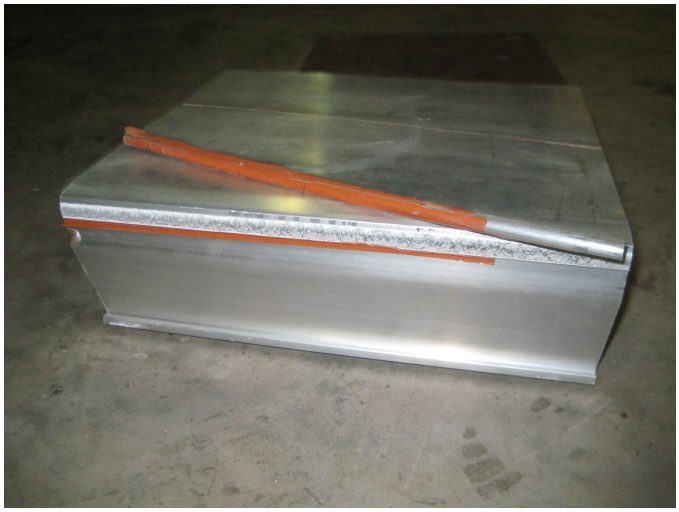

Figure 2.33 Failure of the Lip

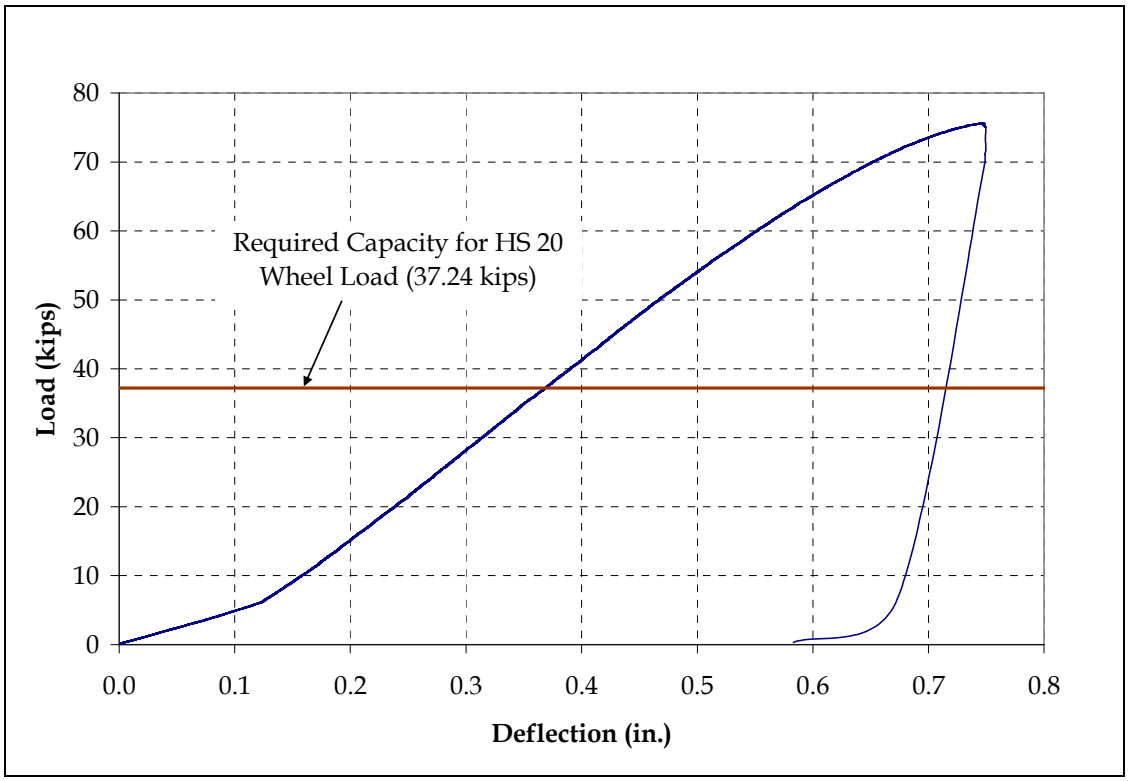

Figure 2.34 Load-Deflection Response for the Lip Test

2.5.5 Fatigue and Residual Strength Tests

Fatigue is a major design consideration for metal structures under repeated load cycles. Most failures of metal structures in the field are by fatigue. Fatigue testing on SAPA aluminum bridge deck panels was performed at the FDOT Structures Lab in Tallahassee. Deck panels were subjected to two million cycles of a sinusoidal load (0.5-18 kips) with a frequency of 4 Hz. The load level followed AASHTO requirements. The test was run continuously for almost six days. Load, displacement, and strain data were recorded after every 1,000 cycles up to 10,000 cycles, and then after every 10,000 cycles up to 2 million cycles. At each interval, eight sinusoidal cycles were continuously recorded for all channels. During and after the test, the deck panels were monitored for cracks in the panels or connections. After the fatigue test, two static tests were performed on the panels to determine their residual strengths. Figures 2.35 to 2.38 show the instrumentation plan, loading configurations, and test setup for the fatigue and residual strength tests.

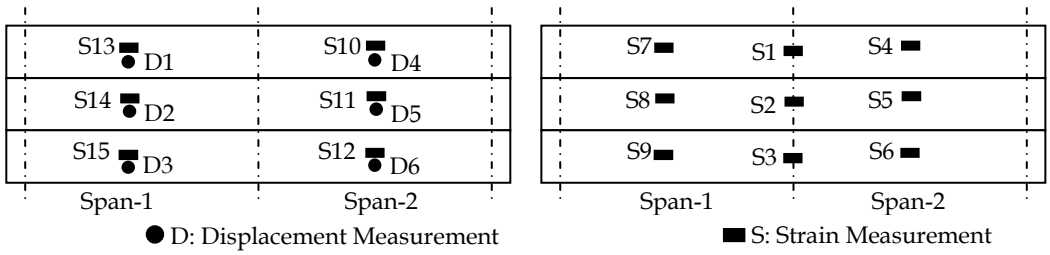

(a) Bottom Surface (view from top) (b) Top Surface

Figure 2.35 Instrumentation Plan

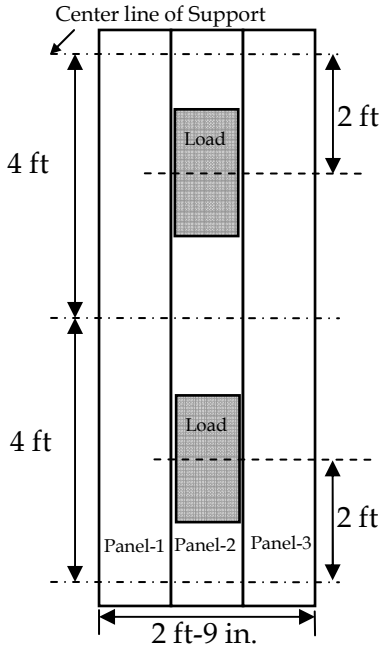

Figure 2.36 Loading Configuration for Fatigue Test

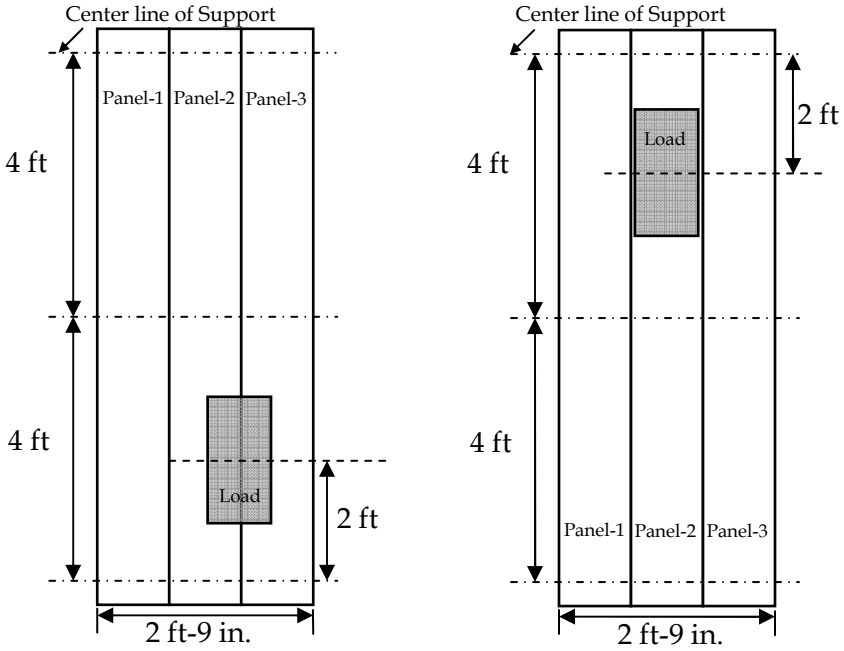

Load on Lip Joint Load on Panel

Figure 2.37 Loading Configurations for Residual Strength Tests

Figures 2.39 and 2.40 show the fatigue load-deflection responses for Spans 1 and 2, respectively. The deflections ranged about 0.05 in. for the load range of 0.5-18 kips. The bolt of the clamp holding the center panel on the interior support failed at about 200,000 cycles, and was replaced with a new one. Installation of the new bolt increased the stiffness of the system as clear in Figures 2.41 and 2.42. There was only one clamp, instead of two, for each panel on every support because the top flanges of the supporting stingers were only 4.5 in. wide and could only accommodate one clamp. Had there been two clamps on each support, as per manufacturer's recommendation, this failure would not have occurred. All other blots performed well throughout the fatigue test. Bolted connections have a tendency of loosening over time and therefore they need routine inspection.

Figures 2.43 to 2.47 show the load-strain responses of deck panels. Strains at all locations remained within the elastic range throughout the fatigue test. The effect of bolt failure is again quite clear in the response curves.

Figure 2.38 Fatigue Test Setup at FDOT Structures Lab

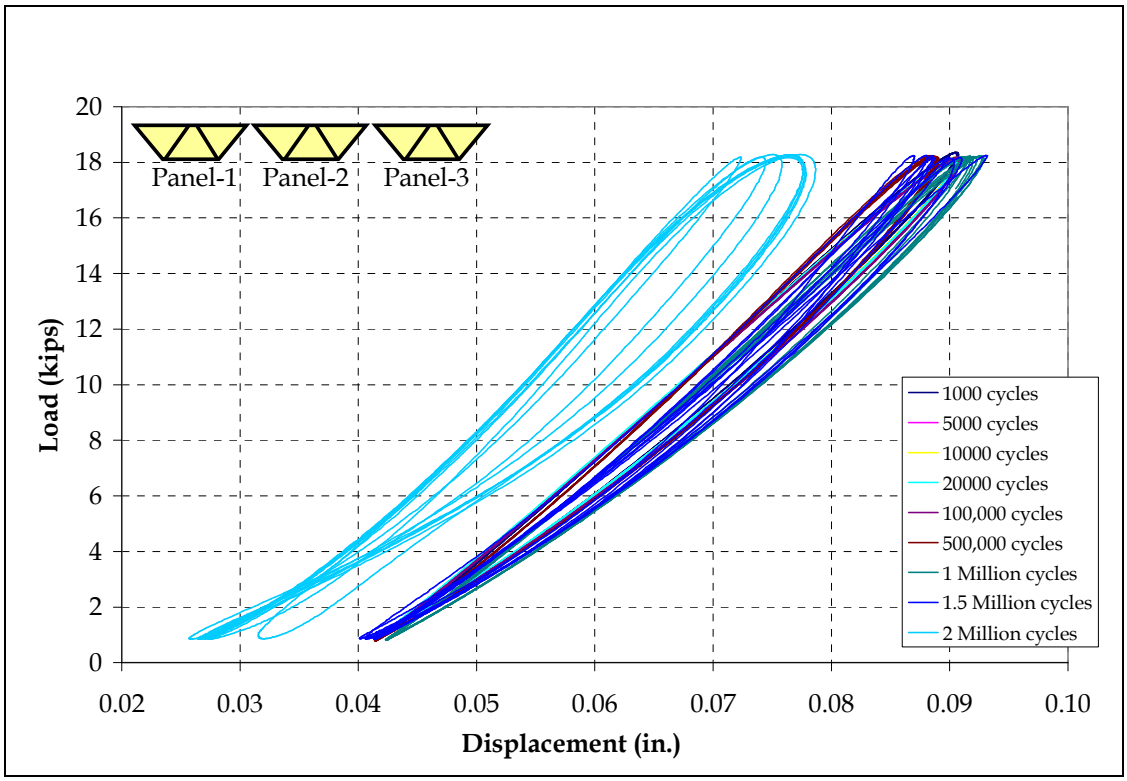

Figure 2.39 Fatigue Load-Deflection Response for Span 1, Panel 2

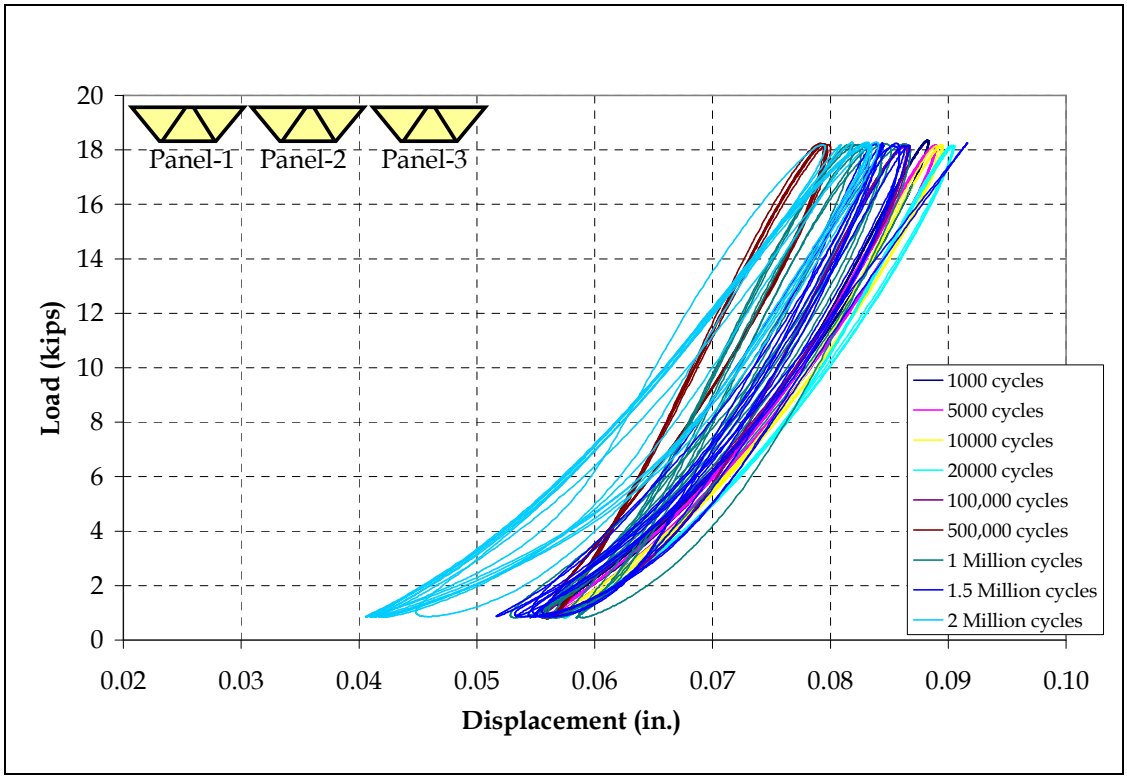

Figure 2.40 Fatigue Load-Deflection Response for Span 2, Panel 2

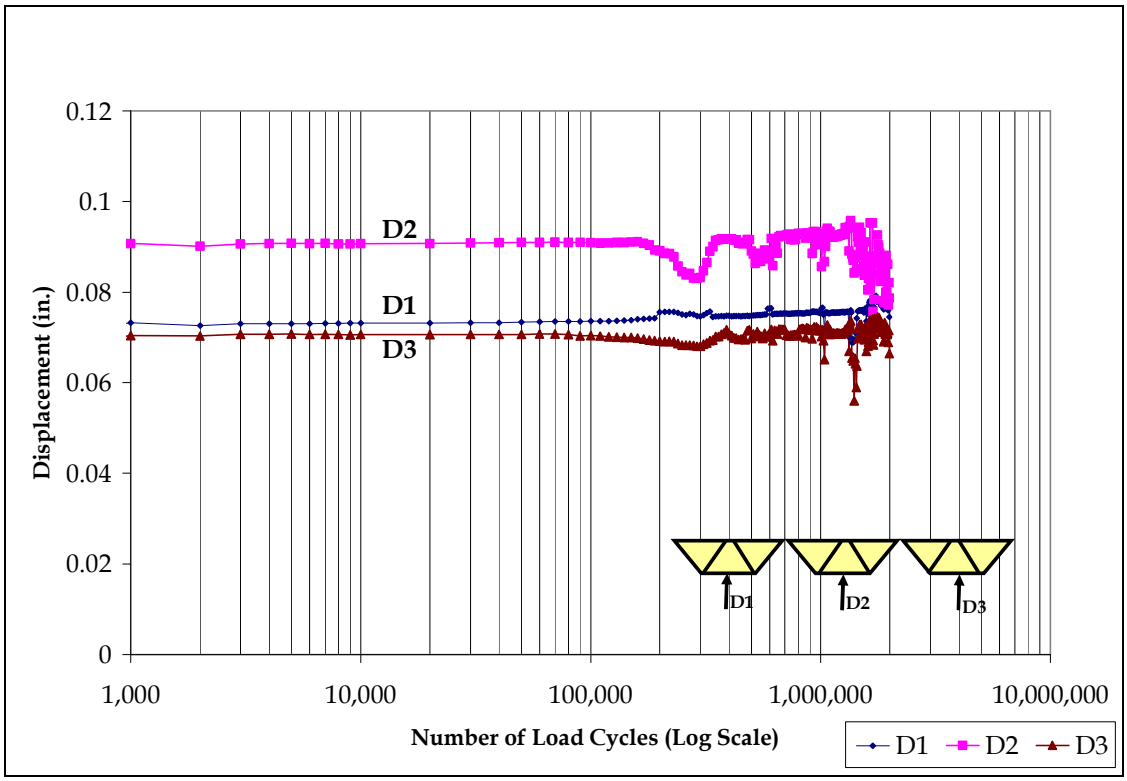

Figure 2.41 Deflection Growth in Span 1 under Fatigue Loading

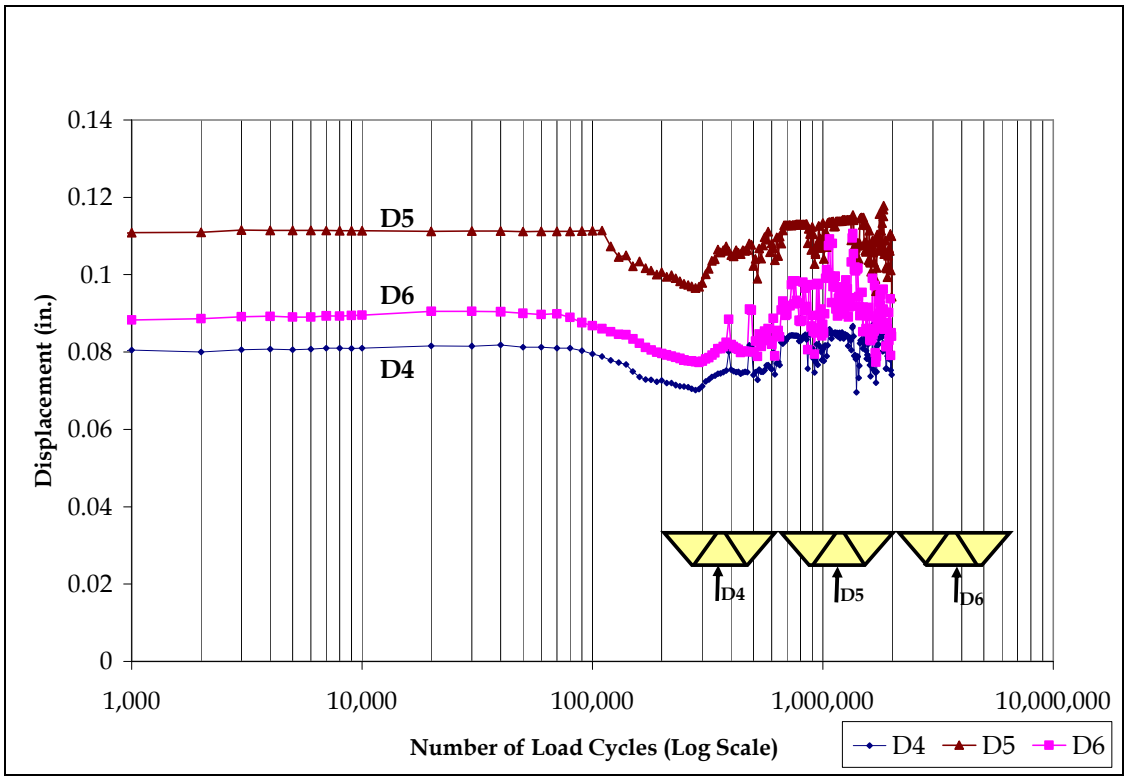

Figure 2.42 Deflection Growth in Span 2 under Fatigue Loading

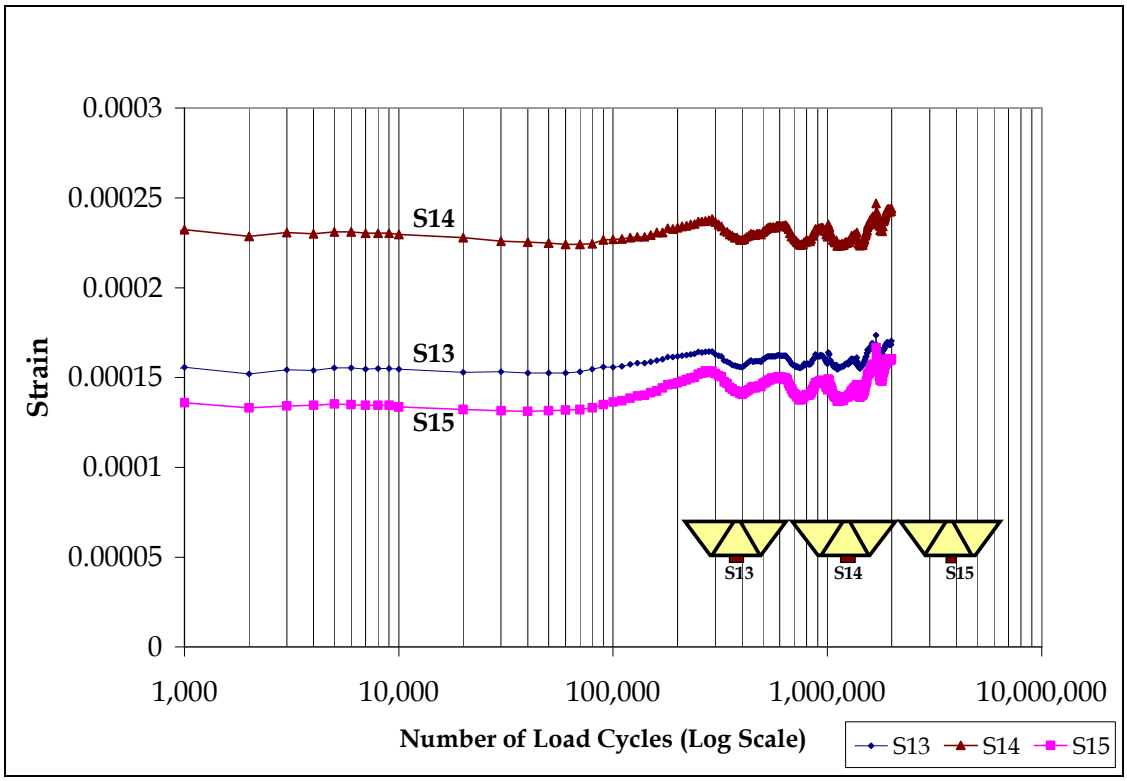

Figure 2.43 Tensile Strain at Middle of Span 1 under Fatigue Loading

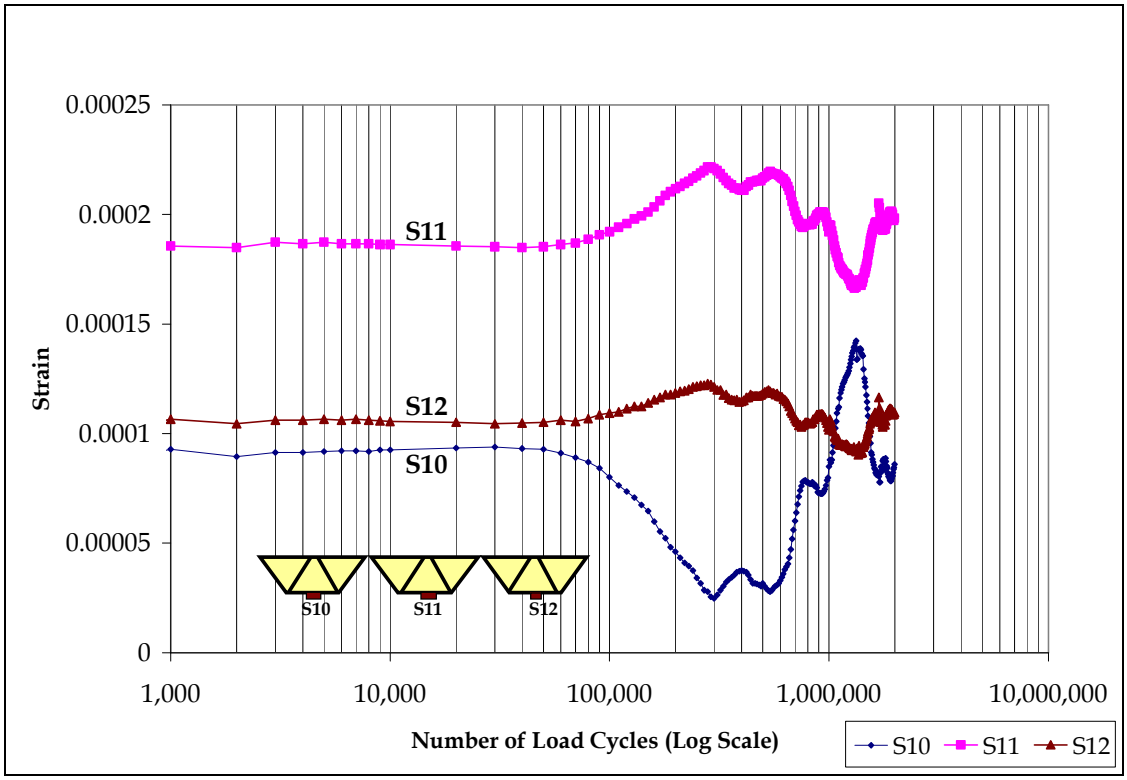

Figure 2.44 Tensile Strain at Middle of Span 2 under Fatigue Loading

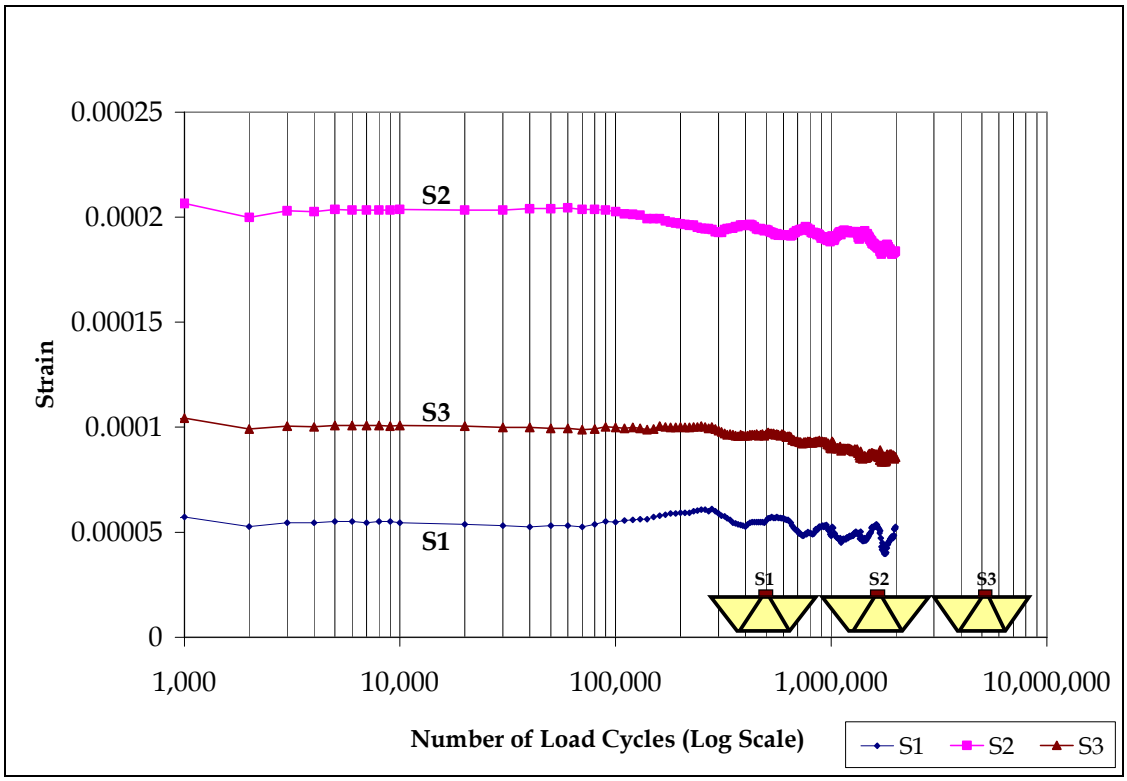

Figure 2.45 Tensile Strain at Center Support under Fatigue Loading

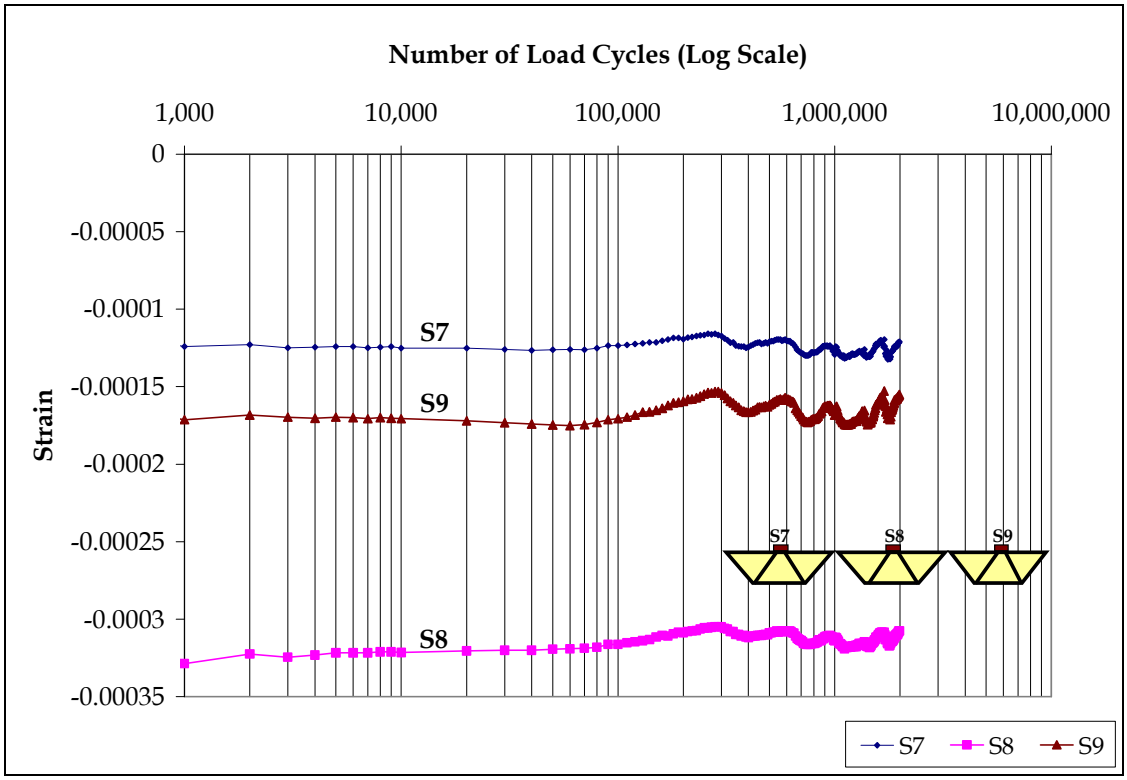

Figure 2.46 Compressive Strain at Middle of Span 1 under Fatigue Loading

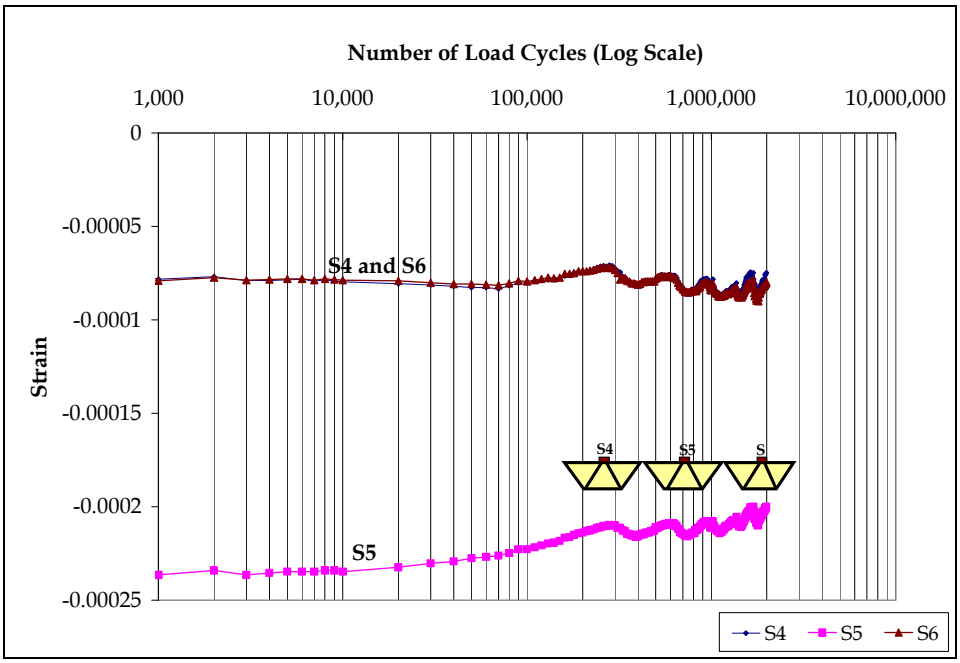

Figure 2.47 Compressive Strain at Middle of Span 2 under Fatigue Loading

Figure 2.48 shows the setup for the two loading configurations in the residual strength tests. Figures 2.49 to 2.52 show the load-deflection and load-strain responses. The diagrams for both loading configurations show that deck panels remained within the linear elastic range. In both cases, the deck panels were loaded up to a level of 100 kips, which is nearly three times the target load of 37.24 kips. The panels and the connections remained intact and did not show any sign of failure. However, some elastic local buckling was observed in the inclined plates. Deflections and strains in the panels adjacent to the loading panels prove that the system is able to develop adequate panel action. This is by the virtue of the tongue and groove connection, which helps to carry the loads in the lateral direction.

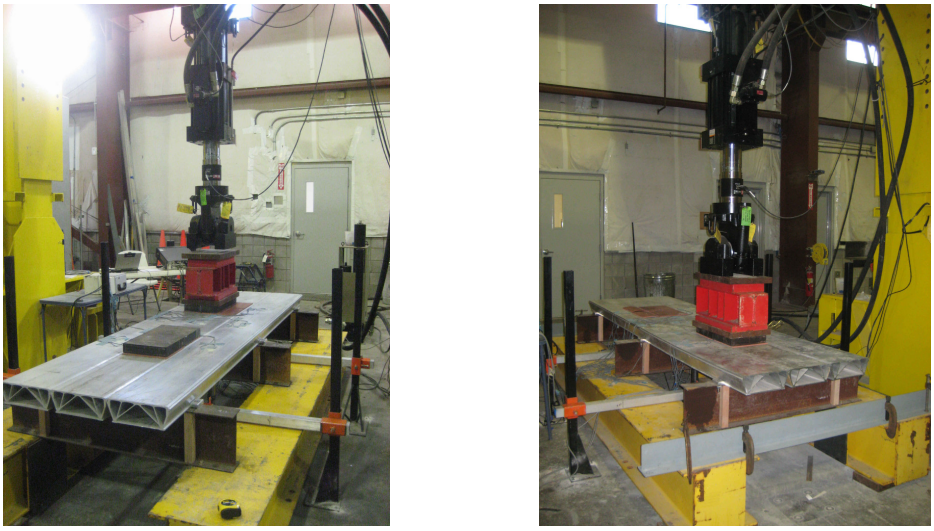

(a) (b)

Figure 2.48 Setup for the Residual Strength Tests: (a) Load Acting on Lip Joint, and (b) Load Acting between Lip Joints

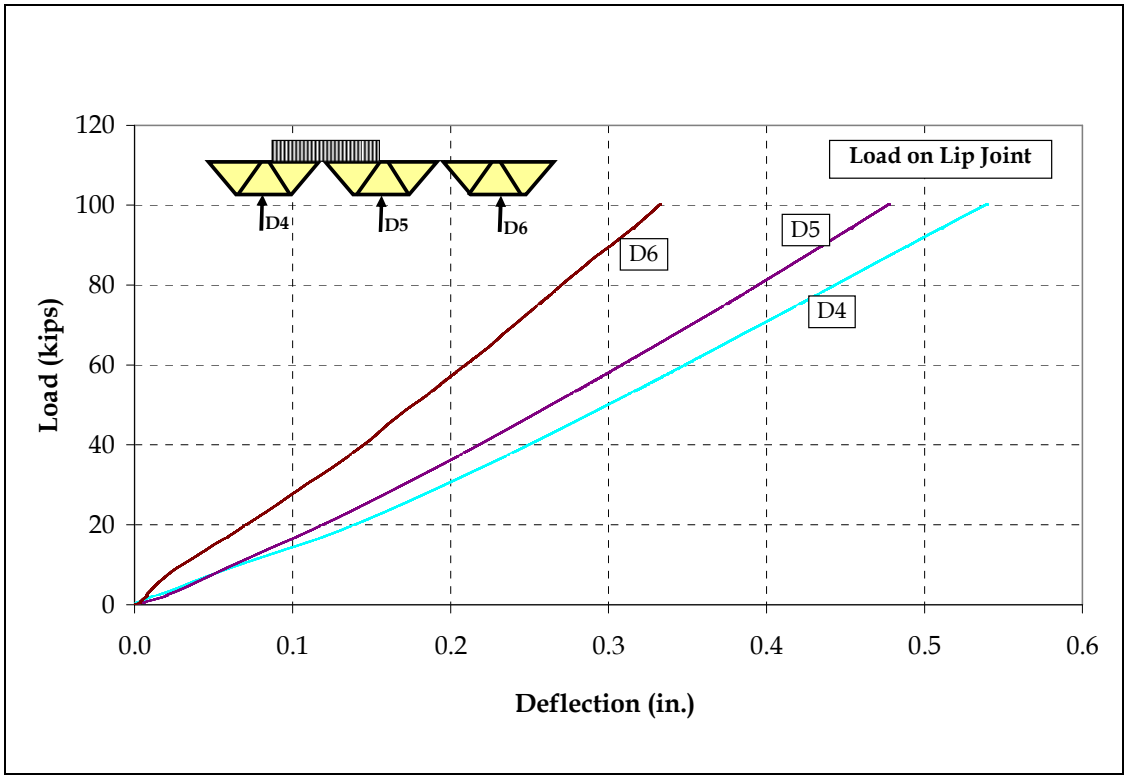

Figure 2.49 Load-Deflection Response for Residual Strength Test on Lip Joint

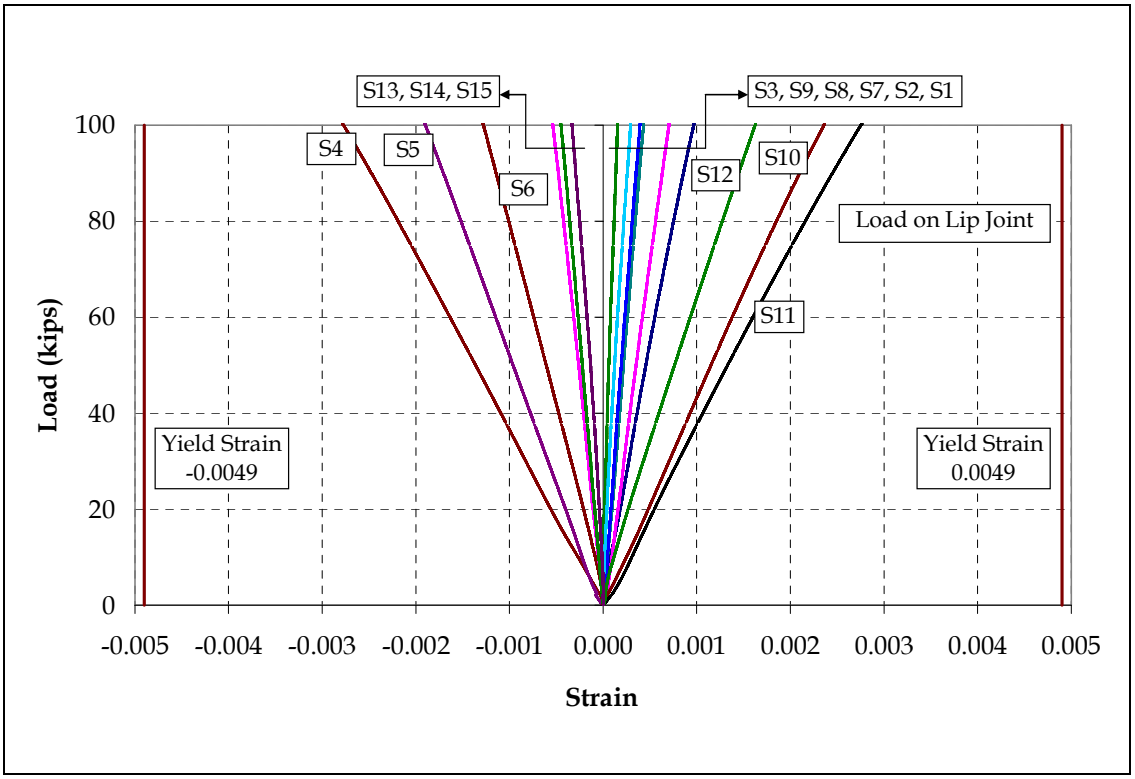

Figure 2.50 Load-Strain Response for Residual Strength Test on Lip Joint

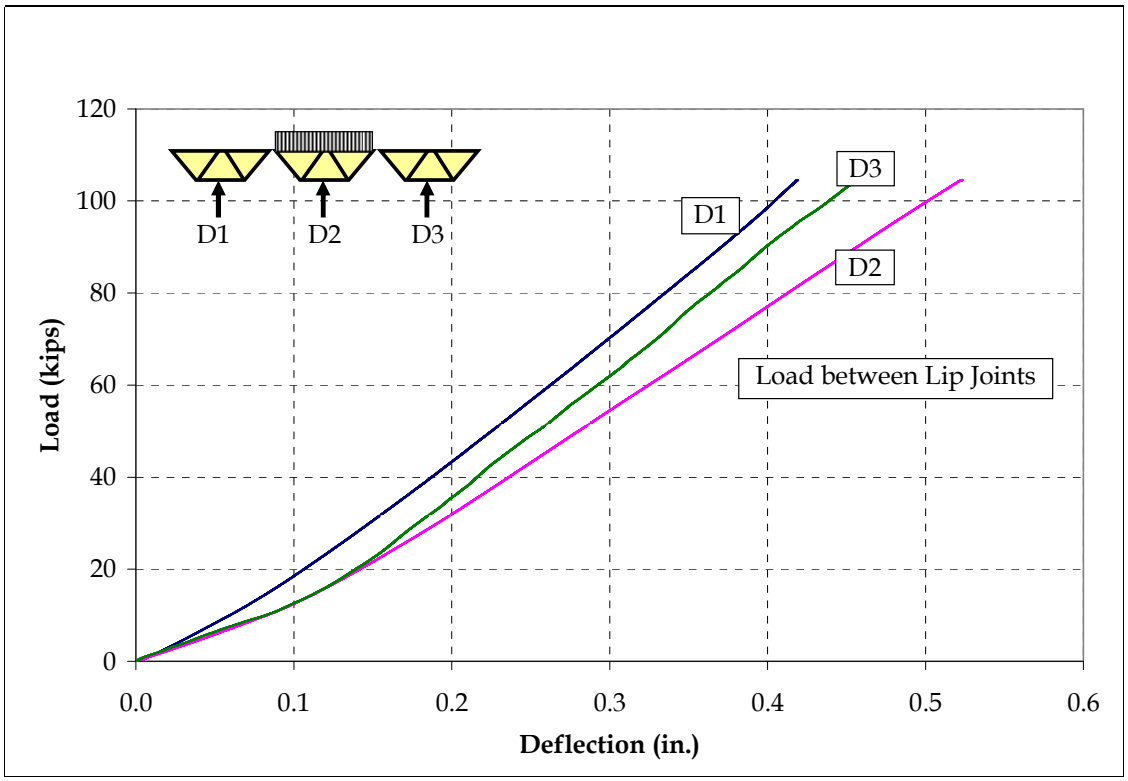

Figure 2.51 Load-Deflection Responses for Residual Strength Test between Lip Joints

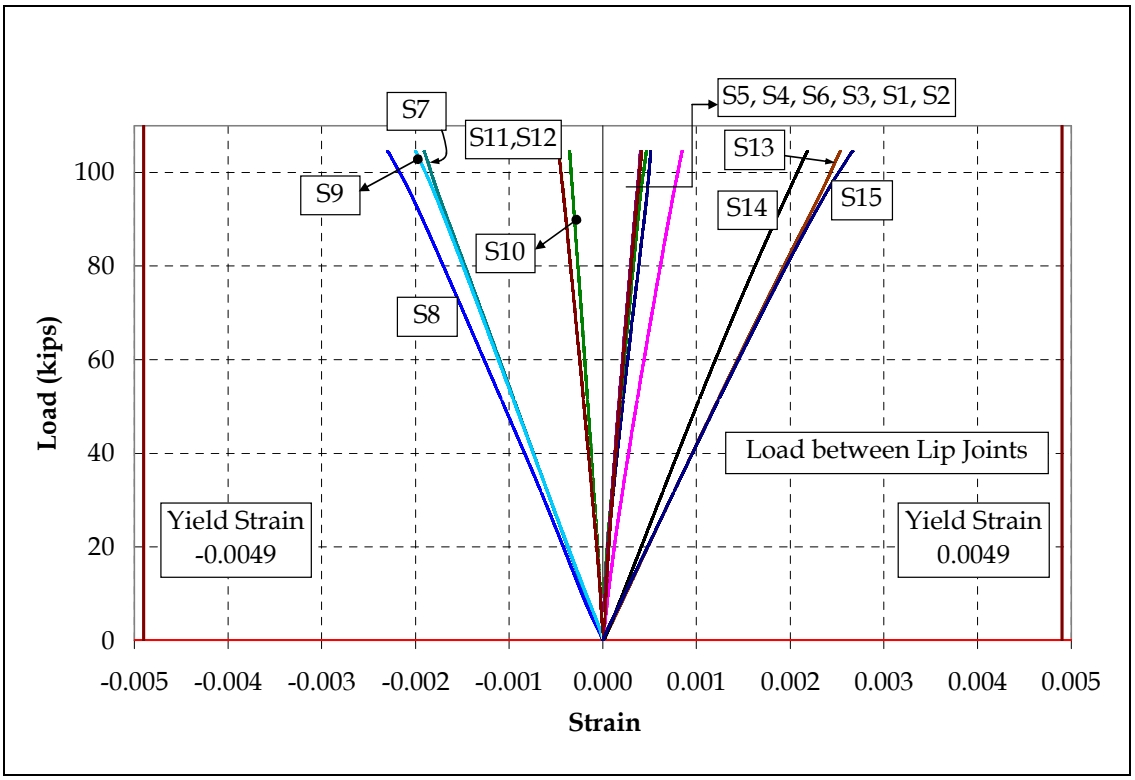

Figure 2.52 Load-Strain Responses for Residual Strength Test between Lip Joints

2.6 Analytical Work

The objective of analytical work was to use elastic and simple plastic analyses to estimate the service deflections and the ultimate load capacity of aluminum decks. The analytical work was first performed on small deck strips and was then expanded to the multi-span, multi-unit deck panels. The analytical work included the following tasks:

1. Determine sectional properties for the deck;
2. Predict the linear elastic stiffness, yielding load, and ultimate strength of the single-span, single-unit deck strip;
3. Predict the linear elastic stiffness, yielding load, and ultimate loading capacity of the two-span continuous, single-unit deck strip;
4. Predict the overall stiffness and ultimate strength of the two-span continuous, three-unit deck panel

In addition, a detailed finite element analysis of the deck was performed.

2.6.1 Sectional Properties for the Analytical Modeling

The geometry of the deck section is shown in Figure 2.53. The sectional properties of the deck are shown in Table 2.2. These properties were calculated from an AutoCAD drawing of the deck section, and are therefore slightly different from the actual properties, as presented in Section 2.3 by the manufacturer. However, this information is necessary for analytical modeling.

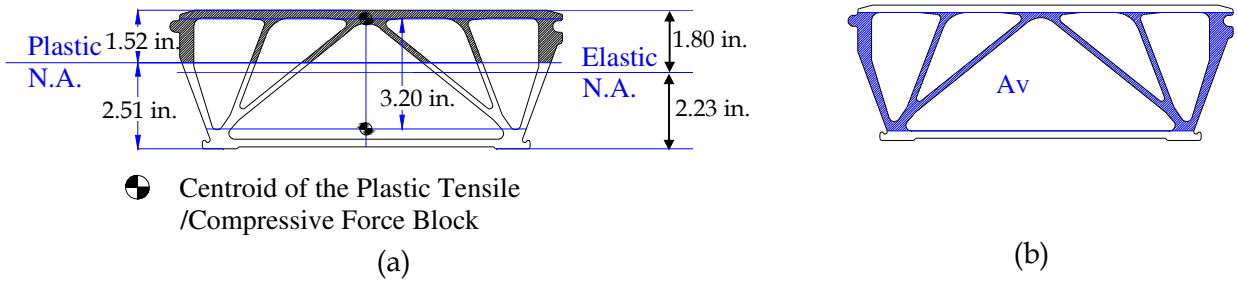

(a) (b)

Figure 2.53 Deck Section: (a) Elastic and Plastic Section Properties, and (b) Shear Resisting Area

Table 2.2 Sectional Properties for Analytical Modeling

Total area	A = 10.23 in^2.
Area resisting shear	A_V = 5.71 in^2. (as shown in Figure 2.53b)
Moment of inertia	I_x = 22.61 in^4.
Distances from top and bottom faces to elastic neutral axis	y_{ct} = 1.80 in., y_{cb} = 2.23 in.
Distances from top and bottom faces to plastic neutral axis	y_{cpt} = 1.52 in., y_{cpb} = 2.51 in.
Plastic moment arm	D_p = 3.2 in.

Based on the above properties, the representative sectional moments are illustrated in Figure 2.54. The initial yield moment M_y is calculated as 25.0 kip-ft. Assuming aluminum material as elastic-perfectly plastic, the full plastic moment M_p can be written as

$$M_p = \frac{A}{2} D_p \sigma_y = 39.6 \text{kip} \cdot \text{ft} \tag{2.7}$$

Assuming aluminum material as bilinear plastic, the ultimate moment M_u can be written as:

$$M_u = \frac{A}{2} D_p \sigma_u = 47.5 \text{kip} \cdot \text{ft} \tag{2.8}$$

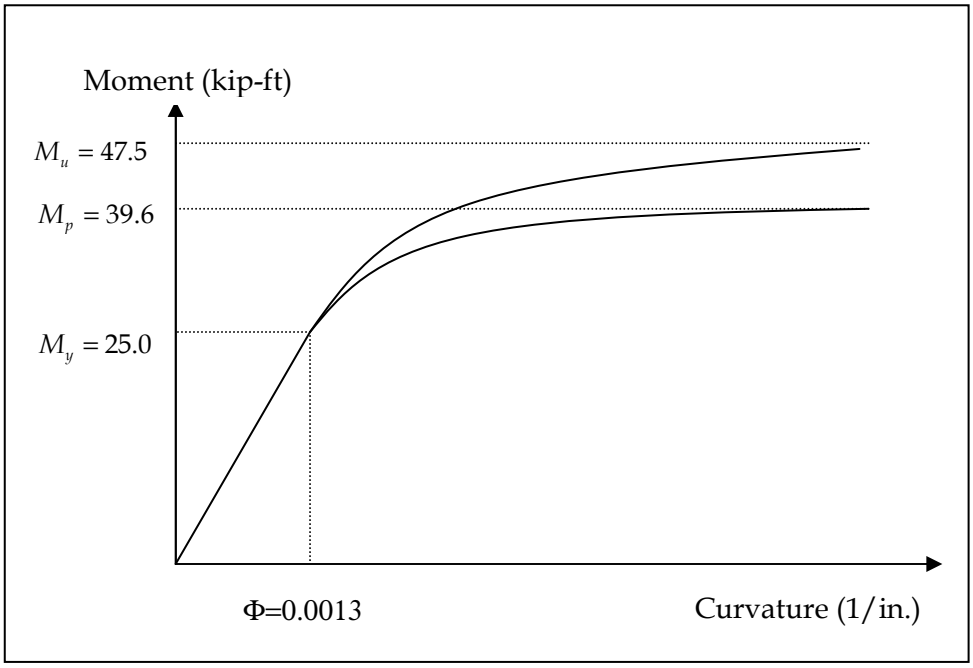

Figure 2.54 Moment-Curvature Responses for Aluminum Deck Section

2.6.2 Analysis of Simple-Span Deck Panel

2.6.2.1 Initial Stiffness

The model of a simply-supported deck strip is shown in Figure 2.55(a). The flexural deflection of the deck can be calculated using an integration method. The deflection under the unit concentrated load shown in Figure 2.55(b) is

$$d\Delta_m = \frac{dP(L-a)}{12EI}(2La - a^2 - \frac{L^2}{4}) \quad \text{When a>L/2, and } dP = \frac{P}{20\text{in}} da \tag{2.9}$$

(a) (b)

Figure 2.55 Simplified Loading Configuration: (a) Distributed load Model, and (b) Unit Concentrated load Model

The deflection at mid-span under the 20 in. distributed wheel load can be calculated by integrating the differential displacements in Eq. (2.9) as:

$$\Delta_{md} = 2\int_{24}^{34} d\Delta_m \tag{2.10}$$

The flexural stiffness is therefore

$$K_f = \frac{P}{\Delta_{md}} = 108 \text{ kip/in} \tag{2.11}$$

Similarly, the deflection due to shear deformations can be calculated using virtual work as:

$$\Delta_V = \int_0^L \frac{k(vV)}{GA_V} dx = \frac{k}{GA_V}\left(\frac{1}{2}P\frac{L}{2}\frac{1}{2} + \frac{1}{2}P\frac{L}{2}\frac{1}{2}\right) = P\frac{k}{GA_V}\frac{L}{4} \tag{2.12}$$

where A_V is the effective area to resist shear force, as shown in Table 2.2, V is the actual shear force, v is the virtual shear force due to unit load, G is the shear modulus of the section, calculated as $E/(2(1+\upsilon))$, and k is the shape factor, assumed as 1.0. The shear stiffness is therefore

$$K_V = \frac{P}{\Delta_V} = 4\frac{GA_V}{kL} = 1{,}862 \text{kip/in} \tag{2.13}$$

The overall stiffness of the simply-supported, single-unit deck strip can be calculated using a parallel combination rule based on the results of Eq. (2.11) and Eq. (2.13) as:

$$K = \frac{1}{\frac{1}{K_v} + \frac{1}{K_f}} = 102.1 \text{ kip/in} \tag{2.14}$$

2.6.2.2 Plastic Load Capacity

The moment diagram at plastic failure is shown in Figure 2.56.

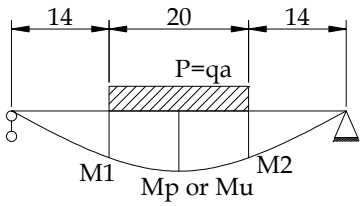

Figure 2.56 Moment Diagram at Plastic Failure

The applied load can be estimated based on the moment at the edge of the wheel loading region, M_1, as:

$$P = V = 2(M_1)/b \tag{2.15}$$

The relation between M_1 and the moment at mid-span is

$$M_p - M_1 = \frac{1}{8}Pa \tag{2.16}$$

Based on Eq. (2.15) and Eq. (2.16), the loading may be calculated as

$$P = \frac{2M_p}{b + a/4} = 50 \text{ kips} \tag{2.17}$$

Using the same method, but assuming the moment at the mid-span is M_u, the ultimate load capacity becomes:

$$P_2 = \frac{2M_u}{b + a/4} = 60 \text{ kips} \tag{2.18}$$

The estimated load capacities are summarized in Table 2.3.

Table 2.3 Load Capacity for Simple-Span Deck

Load Label	**Mid-Span Moment**	**Estimate Load (kips)**
P_1	M_p	50
P_2	M_u	60

2.6.3 Analysis of Two-Span Continuous Deck Panel

2.6.3.1 Initial Stiffness

The simplified load model of the two-span continuous, single-unit deck panel is shown in Figure 2.57(a). The flexural deflection can be calculated using a similar method as that for the simple-span panel. The unit concentrated load model with the appropriate boundary condition is shown in Figure 2.57(b), and the deflection along the beam length is:

$$d\Delta_{m1} = \frac{dP(L-a)^2}{24EIL^2}\left(\frac{11}{4}aL^2 - \frac{L^3}{2}\right) \quad \text{When a>L/2, or}$$

$$d\Delta_{m2} = \frac{dPa}{48EIL}\left(\frac{3L^3}{2} - \frac{5}{2}a^2L\right) \quad \text{When a<L/2, in which } dP = \frac{P}{20in}da \tag{2.19}$$

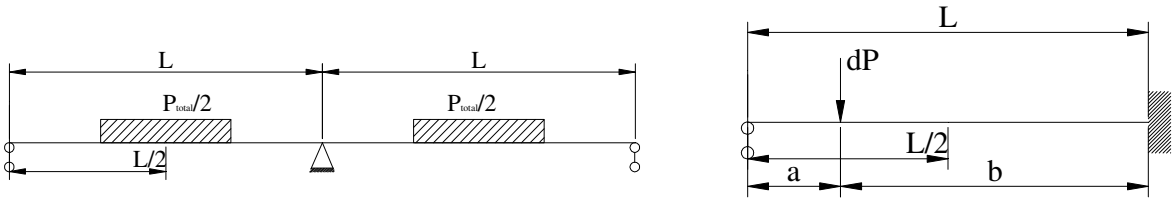

(a) (b)

Figure 2.57 Simplified Loading Model: (a) Distributed Load Model, (b) Unit Concentrated Load Model

The flexural deflection at the mid-span under the 20 in. wide distributed wheel load can be calculated as:

$$\Delta_{md} = \int_{24}^{34} d\Delta_{m1} + \int_{14}^{24} d\Delta_{m2} \tag{2.20}$$

Thus, the flexural stiffness is:

$$K_f = \frac{P_{total}}{\Delta_{md}} = 508 \text{ kip/in. where } P_{total} = 2P \tag{2.21}$$

The mid-span deflection due to shear deformations can be obtained using the virtual work method, as:

$$\Delta_V = \int_0^L \frac{k(vV)}{GA}dx = \frac{k}{GA_V}\left(\frac{5}{16}\frac{P_{total}}{2}\frac{L}{2}\frac{5}{16} + \frac{11}{16}\frac{P_{total}}{2}\frac{L}{2}\frac{11}{16}\right) = P_{total}\frac{k}{GA_V}\frac{L}{7.01} \tag{2.22}$$

Assuming k = 1.0, and G and A_V are as stated previously, the shear stiffness can be calculated as:

$$K_V = \frac{P_{total}}{\Delta_V} = 7.01\frac{GA_V}{kL} = 3{,}263 \text{ kip/in} \tag{2.23}$$

The overall stiffness of the two-span continuous, single-unit deck strip can then be determined using the parallel rule based on results of Eq. (2.20) and Eq. (2.22), as:

$$K = \frac{1}{\frac{1}{K_v} + \frac{1}{K_f}} = 440 \text{ kip/in} \tag{2.24}$$

2.6.3.2 Plastic Load Capacity

The moment diagram under the distributed loads for the plastic failure scenario is shown in Figure 2.58.

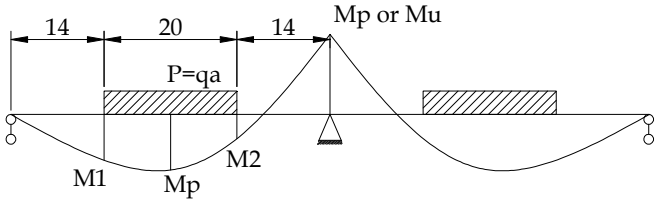

Figure 2.58 Moment Diagram at the Plastic Failure Stage

Since the shear force equals the slope of the moment diagram, the loading on the left span can be estimated as the summation of the left and right shear forces, given by

$$P = V = (M_1)/L_1 + (M_2 + M_p)/L_1 = (M_p + M_1 + M_2)/L_1 \tag{2.25}$$

The relation between the moment at the loading edge and at the middle span is given as:

$$M_p - \frac{1}{2}(M_1 + M_2) = \frac{1}{8}Pa \tag{2.26}$$

Solving $(M_1 + M_2)$ in Eq. (2.26) and then substituting into Eq. (2.25), the loading can then be determined as:

$$P = \frac{3M_p}{L_1 + a/4} = \frac{M_p}{6.33in} = 75 \text{ kips} \tag{2.27}$$

Thus, the first fully plastic loading on both spans becomes

$$P_1 = 2P = 150 \text{ kips} \tag{2.28}$$

If the positive moment reaches M_P, while the negative moment reaches M_u, then Eq. (2.25) becomes:

$$P = \frac{M_u + 2M_p}{L_1 + a/4} \tag{2.29}$$

The second fully plastic force can then be calculated based on Eq. (2.29) and Eq. (2.26), as:

$$P_2 = 2P = 160 \text{ kips} \tag{2.30}$$

If the positive and negative moments both reach M_u, then Eq. (2.25) becomes:

$$P = \frac{3M_u}{L_1 + a/4} \tag{2.31}$$

and Eq. (2.26) becomes:

$$M_u - \frac{1}{2}(M_1 + M_2) = \frac{1}{8}Pa \tag{2.32}$$

Using Eq. (2.31) and Eq. (2.32), the loading then can be determined as:

$$P = 90 \text{ kips}$$

$$P_3 = 2P = 180 \text{ kips} \tag{2.33}$$

A summary of all estimated loading capacities for two-span decks are presented in Table 2.4.

Table 2.4 Load Capacity for Two-Span Deck

Load Label	**Inner Support Moment**	**Mid-span Moment**	**Estimate Load (kips)**
P_1	M_p	M_p	150
P_2	M_u	M_p	160
P_3	M_u	M_u	180

2.6.4 Analysis of Two-Span Continuous Three-Units Deck System

2.6.4.1 Stiffness of the Deck Joint

The expansion of the analytical work from the single-unit deck strip to multiple-unit deck panel requires information about the stiffness and strength of the connections between the panels, which in this case implies the stiffness and strength of the lip joint. The experimental results on a 12 in. long lip were shown in Section 2.5.4. The joint stiffness was 105 kip/in. for a 12 in. long lip, and the ultimate load capacity was more than 70 kips.

2.6.4.2 Initial Stiffness of the Two-Span Continuous Three-Unit Deck System

It is assumed that the flexural stiffness of the 12 in. long deck piece is negligible, and it is in series with the two side panels. The stiffness contribution of the side panel can be calculated

assuming that the lip and the deck itself are connected in parallel. The equivalent stiffness k_0 of the 12 in. long lip at one side is then determined as:

$$2\frac{k_0 K_1}{k_0 + K_1} = 105\text{kip/in} \tag{2.34}$$

where K_1 estimated as 102 kip/in. is the stiffness of the single-span, single-unit deck strip. From Eq. (2.34), k_0 is calculated as 108 kip/in. For the two-span continuous, three-unit deck panel, the total stiffness of the 96 in. long lip (2 spans) at one side is estimated as $8k_0$=864 kip/in., whereas the stiffness of two-span continuous, single-unit deck panel is estimated as $K_2 = 440$ kip/in. Using the same concept as that of Eq. (2.34), the stiffness of the three-unit panel can be estimated as:

$$2\frac{8k_0 K_2}{8k_0 + K_2} + K_2 = 1{,}023 \text{ kip/in} \tag{2.35}$$

For the loading range from 1 kip to 18 kip, the net deflection is then estimated as 0.033 in. for each span.

2.6.4.3 Ultimate Load Capacity of Two-Span Three-Unit Deck System

Case A: Load on only one span and on the lip

As the three panels were clamped to the stringers, the chance for the lip to open is very small. Also, as the loading is only applied on one span, the failure load of the three-unit deck was estimated based on the one-span, one-unit deck strip. The estimated load capacity is 70kip*2*0.9*0.9=113.4kip. The first 0.9 factor accounts for the different moment distribution, while the second 0.9 factor accounts for the negative influence of rotation. The additional factor of 2 implies that only two panels were taken into account, so the estimated load capacity would be on the conservative side.

Case B: Load on only one span and on top of the middle panel

The load capacity under this scenario comes from the middle panel with the help from the side panels through the lips. The load capacity under this loading configuration is estimated as:

$$\text{P=70kip*0.9+70kip*0.9*}\eta\text{*2} \tag{2.36}$$

where η is the participating ratio of the side panel and can be estimated based on the relative stiffness as:

$$\eta = \frac{\dfrac{1}{\dfrac{1}{440\text{kip/in}} + \dfrac{1}{864\text{kip/in}}}}{440\text{kip/in}} = 0.66 \tag{2.37}$$

Therefore, the ultimate load capacity may be estimated as 146.2 kips.

2.6.5 Comparison with the Experiments

The initial stiffness and ultimate load capacity obtained from the experiments are listed in Table 2.5 along with the analytical predictions derived earlier in this section.

Table 2.5 Comparison between Experimental and Analytical Results

Specimen	Results	Experiments	Analysis	Difference
Single-span, single unit	Initial stiffness	90 kip/in.	102.1 kip/in.	13.4%
	Ultimate load	70 kips	60 kip (Max)	-16.7%
Two-span continuous, single unit	Initial stiffness	410 kip/in.	440 kip/in.	7.3%
	Ultimate load	168 kips	180 kip (Max)	7.1%
Two-span continuous, three-unit	Ultimate load (one span loading on lip)	>100 kips	113.4 kips	N/A
	Ultimate load (one span loading on middle)	>100 kips	146 kips	N/A

The table confirms that the elastic and simple plastic analyses may be used to roughly predict the initial stiffness and ultimate load capacity of the single-unit deck strip. The structural properties of the multi-unit deck panel can be estimated based on the single-unit deck properties and the test results of the deck lip joints. The differences between the analytical estimates and experimental results arise from several assumptions, such as the boundary conditions, the shear resisting area of the deck section, and the material properties. More sophisticated finite element models are necessary to simulate the response of the deck system, particularly when there are more complex interactions between the panels due to the lip joints.

2.6.6 Finite Element Analysis

A three-dimensional finite element (FE) model was developed using the general purpose finite element program SAP 2000. Four-noded quadrilateral thin shell elements with in-plane and out-of-plane bending resistance were used to model the top, bottom, vertical and inclined plates of the deck section (CSI Analysis Reference Manual for SAP 2000). Element identification of various cross-sectional components is presented in Figure 2.59.

The mesh size was selected upon a sensitivity analysis of various mesh configurations from coarse to fine, and comparing the results with experimental data. A mesh size of 1 in^2. was finally selected based on the accuracy of results and acceptable computational time demand. The mesh size was smaller near the load to accommodate the accurate size of the load. Uniform shell pressure was used to apply the wheel load of an HS 20 truck on an AASHTO recommended footprint of 20 in. x 10 in. with the 20 in. dimension perpendicular to the direction of traffic. Deflection data was used to check the accuracy of the model.

Data from the residual strength tests showed that the deck response was well within the linear elastic range. Therefore, a simplified linear elastic analysis was performed. An elastic modulus of 10.15×10^6 psi, a Poisson's ratio of 0.33, and a yield strength of 29 ksi were used. A single-unit simple-span model was first developed to check the accuracy of the modeling technique. This model was then expanded to the two-span single-unit model and finally to the two-span three-unit model. Figures 2.60 to 2.63 present the deformed shapes and comparisons of analytical and

experimental load-displacement responses of single-unit simple-span and two-span specimens. The comparisons show close agreements between the FE analysis and the experimental results.

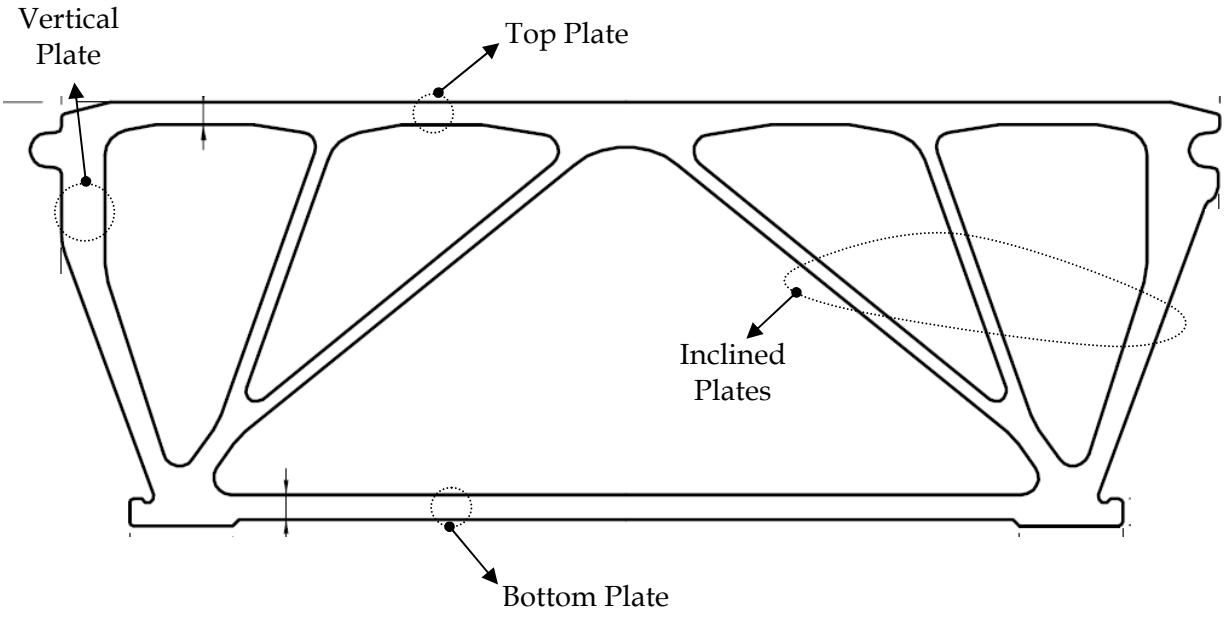

Figure 2.59 Identification of Elements

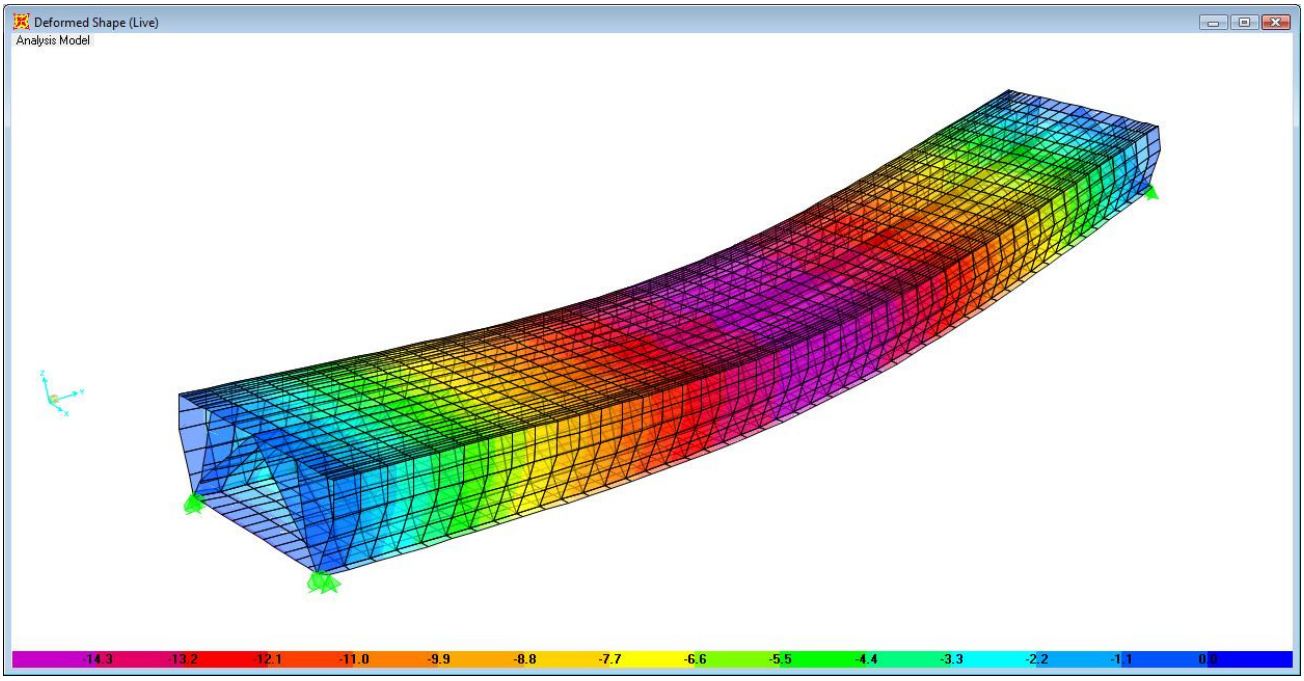

Figure 2.60 Deformed Shape of Simple-Span FE Model

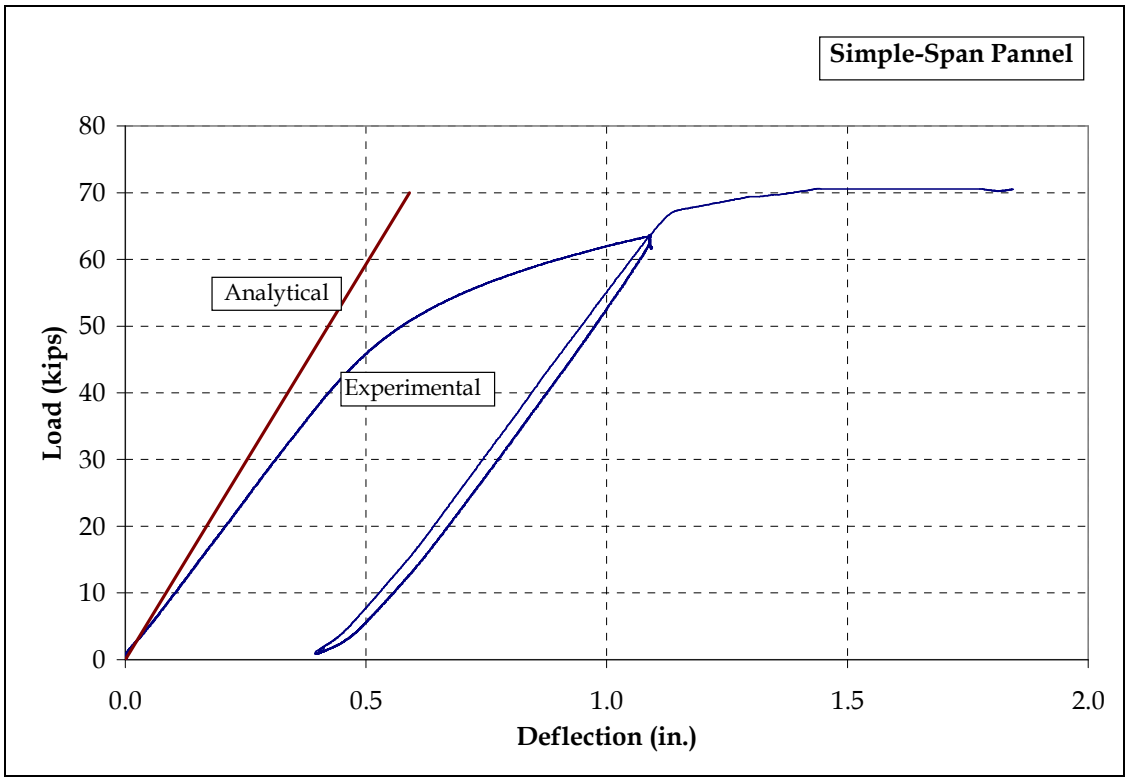

Figure 2.61 Comparison of Load-Deflection Responses from FE Analysis and Experiment

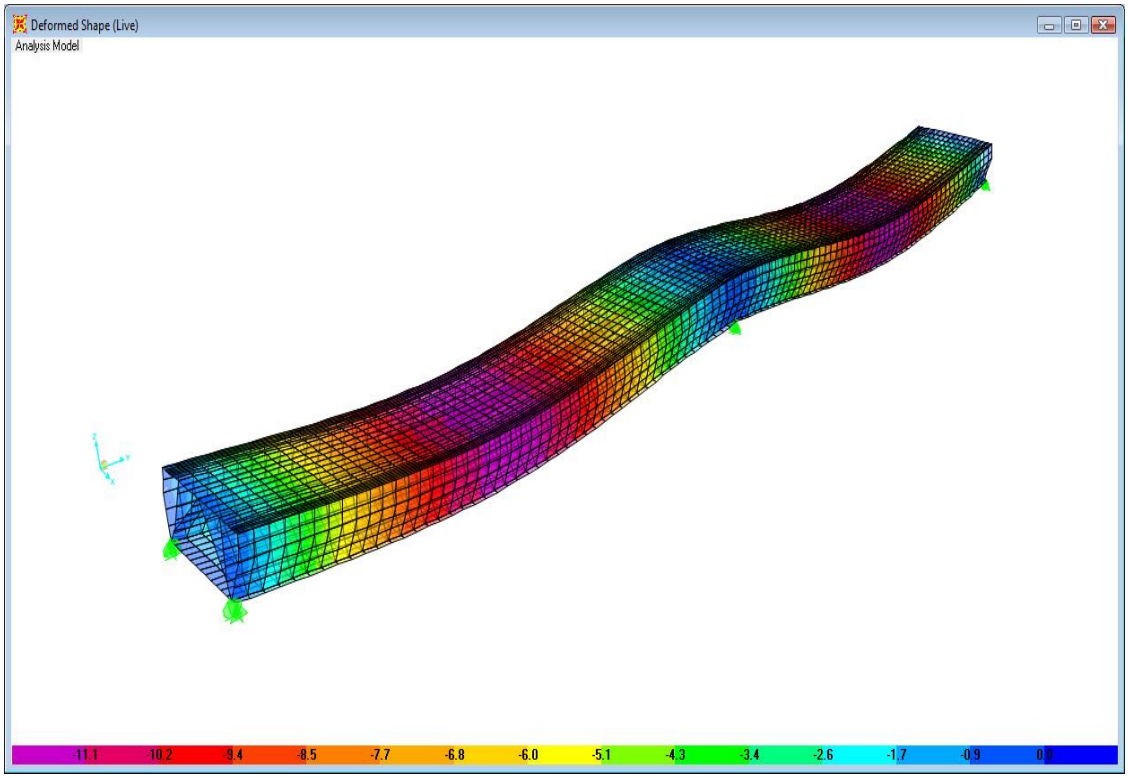

Figure 2.62 Deformed Shape of Two-Span FE Model

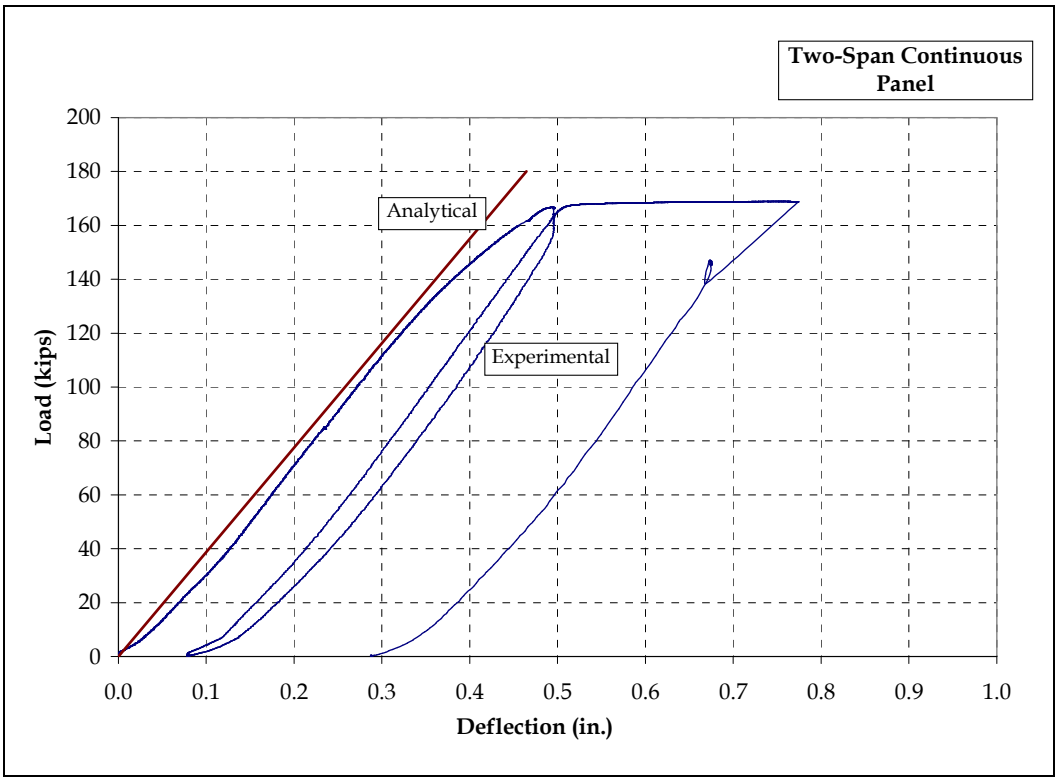

Figure 2.63 Comparison of Load-Deflection Responses from FE Analysis and Experiment

Figure 2.64 shows the deformed shape for the two-span specimen load in both spans. Prior to the fatigue test, the deck panels were loaded up to 18 kips to record the virgin stiffness of the system. Load deflection response from this initial loading is compared with the FE analysis in Figure 2.65.

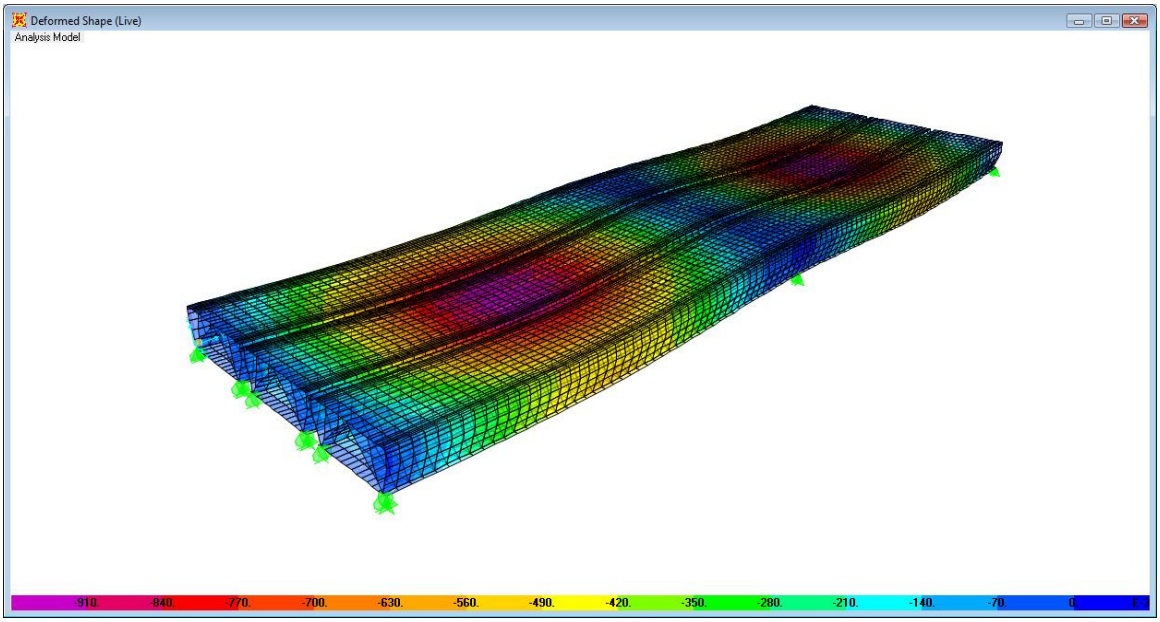

Figure 2.64 Deformed Shape for the Load on Both Panels

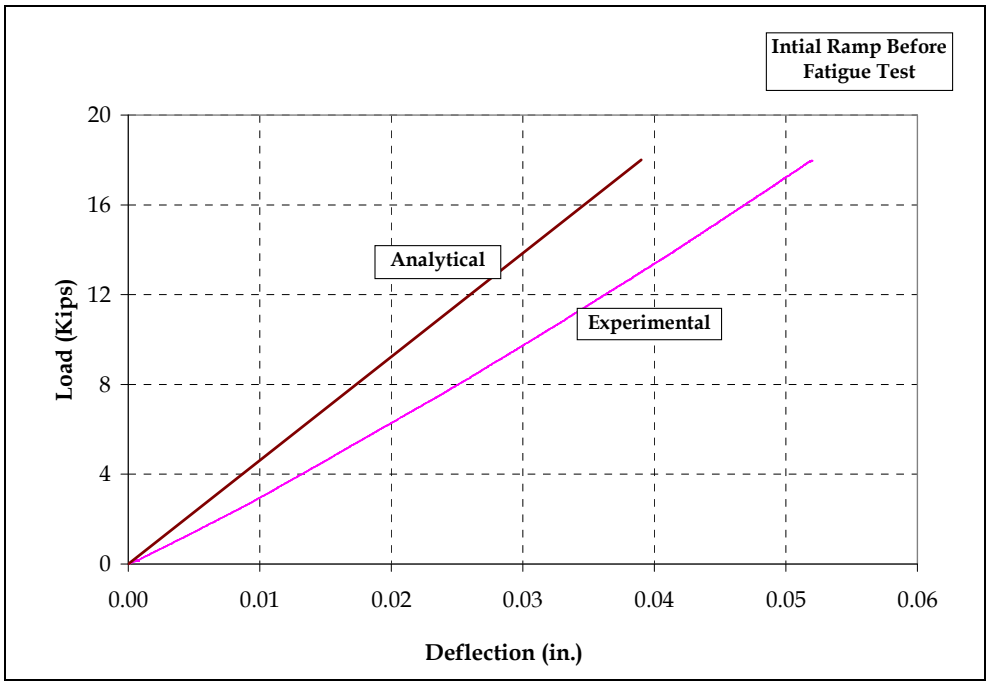

Figure 2.65 Comparison of Load-Deflection Responses from FE Analysis and Experiment

Figures 2.66 and 2.67 present the deformed shape of the full scale FE model for the load on tongue and groove connection, and the center panel, respectively. Figures 2.68 to 2.73 present the comparisons of load-deflection responses from the FE analysis and the two ultimate load tests. The specimens used to perform the ultimate load tests had already been subjected to two (2) million cycles of fatigue loading. The larger discrepancies between the experimental and analytical stifnesses may be due to the fatigue loading, which was not considered in the FE model. However, a smaller discrepancy between the experimental and the analytical stiffnesses was noted even in virgin specimens. This may be attributed to support rotation and seating effects in the experiments, neither of which was accounted for in the FE model.

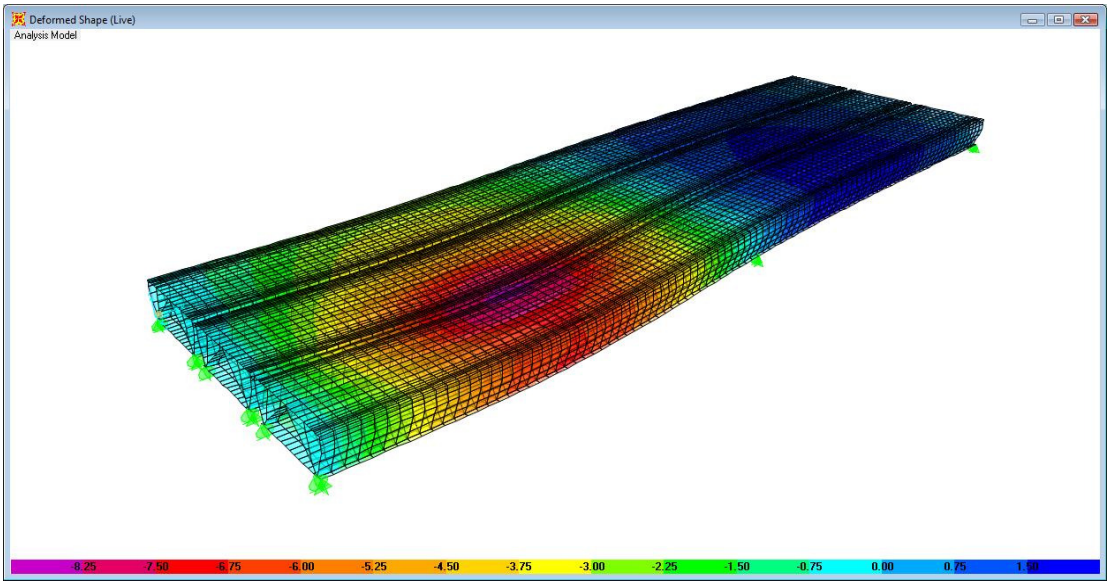

Figure 2.66 Deformed Shape for the Load on Lip Joint

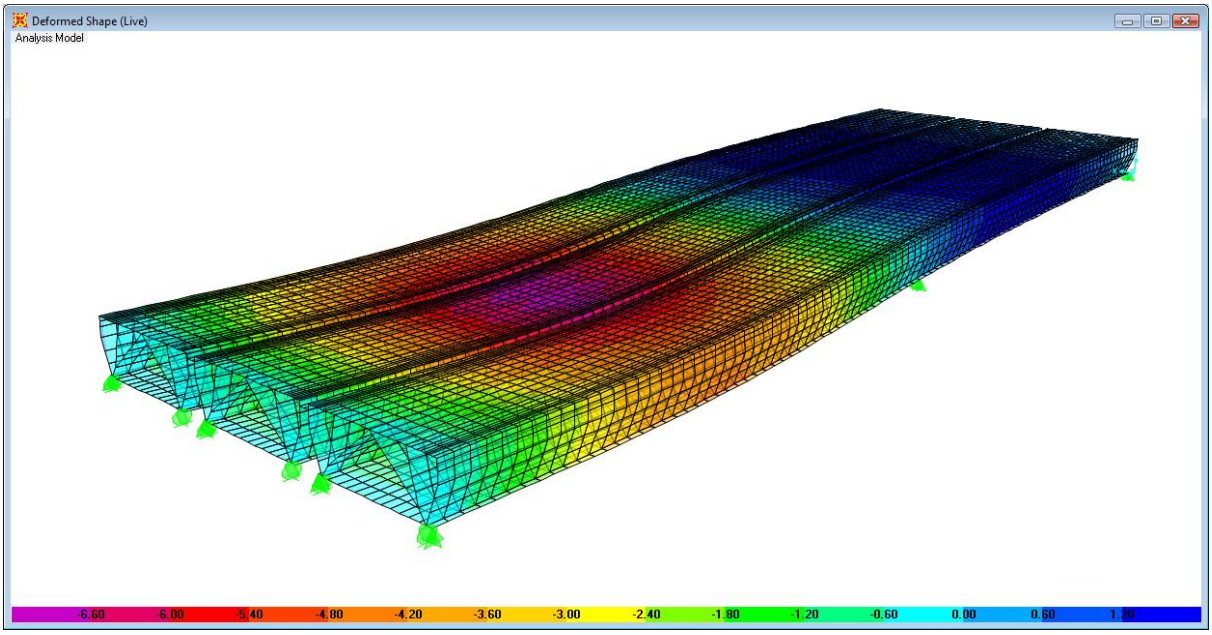

Figure 2.67 Deformed Shape for the Load between Lip Joints

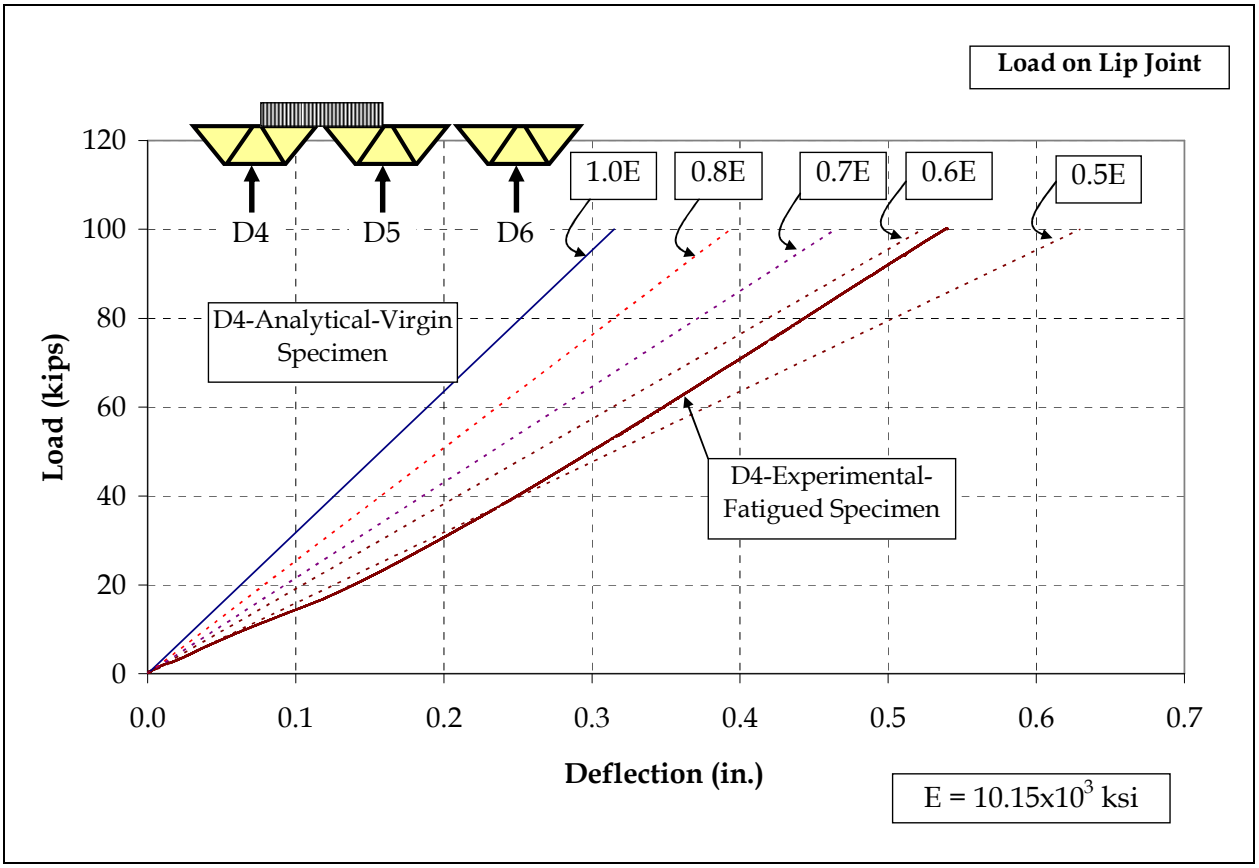

Figure 2.68 Comparison of Analytical and Experimental Load-Deflection Responses

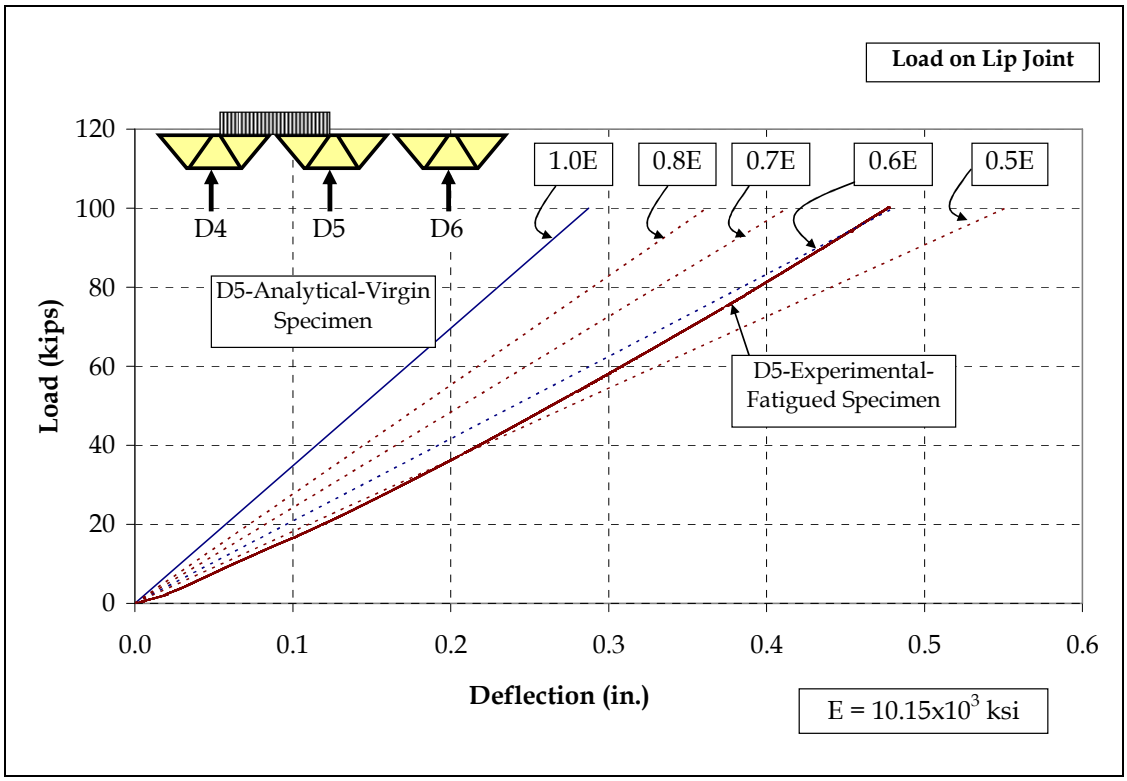

Figure 2.69 Comparison of Analytical and Experimental Load-Deflection Responses

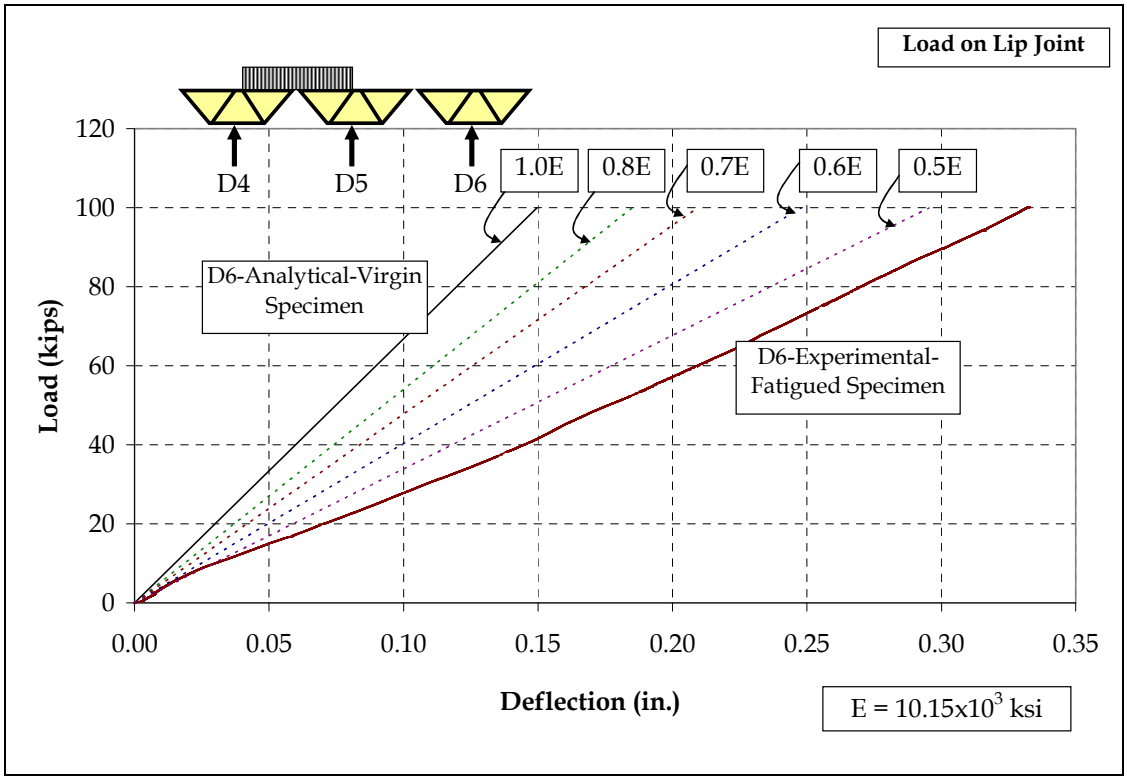

Figure 2.70 Comparison of Analytical and Experimental Load-Deflection Responses

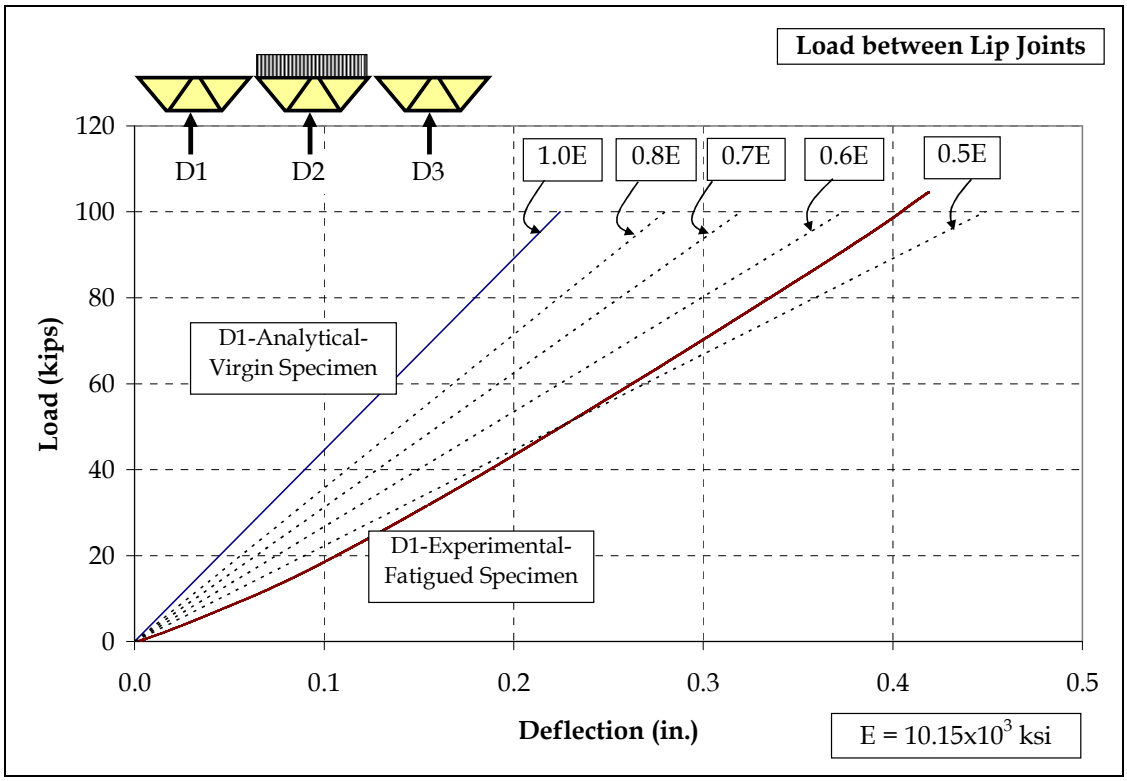

Figure 2.71 Comparison of Analytical and Experimental Load-Deflection Responses

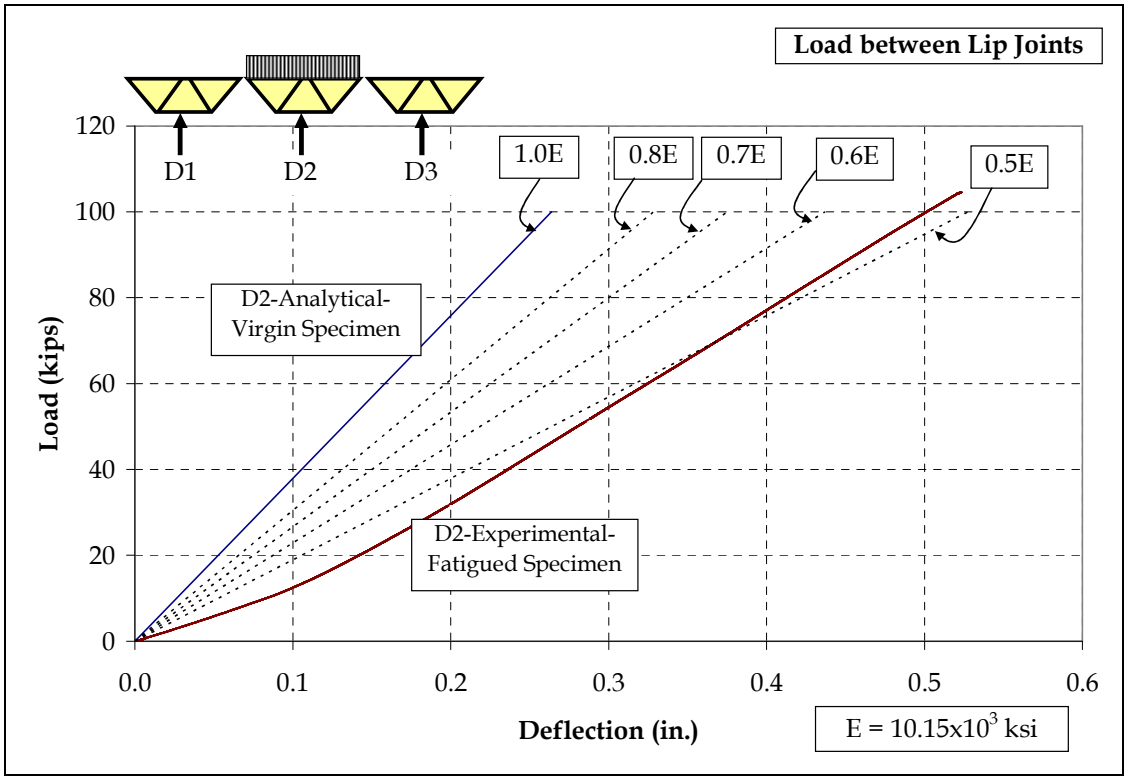

Figure 2.72 Comparison of Analytical and Experimental Load-Deflection Responses

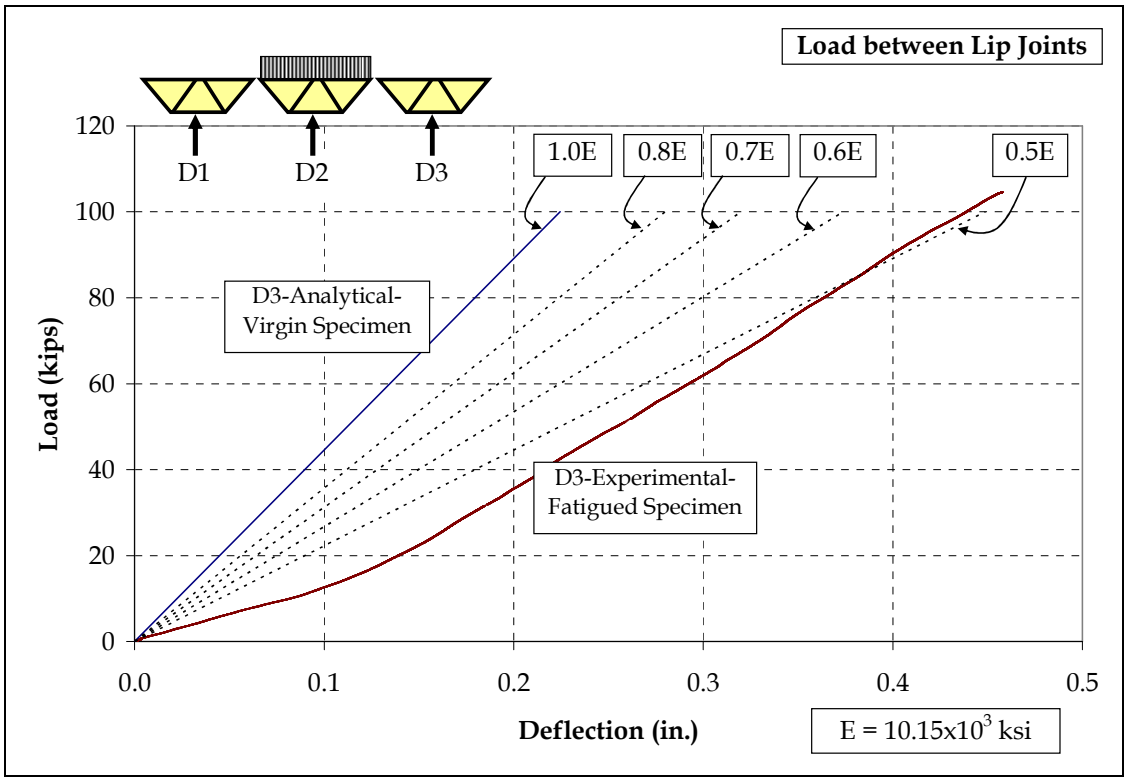

Figure 2.73 Comparison of Analytical and Experimental Load-Deflection Responses

2.7 Conclusions

A detailed experimental and analytical evaluation of SAPA aluminum deck panels led to the following conclusions:

1. SAPA aluminum bridge deck panel is a feasible alternative to the open grid steel decks from both the strength and serviceability points of view.

2. Two million cycles of AASHTO-specified fatigue loading on deck panels did not show any sign of global or local failure in the deck panels. Failure of a bolted connection during the fatigue testing was attributed to the fact that only half of the manufacturer-specified bolted clamps were used in the tests due to the narrow flanges of the stringers.

3. Even though deck panels were loaded up to 100 kips in the two residual strength tests, the extreme fiber stresses remained well within their elastic range.

4. Deck-to-girder connections proved adequate for uplift wind and the braking force, although sudden failure of connections was observed in shear and uplift tests.

5. Elastic and simple plastic analyses may provide adequate estimates for the initial stiffness and ultimate load capacity of aluminum decks.

2.8 Recommendations for Implementation and Future Research

SAPA aluminum deck system has gone through a rigorous set of component, system, and fatigue load testing. It has proven to easily satisfy the AASHTO loading requirements, without being susceptible to fatigue or localized failure modes. While the system is ready for implementation, perhaps even as a test section on an existing bridge deck, the following issues still need to be further investigated:

1. Evaluation of available wearing surfaces, such as Acrydur®, poured mastic asphalt, or Ductal®.
2. Field monitoring of aluminum deck under ambient traffic and designated truck loading.

Chapter-3

SYSTEM 2-Ductal®-MMFX Steel Deck

3.1 Introduction

The schematics of the proposed waffle deck system is shown in Figure 3.1. A transverse strip of the deck acts as a T-beam, and transfers the wheel load to steel girders. The reinforced longitudinal webs help distribute the wheel load to the adjacent transverse deck units. The waffle shape helps make full use of the materials thus achieving high strength with light weight.

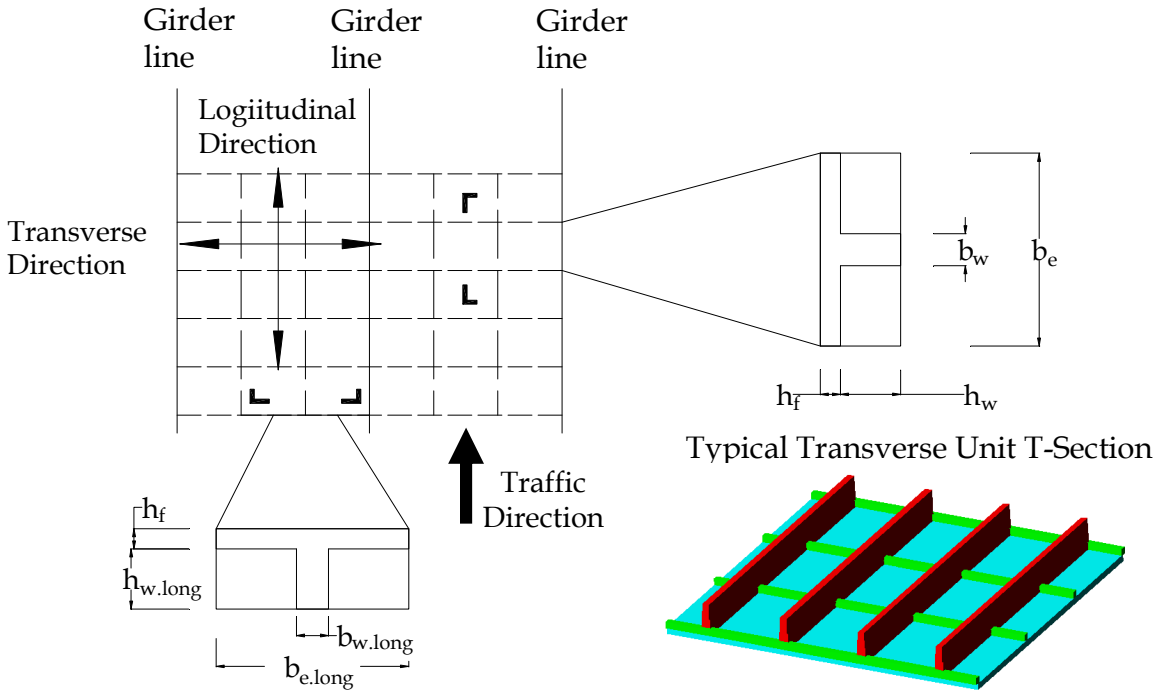

Typical Transverse Unit T-Section

Typical Longitudinal Unit T-Section

3D Deck Model(upside down)

Figure 3.1 Schematics of Proposed Deck System

Due to the limitations on self-weight of the deck, as well as overall depth, ultra-high performance concrete (UHPC) was suggested as an alternative to open grid steel deck. Several UHPC products are available on the market. The most widely used product in the U.S. is Ductal®, which is developed from the joint research of three French companies Bouygues, Lafarge, and Rhodia. The constituent materials of Ductal® include cement, silica fume, ground quartz, sand, metallic fibers, super-plasticizer (third generation), and water. Ductal® products include Ductal®-FM (metallic fibers), Ductal®-AF (additional fiber resistance), and Ductal®-FO

(low strength, architecture purpose) based on application requirements. For this project, Ductal®-FM was used, which included 2% fibers by volume. The high-strength steel fibers have a 0.008 in. diameter and a ½ in. length.

Since the section needs to be very thin, concrete cover for steel reinforcement is a concern. Thinner cover may cause corrosion of reinforcement over time, especially in marine environment. To mitigate the corrosion problem, high-strength steel rebars of MMFX Technologies of Irvine, CA, were used. This project marks the first time that MMFX rebars are used in combination with Ductal®. The dense and uniform UHPC material provides adequate protection for the embedded rebars as well as fairly high bond strength between the two materials.

3.2 Literature Review

3.2.1 Material Properties of UHPC

The unit weight of Ductal® is similar to that of normal concrete (153 lb/ft^3). Its thermal coefficient is 0.00000655/°F. The most distinguishing characteristic of Ductal® is the lack of coarse aggregate, the use of fibers, and the low water/cement ratio. The use of only fine sand creates a dense matrix with minimal voids, which in turn results in a significant increase in strength. The fibers in the concrete matrix are designed to provide bond at the micro level and control cracking. In turn, they act as micro-reinforcement similar to mild steel reinforcement in conventional reinforced concrete at the macro level (Perry 2003, Harris and Roberts 2005).

Low creep and shrinkage are two important features of Ductal®. Whereas for normal concrete the creep coefficient can reach a value of 4, the coefficient for Ductal® is less than 0.8, and after the application of heat treatment, the value can be as low as 0.2. Because the water/cement ratio is very low, Ductal® does not exhibit any drying shrinkage. AFGC (2002) suggests using a value of 0.00055 if no other information is available for preliminary design. However, with heat treatment, the shrinkage process is concluded at the end of the treatment, and no additional shrinkage occurs ever after.

Ductal® has 4-8 times higher compressive strength than conventional concrete. The compressive tests on Ductal® were conducted on 2¾ in. diameter, 5½ in. long cylinders with heat treatment. Based on the test results on 196 specimens, a mean compressive strength of 33 ksi was reported, indicating a characteristic value of 28 ksi with 95% confidence (AFGC 2002). The modulus of elasticity varied between 8,300 ksi and 8,900 ksi. The compression tests have shown a linear behavior until failure, as seen in Figure 3.2. The presence of fibers can prevent a burst failure. A high loading rate of 150 psi/second was used, as compared to the standard 35 psi/second for normal concrete. The use of higher loading rate was justified by the test results, and will be used in this study as well. The cement paste of Ductal® needs 12-24 hours to fully set. Only two (2) hours after setting, according to Graybeal (2006), the compressive strength of the cylinders in the lab environment can reach 10 ksi. Afterwards, the strength gain slows down.

Tensile strength of Ductal® is characterized by two main phenomena: the first crack strength and the post-crack behavior. While the fiber content has a limited impact on the first crack strength (Chanvillard and Rigaud), it dominates the post-crack behavior by providing the bridging over the micro cracks. Four different tensile tests (flexural prism test, split cylinder test,

direct tension test, and mortar briquette test) were performed by Graybeal (2006), and the best estimation of the first crack strength of Ductal® was 0.9 to 1.7 ksi depending on its curing method. For the post-crack behavior, the 2¾ in. x 2¾ in. x 11 in. prism with a 0.4 in. deep notch was used in the flexural test under concentrated load at the middle to ensure the post-crack response is fully developed at the notch (Chanvillard and Rigaud). The post-crack behavior is then modeled based on crack opening and the strain value.

In addition to the high tensile strength, Ductal® can achieve flexural strengths ranging from 5 to 7.2 ksi based on standard flexural beam tests (Perry and Zakariasen 2003). Ductal® is therefore capable of supporting significant loads well beyond cracking (Figure 3.3).

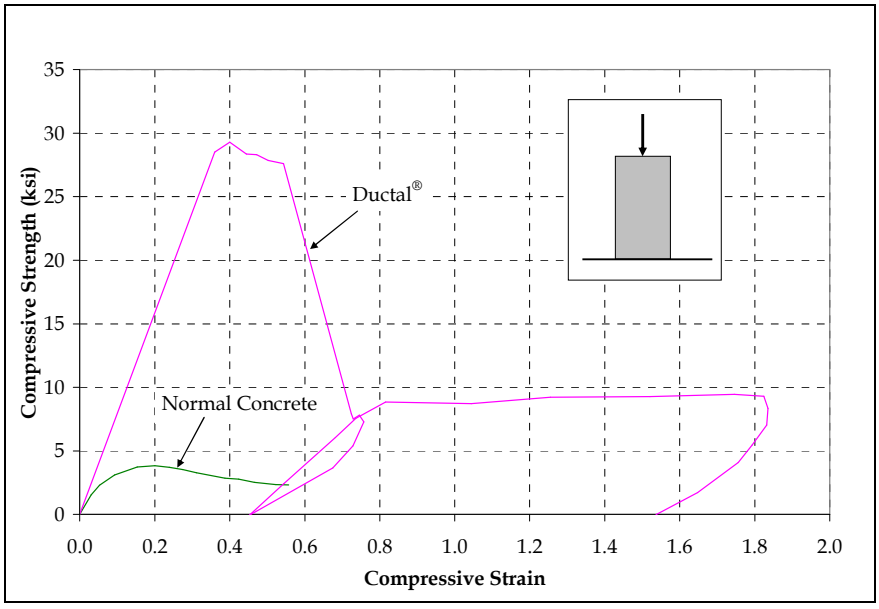

Figure 3.2 Compression Test on Ductal®

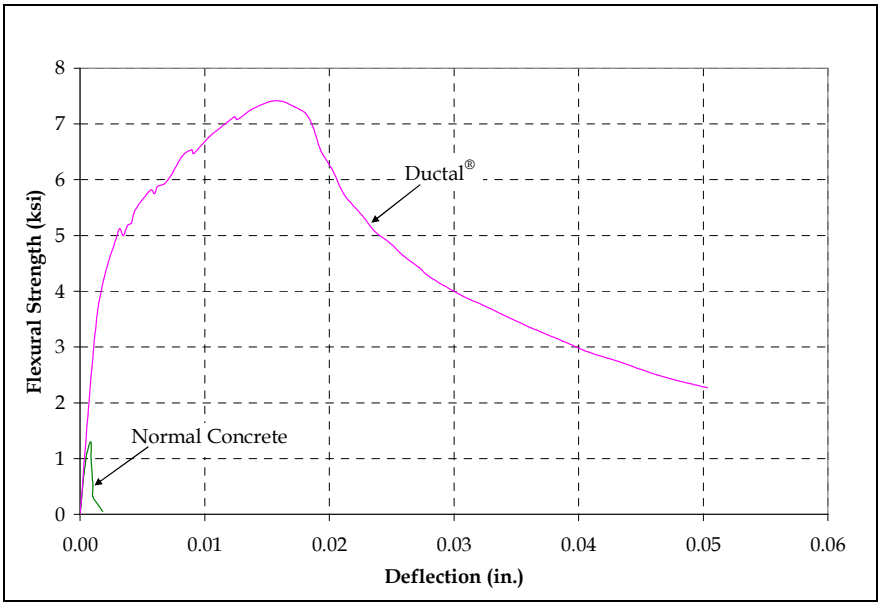

Figure 3.3 Flexural Test on Ductal®

Durability is another key feature of Ductal®. Because the material is relatively new, and that related projects have only existed for a short period of time, the research on durability of Ductal® is mainly through accelerated lab experiments. The crack openings during the strain hardening stage are usually smaller than 0.012 in., which is normally regarded as invisible, due to the existence of 2% steel fibers, representing 1.4 million fibers per cubic feet of concrete. A series of durability tests, including rapid chloride ion penetrability test, chloride penetration test, scaling resistance test, abrasion resistance test, freeze-thaw resistance test, and alkali-silica reaction test, were conducted by Graybeal (2006). Results have confirmed the high durability of Ductal® against both chemical and physical attacks.

3.2.2 Research on UHPC Application in Bridge Decks

Deck systems made of UHPC feature a rapid construction and much better durability over an expected 100-year life span. Although the initial cost of the UHPC deck may be considerably higher, the life-cycle cost is expected to be comparable to the existing cast-in-place concrete deck systems.

Graybeal (2007) proposed a conceptual two-way waffle UHPC deck and performed a design verification based on the simplified material properties. The deck panel is 8 in. thick with ribs spaced at 24 in. in both directions. The thickness of the slab portion is 2½ in., and the minimum width of the ribs is 3 in. The pre-stressing strands used in both directions had a ½ in. diameter.

Perry (2007) developed a precast UHPC bridge deck with no ribs, and implemented it on a bridge at Rainy Lake, near Fort Francis, Ontario, Canada. The deck panels included GFRP rebars on top to prevent corrosion caused by deicing materials. The decks also included mild steel rebars at the bottom where corrosion is not an issue. The total height of the deck is 8-7/8 in. The UHPC was cast on site in the pocket left in the panel to form the composite action between the deck and girders. The 8 in. joint width of two panels in the longitudinal direction was also filled by UHPC to form continuity in the decks.

Toutlemonde (2007) performed a series of fatigue tests on two-way ribbed UHPC decks in Europe. The height of the deck section was 15 in. with the slab portion only 2 in. thick. The width of the ribs was 4 in. at the top and 2¾ in. at the bottom. The height of the ribs was the same in both directions. The length of the deck segment was about 8 ft due to transportation limits. Two pretensioned strands were used in the transverse direction, while post tensioning was applied in the longitudinal direction to assemble the deck segments. The deck joint was filled by casting UHPC on site. The experiment showed the fatigue initiation was consistently associated with a tensile stress larger than the first crack strength. A punching shear failure was observed when using a small load zone. It was found that the mean shear stress along the load surface was close to the tensile strength of UHPC, which justified the design method for punching shear.

Harris and Roberts (2005) reported on punching shear experiments for UHPC decks. Twelve 45 in. x 45 in. slabs with thicknesses as 2 in., 2½ in. and 3 in. were tested with small load zones of 1 in. x 1 in. and 3 in. x 3 in. The modified ACI equation for punching shear provided the best estimation. In addition, three larger slabs were tested by the standard wheel load and no punching shear failure was observed. The analysis, verified by the experiment, suggested a

minimum thickness of 1 in. of the slab to prevent the punching shear failure under the 8 in. x 20 in. wheel load.

3.2.3 Design Guidelines for UHPC

The Australian Code on UHPC published in 2000 was drafted by Gowripalan and Gilbert (2000). It followed Australian Standard for Concrete Structures (AS3600-1994), and provided the design method for prestressed concrete beams made of UHPC.

In 2002, the French code was published by the Association Française de Génie Civil (AFGC) and provided the basis for design guidelines. The code is based on the French 'BPEL' code (BAEL 91 limit state reinforced concrete rules, 1999 revision), and combined with a few elements of the 'BAEL' codes (BPEL 91 limit state prestressed concrete rules, 1999 revision). The French code covers the material properties for service and ultimate limit states design, as well as the design methods for flexure, shear, and torsion.

In 2004, the concrete committee of Japanese Society of Civil Engineers (JSCE) published its recommendations for design and construction of ultra high strength fiber reinforced concrete structures. The code was based on the knowledge and engineering experience gained through the construction of the Sakata-Mirai bridge and also the use of French code as a main reference. The English version of this code was published later (JSCE 2006).

3.2.4 Field Applications of UHPC

In recent years, Ductal® has been used in bridge construction all over the world. Papatoetoe foot bridge in New Zealand, Bridge of Peace in Seoul (foot bridge), Sakata Mirai foot bridge in Japan, and Shepherd Bridge in Sydney with Ductal® girders represent few examples (www.ductal-lafarge.com). Wapello County, IA, with the help of Federal Highway Administration (FHWA), is in the midst of installing UHPC bridge deck panels on a small bridge in the northeast corner of Ottumwa (www.heartlandconnection.com).

3.2.5 Material Properties of MMFX Reinforcement

Microcomposite steel rebar (MMFX) is an uncoated, high-strength, corrosion-resistant rebar made from a low-carbon, chromium alloy steel (America 2007), as shown in Figure 3.4. The typical stress-strain behavior is also shown in Figure 3.4 (Yotakhong 2003). Test results meet the requirement of ASTM A615 Grade 75 (2007) and ASTM A1035 (2006) Grade 100. The bond strength and splice length of MMFX rebar were investigated by El-Hacha et al. (2006). It was reported that MMFX has similar bond behavior with convention concrete as normal carbon steel rebar, but due to its higher strength, longer embedment is needed to fully yield the rebar and thus utilize its high strength.

The MMFX rebar has already been used in field applications. Both Iowa and Kentucky Departments of Transportation have used MMFX rebars as reinforcement in bridge decks. Delaware Department of Transportation considered using MMFX rebars in its I-95 Service Road Bridge 1-712-B in 2005 (Chajes et al. 2005). Florida DOT District 4 has used MMFX rebars in foundations.

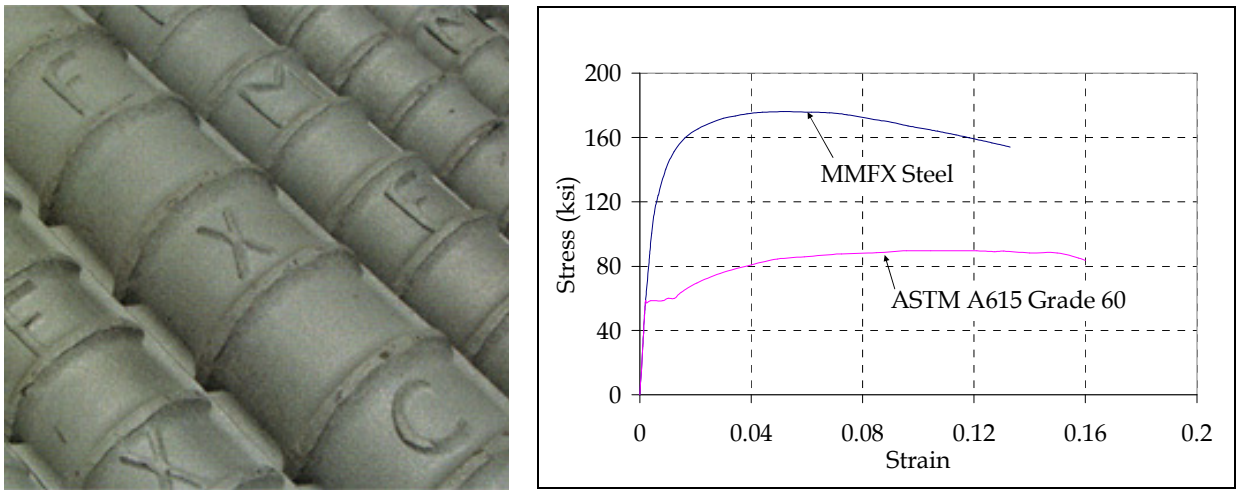

Figure 3.4 MMFX Rebar with Typical Stress-Strain Response
Source: Product Guide on MMFX

3.3 Preliminary Design

The simplified stress-strain relation (Graybeal 2007) was used for the preliminary design for UHPC, as shown in Figure 3.5. An elastic-perfectly plastic model was used for the high-strength MMFX rebar, with a yield strength of 75 ksi.

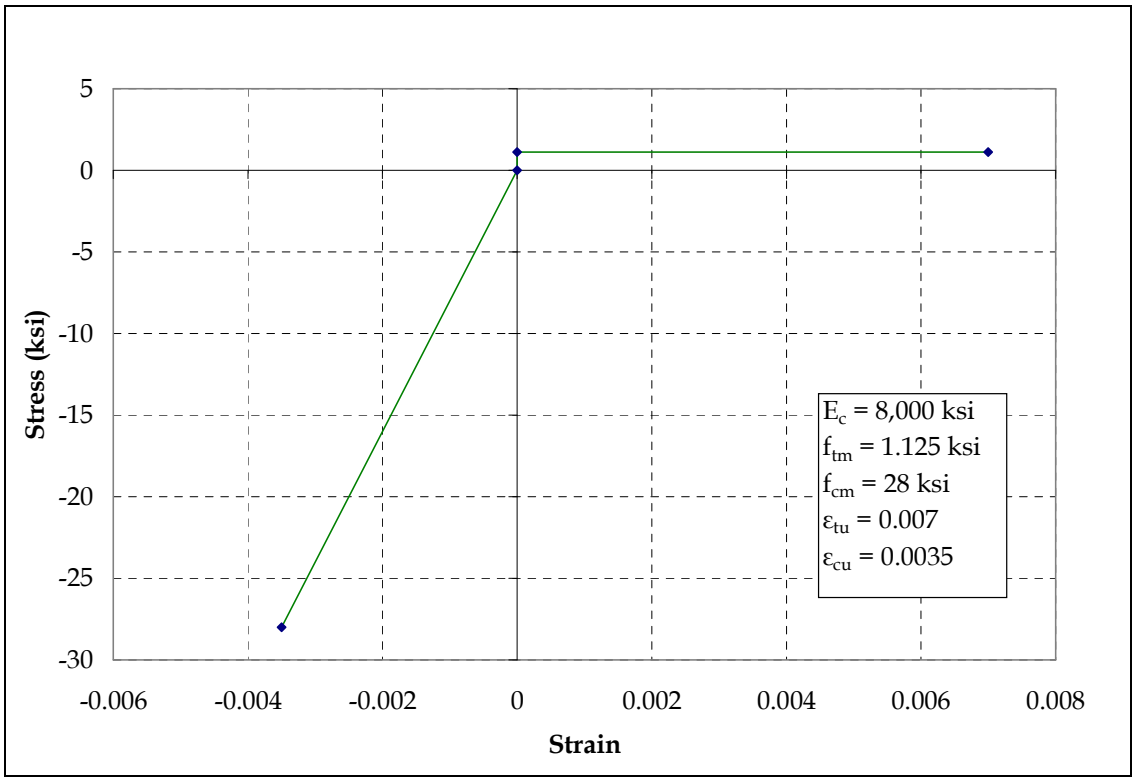

Figure 3.5 Stress-Strain Relation Used in Preliminary Design for UHPC

Figure 3.6 shows the schematics of sectional analysis, assuming that tension steel yields. Two cases are considered, depending on whether the neutral axis is in the flange or in the web. As a design example, consider a section with a flange width b_e of 12 in., web width b_w of 2 in., flange thickness h_f of 1¼ in., overall depth h of 4¾ in., concrete cover of ½ in., and one #6 bar. In this case, the neutral axis would be in the flange, and the moment capacity would be 146 kip-in. This moment capacity corresponds to a 12.2 kips load at the mid-span of 4 ft long span. The compressive strain in concrete turns out to be 0.0016, which is less than half of its crushing strain.

Several sensitivity analyses were carried out to help with sizing of the proposed deck system. Factors considered included reinforcement ratio, and flange width and thickness. Figure 3.7 shows the moment capacity as a function of reinforcement ratio, indicating a linear relation. Figures 3.8 and 3.9 show the moment capacity as a function of flange width and thickness, respectively. In both cases, a nonlinear relationship was observed.

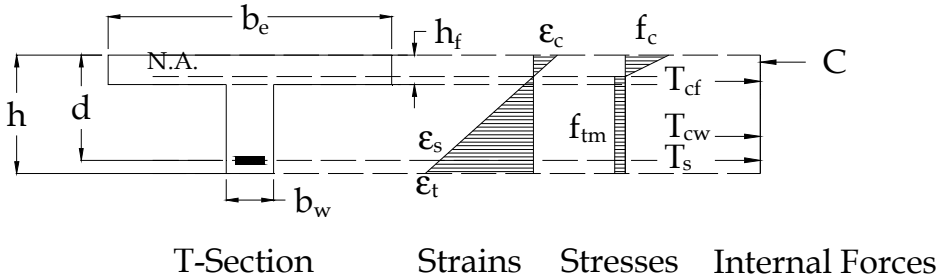

(a) Neutral Axis in the Flange

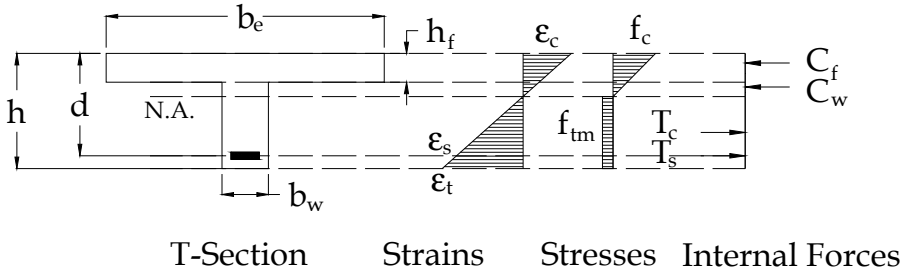

(b) Neutral Axis in the Web

Figure 3.6 Sectional Analysis for Design of Ductal®-MMFX T-Section

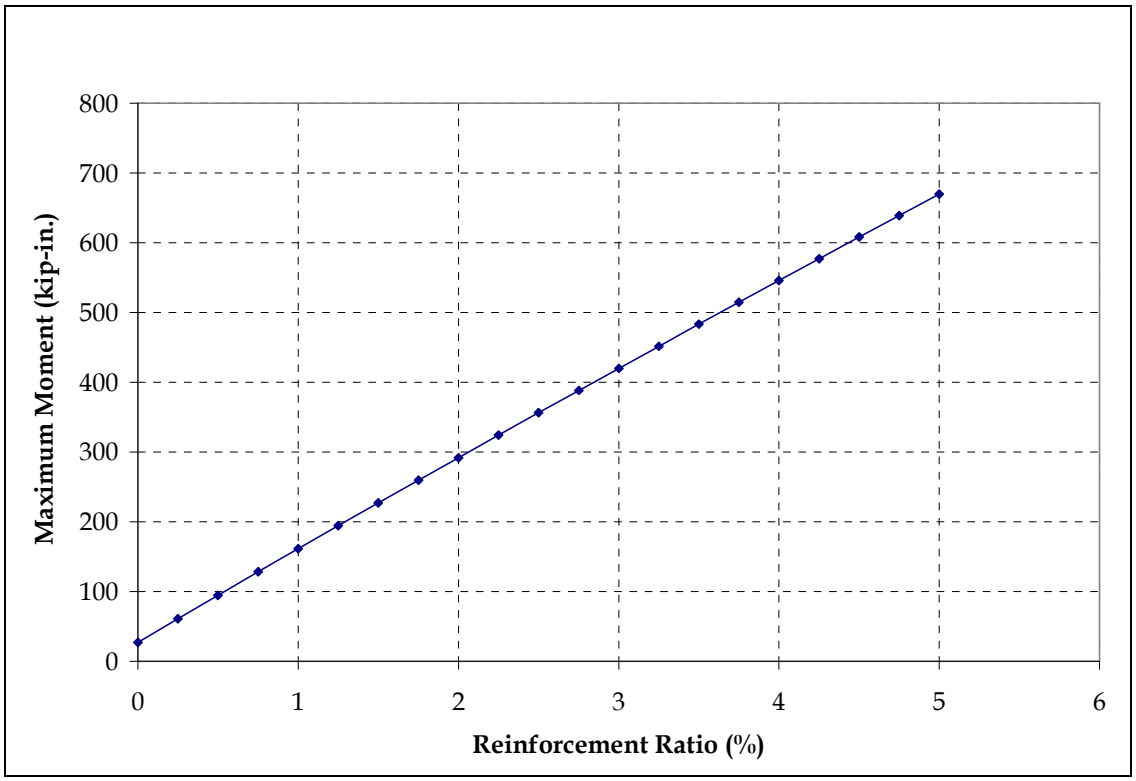

Figure 3.7 Sensitivity Analysis on Reinforcement Ratio

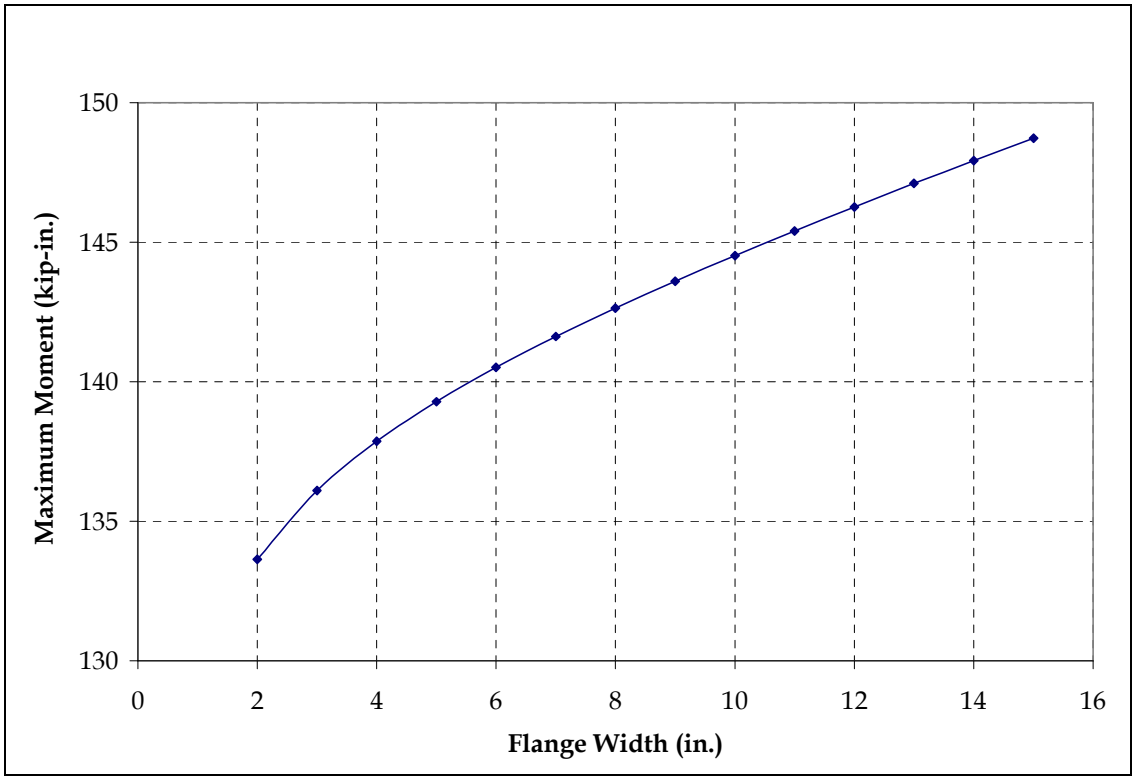

Figure 3.8 Sensitivity Analysis on Flange Width

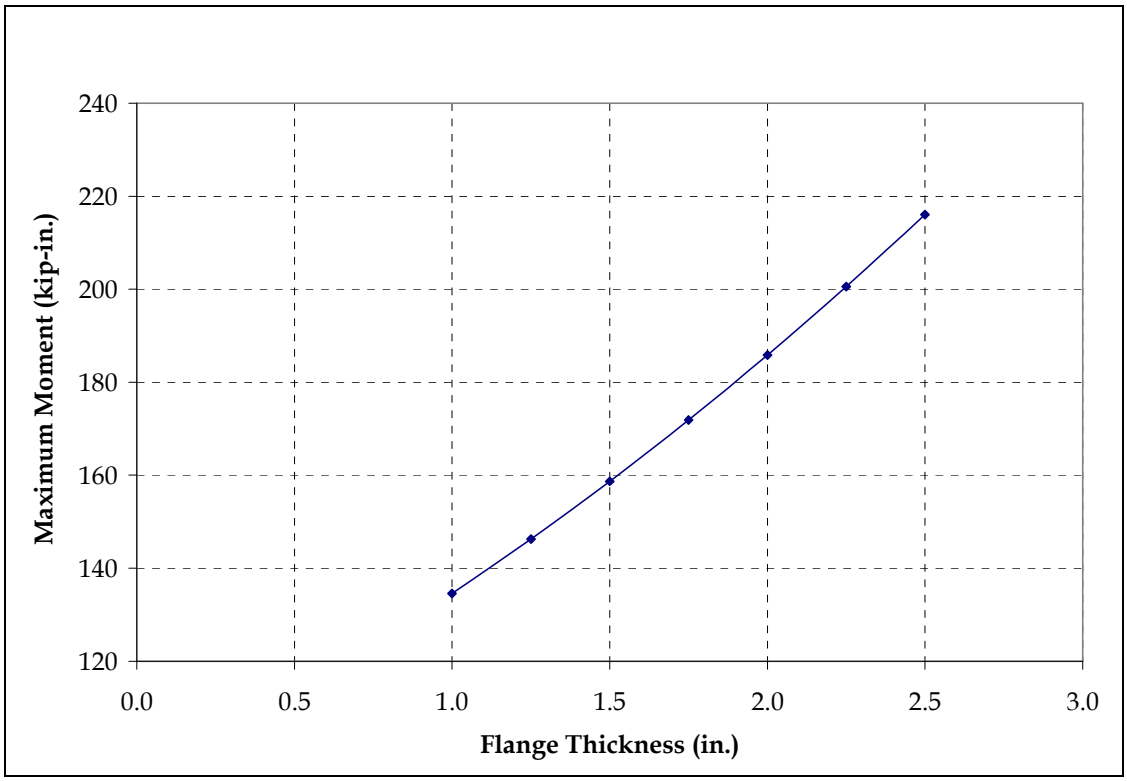

Figure 3.9 Sensitivity Analysis on Flange Thickness

Based on the above discussion, and given the ultra-high compressive strength of Ductal®, the neutral axis is expected to stay within the flange. The preliminary design indicates that the deck can potentially carry an AASHTO wheel load.

The maximum flange thickness is 2 in., given the weight limit of 25 lb/ft². As recommended by Harris (2005), a minimum flange thickness of 1 in. must be maintained to avoid catastrophic punching shear. Moreover, a minimum cover of ½ in. must be maintained to help with the bond between Ductal® and MMFX bars.

Based on the self-weight limit of 25 lb/ft², a series of cross-sections were assessed with different flange width and thickness, as well as rib depth and thickness in both directions. The acceptable ranges of parameters, based on self-weight limits, are as follows:

- Flange width between 6 and 15 in.
- Flange thickness between 1 and 2 in.
- Rib width between 2 and 3 in.
- Rib depth between 3 and 4½ in.

Similarly, corresponding reinforcement was selected based on the rib width. For 2 in. wide ribs, a maximum bar size of #7 provides a minimum cover of ½ in. For 3 in. wide ribs, #8 bars may be used.

Finally, a finite element model was developed to assess the distribution factor for the proposed slab. Figure 3.10 shows the FE model of the proposed slab with five longitudinal ribs and two

transverse ribs. The flange and ribs were modeled using shell elements, whereas truss elements were used for the reinforcement. Perfect bond was assumed between Ductal® and MMFX reinforcement.

Figures 3.11 and 3.12 show the results of FE analysis in terms of maximum deflection as a function of number of ribs and percentage of full service load taken by each rib. The distribution factor appears to be about 36.3%.

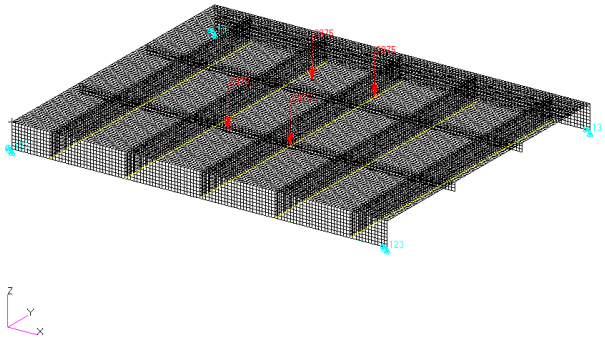

Figure 3.10 FE Model of the Proposed Slab

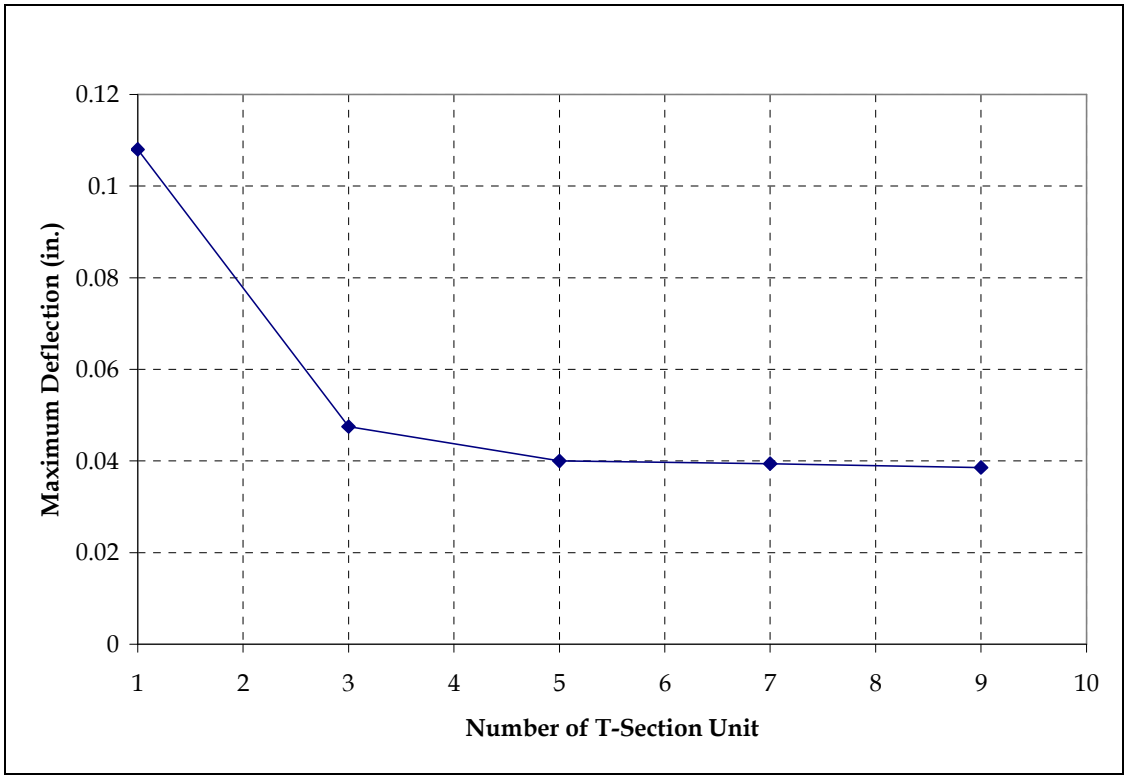

Figure 3.11 FE Analysis Results for Deflections of T-Section Units

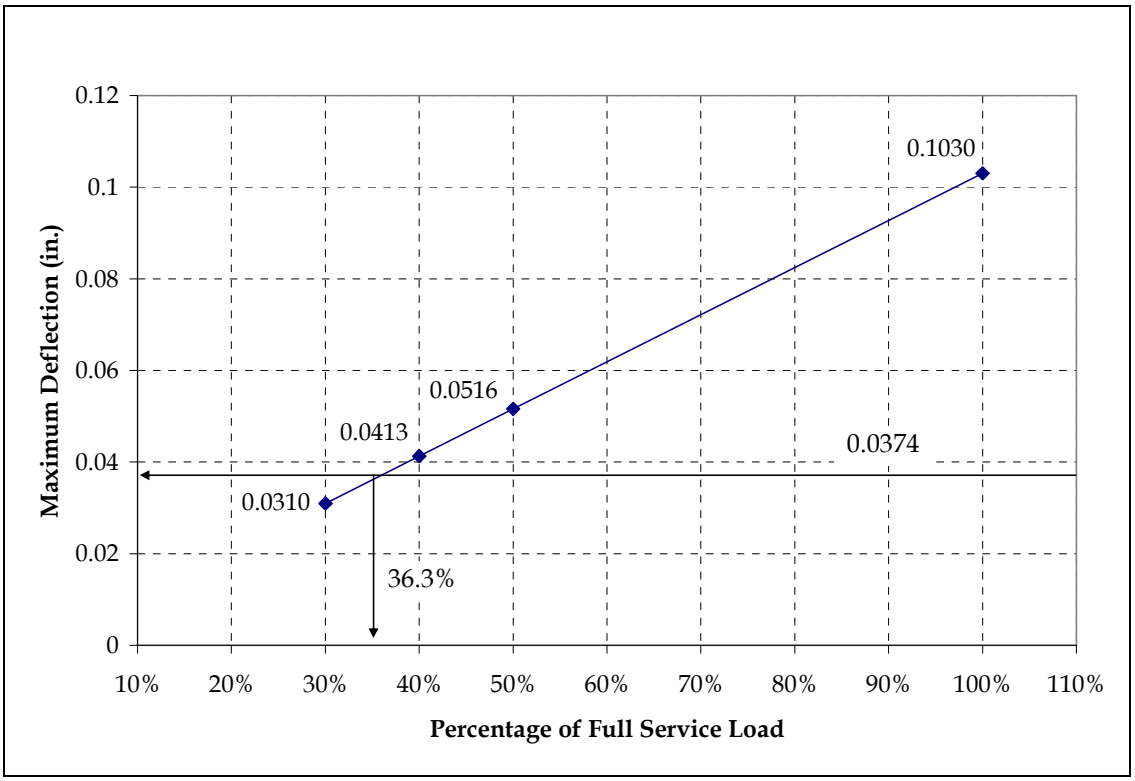

Figure 3.12 FE Analysis Results for Elastic Load Distribution Factor

3.4 Experimental Work

3.4.1 Overview

A comprehensive experimental study was carried out to establish the behavior of Ductal®-MMFX steel decks at service and ultimate load levels. Different configurations of deck profiles were constructed in five separate castings. The same Ductal® mix design was used for all five castings. The constituent materials are listed in Table 3.1.

Table 3.1 Ductal® Constituent Materials

Constituent Materials	Largest Dimension	Mix Design	
		Unit Weight (lb/ft^3)	Percentage by Weight (%)
Cement	0.0006 in.	44.32	28.6
Silica Fume	-	14.36	9.3
Ground Quartz	0.0004 in.	13.11	8.5
Fine Sand	0.006-0.023 in.	63.68	41.1
Metallic Fibers	0.5 in. Long	9.99	6.4
Superplasticizer	--	0.812	0.5
Water	--	8.74	5.6

The mixing of Ductal® requires a high shear mortar mixer with rolling shear pads. The premix, water, super plasticizer, and steel fibers were poured into the mixer in a certain sequence based on the time of mixing and the temperature of the paste. The molds for specimens were initially

made of woods. However, at the later stages of the study solid foam was used instead to form the specimens. The foam panels were cut precisely at the University of Central Florida, and were than glued together to shape the space for the flow of Ductal®. Foam made it easier to control the dimensions as well as the shapes of the specimens. Ductal® is self-compacting and flows well in the molds with limited spaces. No internal or external vibrations were applied during the casting. It was found that the orientation of the fibers tends to align with the formwork (Fehling and Bunje 2008), which causes a non homogenous distribution of the fibers. The uneven distribution was confirmed using electric resistance measurement (Lataste et al. 2008). It was decided to cut the specimens after testing and examine the spatial distribution of fibers, as will be discussed later.

Curing is very important for Ductal® to develop its high strength. The recommended curing is heat treatment at 194°F with 95% humidity for 48 hours, excluding the extra hours for ramping up and down the temperature (AFGC 2002). A 72 hour duration heat treatment curing at 140°F with 95% humidity is suggested by the manufacturer as an alternative. The full strength of Ductal® is assured at the conclusion of the heat treatment. Initially, it was decided to apply the thermal treatment in the lab but the desired temperature could not be achieved. Therefore, it was decided to adopt the regular method of curing instead. The specimens were sealed with plastic sheets for 28 days to prevent the loss of moisture. The strengths achieved without thermal treatment were sufficient to ensure necessary bond strength to yield the MMXF rebar and thus satisfy the ultimate load requirement.

3.4.2 Material Properties Calibration Tests

3.4.2.1 Compressive Strength of Ductal®

Table 3.2 presents the average compressive strengths of concrete for the five castings carried out throughout this project.

Table 3.2 Average Cylinder Strengths for the Five Castings

Casting No.	Date of Casting	28-Day Compressive Strength (ksi)
1	March 26, 2008	28
2	August 5, 2008	26
3	December 23, 2008	27
4	March 6, 2009	22
5	June 19, 2009	27

Based on the strengths of the five castings, it was found that the compressive strength is quite consistent, except for Casting No. 4. The premix used for this casting was older than 6 months. The specimens were not subjected to heat treatment, and therefore, all resulted in lower strengths than those prescribed by the manufacturer.

3.4.2.2 Tensile Properties of Ductal®

Tensile properties of Ductal® were confirmed based on the four-point bending test according to ASTM C1018 Standard Test Method for Flexural Toughness and First-Crack Strength of Fiber-Reinforced Concrete. Load-deflection response for three prisms is shown in Figure 3.13. The prisms were all made from Casting No. 1.

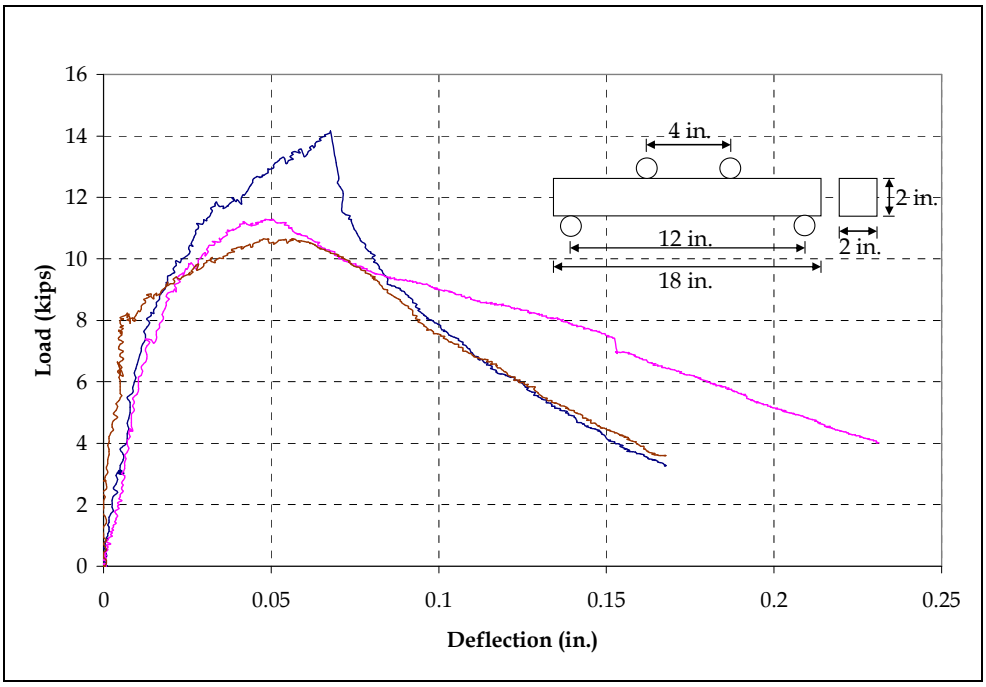

Figure 3.13 Load-Deflection Responses of Prisms

3.4.2.3 Tensile Properties of MMFX Rebar

MMFX bars of size No. 4 and No. 7 were tested using an Instron Universal Testing Machine with 1 in. gauge length extensometers. The stress-strain relation was recorded up to a strain level of 28%, also shown in Figure 3.14.

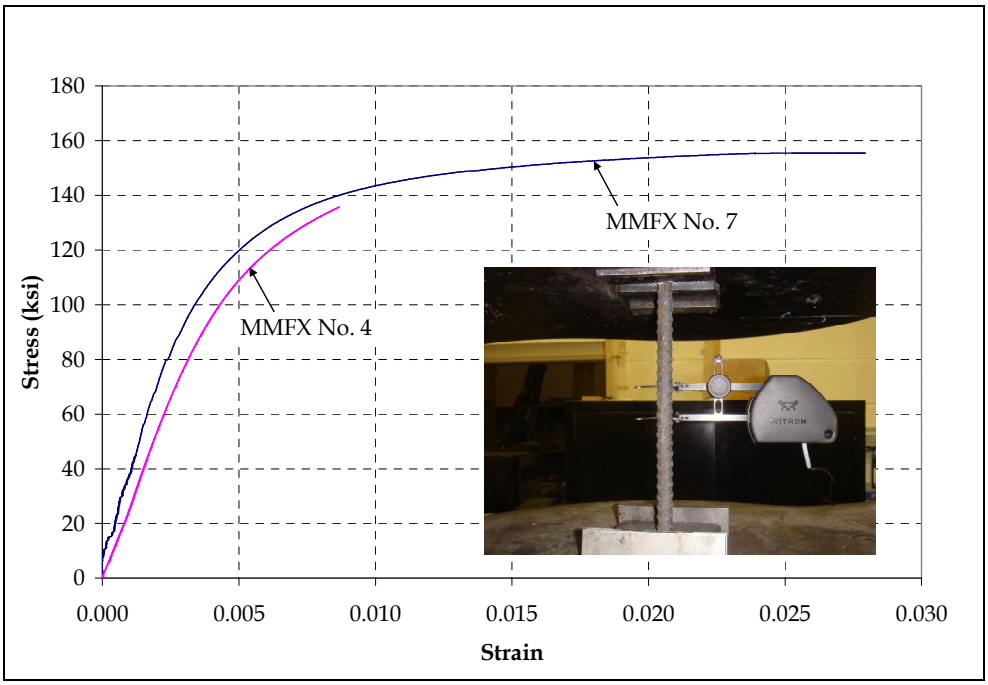

Figure 3.14 Tension Test Results of MMFX Bars

3.4.2.4 Bond between MMFX and Ductal®

Bond strength of MMFX-Ductal® interface was examined using a pullout test, as shown in the inset of Figure 3.15. The specimen had a 2 in. x 5 in. cross-section with ½ in. clear cover on three sides to simulate the proposed deck system. A No. 4 MMFX bar was used with an embedment length of 16 times its diameter. The specimen failed by crushing of concrete, with rebar stress recorded above 125 ksi. More pullout tests are needed to characterize the interface bond between MMFX and Ductal®.

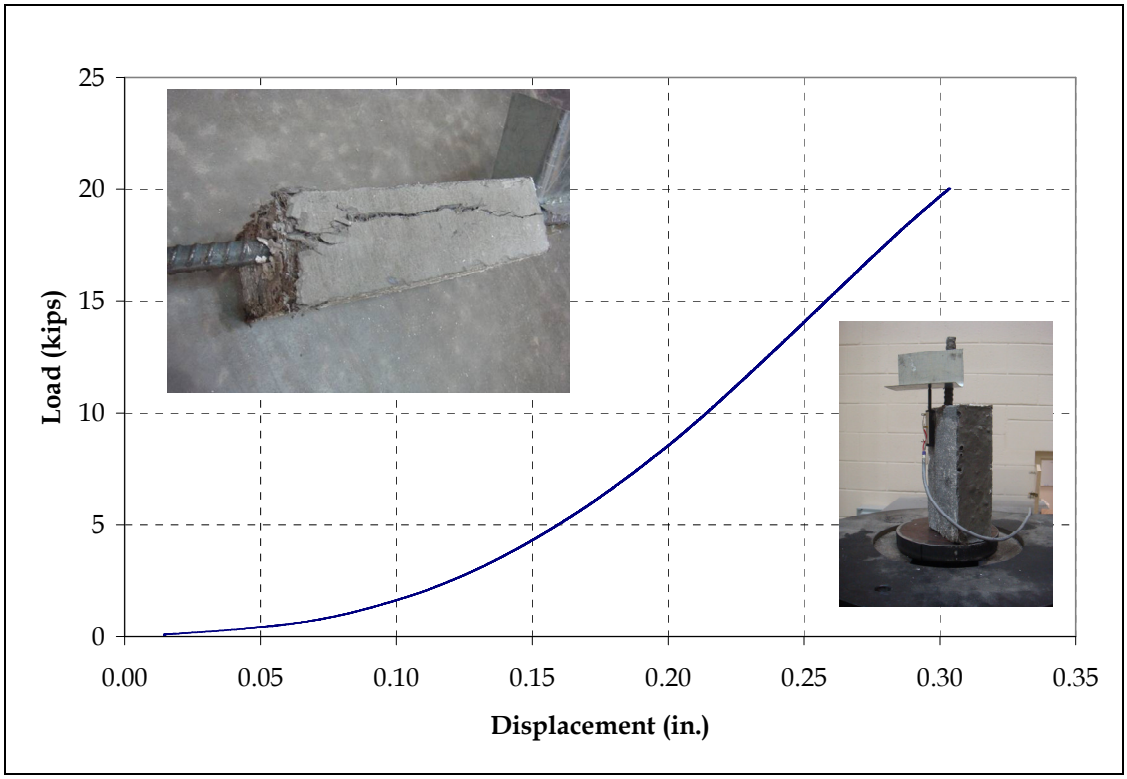

Figure 3.15 Pullout Test Results

3.4.3 Component Specimen Test Matrix

Initially, single-T simple-span (1T1S) specimens were tested with different flexural reinforcements, with and without shear reinforcement, and with different end anchorages. Based on the results of simple-span specimens, it was decided to use 1#7 as the flexural reinforcement, not to use shear reinforcement, and use an inclined 180° hook for end anchorage. The design was then expanded to four-T simple-span (4T1S), single-T two-span (1T2S), and three-T two-span (3T2S) specimens. The specimen test matrix is summarized in Table 3.3.

Simple-span specimens were subjected to a single load, whereas the two-span specimens were loaded at the middle of each span. Load was applied on an AASHTO prescribed foot print (20 in. x 10 in.) of an HS 20 truck dual-tire wheel. Strain gauges and string potentiometers were installed at important locations to acquire the strains in concrete and steel, as well as deflection data. The instrumentation plan for the single-T simple-span specimen is shown in Figure 3.16. A hydraulic actuator was used to apply the load. Displacement control procedure was adopted for all tests with a displacement rate of 0.015 in./min. The simple-span specimens had a 4 ft center to center (c/c) span, and each span in two-span specimens was also 4 ft c/c.

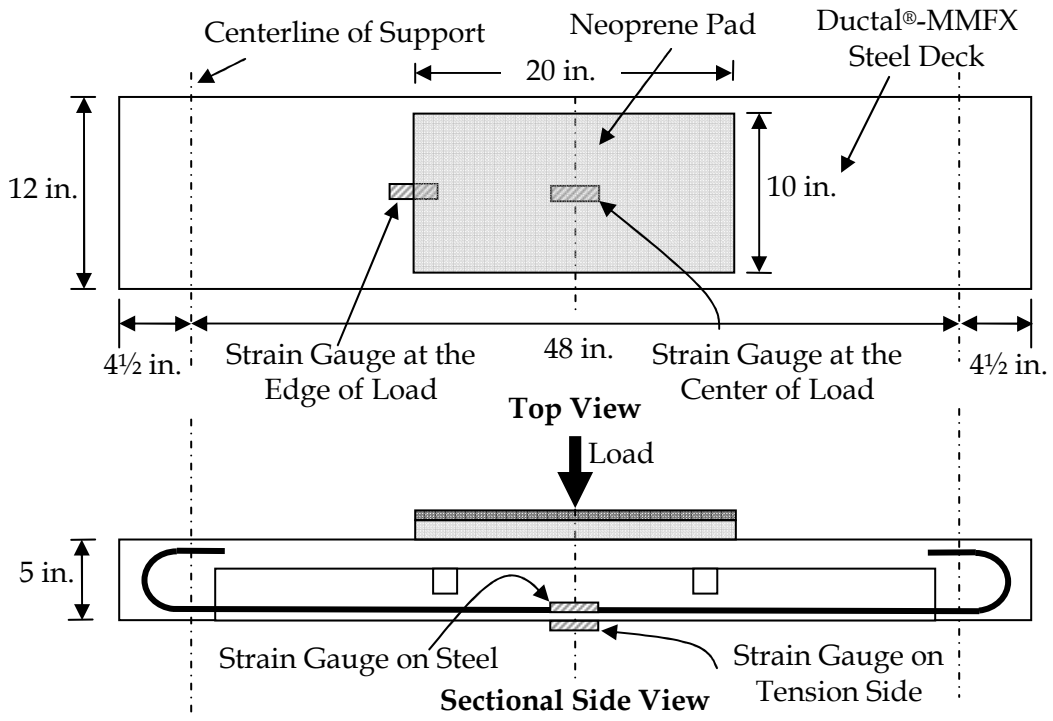

Figure 3.16 Instrumentation Plan for the Single-T Simple-Span Specimens

Table 3.3 Test Matrix for Ductal®-MMFX Steel Deck

No.	Specimen Name	Quantity	Casting No.	Flexural Reinforcement	Shear Reinforcement	End Anchorage
1	1T1S*	1	1	1# 7	No	Anchored
2	1T1S	1	1	1# 7	No	Un-anchored
3	1T1S	2	2,3	1# 7	No	180° Hook
4	1T1S	1	3	1# 7	#2 single leg	180° Hook
5	1T1S (TF**)	1	3	1# 7	No	180° Hook
6	1T1S	1	3	2#4	No	180° Hook
7	1T1S	1	3	1#4 + 2#3 (bent up)	2#3 bent up bars	180° Hook
8	4T1S	1	2	1# 7 (in each rib)	No	180° Hook
9	1T2S	1	4	1#7	No	180° Hook
10	3T2S	1	5	1#7 (in each rib)	No	180° Hook

*1T1S means single-T simple-span (4 ft) specimen.
**TF: Tapered flange designed for self-weight reduction purpose.

3.4.4 Test Observations and Results

3.4.4.1 1T1S Series Specimens with No Shear Reinforcement

Figures 3.17 and 3.18 show the test setup and failure pattern of the 1T1S specimen with anchored steel bar. A 2 in. x 2 in. steel plate was welded at each end of the flexural steel bar to provide end anchorage. Load-deflection and load-strain responses are shown in Figures 3.19 to 3.21. The strain gauge applied to the flexural steel at the mid-span was detached during the test, and therefore no accurate data was recorded. Large shear cracks were developed at both ends near the supports, but failure took place due to the fracture of the end plate weld. Failure was sudden with a loud sound, and notable from the sudden drop in the load-deflection response (Figure 3.19). Although failure was sudden, the specimen managed to exceed the target load of 37.24 kips. Figure 3.20 shows that the strain at the center of the load is smaller than that at the edge of the load. However, the strain data at the center may not be very reliable because the strain gauge was sandwiched between concrete and the neoprene pad, which may effect the free movement of the strain gauge.

Figure 3.17 Test Setup for Specimen 1T1S with End Anchorage

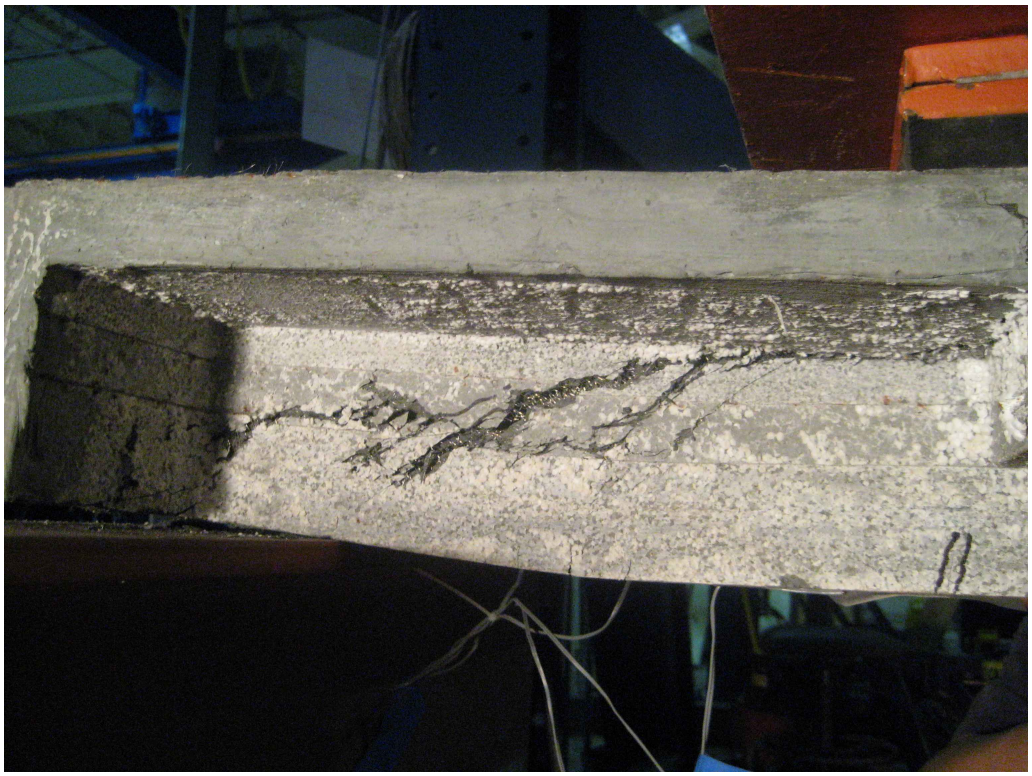

Figure 3.18 Shear-Bond Failure of Specimen 1T1S with End Anchorage

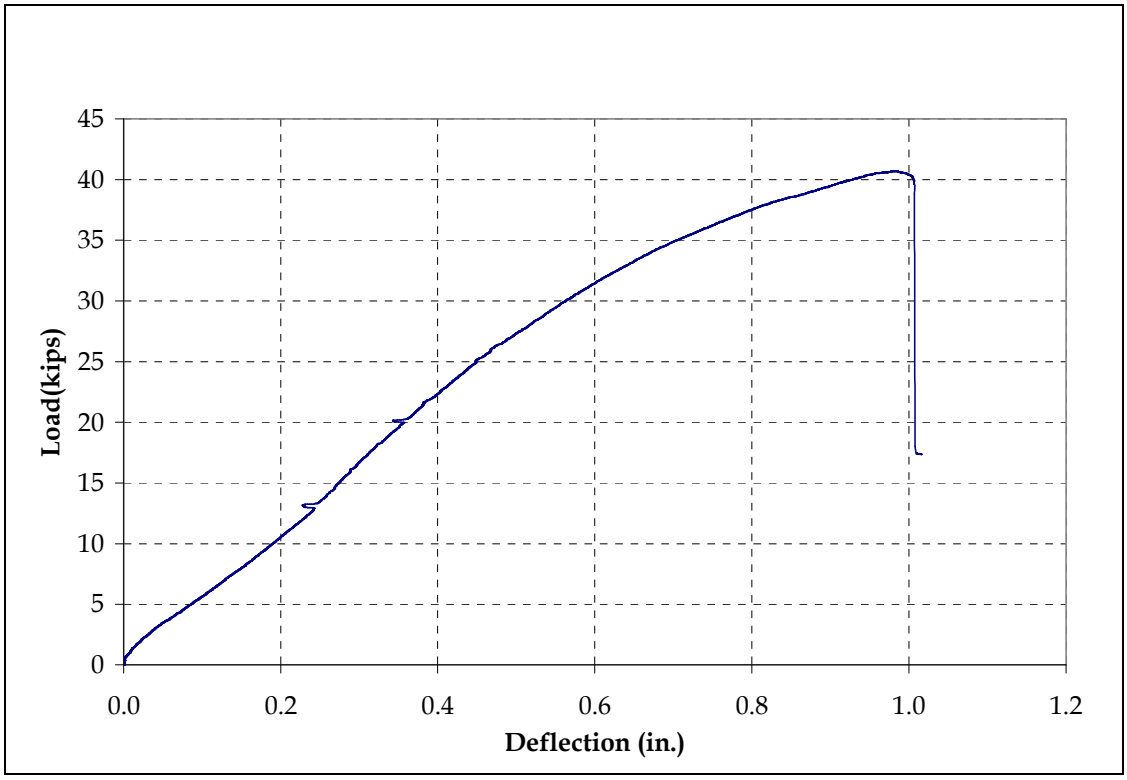

Figure 3.19 Load-Deflection Response for Specimen 1T1S with End Anchorage

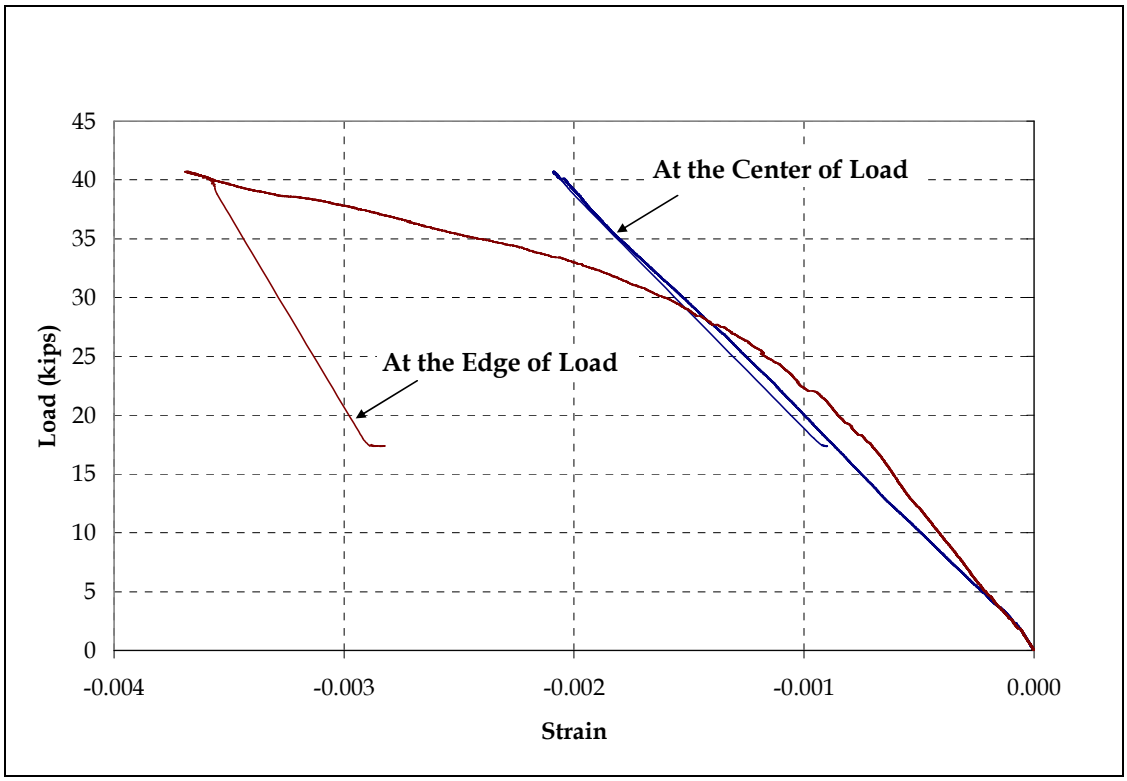

Figure 3.20 Top Concrete Strain in Specimen 1T1S with End Anchorage

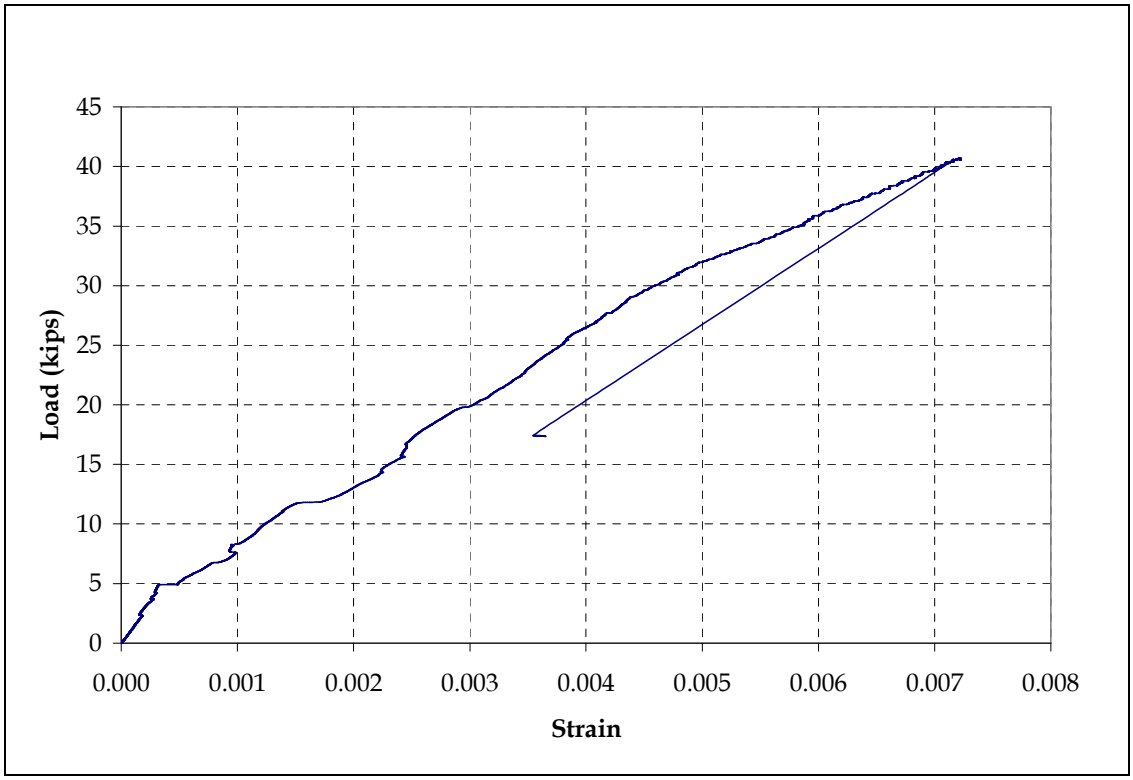

Figure 3.21 Bottom Concrete Strain at Mid-Span in Specimen 1T1S with End Anchorage

Figures 3.22 and 3.23 present the failure pattern of Specimen 1T1S without end anchorage. The specimen failed in shear at an ultimate load of 33 kips. The failure was more ductile than the first specimen with end anchorage. Shear cracks appeared near both supports and gradually opened up. These cracks moved towards the top flange which was subsequently crushed at the ultimate load. Figures 3.24 to 3.26 show the load-deflection and load-strain responses. The ultimate load for this specimen was less than the target load, which emphasized the need for end anchorage.

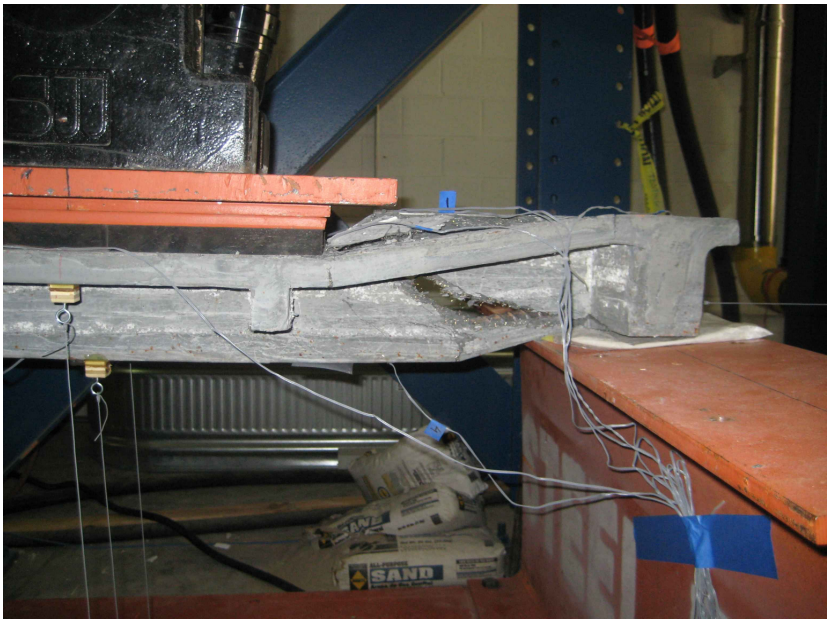

Figure 3.22 Shear-Bond Failure of Specimen 1T1S without End Anchorage


Figure 3.23 Flange Failure in Specimen 1T1S without End Anchorage (Bottom View)

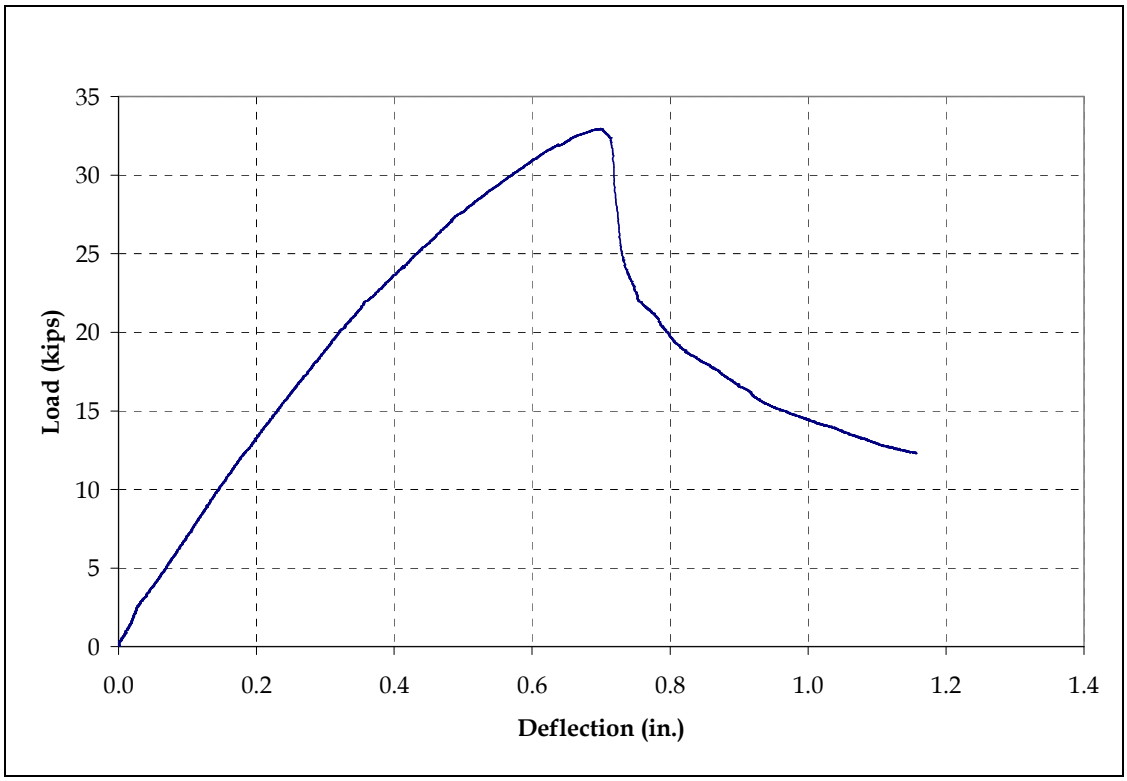

Figure 3.24 Load-Deflection Response for Specimen 1T1S without End Anchorage

Figure 3.25 Top Concrete Strain in Specimen 1T1S without End Anchorage

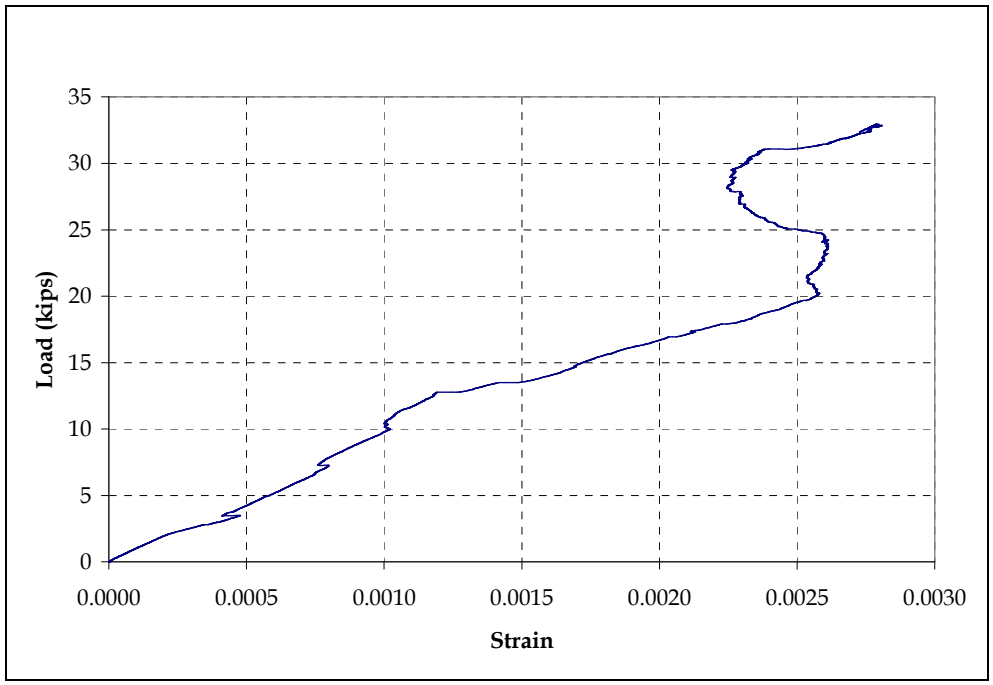

Figure 3.26 Bottom Concrete Strain at Mid-Span in Specimen 1T1S without End Anchorage

Figure 3.27 compares the crack patterns for the first two 1T1S specimens with and without end anchorage. It is clear that shear cracks extend well into the top flange in the absence of end anchorage, and thus lower the load capacity of the slab.

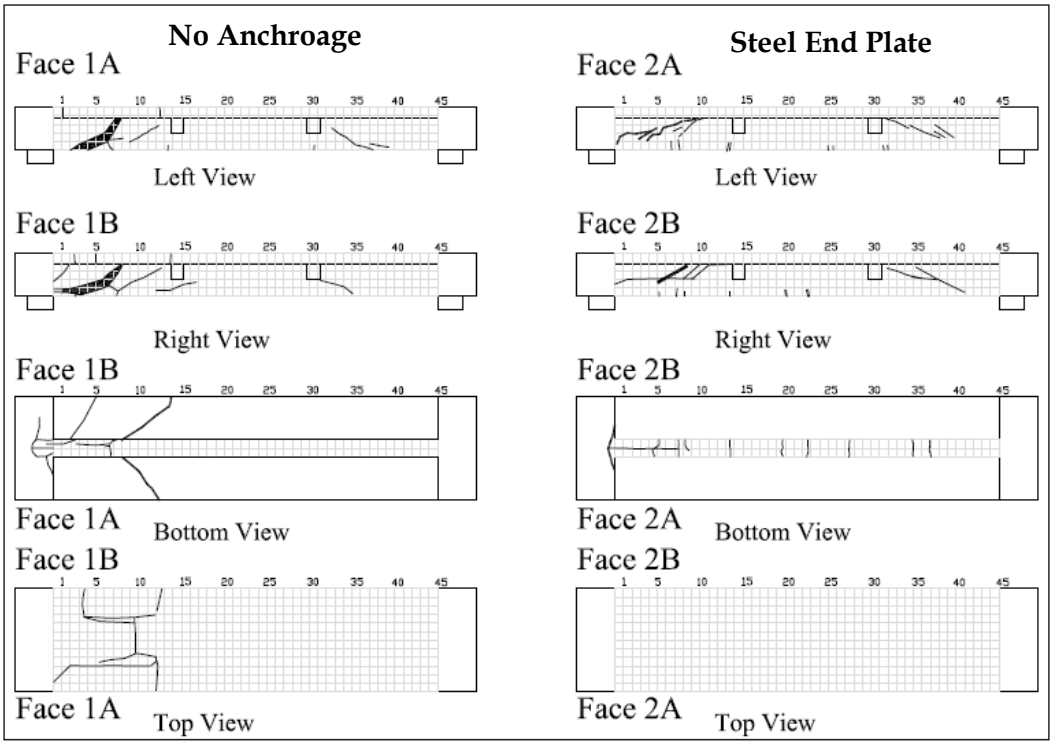

Figure 3.27 Crack Patterns in the First Two 1T1S Specimens with and without End Anchorage

Based on the results of the first two tests, it was decided to use ACI standard 180° hooks for the third specimen to avoid bond failure. Figure 3.28 shows the failure pattern for Specimen 1T1S with 180° hooks. The hooks worked well and the failure was pure shear at an ultimate load of 40 kips (see Figure 3.29). Although the 180° hooks restricted the bond failure, the ultimate load was the same as the specimen with end anchorage. The reason was the lower 28-day cylinder strength for the third specimen. Figures 3.29 to 3.32 show the load-deflection and load-strain responses. Figure 3.31 shows that the bottom concrete stain gauge was damaged at 30 kips which indicates the presence of flexural cracks albeit not visible with naked eye. For this specimen, the steel strain gauge worked very well because adequate protective coating and mastic tape were applied.

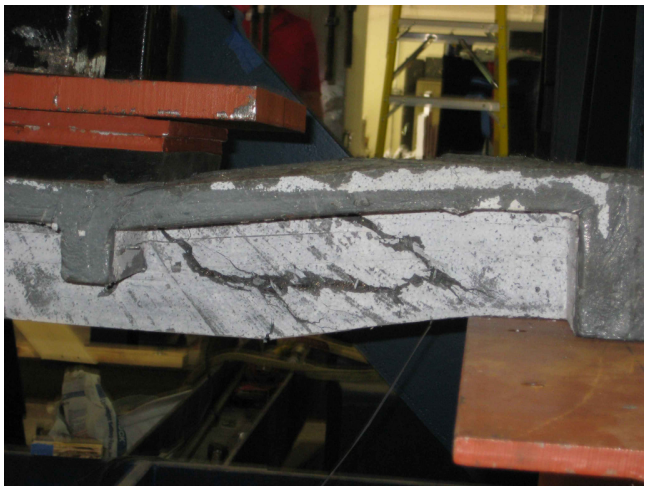

Figure 3.28 Pure Shear Failure of Specimen 1T1S with 180° Hook

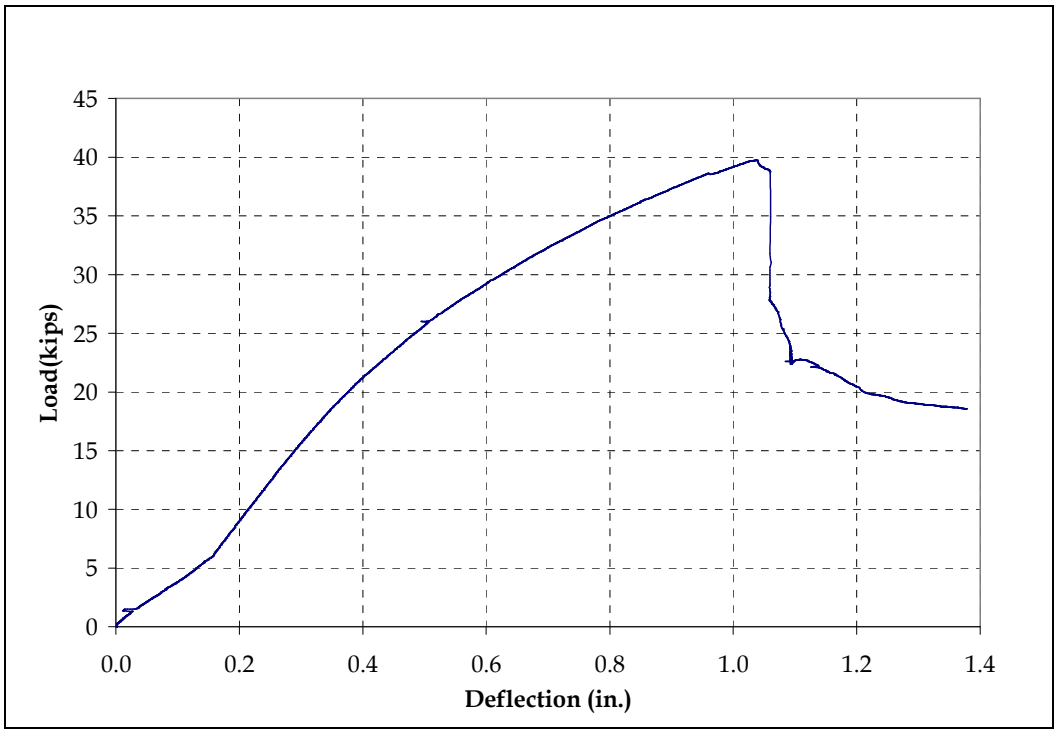

Figure 3.29 Load-Deflection Response for Specimen 1T1S with 180° Hook

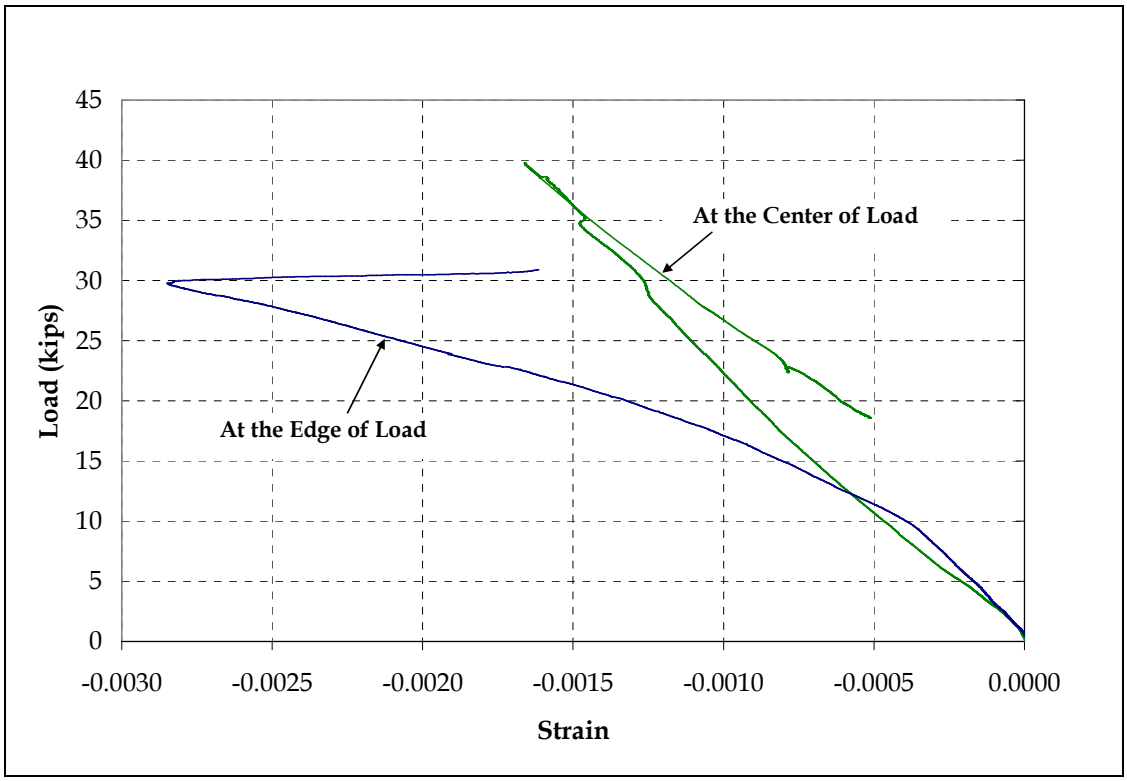

Figure 3.30 Top Concrete Strain in Specimen 1T1S with 180° Hook

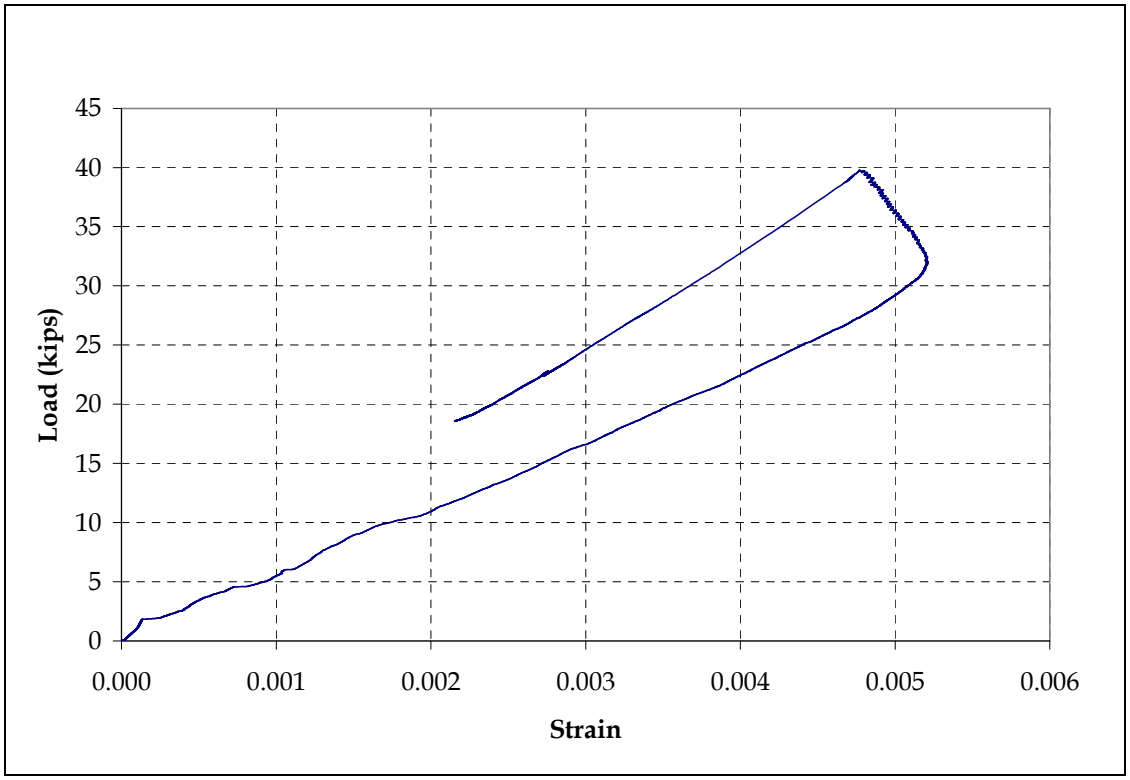

Figure 3.31 Bottom Concrete Strain at Mid-Span in Specimen 1T1S with 180° Hook

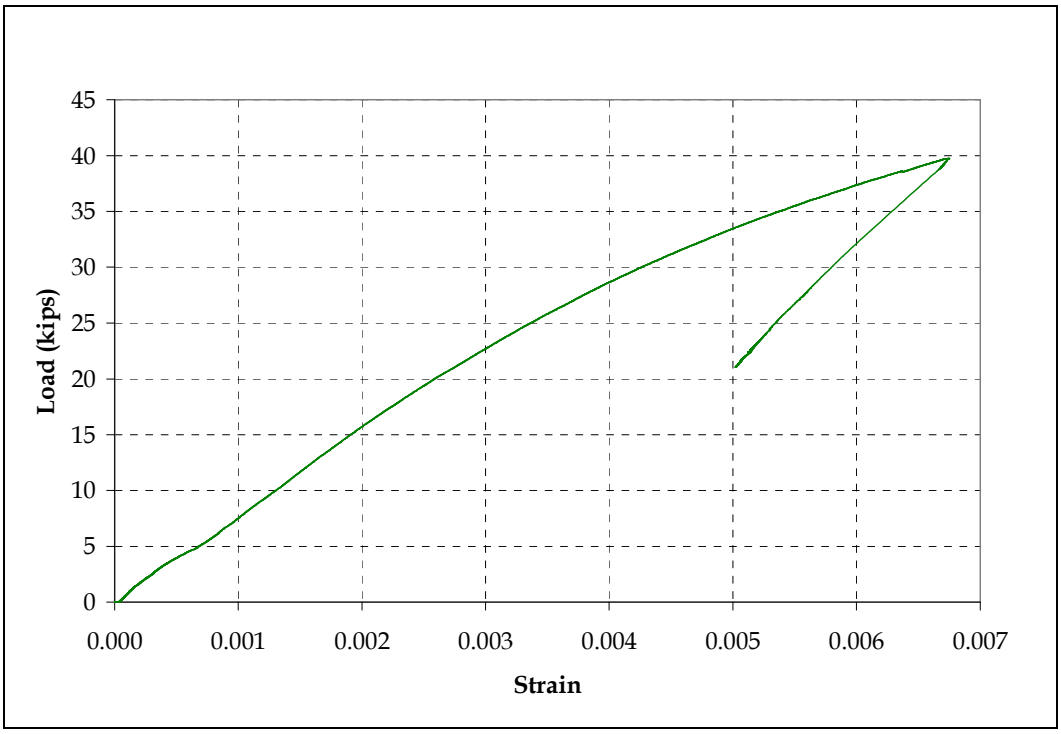

Figure 3.32 Bottom Steel Strain at Mid-Span in Specimen 1T1S with 180° Hook

Figures 3.33 and 3.34 show the failure pattern of the second 1T1S specimen with 180° hooks. The second specimen was necessary because the first test did not provide realistic estimate of the ultimate load due to the lower material strength. The first shear crack appeared at 26 kips, and the specimen failed in shear at 47 kips. Unlike the previous test, the failure was not sudden. Figures 3.35 to 3.38 show the load-deflection and load-strain responses. There were very small flexural cracks, which damaged the bottom concrete strain gauge at around 30 kips.

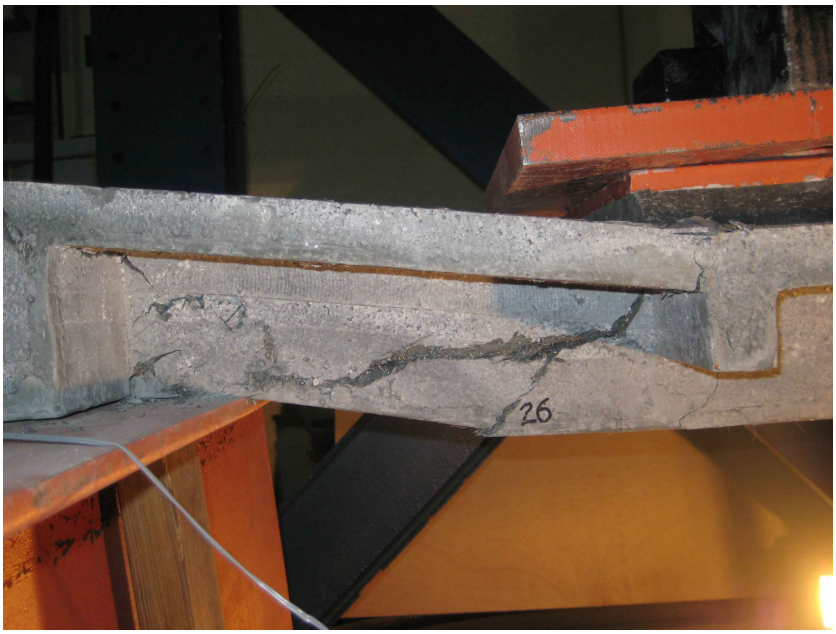

Figure 3.33 Wide Shear Crack in Specimen 1T1S with 180° Hook near North Support

Figure 3.34 Shear Cracks in Specimen 1T1S with 180° Hook near South Support

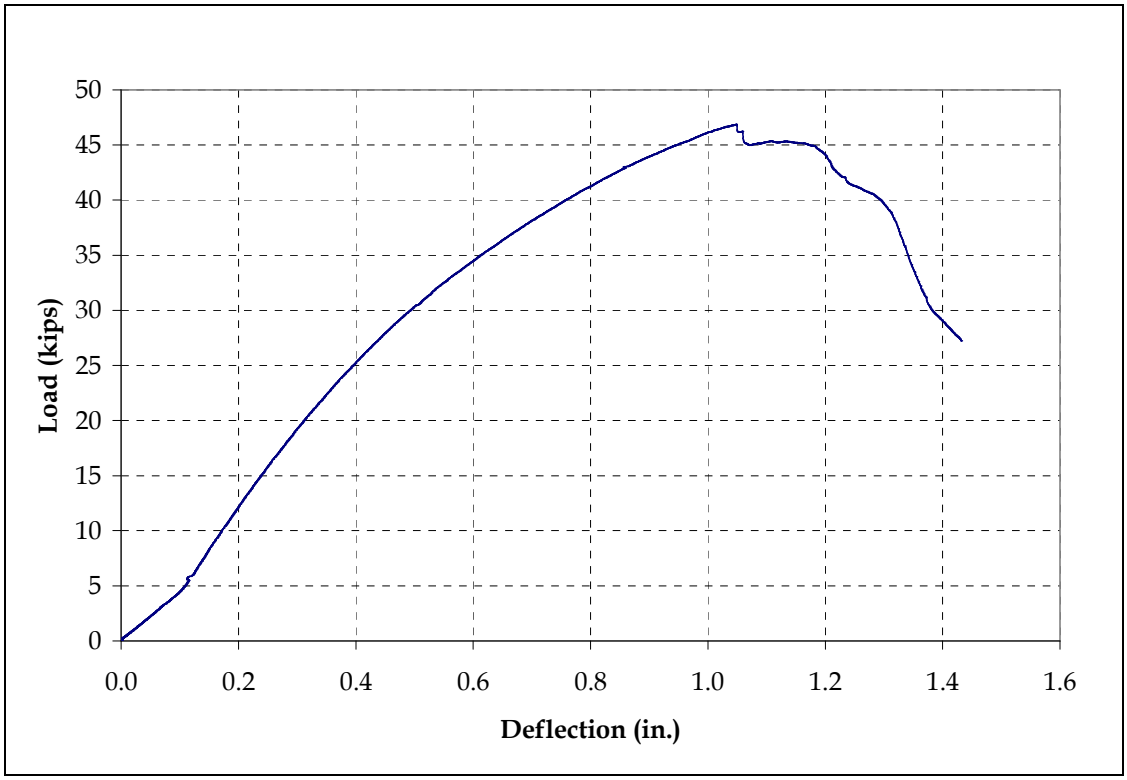

Figure 3.35 Load-Deflection Response for Specimen 1T1S with 180° Hook

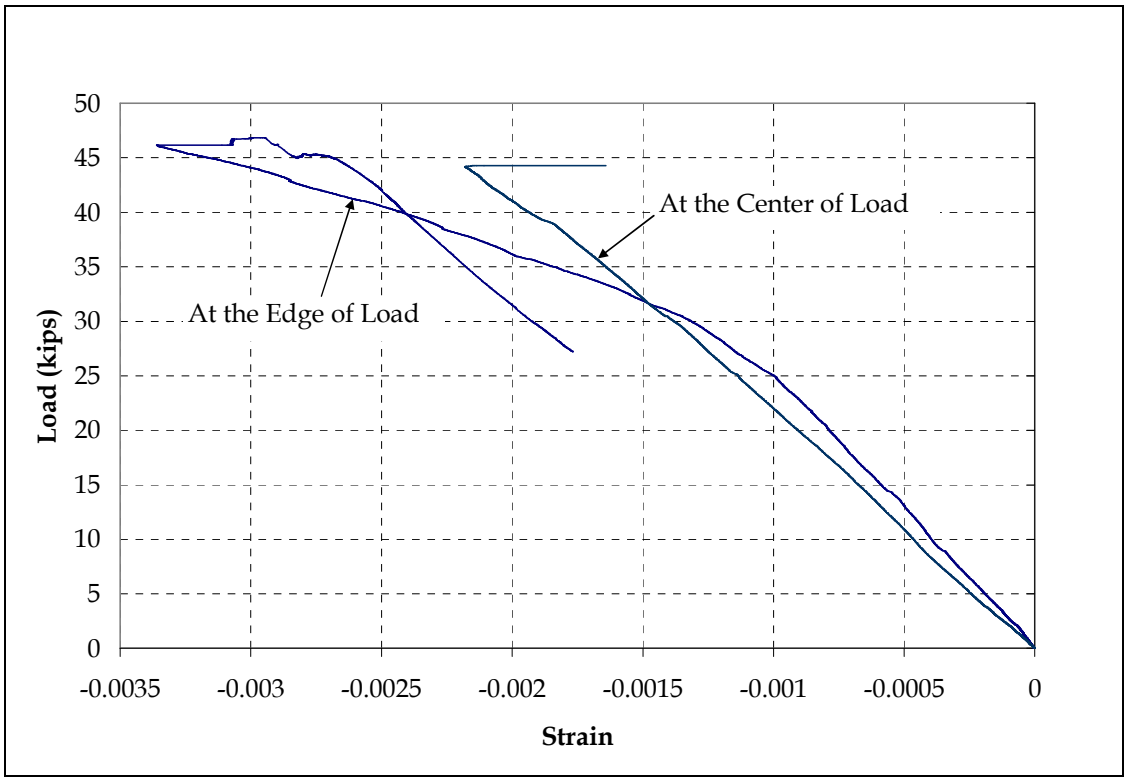

Figure 3.36 Top Concrete Strain in Specimen 1T1S with 180° Hook

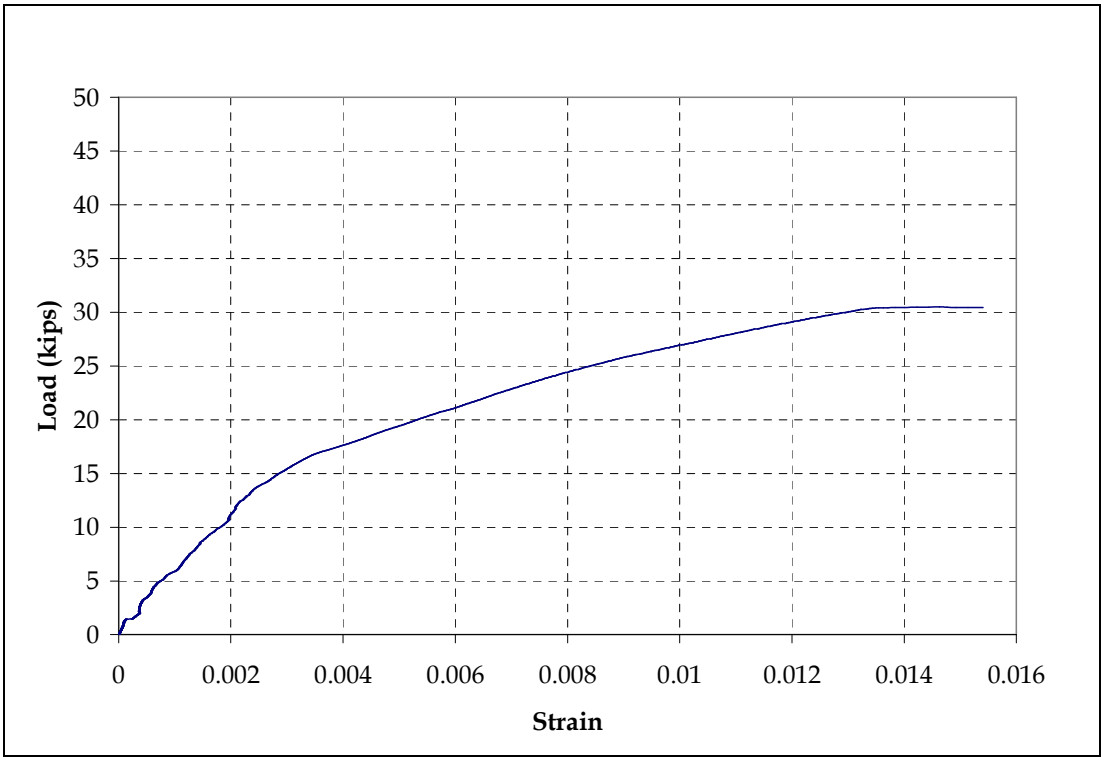

Figure 3.37 Bottom Concrete Strain at Mid-Span in Specimen 1T1S with 180° Hook

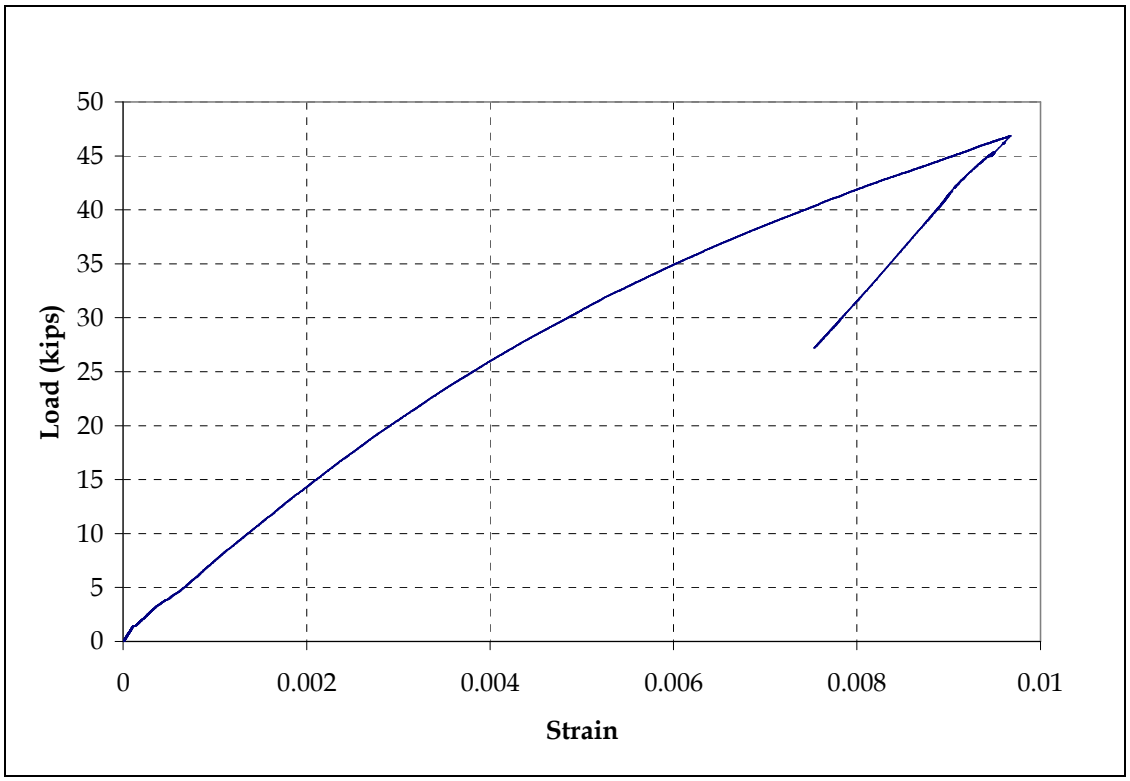

Figure 3.38 Bottom Steel Strain at Mid-Span in Specimen 1T1S with 180° Hook

Figures 3.39 and 3.40 show the failure pattern of Specimen 1T1S with a tapered flange. The intention to taper the flange was to further reduce the self-weight without affecting the strength. Figures 3.41 to 3.44 show the load-deflection and load-strain responses. Unlike all earlier tests, this specimen developed significant flexural cracks in addition to shear cracks. The first shear crack appeared at 17.5 kips and the specimen failed at 35 kips. The tapered flange was not the reason for the flexural cracks and the lower ultimate load, but rather the under-strength flexural reinforcement. Here, the widening of the flexural cracks is because of the yielding and plastic deformation of the rebar. Before rebar yielding, the strong bond between the rebar and concrete would not allow the crack to widen as there was only ½ in. cover. In Figure 3.42, nonlinear compressive strain was observed as the section lost its rigidity due to yielding of the rebar. The load-strain response (see Figure 3.44) shows that the steel bar was not the high-strength MMFX rebar but rather a regular hot-rolled rebar with a wide yielding plateau. This steel bar was inadvertently used in place of the MMFX bar. The test results however, showed that a tapered section was feasible, and that the use of mild steel affects not only the ultimate strength of the section, but also the crack pattern.

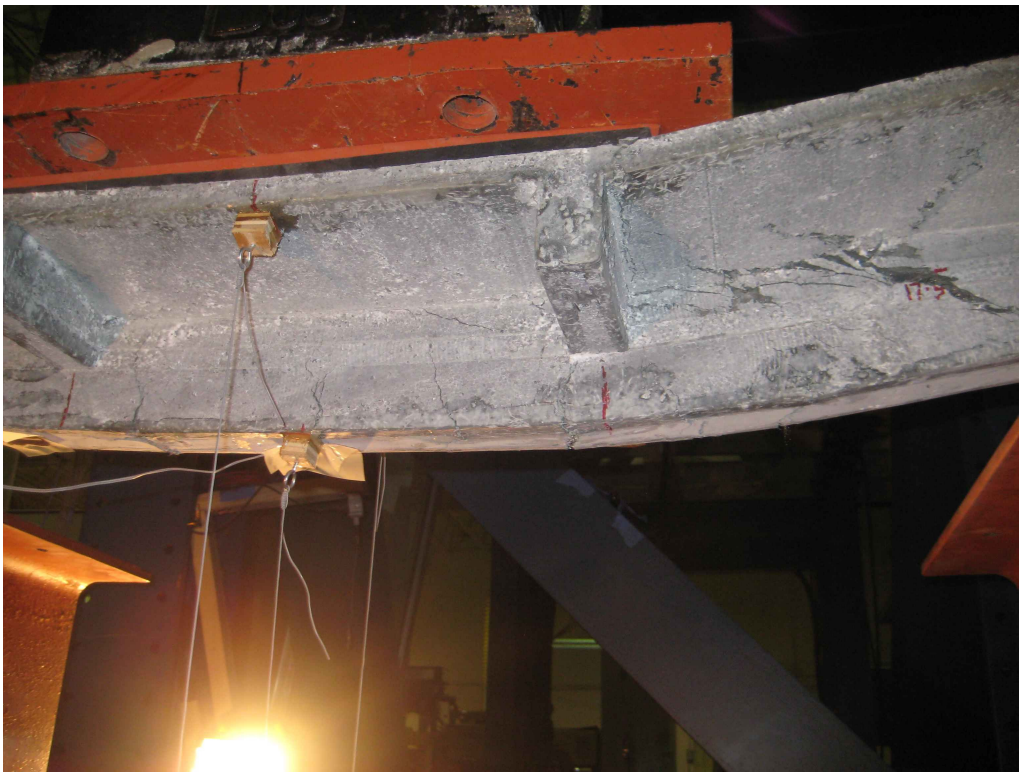

Figure 3.39 Flexural and Shear Cracks in Specimen 1T1S with Tapered Flange

Figure 3.40 Shear Cracks in Specimen 1T1S with Tapered Flange

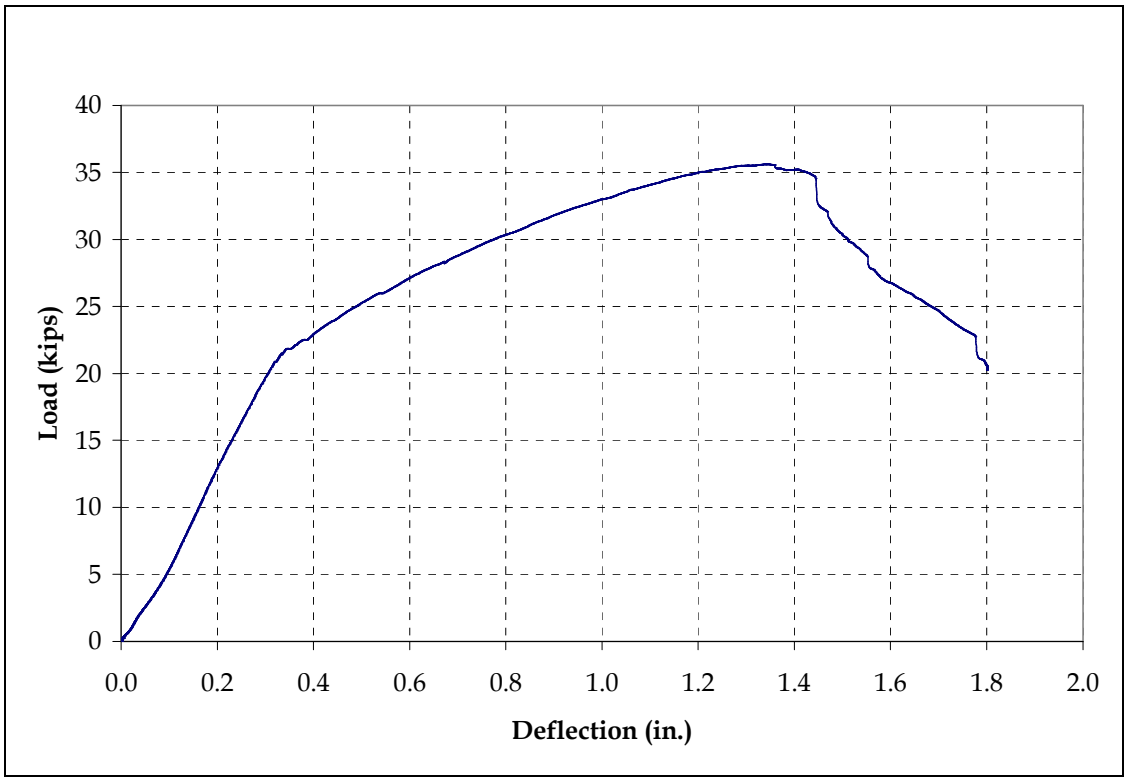

Figure 3.41 Load-Deflection Response for Specimen 1T1S with Tapered Flange

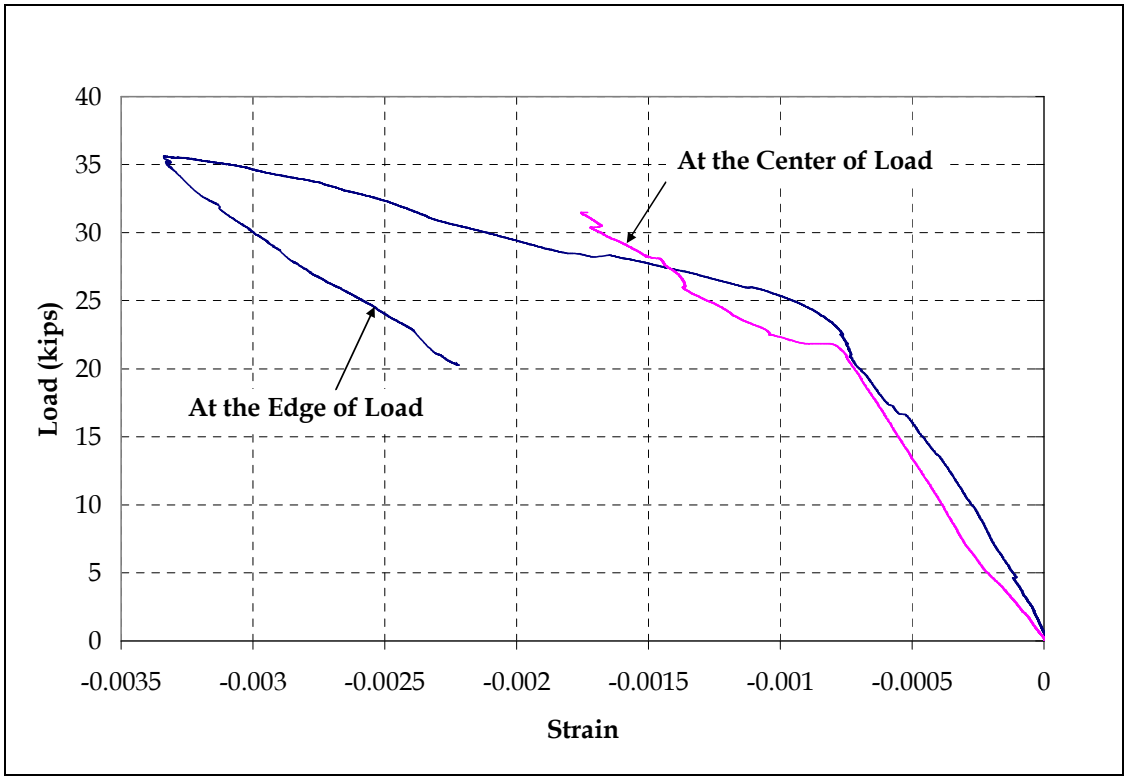

Figure 3.42 Top Concrete Strain in Specimen 1T1S with Tapered Flange

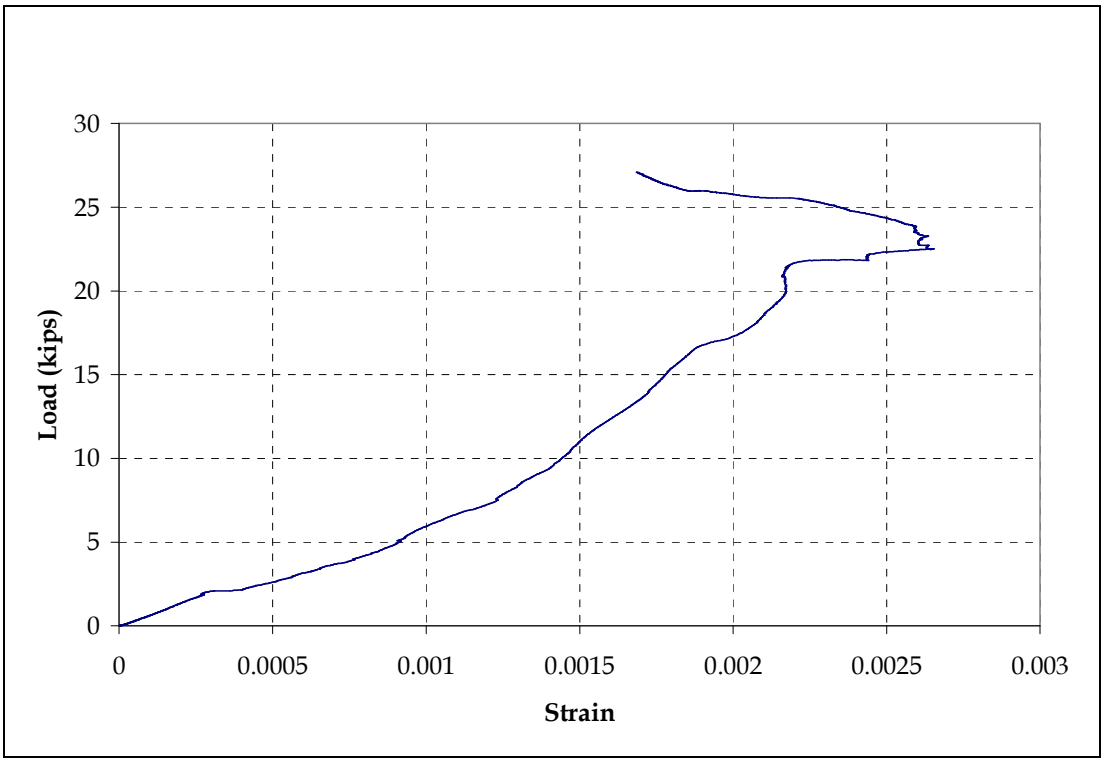

Figure 3.43 Bottom Concrete Strain at Mid-Span in Specimen 1T1S with Tapered Flange

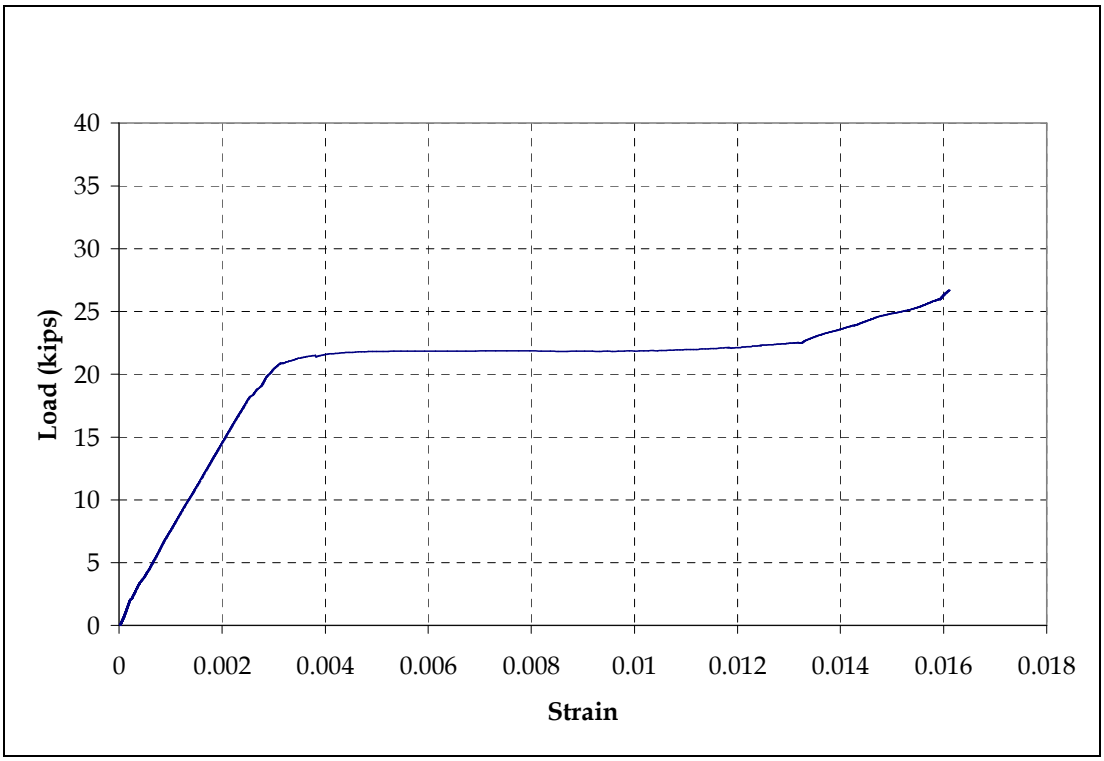

Figure 3.44 Bottom Steel Strain at Mid-Span in Specimen 1T1S with Tapered Flange

3.4.4.2 1T1S Specimens with Various Types of Shear Reinforcement

Figures 3.45 and 3.46 show the failure pattern of Specimen 1T1S with shear reinforcement. Shear stirrups (#2 @ 2 in. c/c, Grade 40) were provided at both sides between the edge of the supporting stringer and the loading pad. Because shear was the dominant mode of failure in all previous specimens, shear stirrups were provided to change the failure mode to flexure, which is generally desirable for bridge decks and slabs. However, the shear reinforcement did not significantly alter the failure mechanism, and the specimen still failed in shear at 48 kips. The ultimate load did not significantly increase either. Therefore, the idea of shear stirrups was not pursued any further. Figures 3.47 to 3.50 show the load-deflection and load-strain responses.

Figure 3.45 Distributed Shear Cracks in Specimen 1T1S with Shear Reinforcement near South Support

Figure 3.46 Distributed Shear Cracks in Specimen 1T1S with Shear Reinforcement near North Support

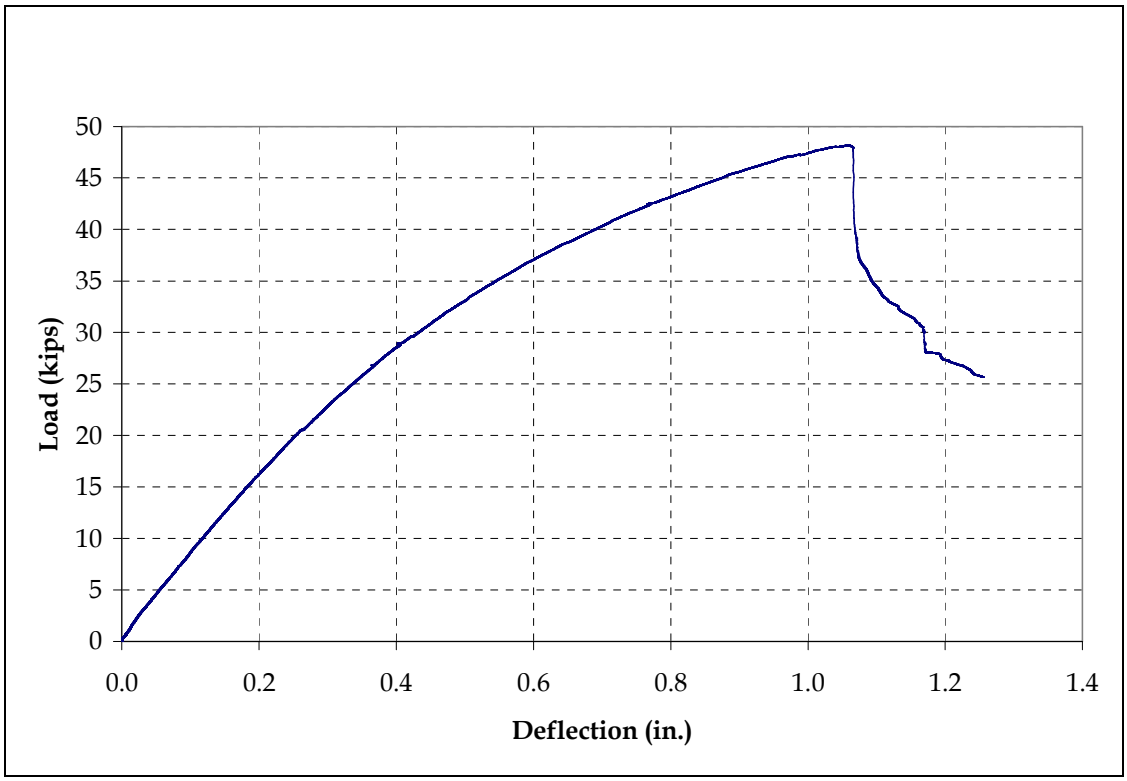

Figure 3.47 Load-Deflection Response for Specimen 1T1S with Shear Reinforcement

Figure 3.48 Top Concrete Strain in Specimen 1T1S with Shear Reinforcement

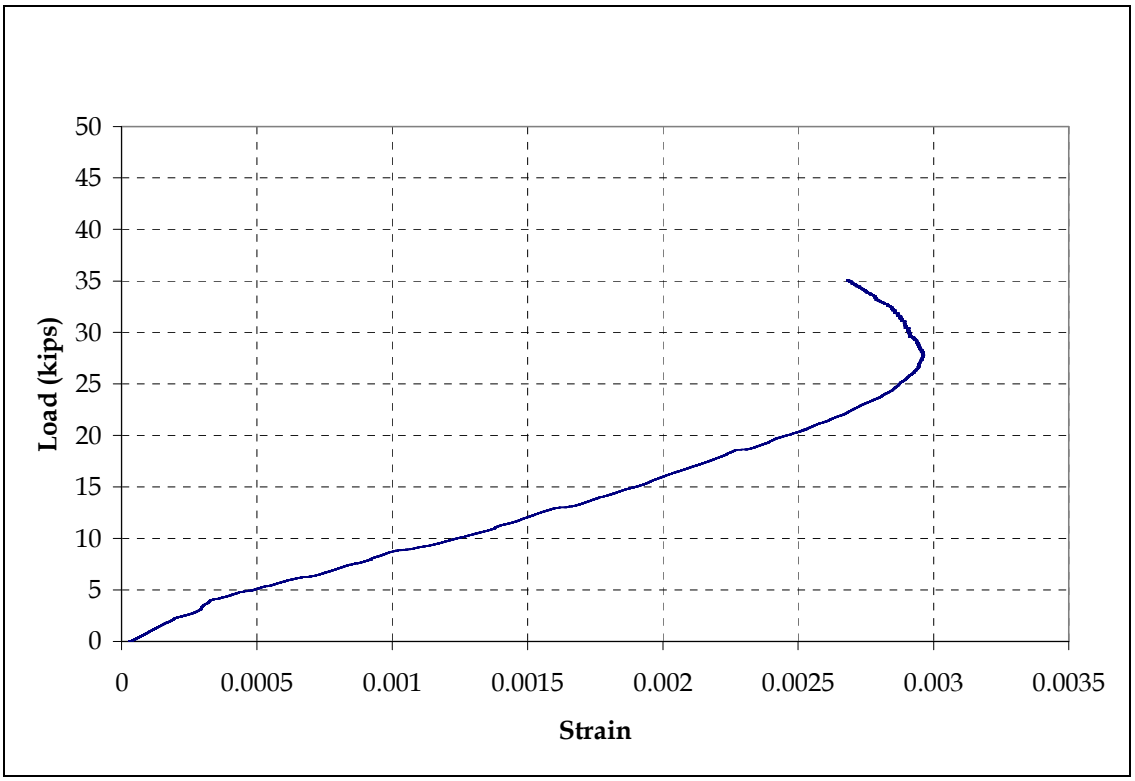

Figure 3.49 Bottom Concrete Strain at Mid-Span in Specimen 1T1S with Shear Reinforcement

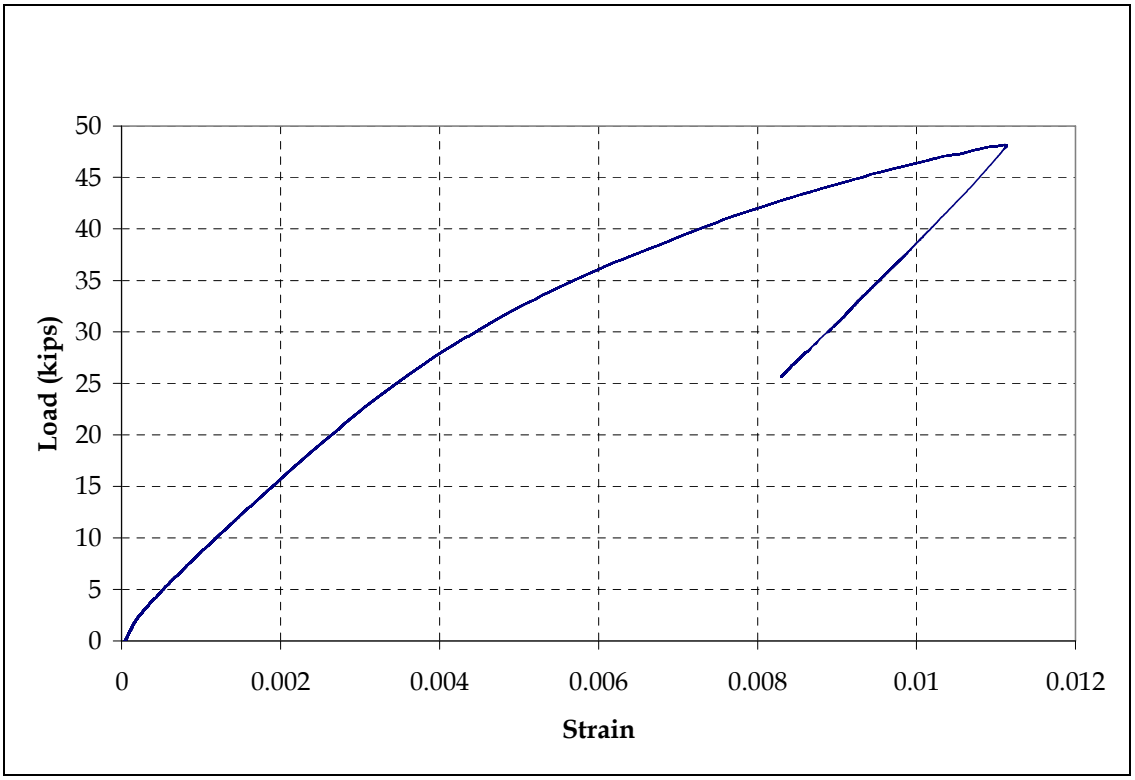

Figure 3.50 Bottom Steel Strain at Mid-Span in Specimen 1T1S with Shear Reinforcement

Figures 3.51 and 3.52 show the arrangement of steel bars, instrumentation plan, and the failure mode of Specimen 1T1S with 1#4 and 2#3 bent-up bars. The idea behind bending up the #3 bars was to prevent shear failure. However, the specimen still failed in shear with the first shear crack appearing at 20.5 kips. Figures 3.53 to 3.56 show the load-deflection and load-strain responses. The failure load was around 35 kips, which is lower than the target load of 37.24 kips. Figure 3.55 shows that the bottom concrete strain gauge remained intact up to the ultimate load indicating that no significant flexural cracks had developed at the mid-span

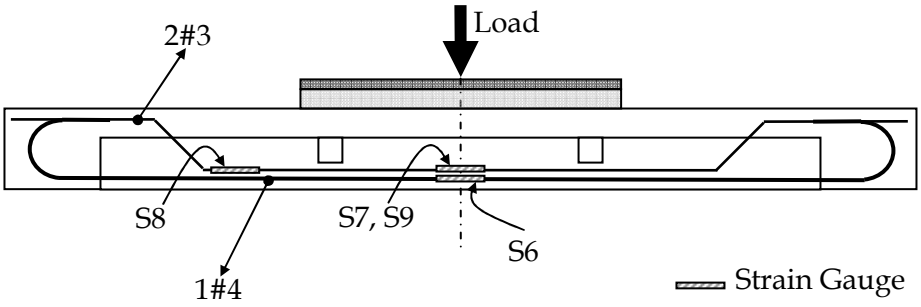

Figure 3.51 Arrangement of Steel Strain Gauges in Specimen 1T1S with 1#4 and 2#3 Bent-up Bars

Figure 3.52 Wide Shear Crack in Specimen 1T1S with 1#4 and 2#3 Bent-up Bars

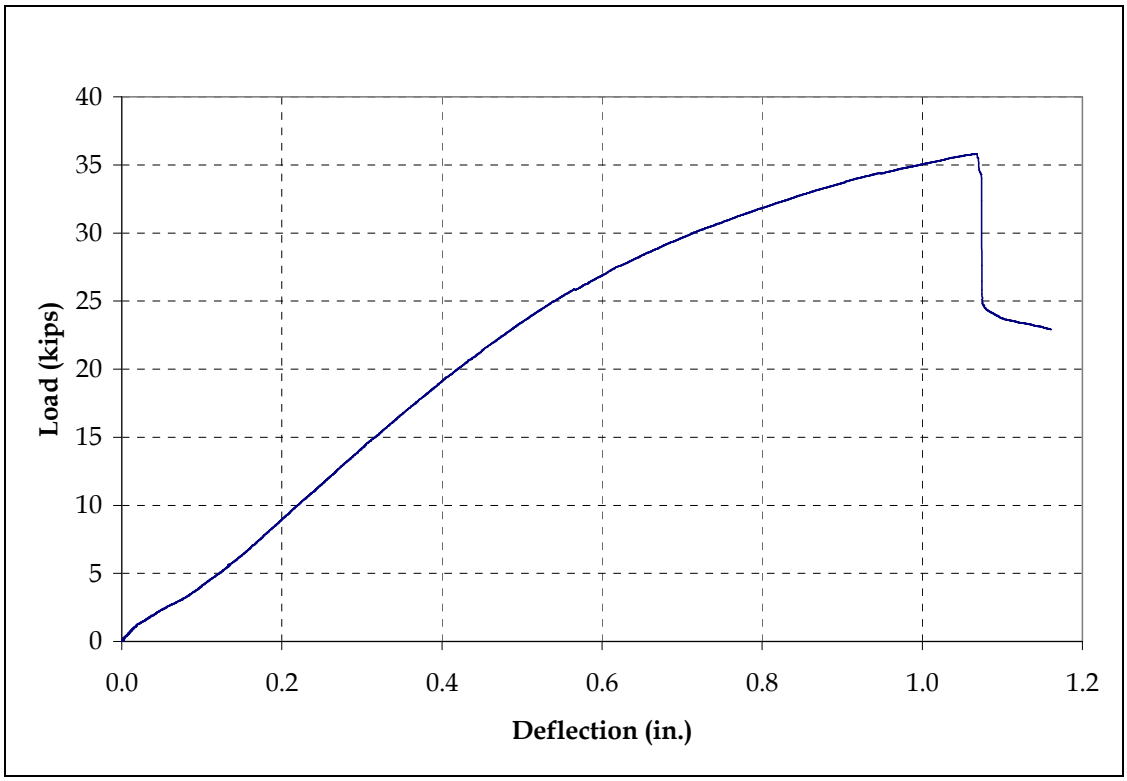

Figure 3.53 Load-Deflection Response for Specimen 1T1S with 1#4 and 2#3 Bent-up Bars

Figure 3.54 Top Concrete Strain in Specimen 1T1S with 1#4 and 2#3 Bent-up Bars

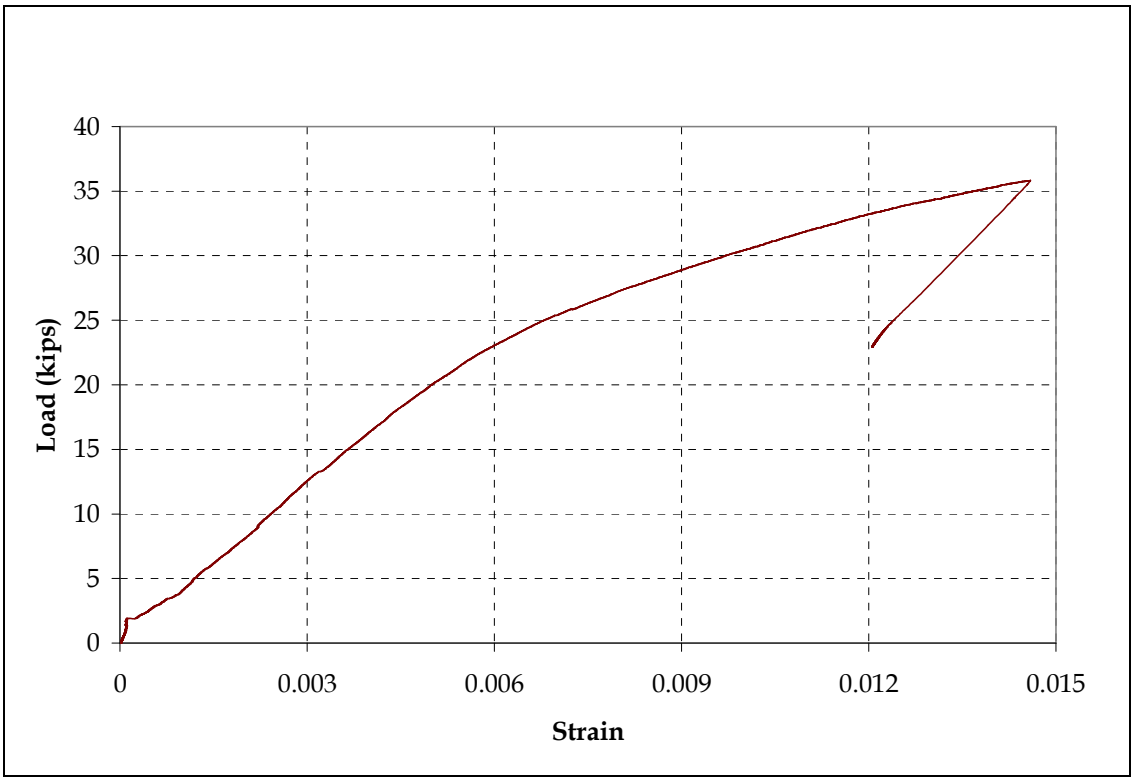

Figure 3.55 Bottom Concrete Strain at Mid-Span in Specimen 1T1S with 1#4 and 2#3 Bent-up Bars

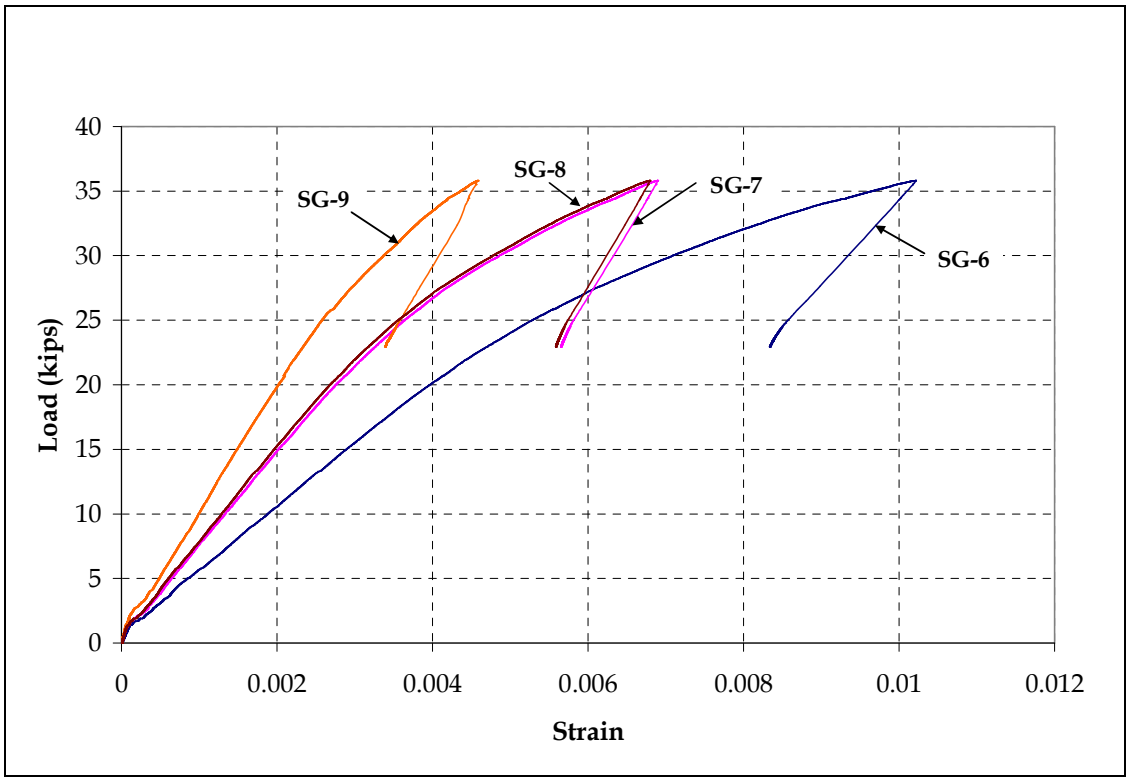

Figure 3.56 Bottom Steel Strains in Specimen 1T1S with 1#4 and 2#3 Bent-up Bars

Figure 3.57 shows the failure mode of Specimen 1T1S with 2#4 bars as flexural reinforcement. This specimen was tested to see whether the mode of failure could be changed to flexure in the under-reinforced case. The specimen however suddenly failed in shear at a relatively low load level of 35 kips. Reduced steel clearly did not change the failure mode. Figures 3.58 to 3.61 show the load-deflection and load-strain responses.

Figure 3.57 Shear Failure of Specimen 1T1S with 2#4 Bars as Flexural Reinforcement

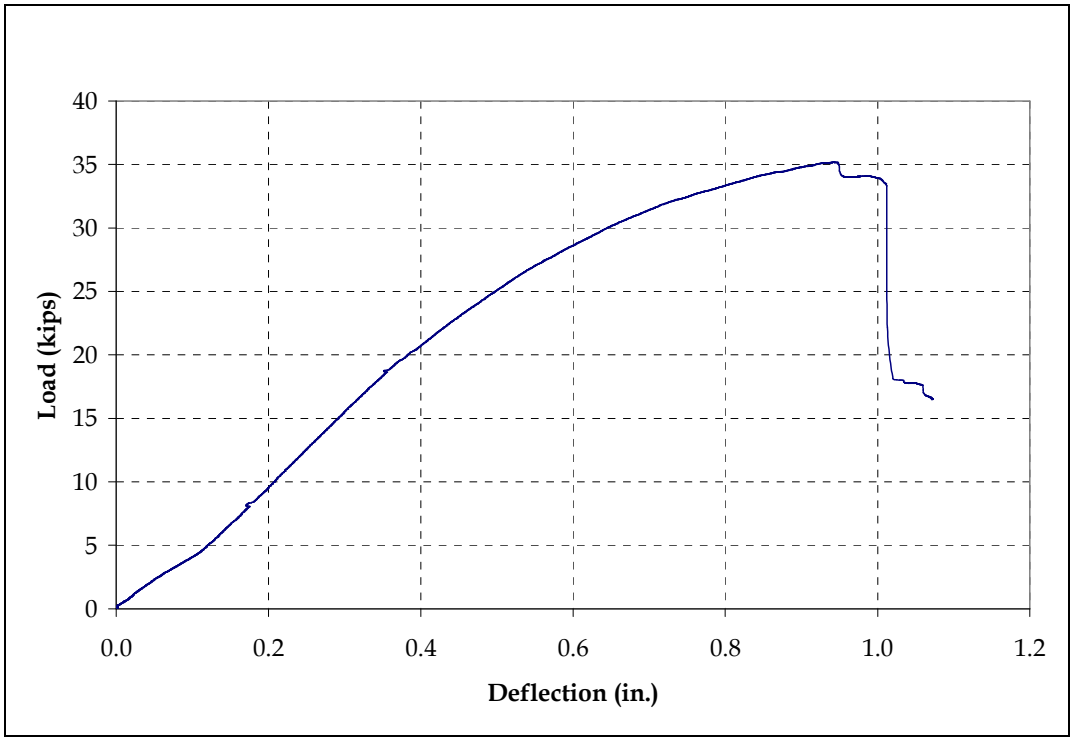

Figure 3.58 Load-Deflection Response for Specimen 1T1S with 2#4 Bars as Flexural Reinforcement

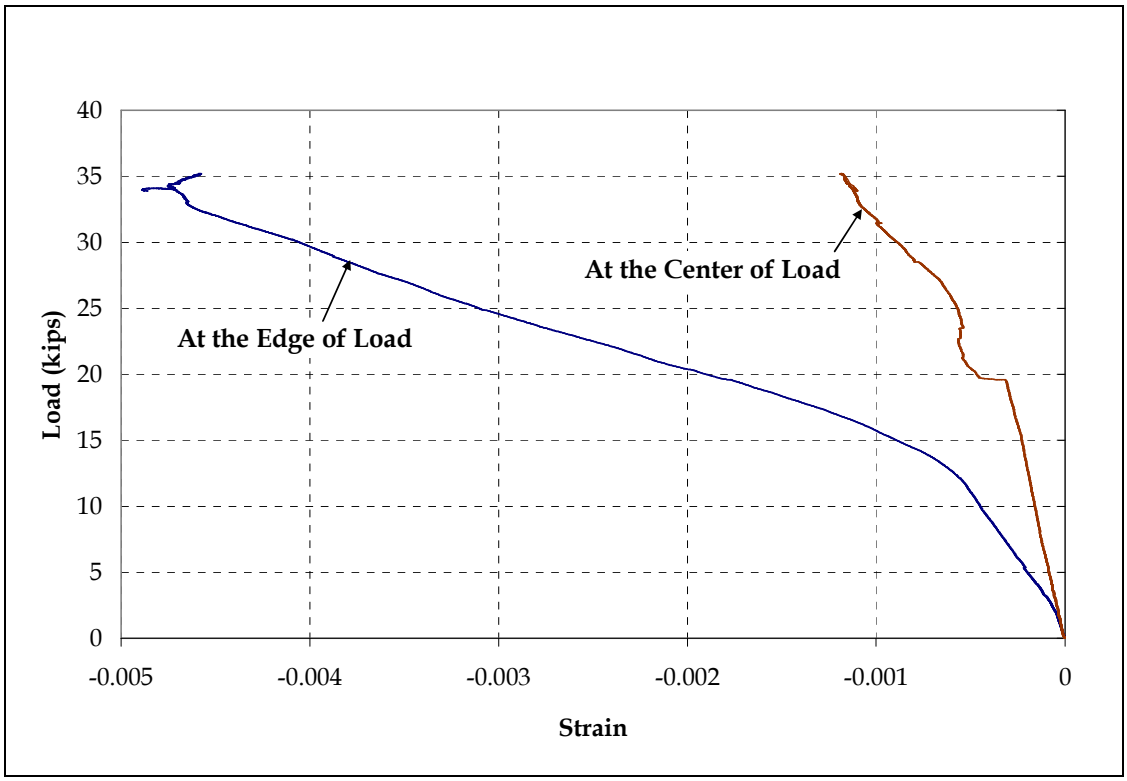

Figure 3.59 Top Concrete Strain in Specimen 1T1S with 2#4 Bars as Flexural Reinforcement

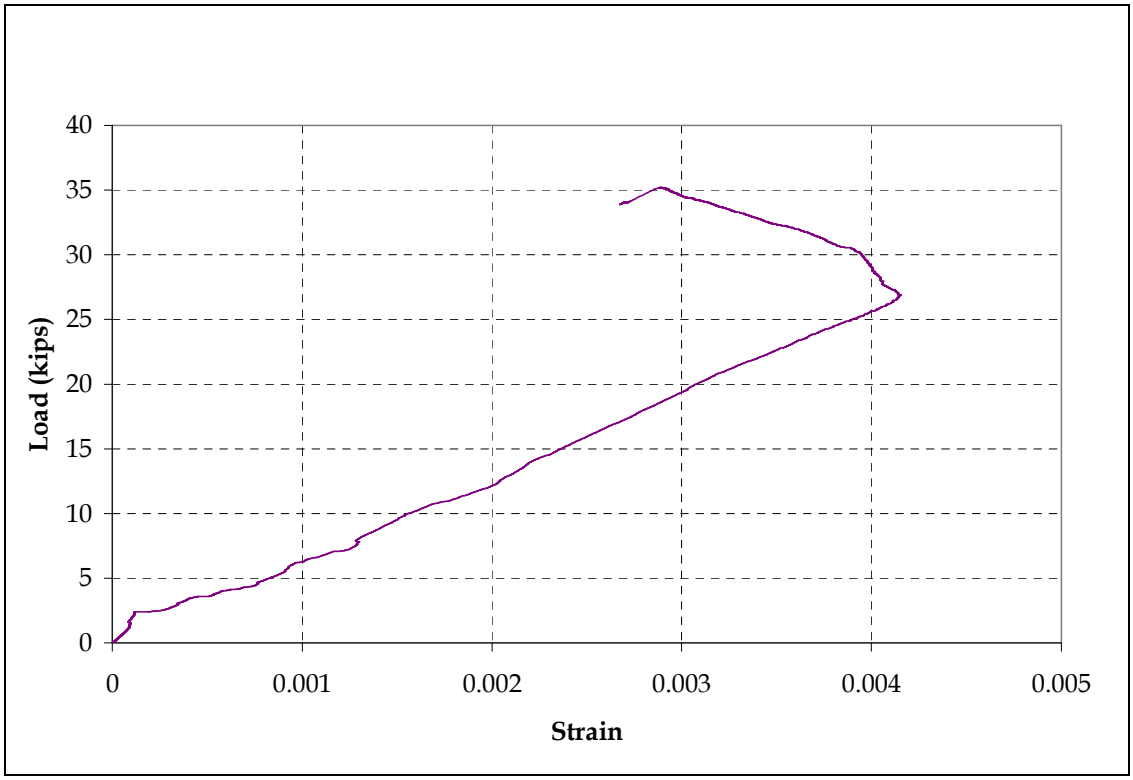

Figure 3.60 Bottom Concrete Strain at Mid-Span in Specimen 1T1S with 2#4 Bars as Flexural Reinforcement

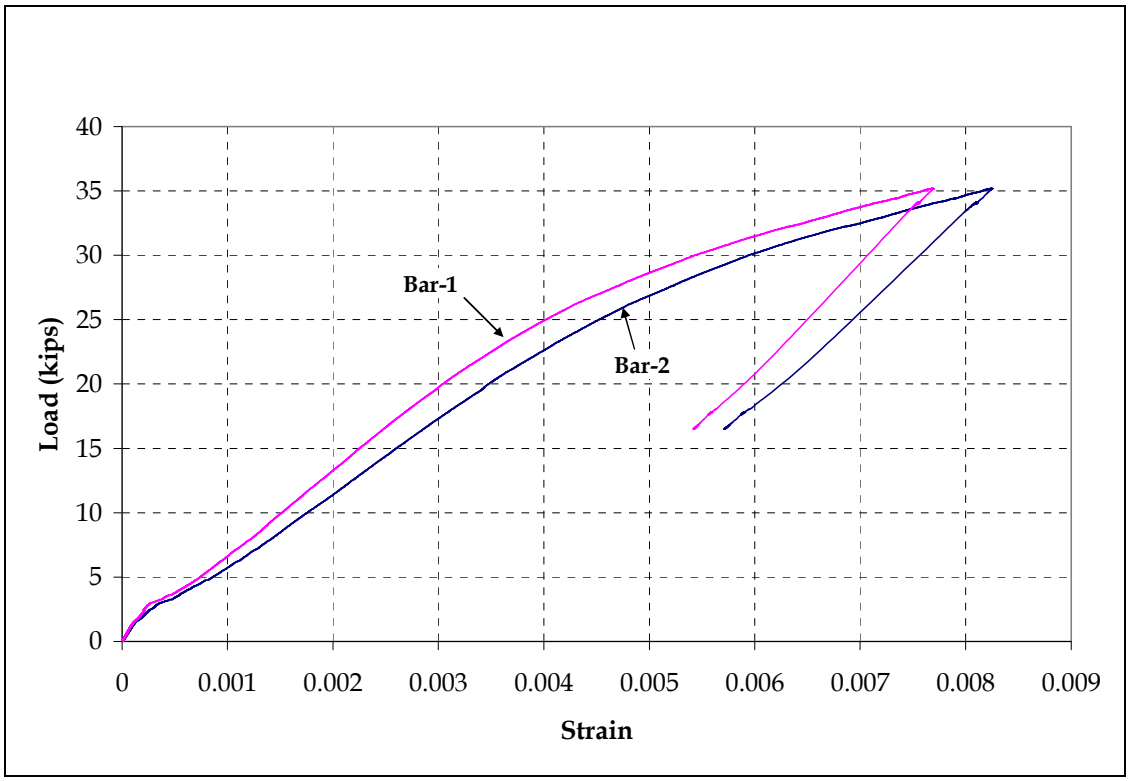

Figure 3.61 Bottom Steel Strains at Mid-Span in Specimen 1T1S with 2#4 Bars as Flexural Reinforcement

3.4.4.3 Multi-Unit Simple-Span Specimen

Figures 3.62 to 3.66 show the instrumentation plan, loading pattern, test setup, and failure pattern for the four-T simple-span (4T1S) specimen. Based on the results of all single-T simple-span (1T1S) specimens, it was decided to use 1#7 bar as flexural reinforcement with 180° hooks, and no shear reinforcement. The deck failed at 83 kips which is more than twice the target load. Shear cracks started appearing at 40 kips, and then gradually grew wider, leading to the punching of neoprene pad into the top flange at the ultimate load. Figures 3.67 to 3.72 show the load-deflection and load-strain responses. The load-deflection diagram (see Figure 3.67) clearly shows that the major load was taken by the three interior ribs. Strain in the transverse steel at mid-span (see Figure 3.72) is nearly 3 times the maximum longitudinal steel strain (see Figure 3.70). Transverse ribs have much smaller stiffness than the longitudinal ribs, which is the major reason for such a high strain.

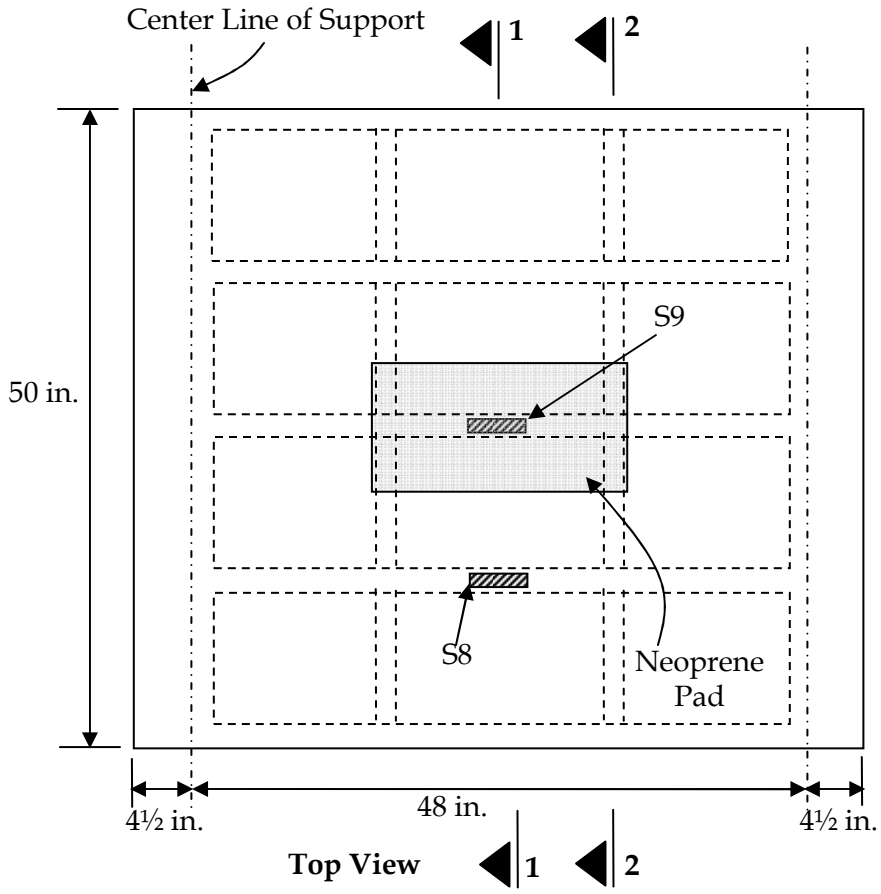

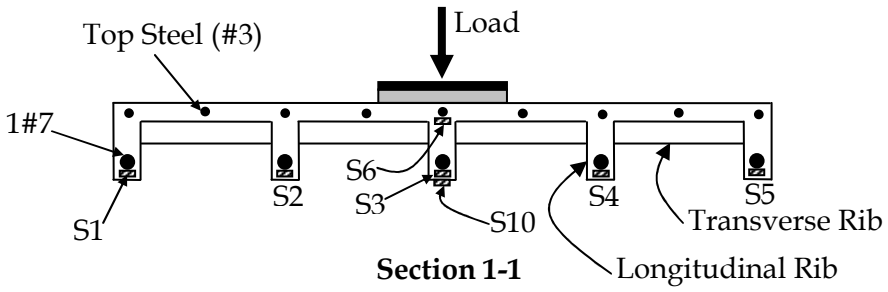

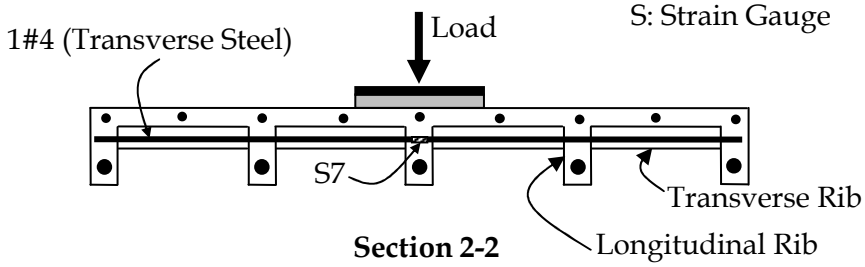

Figure 3.62 Instrumentation Plan and Loading Configuration for Specimen 4T1S

The load distribution between the ribs can be calculated based on the rebar strains at the bottom, which are 0.001, 0.0025, and 0.004, respectively for the external, side, and middle webs at the final load level. The distribution factor for the center unit is therefore 0.364, which means only 36.4% of the total load is carried by the middle unit. This value is very close to the factor derived from an elastic FE analysis during the preliminary design stage in Section 3.3. The reason is that all units behave within their linear range before failure, as shown by the load-strain curves. The flattening and drop in the load-deflection curve is attributed to the yielding and fracture of the longitudinal #4 rebar as this changed the load distribution between all ribs and caused punching shear failure when the entire load was finally concentrated on the middle rib.

The low strain value for the top rebar was expected as the neutral axis remained within the top flange. The top rebar will be effective to resist the negative moment at interior supports for multi-span specimens.

Figure 3.63 Test Setup for Specimen 4T1S

Figure 3.64 Shear Cracks in Specimen 4T1S

Figure 3.65 Bottom View of Punching Shear Pattern in Specimen 4T1S

Figure 3.66 Top View of Punching Shear Pattern in Specimen 4T1S

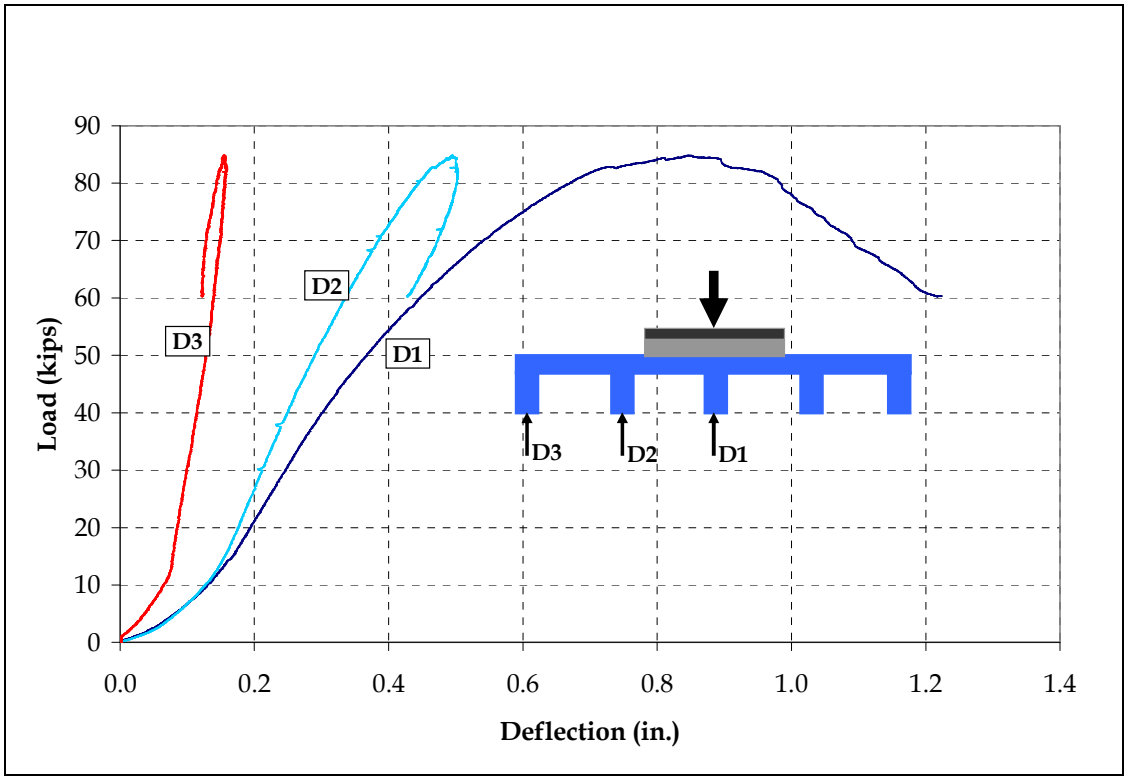

Figure 3.67 Load-Deflection Responses for Specimen 4T1S

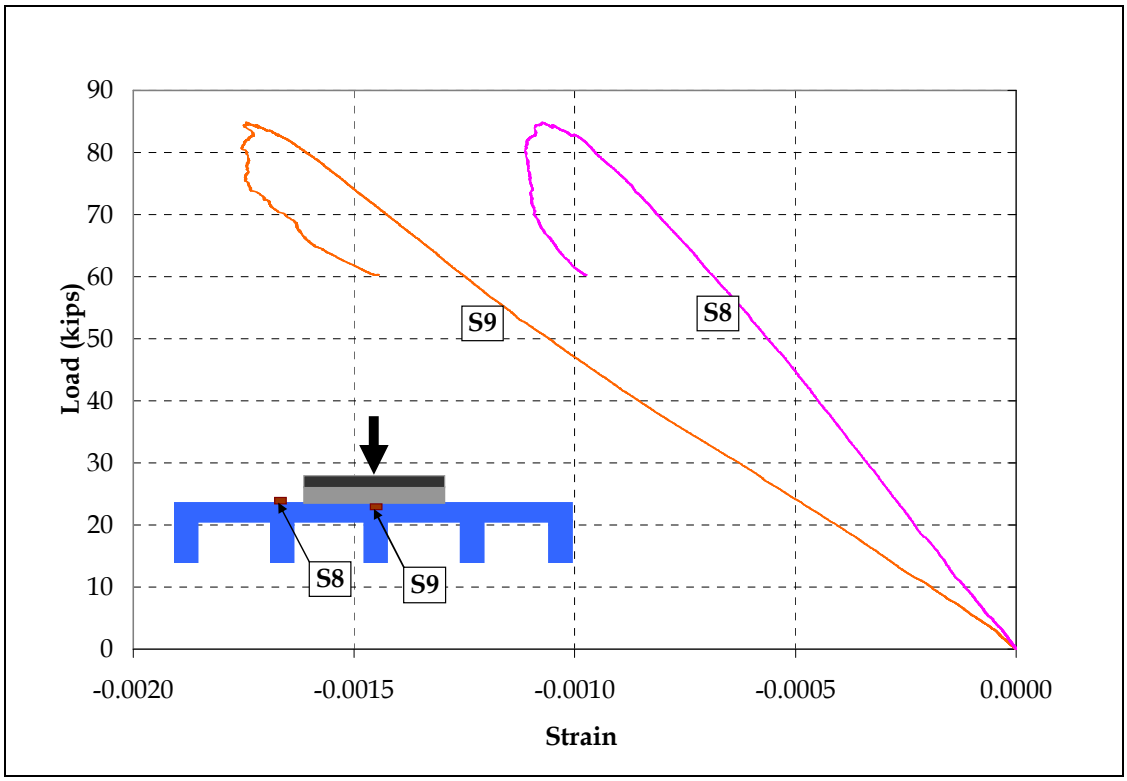

Figure 3.68 Top Concrete Strains in Specimen 4T1S

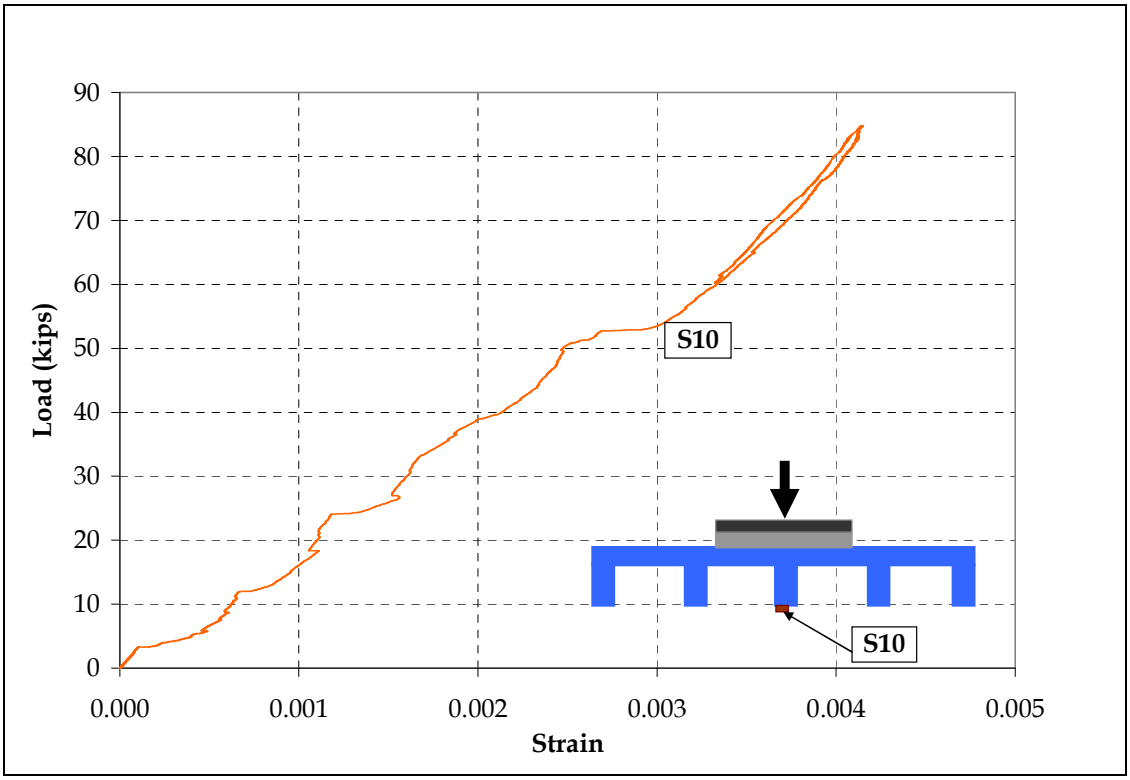

Figure 3.69 Bottom Concrete Strain at Mid-Span in Specimen 4T1S

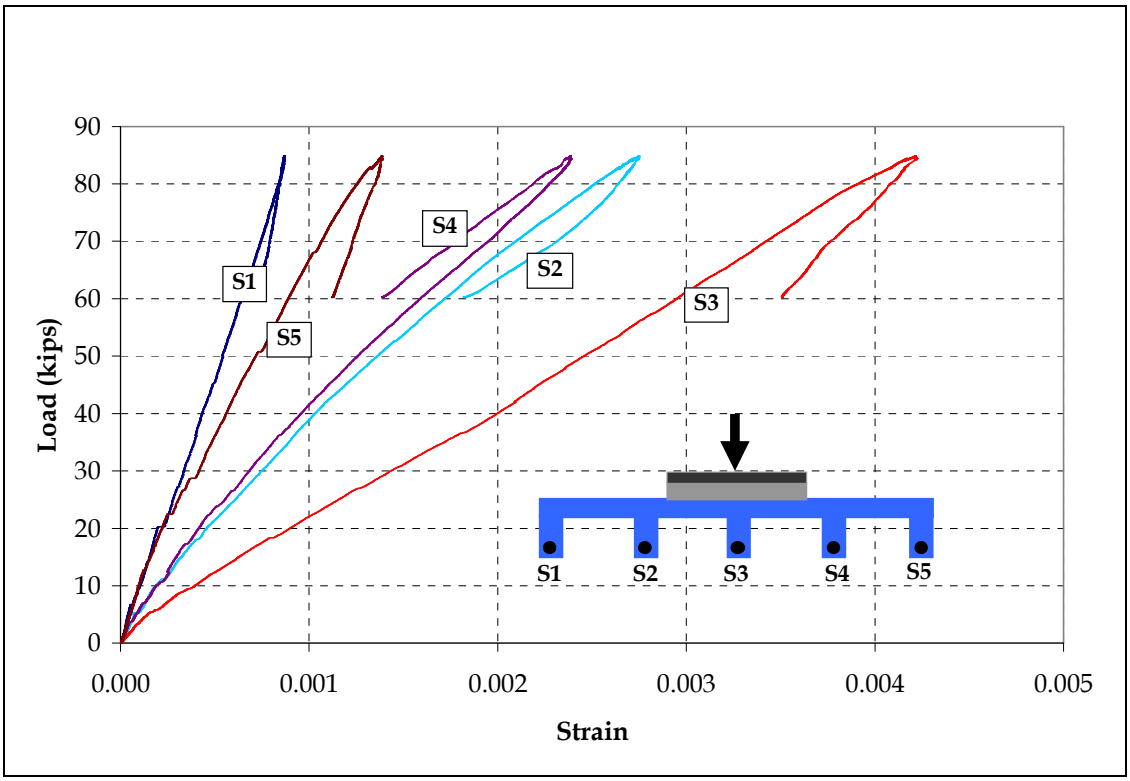

Figure 3.70 Bottom Steel Strains at Mid-Span in Specimen 4T1S

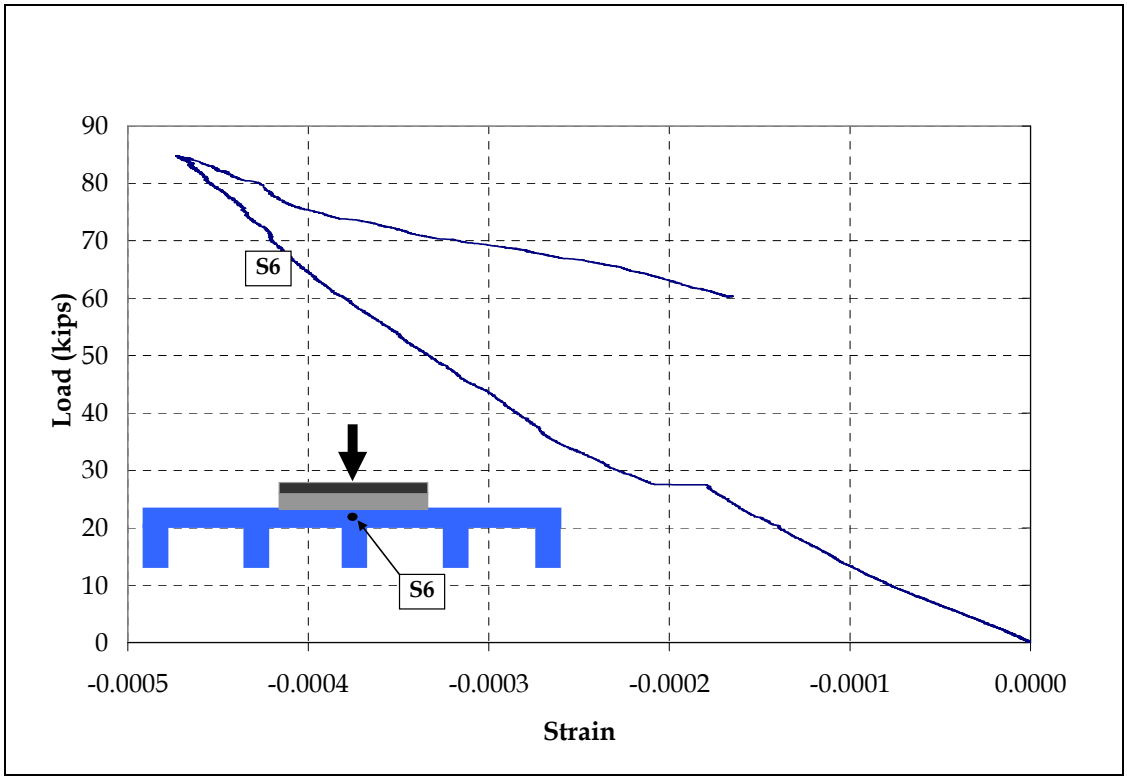

Figure 3.71 Top Steel Strain at Mid-Span in Specimen 4T1S

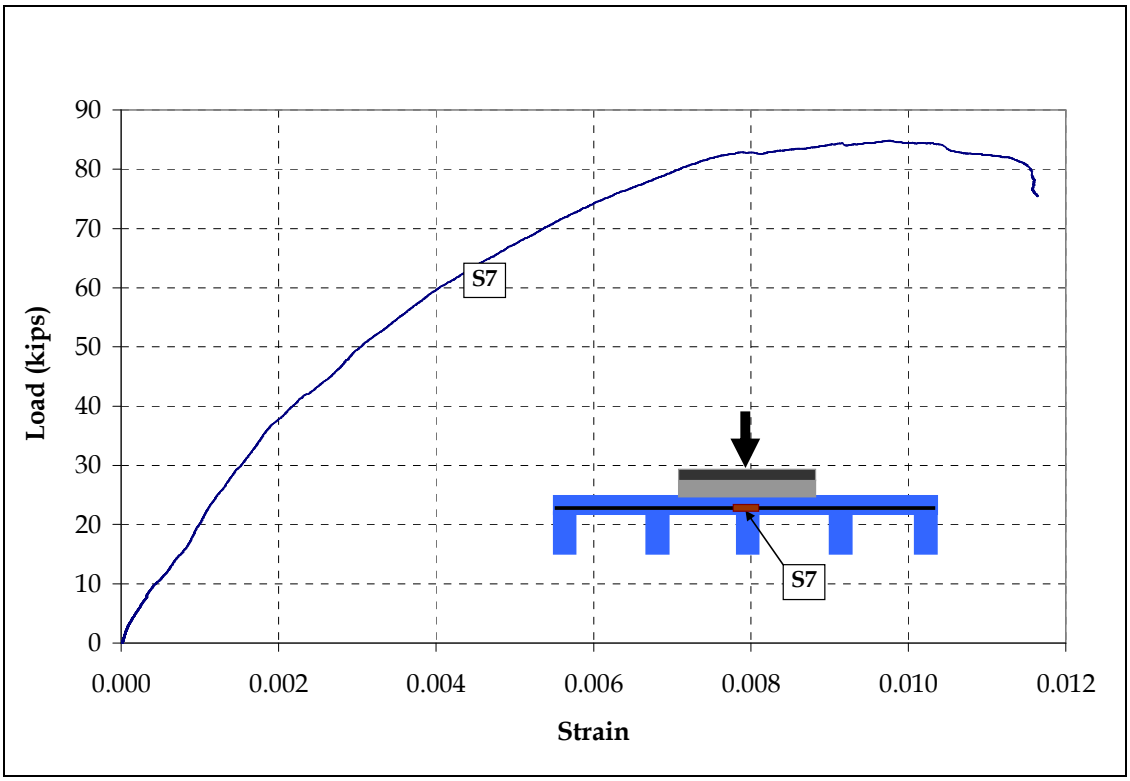

Figure 3.72 Transverse Steel Strain in Specimen 4T1S

3.4.4.4 Single-Unit Two-Span Specimen

Figures 3.73 to 3.77 show the instrumentation plan, loading configuration, test setup, and failure pattern of the single-T two-span (1T2S) specimen. The purpose of this test was to establish the behavior of the deck under negative moment. Figures 3.78 to 3.80 show the load-deflection and load-strain responses. Initially, the plan was to load the specimen beyond the plastic hinge formation at the interior support section. However, the test was stopped at 55 kips, when the spreader beam was about to touch the specimen due to excessive deflection. The first shear crack appeared near the interior support at 24 kips. At the later stages, shear cracks also appeared near the exterior supports with some flexural cracks at the two mid-spans.

It is evident that when the strain in the top rebar reaches 0.025, both the load-deflection and the load-strain curves begin to soften significantly. This may be attributed to the top rebar losing its bond strength at the cracked region. The gain in strength from rebar counteracts the loss from the pull-out of fibers. Therefore, large displacements occur with crack widening.

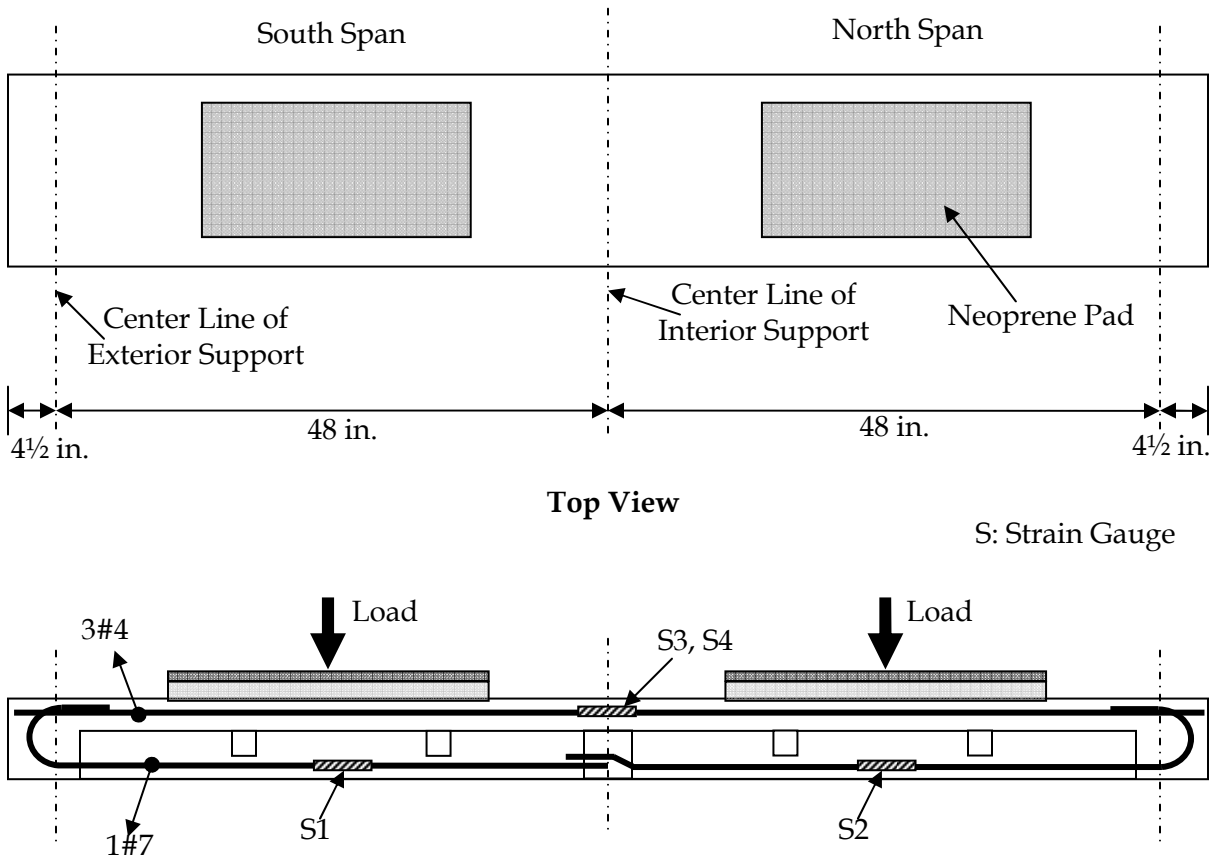

Figure 3.73 Instrumentation Plan and Loading Configuration for Specimen 1T2S

Figure 3.74 Test Setup for Specimen 1T2S

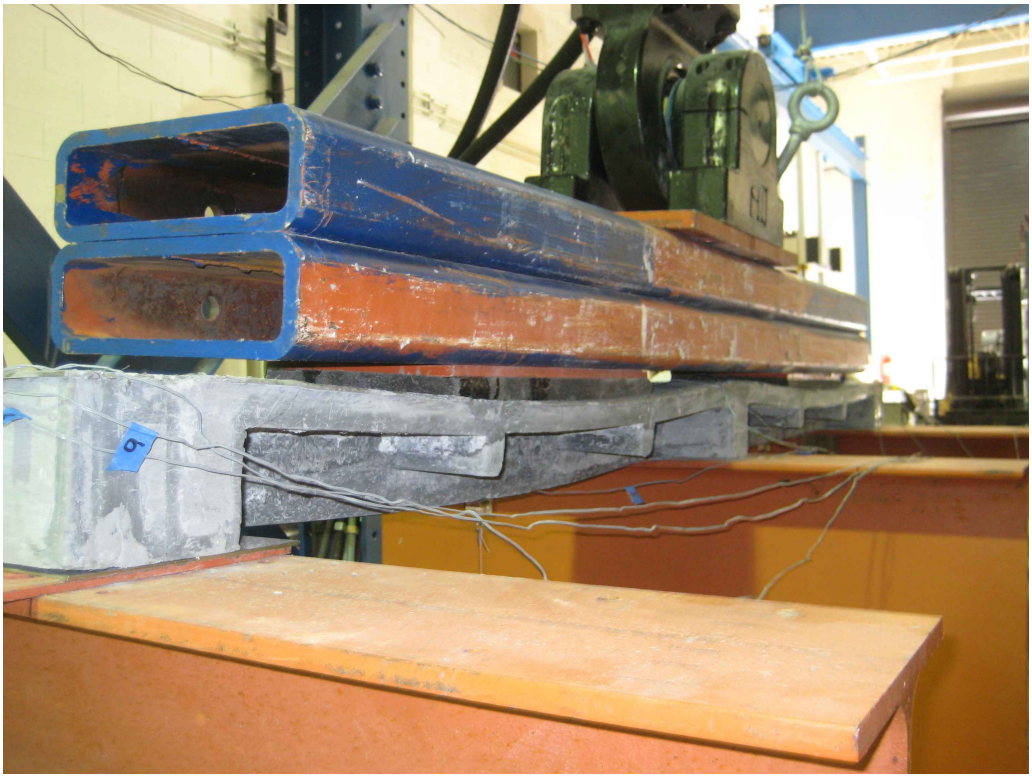
Figure 3.75 Deformed Shape of Specimen 1T2S at 55 kips

Figure 3.76 Shear Cracks in Specimen 1T2S

Figure 3.77 Flexural and Shear Cracks in Specimen 1T2S

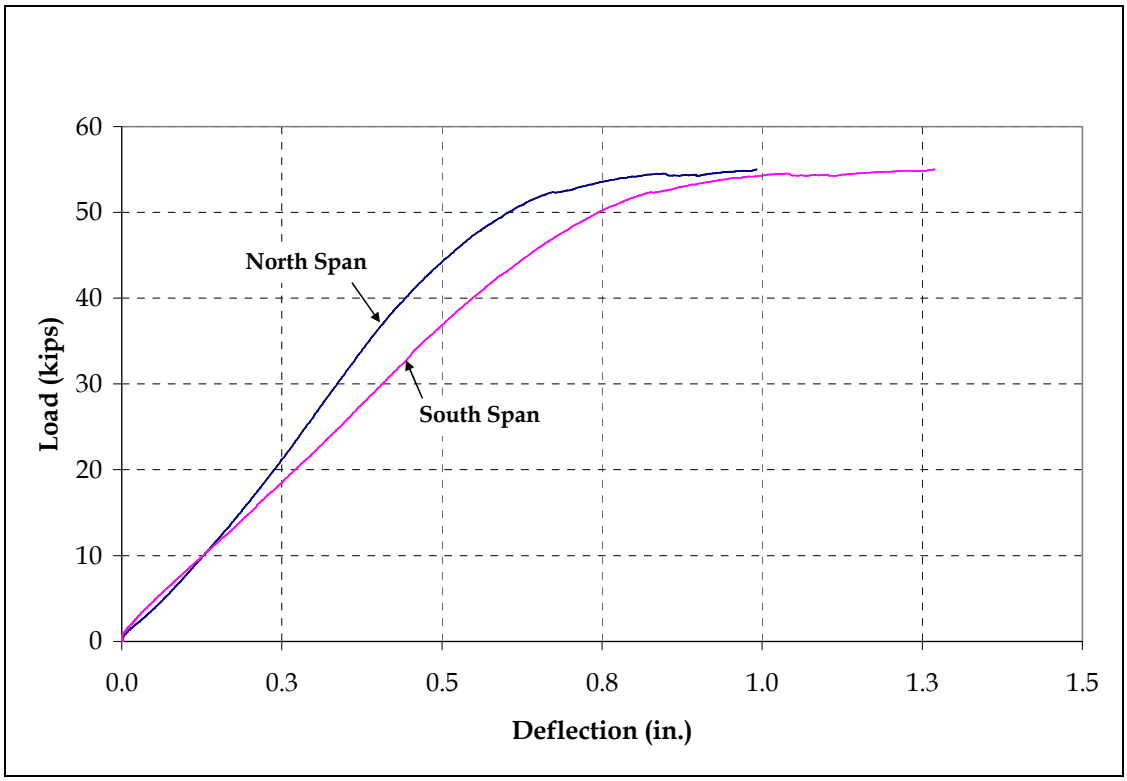

Figure 3.78 Load-Deflection Responses for Specimen 1T2S

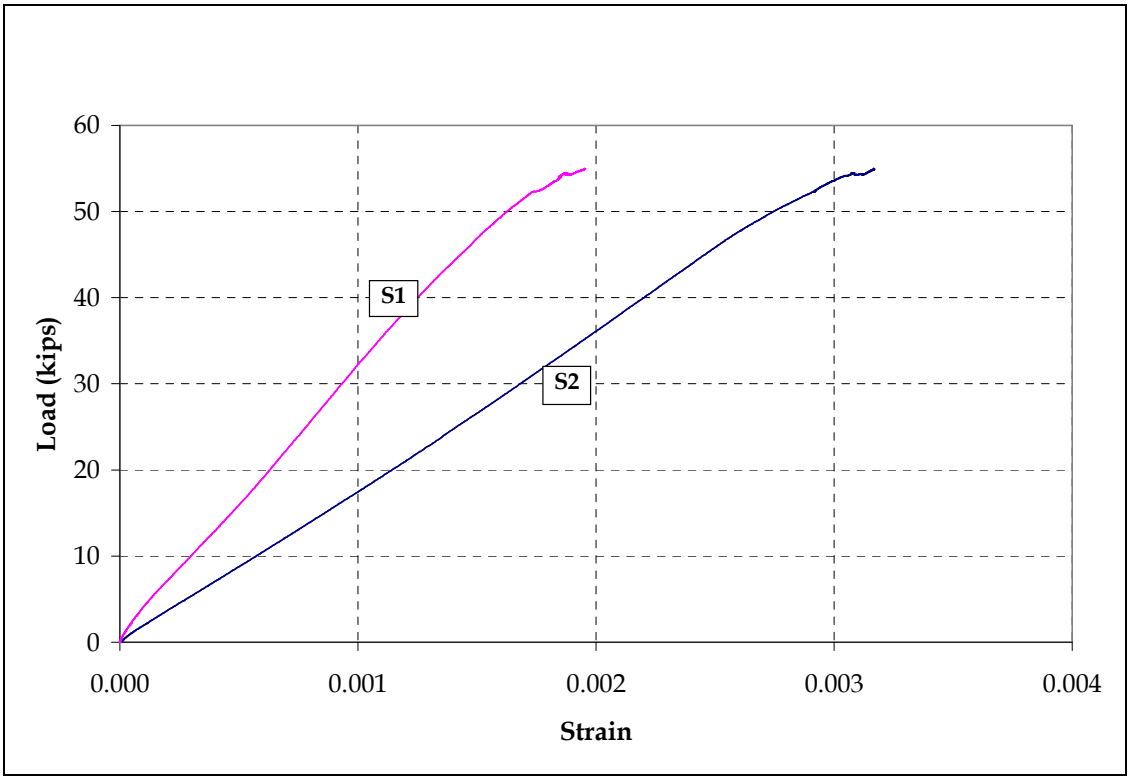

Figure 3.79 Bottom Steel Strains in Specimen 1T2S

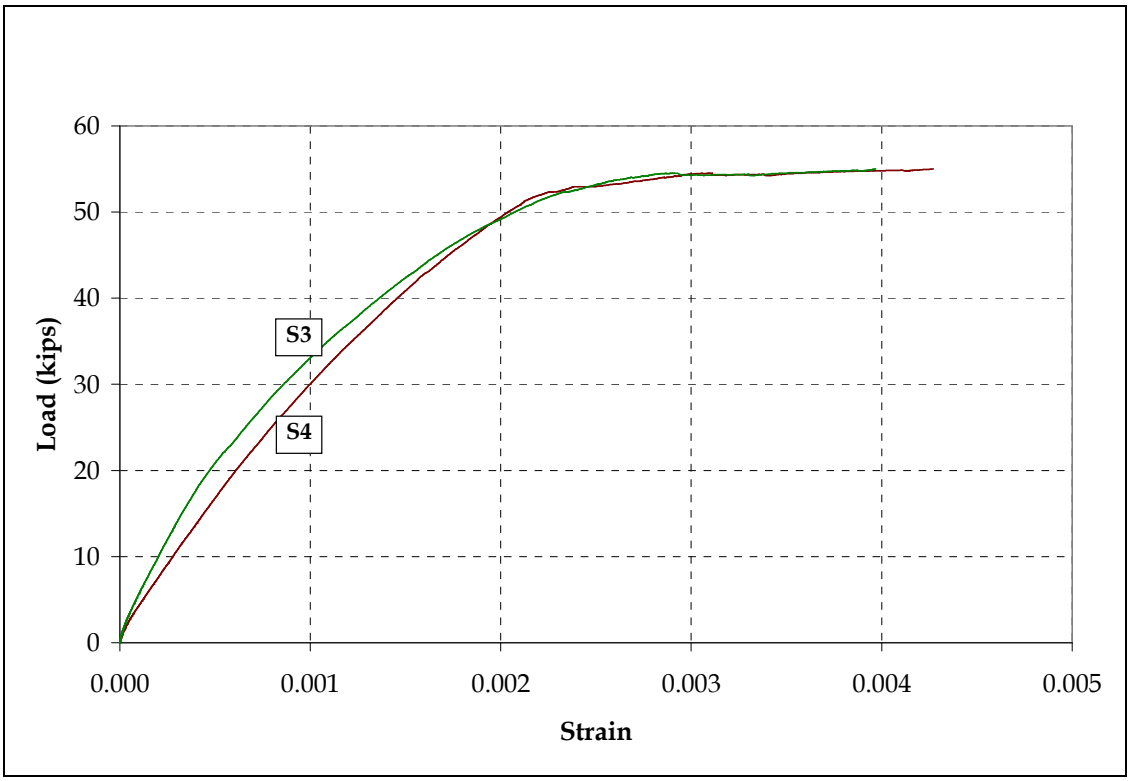

Figure 3.80 Top Steel Strains at Interior Support in Specimen 1T2S

3.4.4.5 Multi-Unit Two-Span Specimen

Figures 3.81 to 3.87 show the instrumentation plan, loading configuration, test setup, and failure pattern of the three-T two-span (3T2S) deck specimen. The objective of this test was to validate the design of the deck at the full-scale level. At the load of 49 kips, a flexural crack appeared in the top flange at the interior support section (see Figure 3.84), followed by the shear cracks on the two interior ribs near the interior support. These cracks kept on growing, which led to the punching of the neoprene pad into the flange. As the punching shear began, the top flexural crack at the support section closed. Punching was more prominent in the north span than the south span. Figures 3.88 to 3.96 show the load-deflection and load-strain responses. The total failure load was 147 kips, i.e., 73.5 kips for each span. This is almost twice the target load of 37.24 kips.

Load-deflection curves (Figures 3.88 and 3.89) show that the majority of the load was taken by the two interior ribs. The top concrete strain at mid-span did not reach its ultimate value of 0.003. However, the bottom compressive strain at the interior support section was very high (0.016), indicating the crushing of concrete. Figure 3.95 shows that the strain gauges at the interior support section on the top steel bars were damaged at around 90 kips. The crack that appeared in the top flange at the interior support section at 49 kips must have likely penetrated to the level of top steel bars and damaged the strain gauges. Similar to the 4T1S deck specimen, the transverse steel strain was high in this specimen, as well. The maximum transverse steel strain reached 0.027. Overall, the specimen performed very well and the target load was achieved.

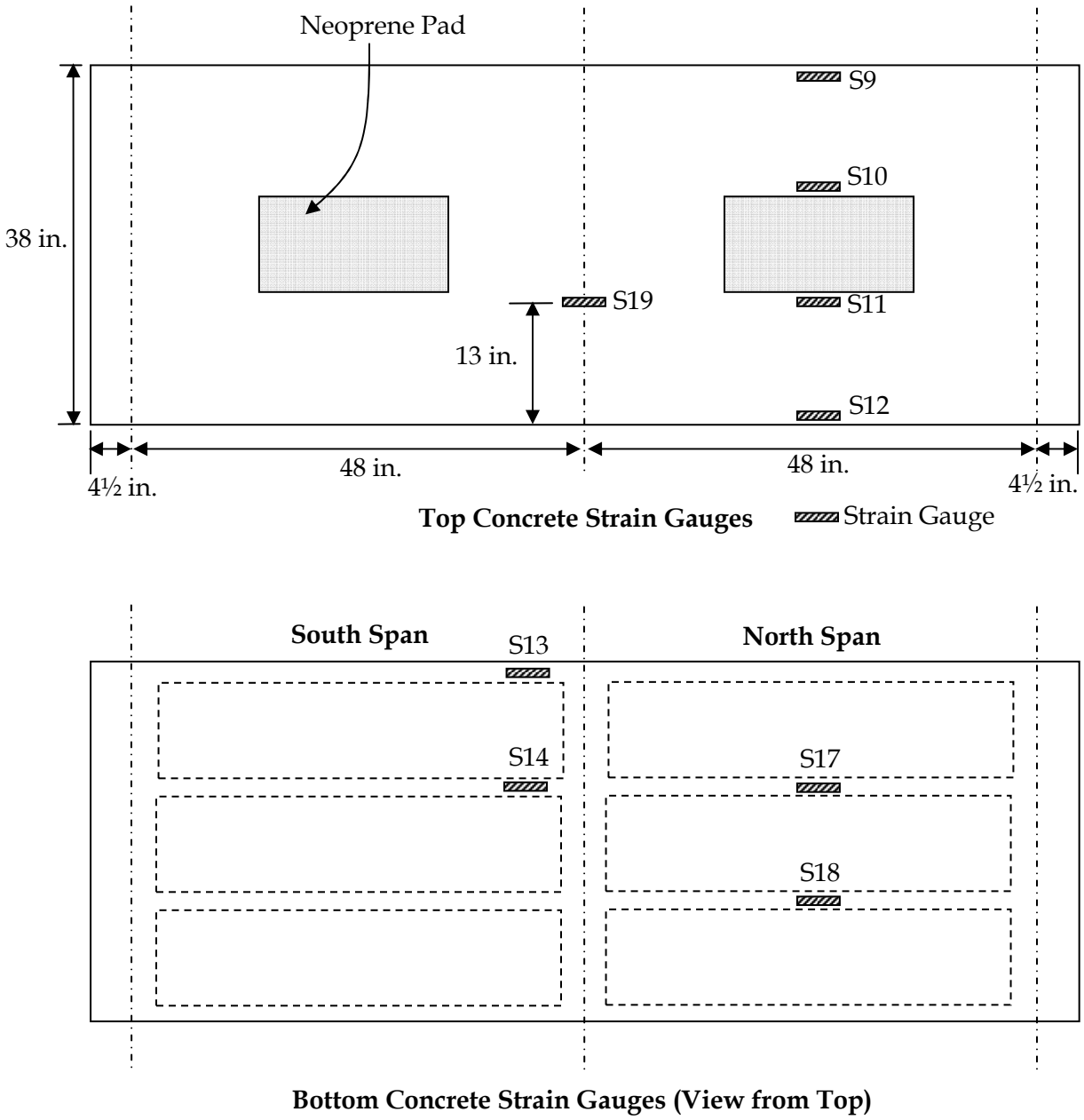

Figure 3.81 Arrangement of Concrete Strain Gauges and Loading Configuration for Specimen 3T2S

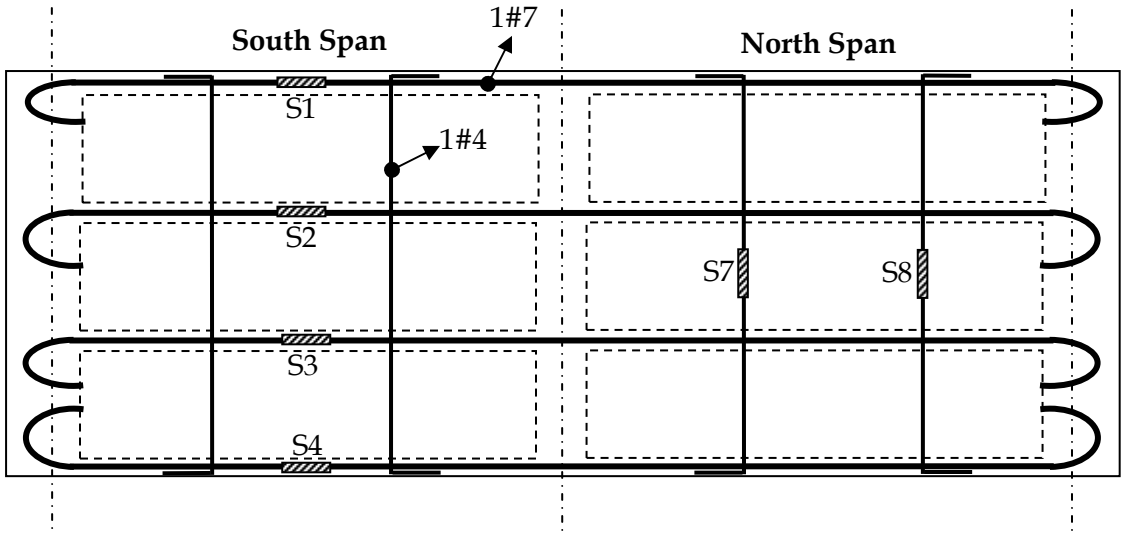

Arrangement of Strain Gauges on Bottom Steel Rebars (View from Top)

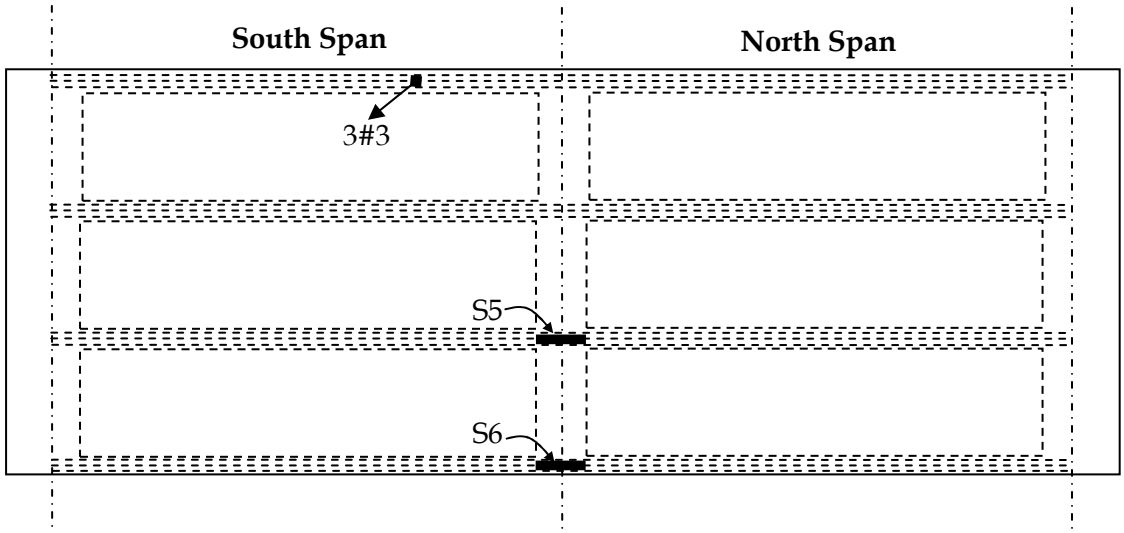

Arrangement of Steel Strain Gauges on Top Steel Rebars (View from Top)

Figure 3.82 Arrangement of Strain Gauges on Steel Rebars in Specimen 3T2S

Figure 3.83 Test Setup for Specimen 3T2S

Figure 3.84 Top Flexural Crack at the Interior Support of Specimen 3T2S

Figure 3.85 Shear Cracks near the Interior Support of Specimen 3T2S

Figure 3.86 Bottom View of Punching Shear Pattern in Specimen 3T2S

Figure 3.87 Top View of Punching Shear Pattern in Specimen 3T2S

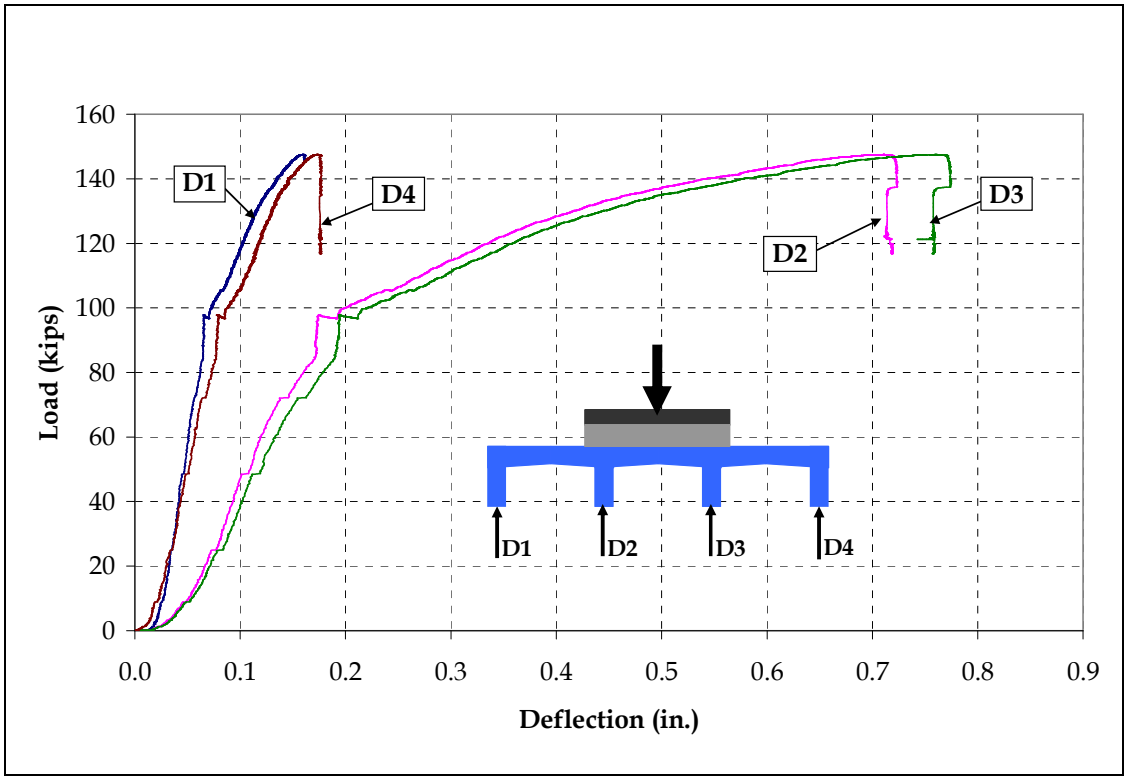

Figure 3.88 Load-Deflection Responses for the North Span of Specimen 3T2S

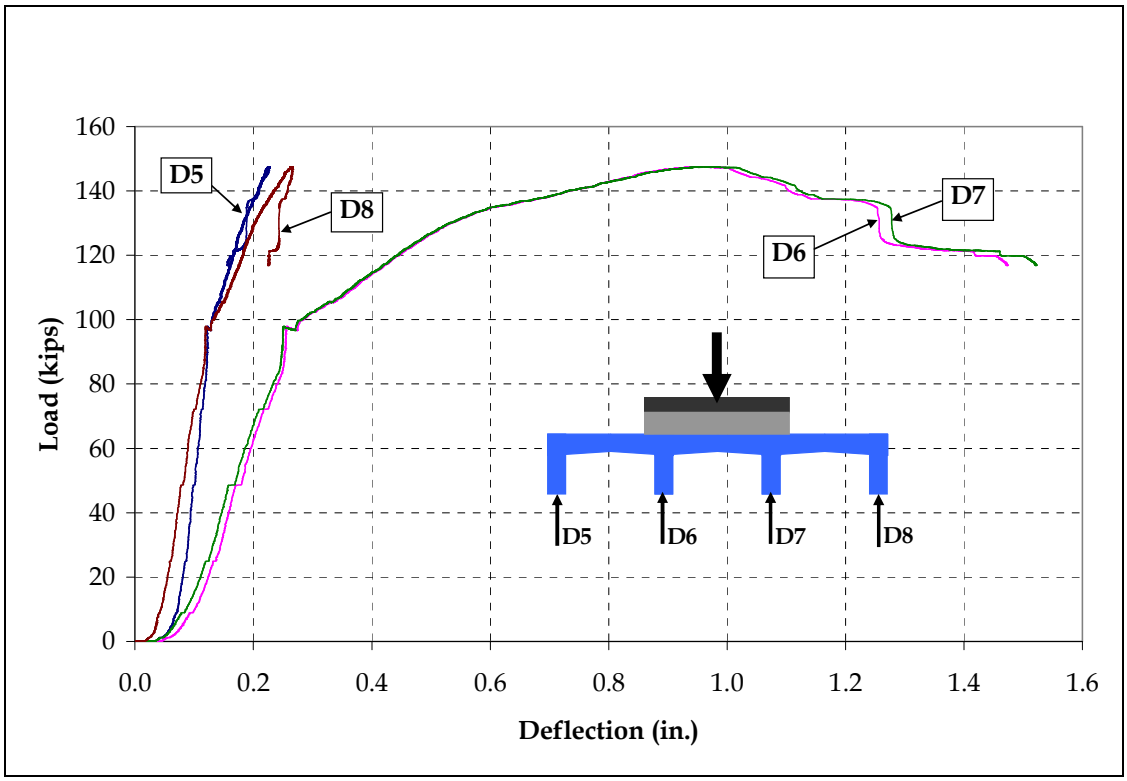

Figure 3.89 Load-Deflection Responses for the South Span of Specimen 3T2S

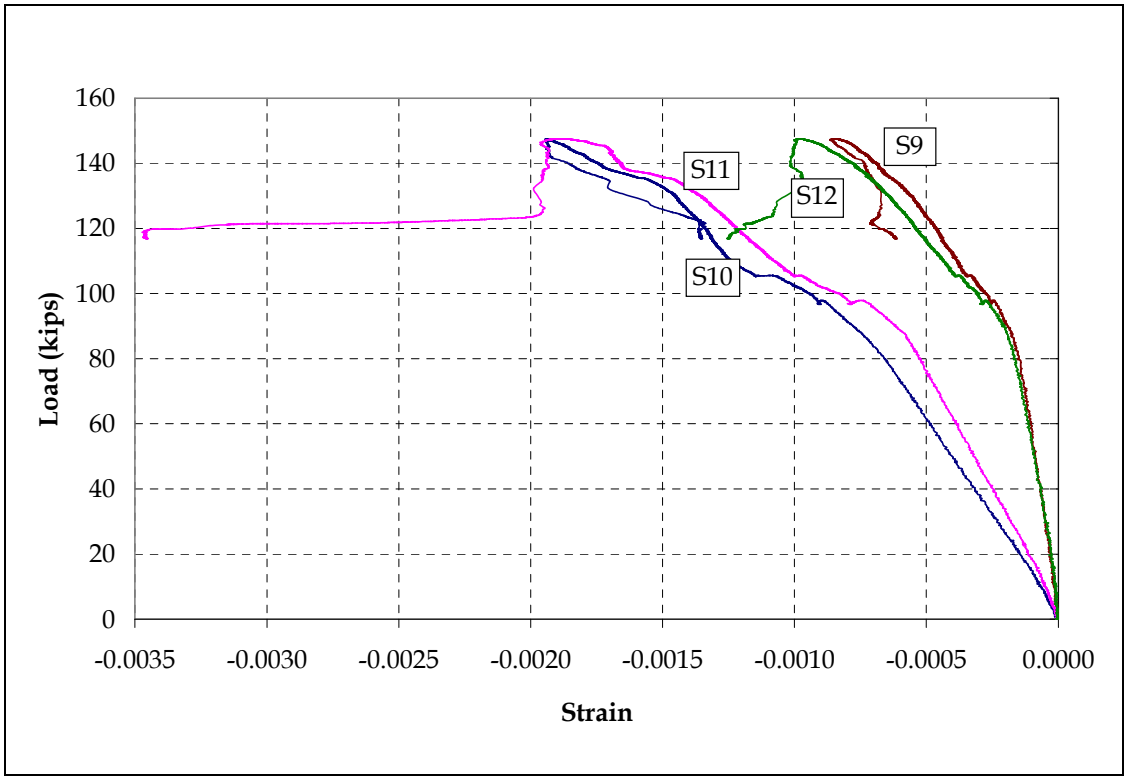

Figure 3.90 Top Concrete Strains in Specimen 3T2S

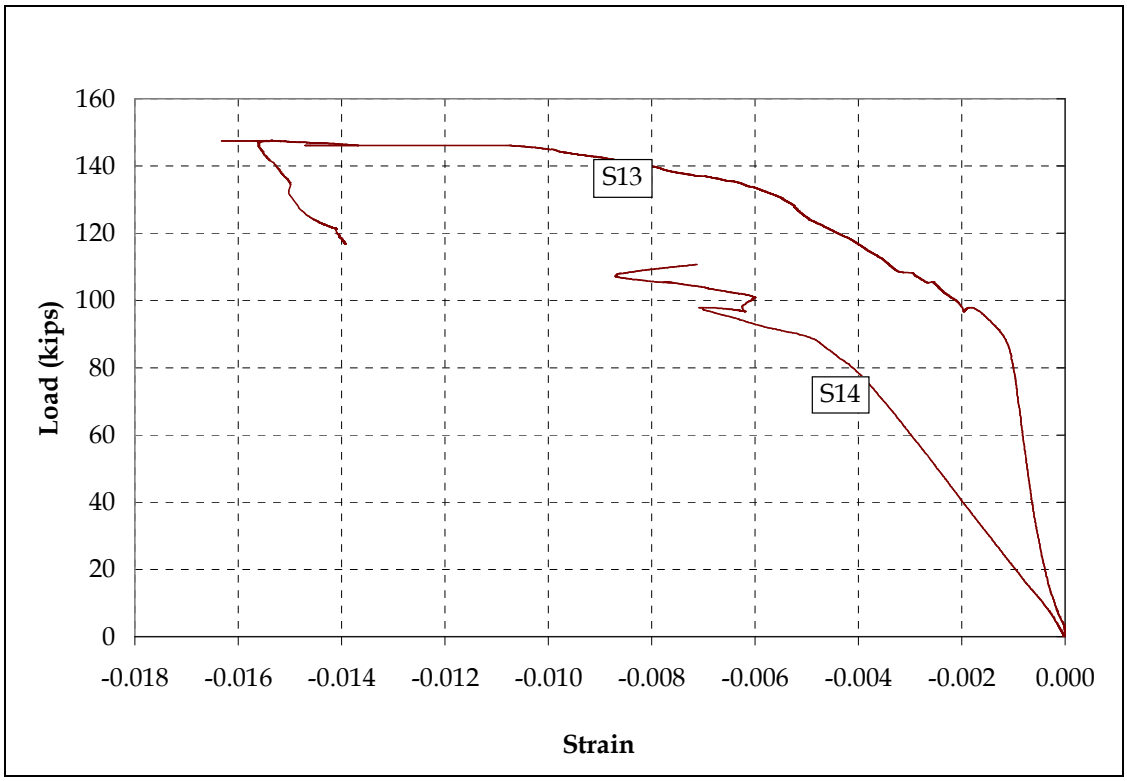

Figure 3.91 Bottom Concrete Strains at the Interior Support of Specimen 3T2S

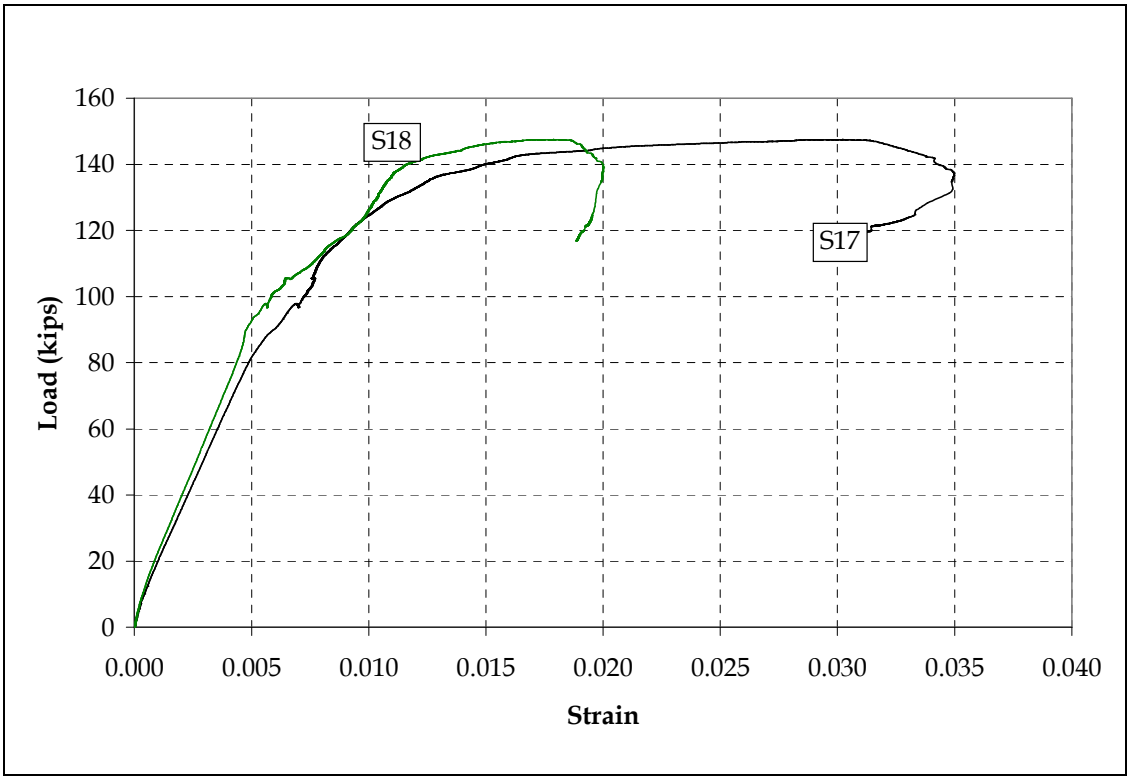

Figure 3.92 Bottom Concrete Strains at the Mid-Spans of Specimen 3T2S

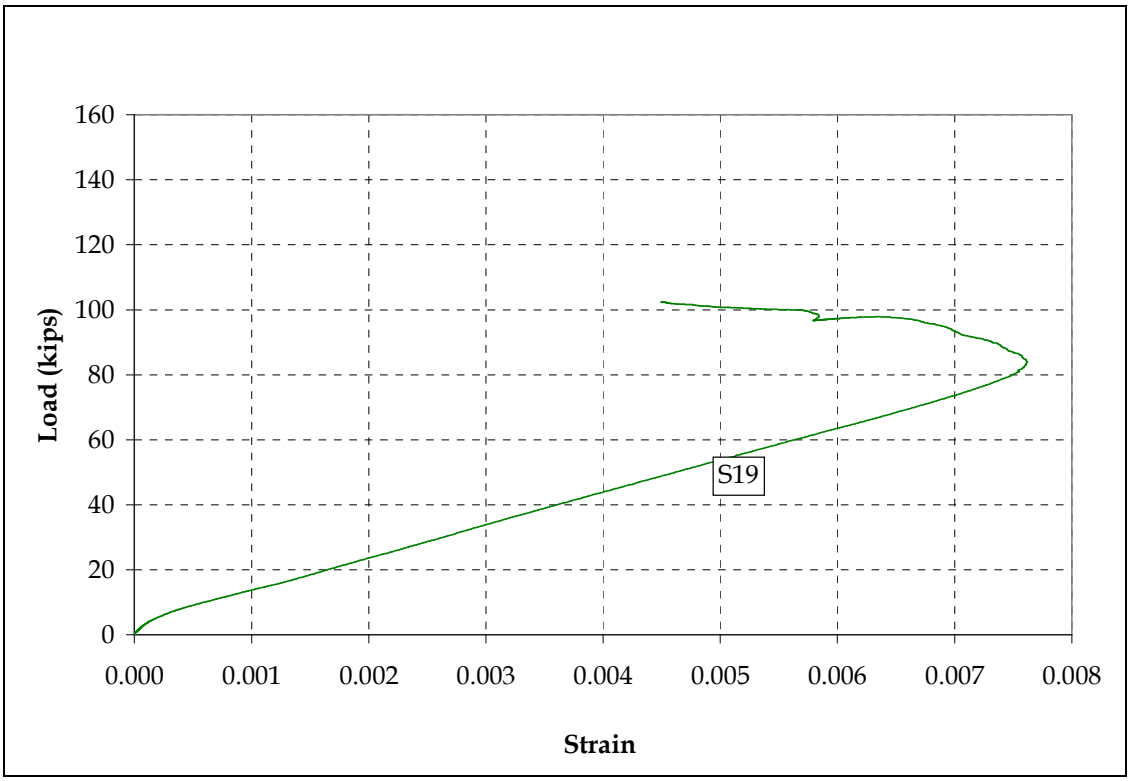

Figure 3.93 Top Concrete Strain at the Interior Support of Specimen 3T2S

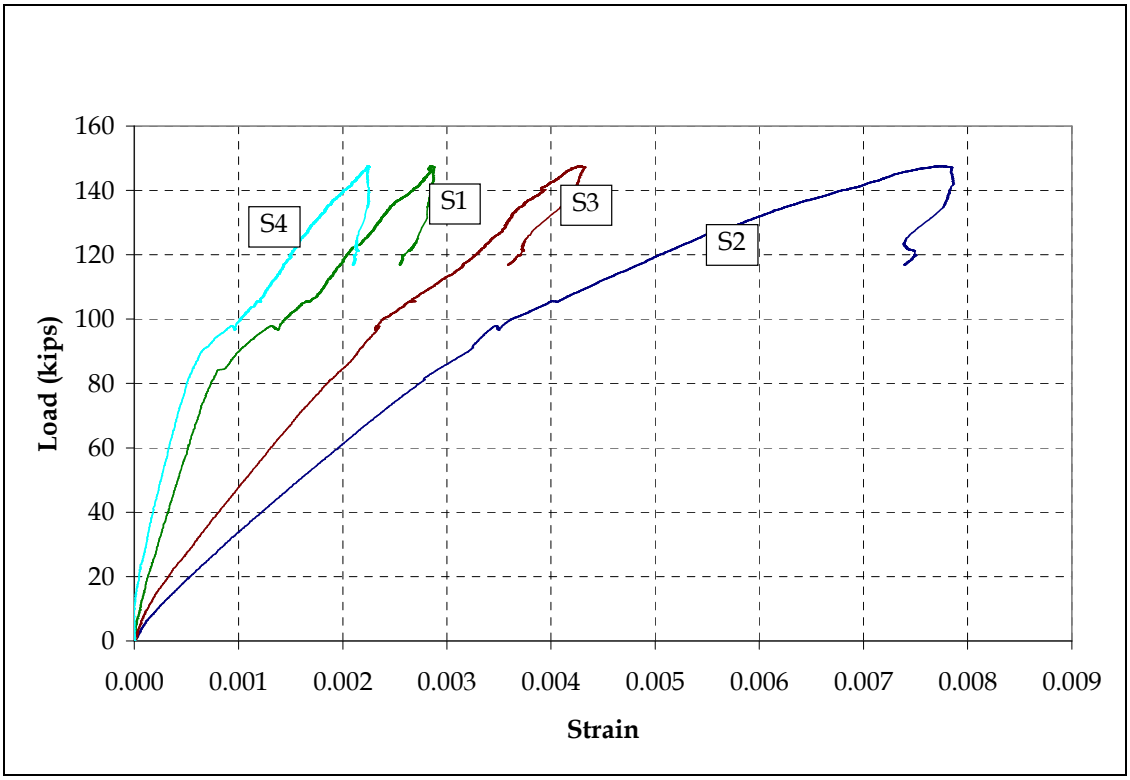

Figure 3.94 Bottom Steel Strain at the Mid-Spans of Specimen 3T2S

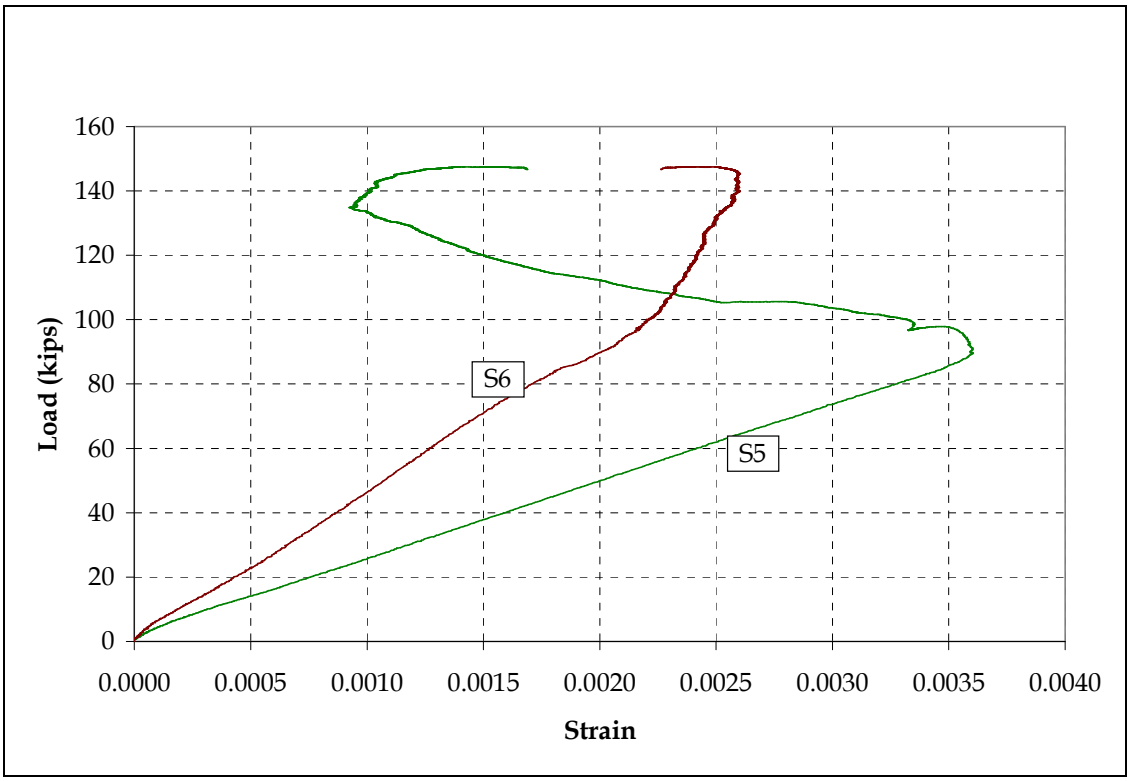

Figure 3.95 Top Steel Strains at the Interior Support of Specimen 3T2S

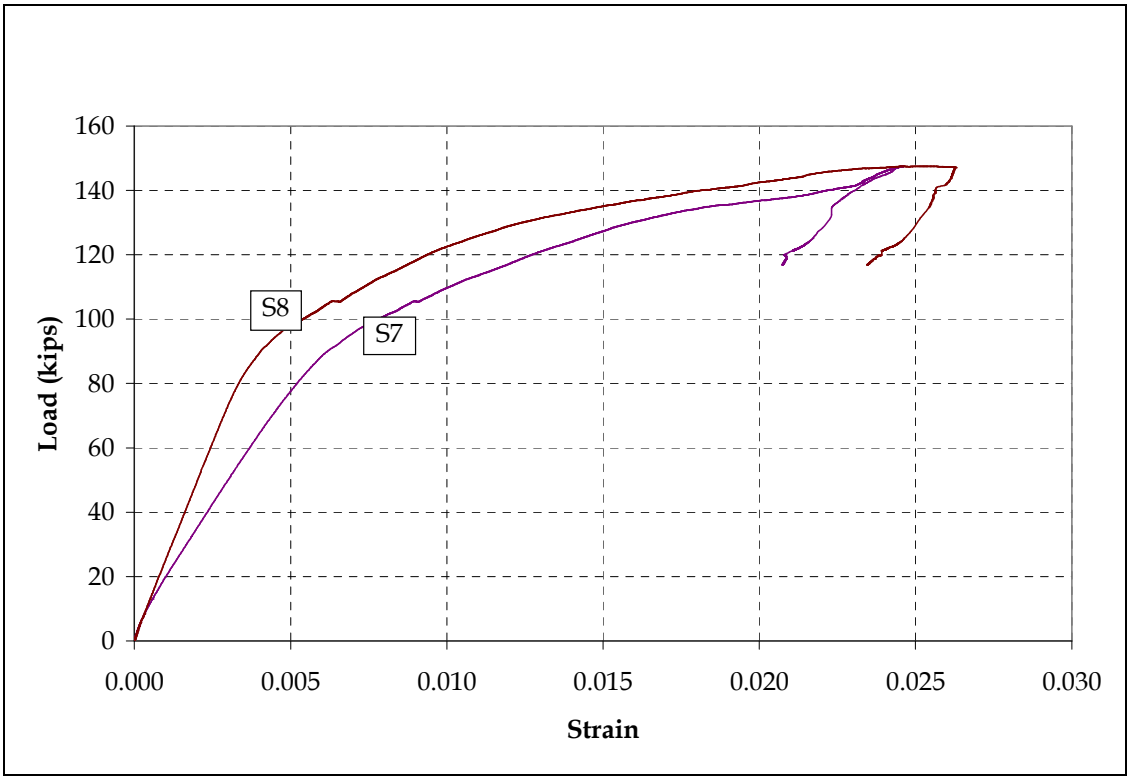

Figure 3.96 Transverse Steel Strain in Specimen 3T2S

3.4.4.6 Comparison of Component Specimens

Figures 3.97 and 3.98 show the comparisons of load-deflection and normalized moment-deflection responses for all specimens, respectively. It is clear that all single-unit specimens have comparable stiffness. Considerable difference in the stiffness and ultimate loads of 4T1S and 3T2S specimens indicates the lateral distribution of load, as expected. The ultimate mid-span load for the four-unit specimen (4T1S) is almost twice as that of the maximum ultimate load for the single-unit (1T1S) specimens. The normalized moment-deflection graph illustrates however that by increasing the number of units the ultimate load does not increase proportionally.

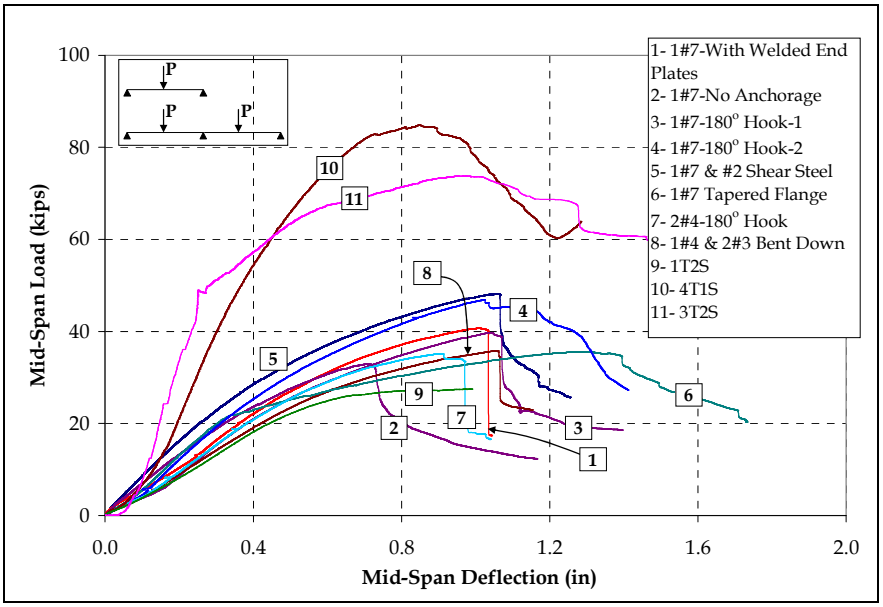

Figure 3.97 Comparison of Load-Deflection Responses for Ductal®-MMFX Steel Deck Specimens

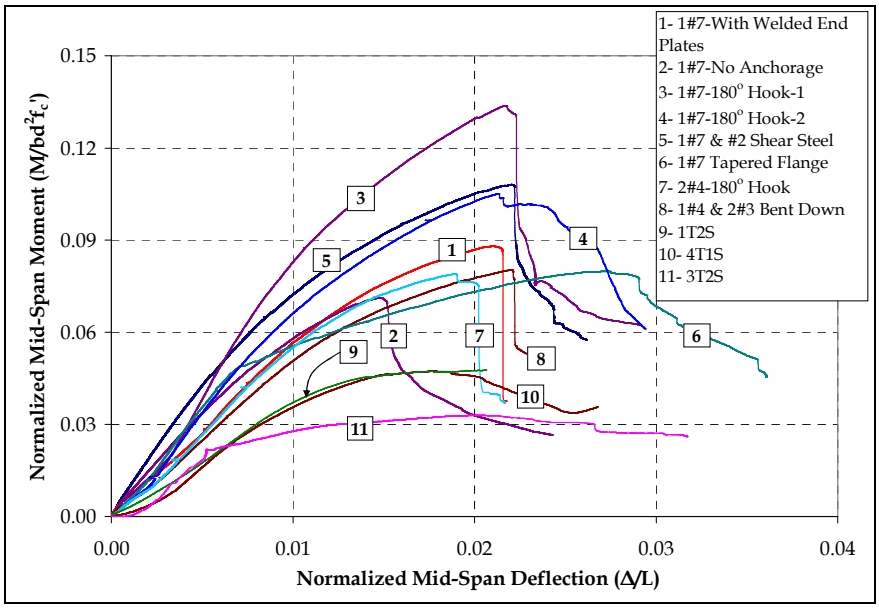

Figure 3.98 Comparison of Normalized Mid-Span Moment-Deflection Responses for Ductal®-MMFX Steel Deck Specimens

3.4.5 Forensic Examination of Specimens after Load Testing

In order to examine the bond between MMFX and Ductal® as well as to assess the distribution of steel fibers, two 1T1S specimens, (one with 180° hook and another with tapered flange, both from Casting No. 3) were cut after the load testing. The blocks cut off from the specimens were numbered, as shown in Figure 3.99.

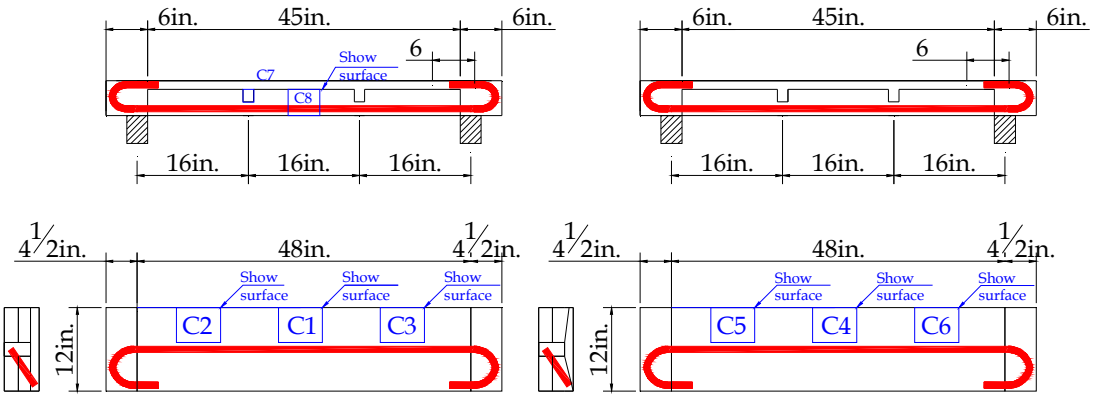

Regular Section Tapered Flange Section

Figure 3.99 Sections Cut From Test Specimens

The photos taken for blocks C1 (C2 and C3 are similar) and C6 (C4 and C5 are similar) are shown in Figure 3.100. These were cut from the flanges. Blocks C1 to C3 were cut from the specimen with 180° hook and had one #3 rebar in the cutting plane. The rebars in the tapered specimen were closer to the web, thus blocks C4-C6 did not include any rebars. It is interesting to note that the #3 rebar bonds well with Ductal® even with less than ½ in. cover. The fibers are the shiny white spots on the surface because of the light reflection on the metal surface. All three cuts from the tapered section show a no-fiber region on top of the flanges with an average depth of about 0.4 in. This was not as prevalent in the specimens with constant flange thickness, perhaps due to the presence of 3 rebar at the top. The photos for blocks C7 and C8 are shown in Figure 3.101. No debonding was noted in either case. Moreover, ample fibers surround the rebar.

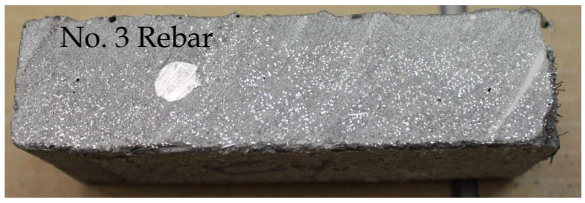

(a) Block C1

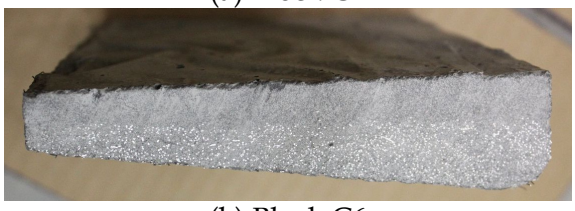

(b) Block C6

Figure 3.100 Image of Blocks C1 and C6

(a) Block C7 (b) Block C8

Figure 3.101 Images from Blocks C7 and C8

3.5 Analytical Work

3.5.1 Shear Resistance

According to the French code, which is the most widely used code for UHPC, the shear resistance of a reinforced UHPC beam is the sum of the contributions from concrete, fibers, and shear reinforcement. The shear reinforcement can be either bent up rebars or stirrups. Shear strength of specimens without shear reinforcement is given by:

$$V_{Rb} = \frac{1}{\gamma_E}\frac{0.21}{\gamma_b}k\sqrt{f_{cj}}b_w d \tag{3.1}$$

where k is the parameter accounting for the normal stress caused by the applied compressive loads, f_{cj} is the nominal compressive strength (in MPa), b_w is the width of the web, d is the depth of tension steel, and γ_E and γ_b are design parameters, specified in detail in the French code. The shear strength of the tested specimen is 8.7 kips using the above equation. This represents an applied load of 17.4 kips, at which level shear cracks start to open.

The contribution from fibers is given by

$$V_f = \frac{S\sigma_P}{\gamma_{bf}\tan(\beta_u)} \tag{3.2}$$

where $\sigma_P = \frac{1}{K}\frac{1}{w_{\lim}}\int_0^{w_{\lim}}\sigma(w)dw$ is the average post-crack stress along the section height calculated based on the crack width, S is the cracked area where fibers have an influence, β_u is 45° for passive reinforcement, and K is the fiber orientation factor to consider the discrepancy of fiber orientation distribution and serves as a strength reduction factor. Using γ_{bf} of 1.0, K of 1.0, and S of the web area, the shear contribution of fibers would range between 4 and 8 kips, depending on the estimated average post-crack stress. The maximum contribution would be 16 kips assuming full post-crack strength at the web area.

The total ultimate load considering contributions from concrete and fibers is between 25.4 to 31.4 kips. The shear resistance estimated using the French code is relatively lower than the test results for Specimen 1T1S with 180° hooks, but closer to the ultimate load of Specimen 1T1S without any anchorage.

3.5.2 Flexural Resistance

Three 1T1S specimens were selected for the moment-curvature and load-deflection analyses to determine flexural resistance of the proposed deck system. They include 1T1S with 180° hooks, 1T1S with two #4 rebars, and 1T1S with tapered flange, all of which were made from the third casting.

Figure 3.102 shows the stress-strain models in tension and compression used for the moment-curvature analysis. No heat treatment was considered, as was the case for the experiments. On the compression side, the models are linear with an elastic modulus of 6,000 ksi until the compressive strength from cylinder tests is reached, after which the stress remains constant until the material crushes at a compressive strain of 0.005. No residual strength is considered afterwards.

On the tension side, three models from the literature (MIT, Soft, and French) are shown in the figure. Because the tensile properties of Ductal® do not significantly affect the load-carrying capacity of the specimens, the material model with the constant softening (the so-called soft model) was chosen for the analysis, with a softening modulus of 5 ksi.

For the MMFX bars, stress-strain response curve obtained from the uniaxial tension test, as shown earlier in Figure 3.14, was used in the analysis.

The load-deflection response curve was developed using the virtual work method from the sectional moment-curvature relations. Figures 3.104 and 3.105 show the comparisons of experimental and analytical load-deflection curves for the two 1T1S specimens with one No. 7 and two No. 4 bars, respectively. Clearly, the method underestimates the ultimate load-carrying capacity of both beams.

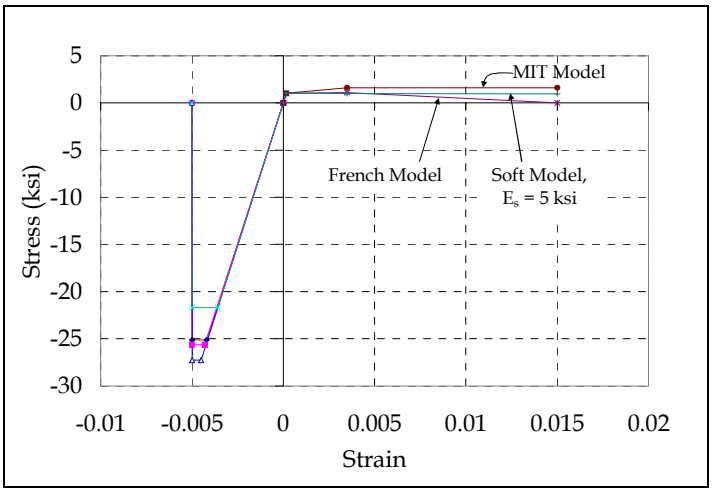

Figure 3.102 Stress-Strain Models used for Moment-Curvature Analysis

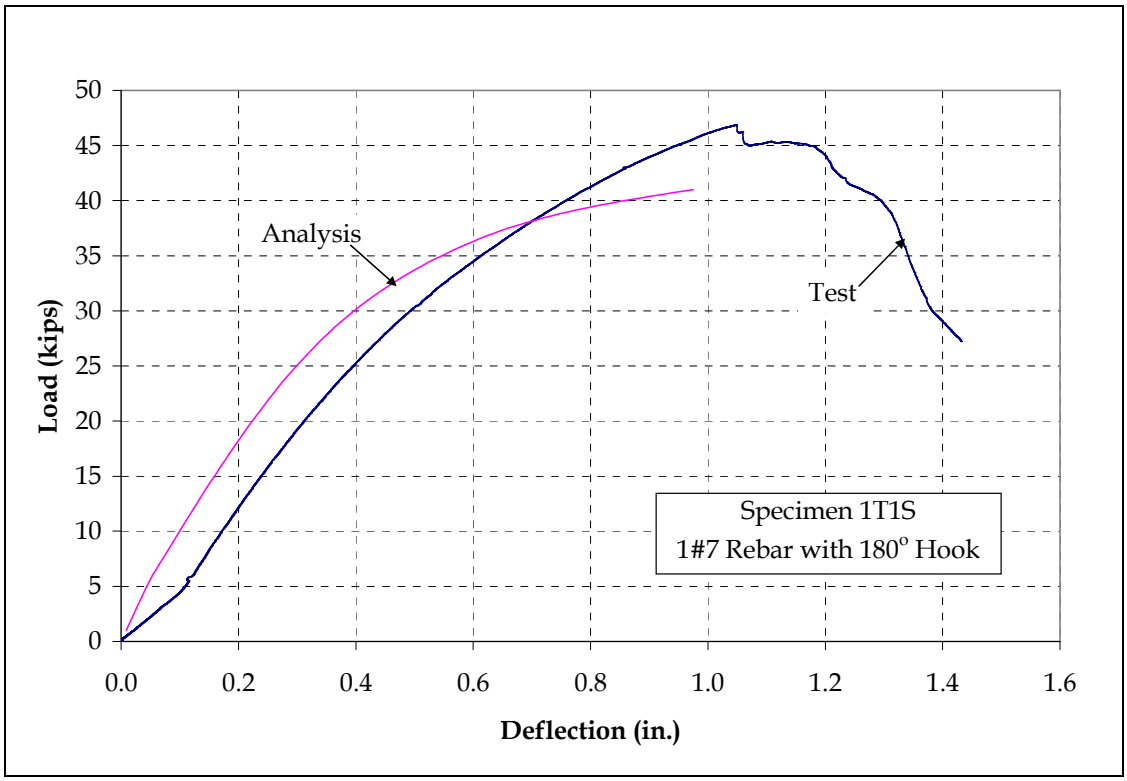

Figure 3.103 Comparison of Analytical and Experimental Results

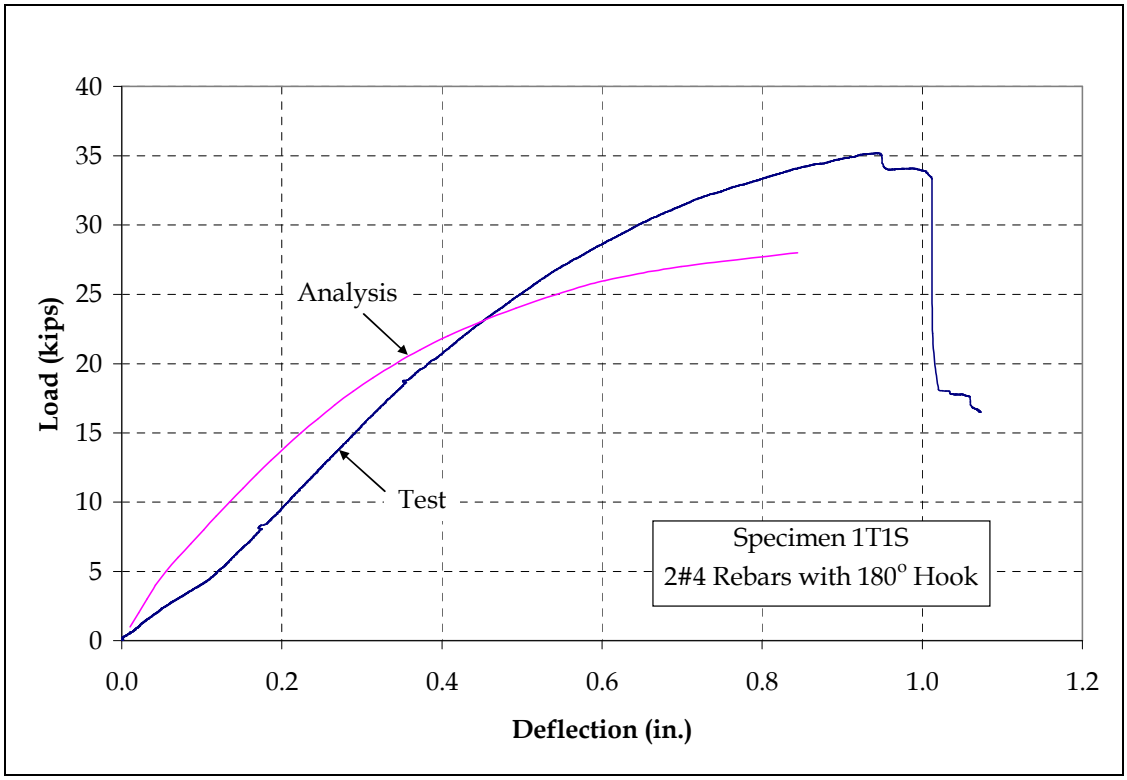

Figure 3.104 Comparison of Analytical and Experimental Results

Figure 3.105 compares the experimental and analytical load-deflection response curves for the 1T1S specimen with tapered flange. The analysis was carried out with both MMFX and mild steel reinforcement, whereas the experiment, as discussed earlier, inadvertently included mild steel reinforcement instead. The initial stiffness of the specimen for both types of reinforcement is the same from the analysis.

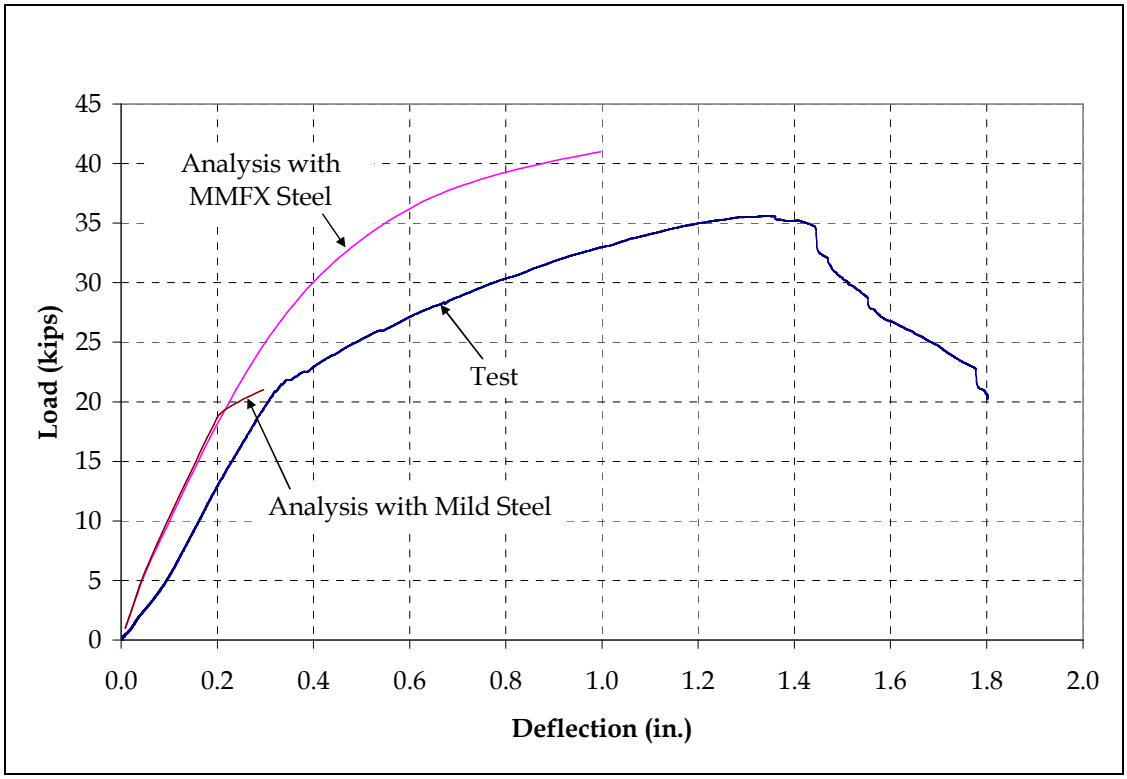

Figure 3.105 Comparison of Analytical Results with Test Data for 1T1S Specimen with Tapered Flange

3.5.3 Finite Element Analysis

Finite element analysis was performed using MSC.Marc®, a commercial software suitable for nonlinear analysis. The single-unit T-beam model (1T1S) as well as the multi-span, multi-unit models (1T2S, 4T1S, 3T2S) were developed using the available elements in the software.

Ductal® was modeled as an elastic-perfectly plastic material with von Mises yield surface. The equivalent yielding stress was set equal to the uniaxial compressive strength of the material.

For tensile properties of Ductal®, the softening material model built in MSC.Marc® was used. This model is quite similar to that used in the moment-curvature analysis with the stress softening behavior, as shown in Figure 3.106. The input parameters for the material model are shown in Table 3.4.

Table 3.4 Material Parameters Used for Ductal® FE Analysis

Item	Description	Typical Value
E	Modulus of elasticity	6,000 ksi
μ	Poisson's ratio	0.17
E_s	Softening modulus	5 ksi*
f_t	Cracking stress	1.125 ksi
f_c	Compressive strength	28 ksi (Untreated)
ε_{crush}	Plastic strain	0.0001
γ_{shear}	Shear retention factor	0.1

*This value is calibrated based on the analyses on the prisms, as shown in the following section.

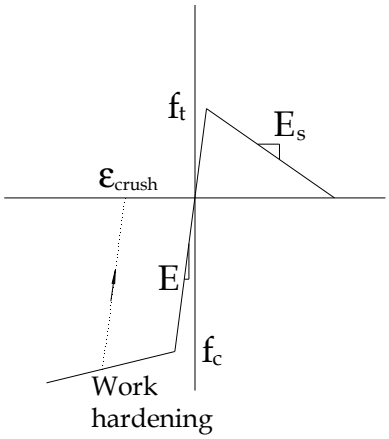

Figure 3.106 Softening Material Model

Cracking was identified by comparing the maximum principal stress with the first cracking stress. Cracked element was treated as orthotropic. The stress that could transfer perpendicular to the cracks would decrease along with the opening of the crack. The reduction in stress would be proportional to the crack opening, which is measured in terms of cracking strain. The relation between cracking strain and the stress loss is the softening modulus E_s. Once the stress is decreased to zero, the crack opening would be treated as permanent, and the stress would remain as zero. MMFX bars were modeled with nonlinear elastic strain hardening.

The model was calibrated using the four-point bending tests of treated and untreated prisms from the literature. The results from the experiment, literature, and FE analysis are plotted in Figure 3.107. The FE model matches the general load-deflection trend of test results and provides conservative values. In order to consider the untreated material properties, the first cracking stress was set to 1.125 ksi, as shown earlier in Table 3.4.

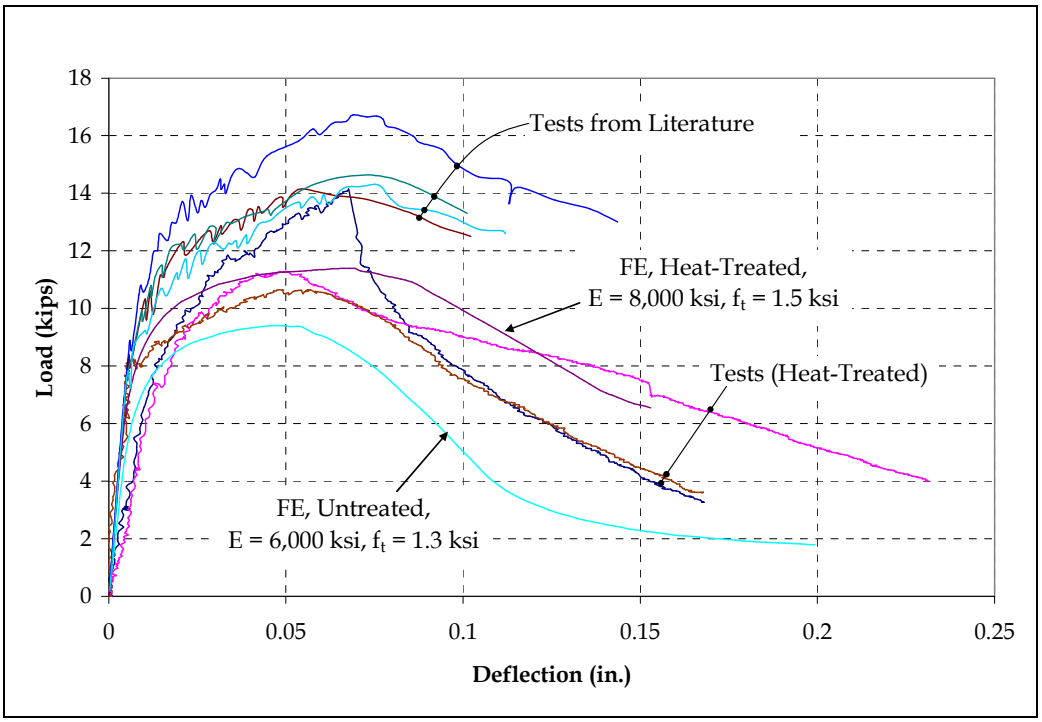

Figure 3.107 Load-Deflection Response Curves

The mesh and geometry of 1T1S model is shown in Figure 3.108. Symmetry was not used to avoid stress concentrations along the boundaries. The initial FE analysis resulted in a softer response than the test results, with failure due to excessive cracking at mid-span, which is not the case in the experiments. In order to ensure that the concrete around the rebar is restrained by the rebar itself, and would not crack at a low stress level, an elastic layer was modeled around the rebar in the FE model. Subsequently, the rebar stress was transformed along the span of the beam, and shear failure was captured. Figures 3.109 to 3.111 compare the load-deflection and load-strain curves from FE analysis with the experiments.

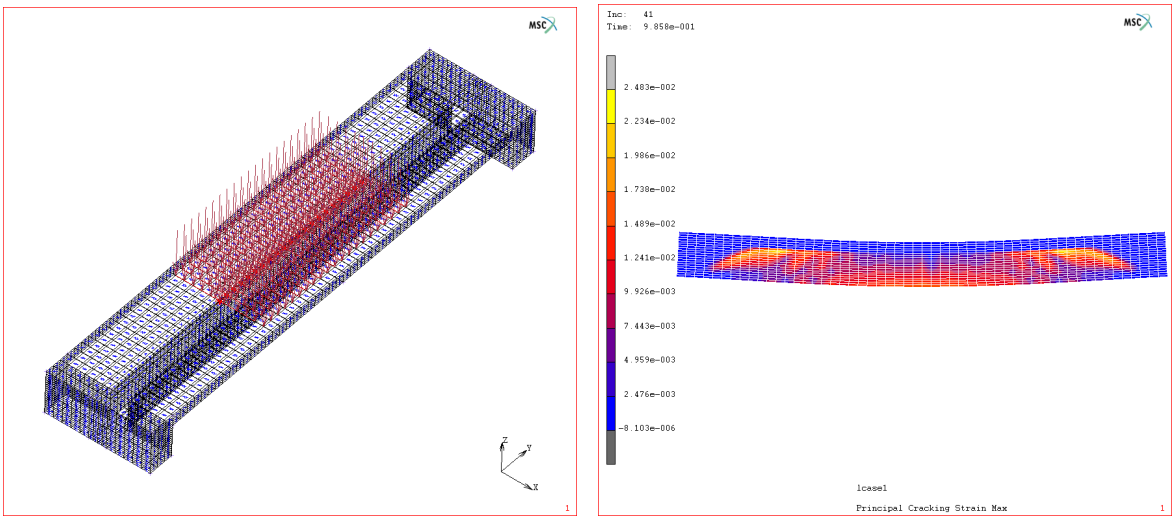

Figure 3.108 Discretized Model and Stress Distribution for Specimen 1T1S with 180° Hook

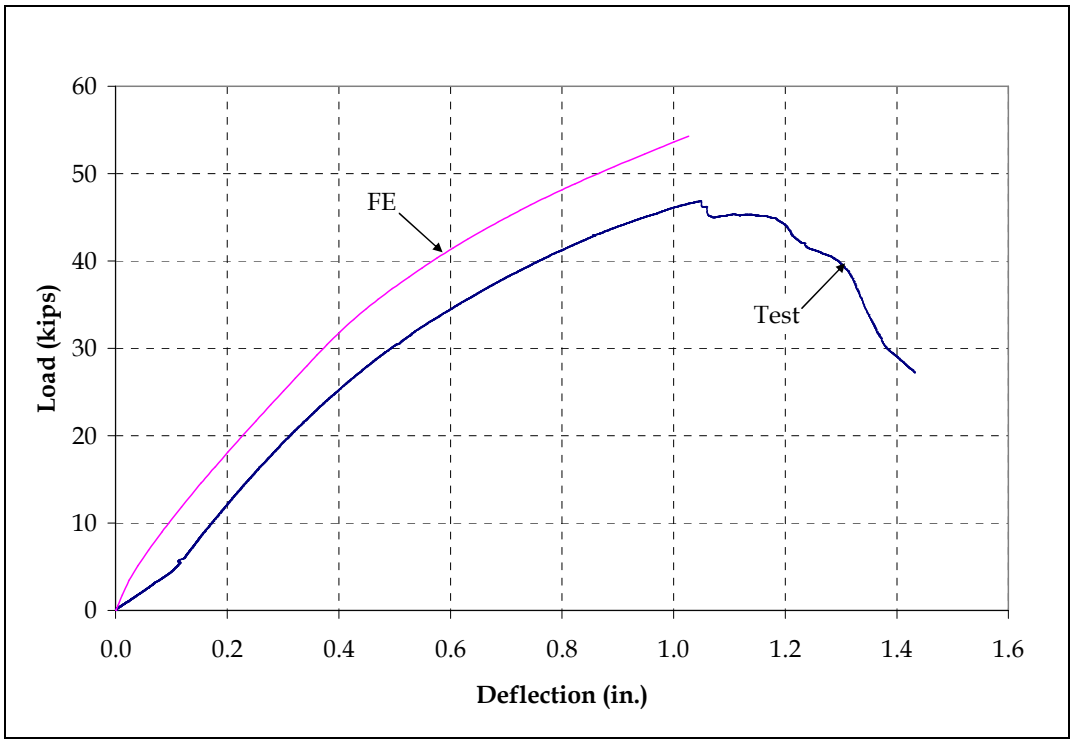

Figure 3.109 Comparison of Analytical and Experimental Load-Deflection Responses for Specimen 1T1S with 180° Hook

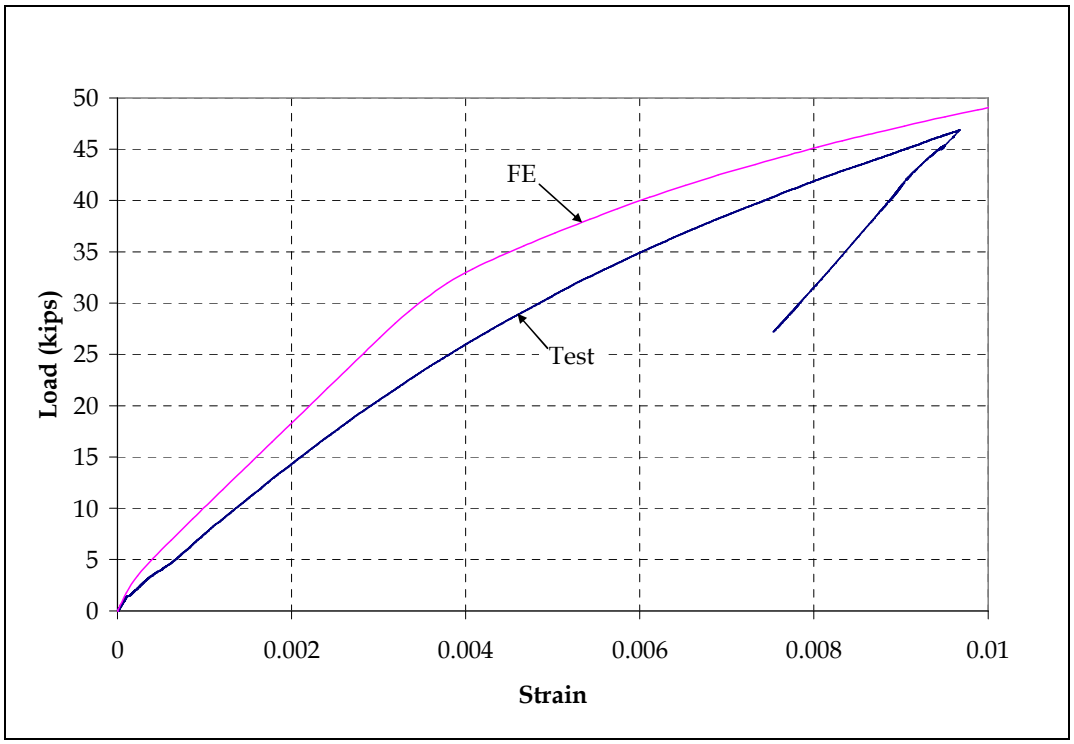

Figure 3.110 Comparison of Analytical and Experimental Load-Steel Strain Responses for Specimen 1T1S with 180° Hook

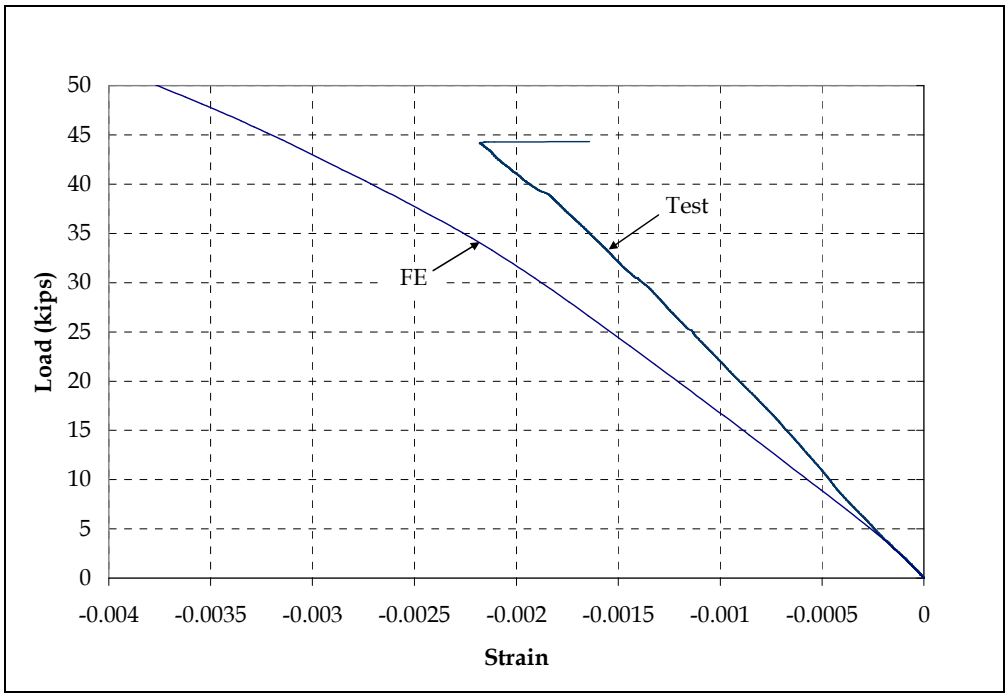

Figure 3.111 Comparison of Analytical and Experimental Load-Concrete Strain Responses for Specimen 1T1S with 180° Hook

The FE results for the un-anchored specimen are shown in Figure 3.112. Whereas the initial stiffness seems close to the experiment results, the model overestimates the load capacity.

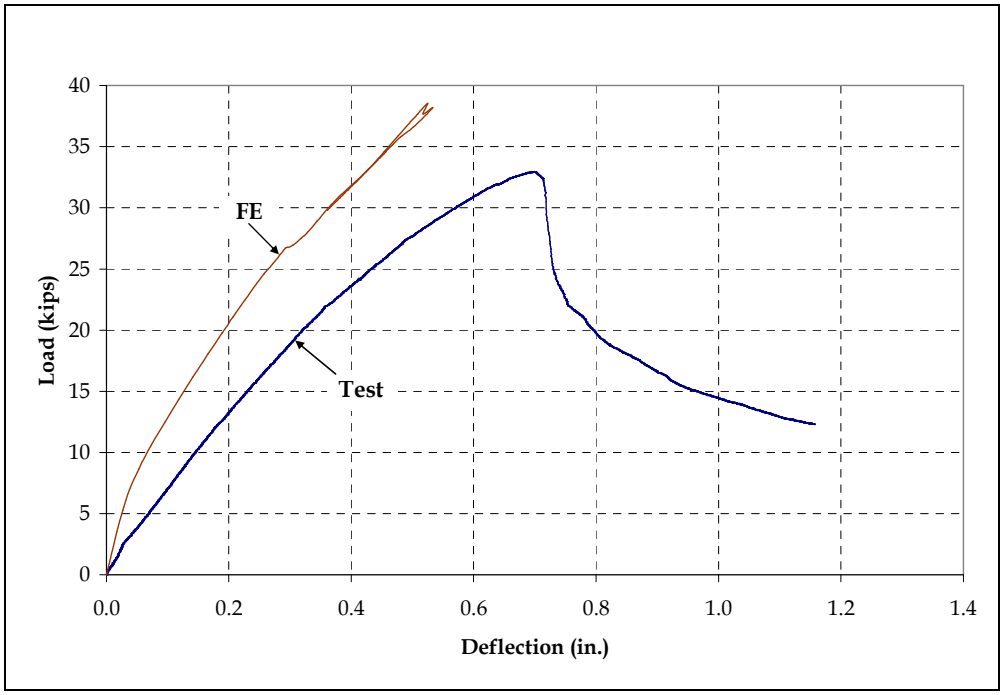

Figure 3.112 Comparison of Analytical and Experimental Load-Deflection Responses for Specimen 1T1S with No Anchorage

The FE model and stress distribution for Specimen 1T2S are shown in Figure 3.113. Comparisons of FE model and test data are shown in Figures 3.114 to 3.116. The difference between analytical and experimental data may be attributed to several factors, including lack of fibers at the top 0.4 in. layer of the flange, and the difference in cracking stress of Ductal® with the model.

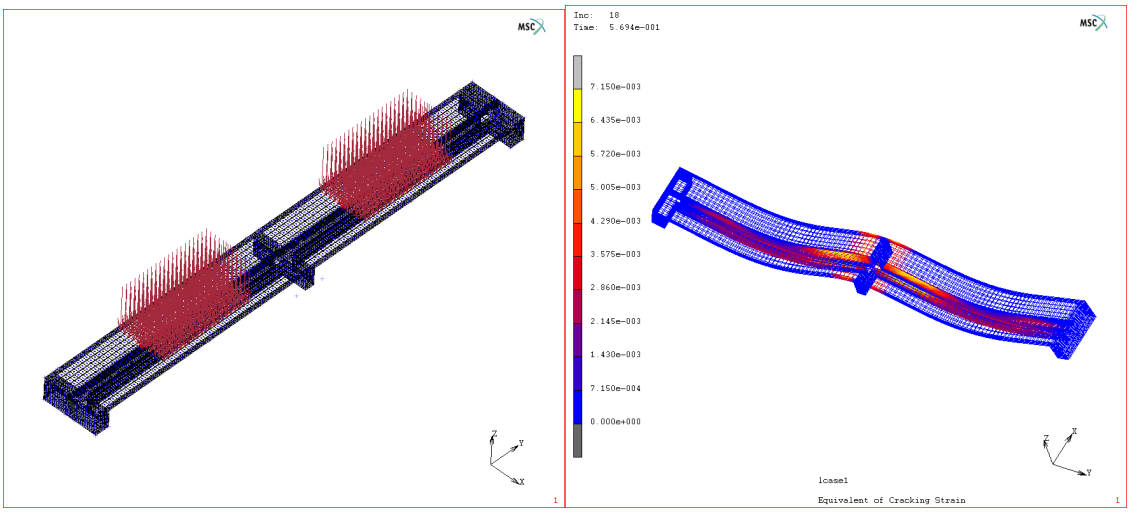

Figure 3.113 Discretized Model and Stress Distribution for Specimen 1T2S

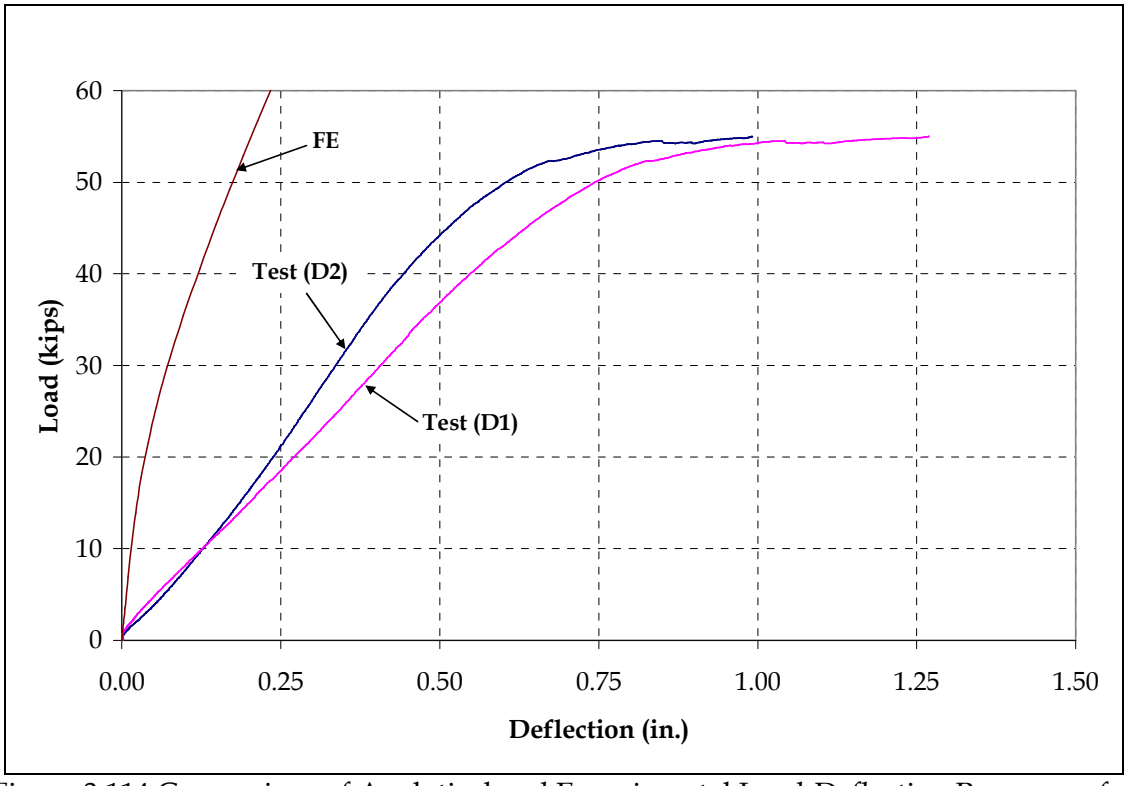

Figure 3.114 Comparison of Analytical and Experimental Load-Deflection Responses for Specimen 1T2S

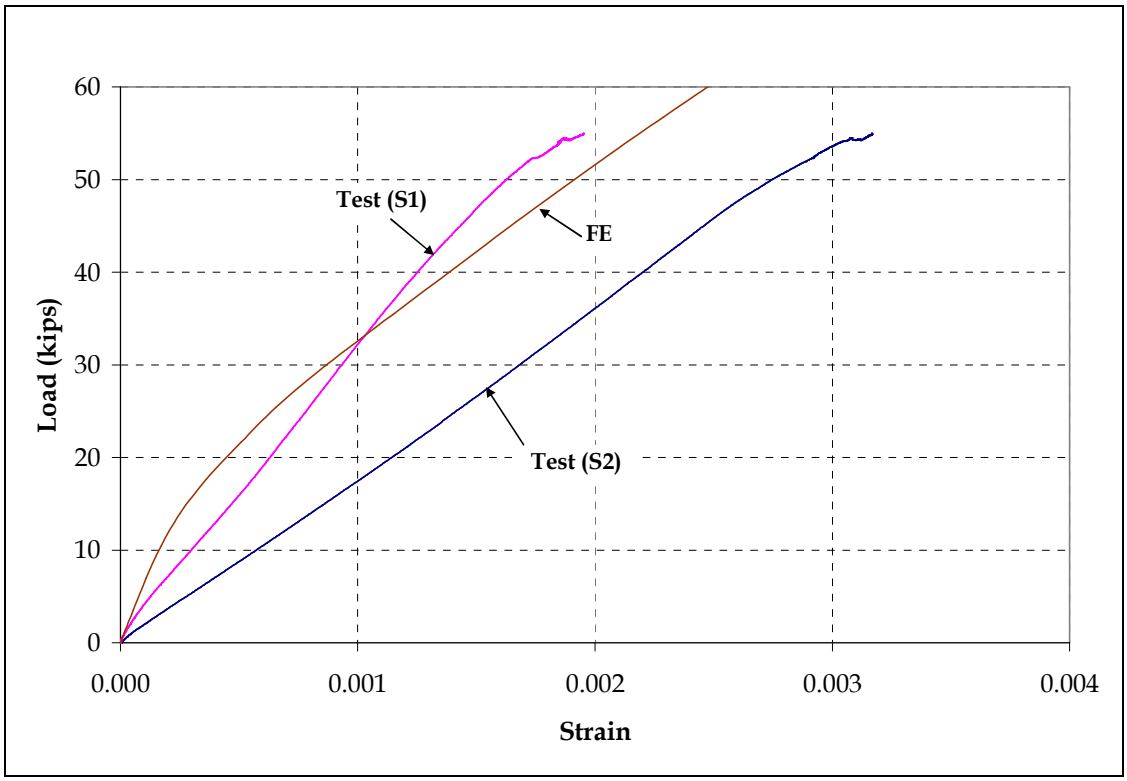

Figure 3.115 Comparison of Analytical and Experimental Load-Strain Responses for Specimen 1T2S

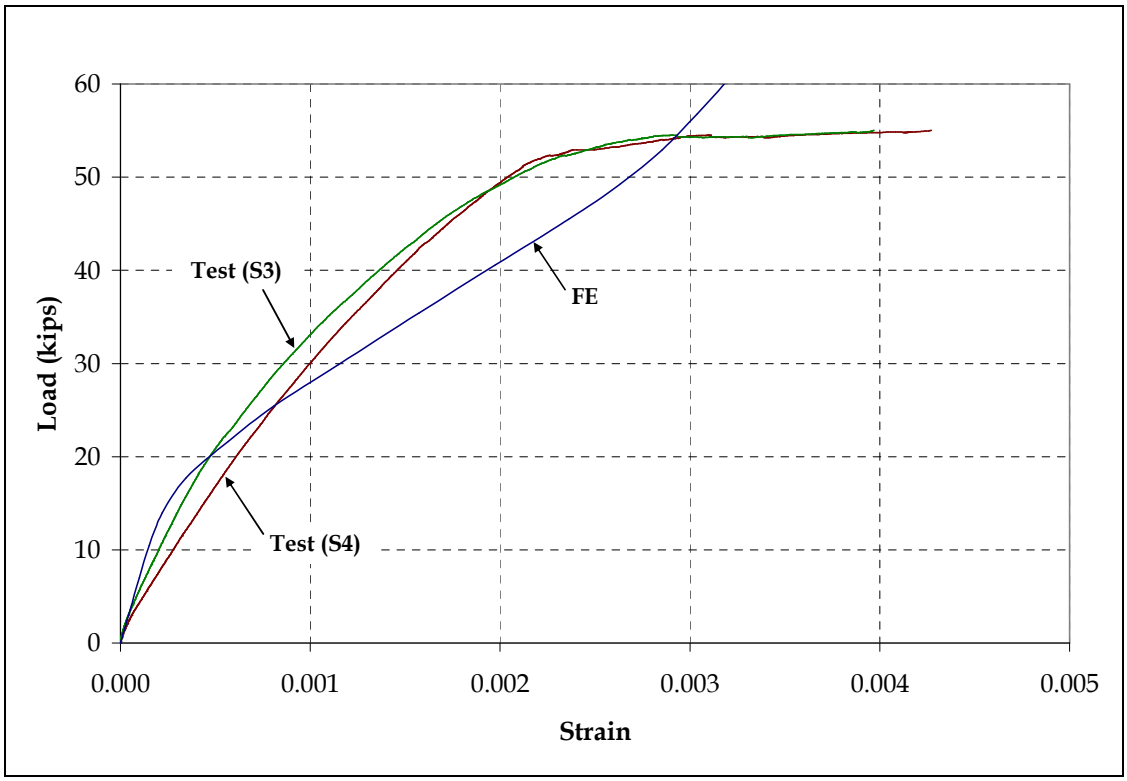

Figure 3.116 Comparison of Analytical and Experimental Load-Strain Responses for Specimen 1T2S

The FE model and stress distribution for the Specimen 4T1S are shown in Figure 3.117. Comparisons of FE model and test data are shown in Figures 3.118 to 3.120. Again, some differences in the analytical and experimental responses are observed, which may be attributed to the assumptions made in the FE model.

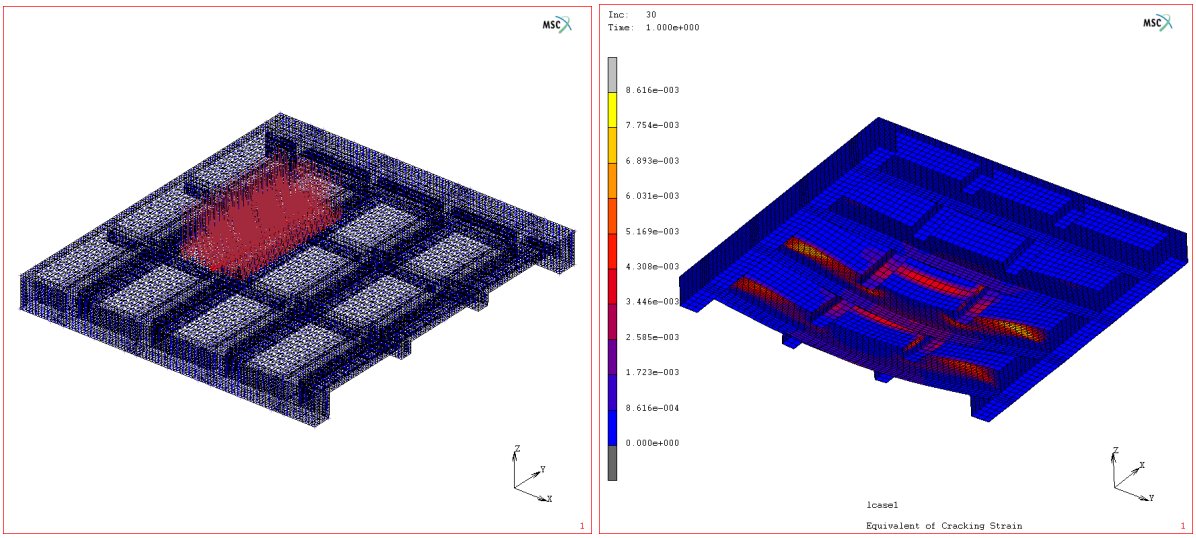

Figure 3.117 Discretized Model and Stress Distribution for Specimen 4T1S

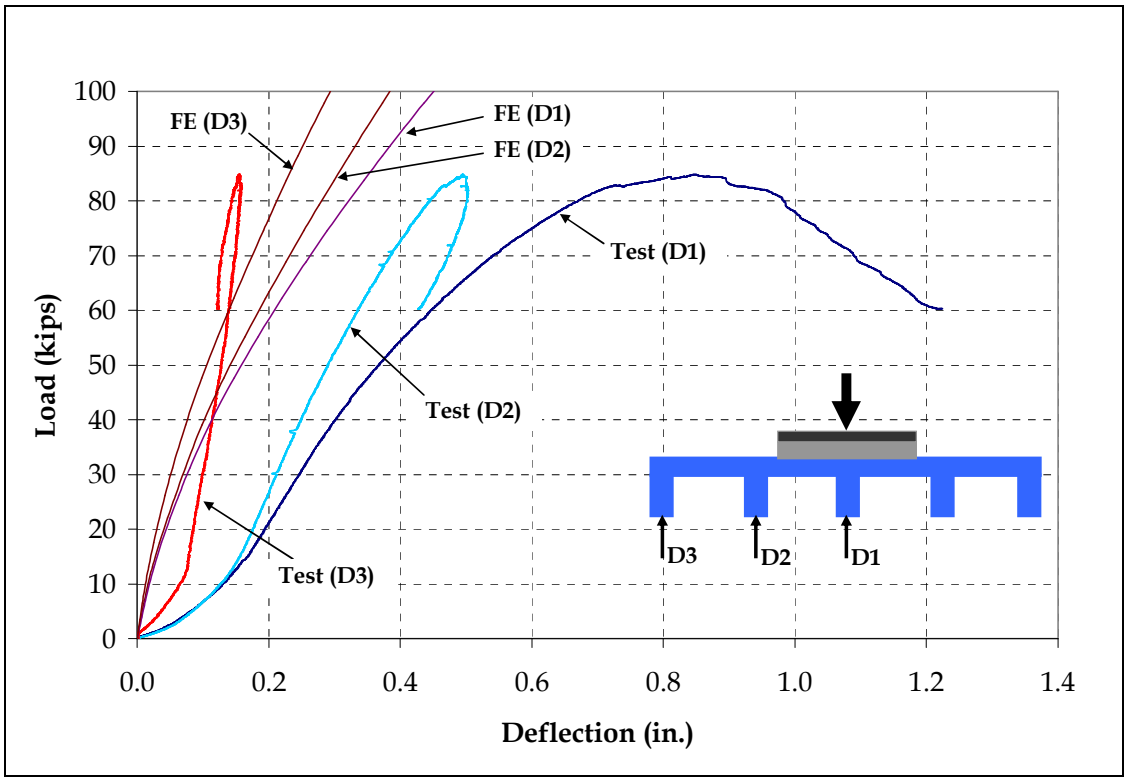

Figure 3.118 Comparison of Analytical and Experimental Load-Deflection Responses for Specimen 4T1S

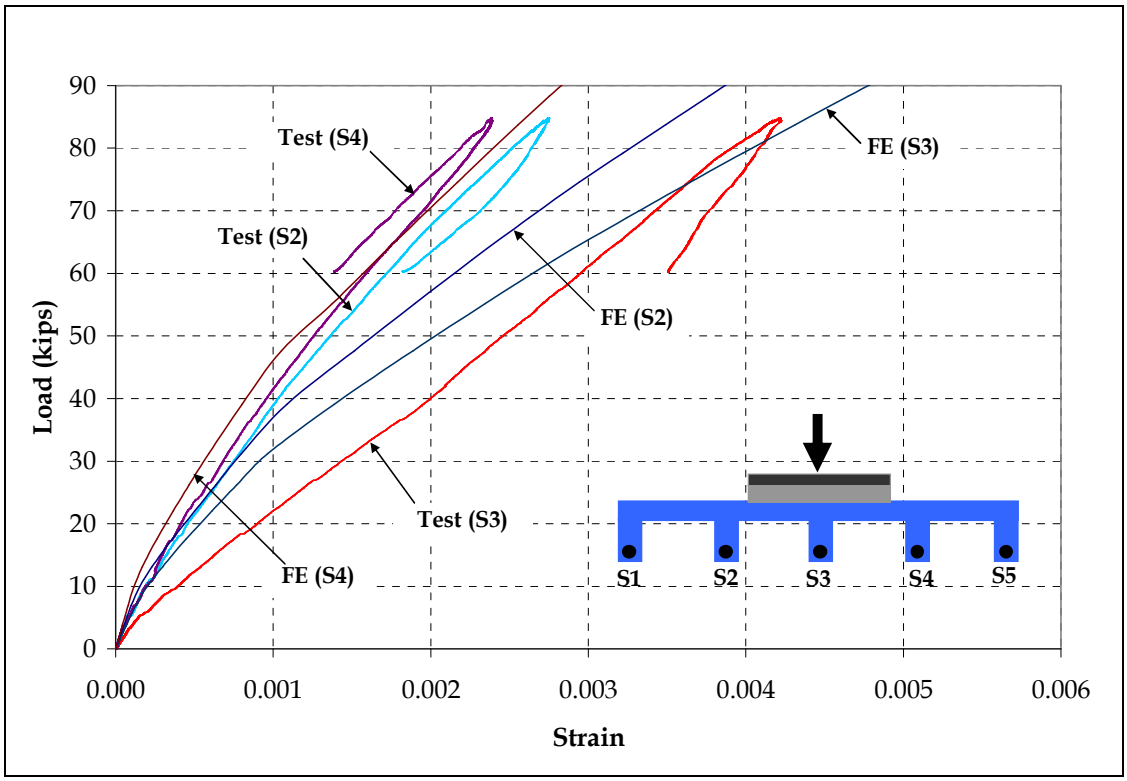

Figure 3.119 Comparison of Analytical and Experimental Load-Strain Responses for Specimen 4T1S

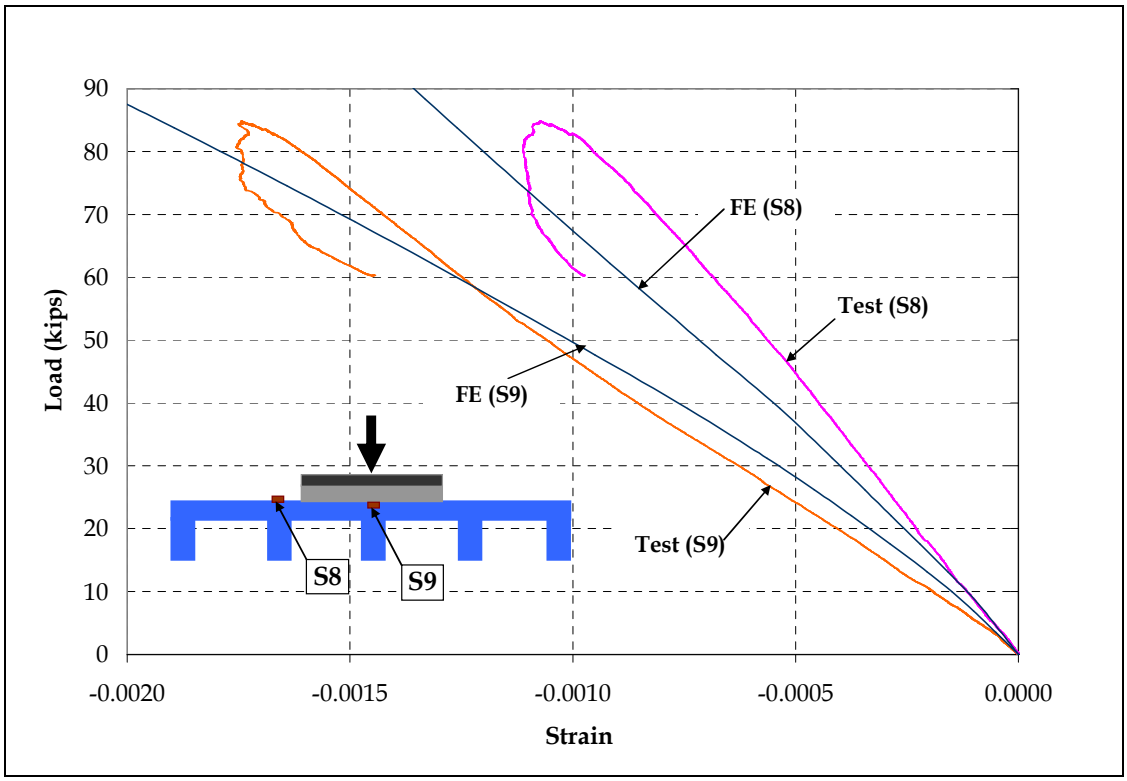

Figure 3.120 Comparison of Analytical and Experimental Load-Strain Responses for Specimen 4T1S

The FE model and stress distribution, and the comparisons of FE model and test data for Specimen 1T1S with tapered flange are shown in Figures 3.121 and 3.122, respectively.

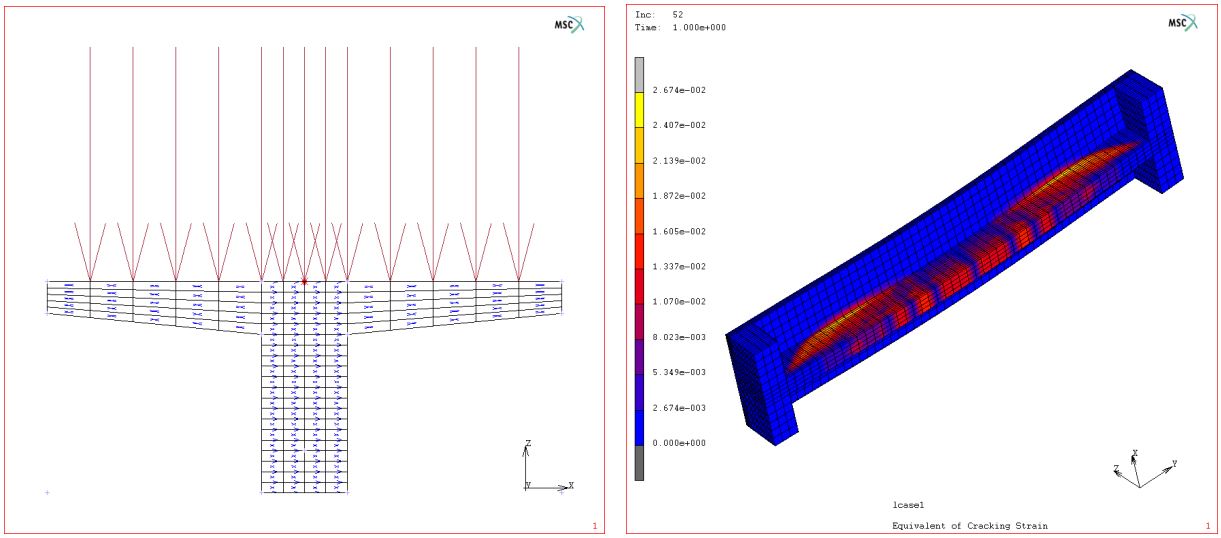

Figure 3.121 Discretized Model and Stress Distribution for Specimen 1T1S with Tapered Flange

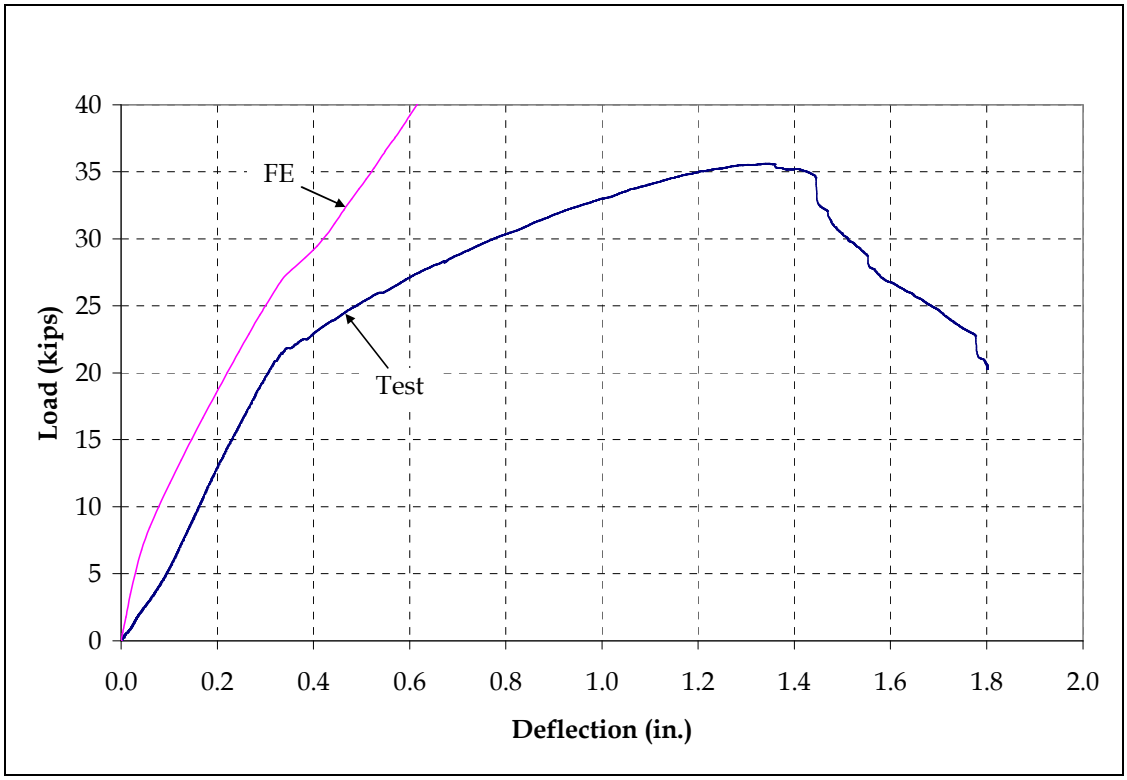

Figure 3.122 Comparison of Analytical and Experimental Load-Deflection Responses for Specimen 1T1S with Tapered Flange

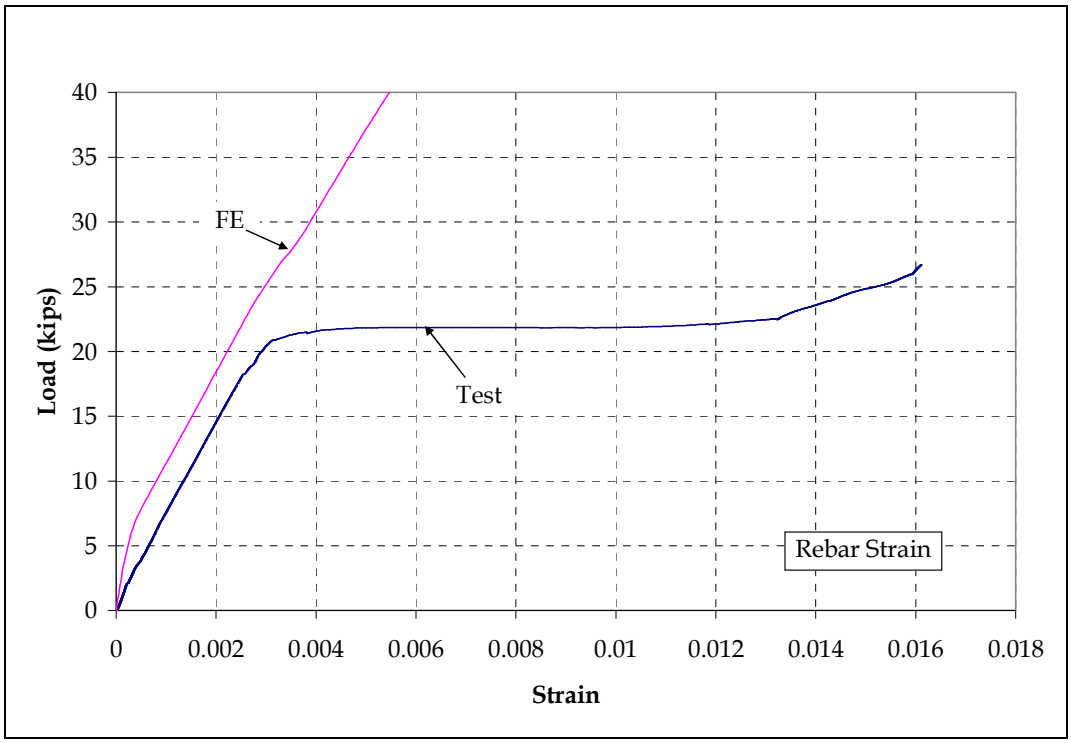

Figure 3.123 Comparison of Analytical and Experimental Load-Strain Responses for Specimen 1T1S with Tapered Flange

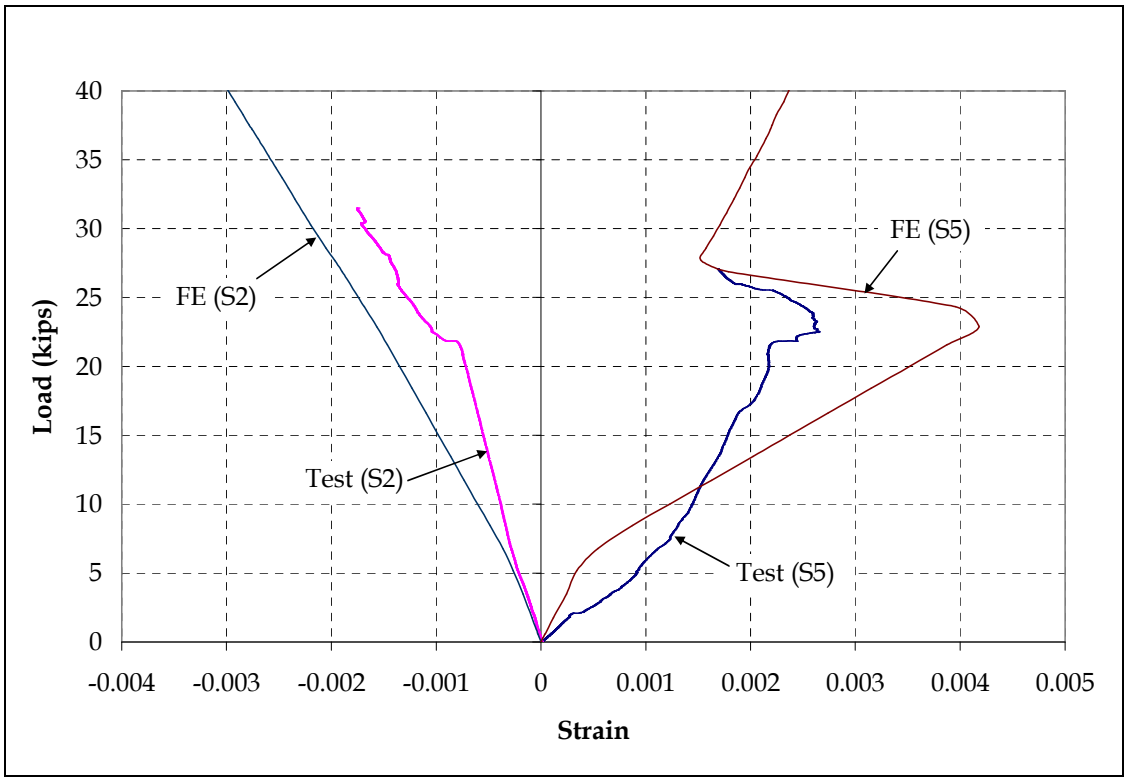

Figure 3.124 Comparison of Analytical and Experimental Load-Strain Responses for Specimen 1T1S with Tapered Flange

Finally, the FE model, stress distribution and comparison of the FE model and test data for Specimen 3T2S are shown in Figures 3.125 and 3.126, respectively. The analysis overestimates the stiffness of the specimen.

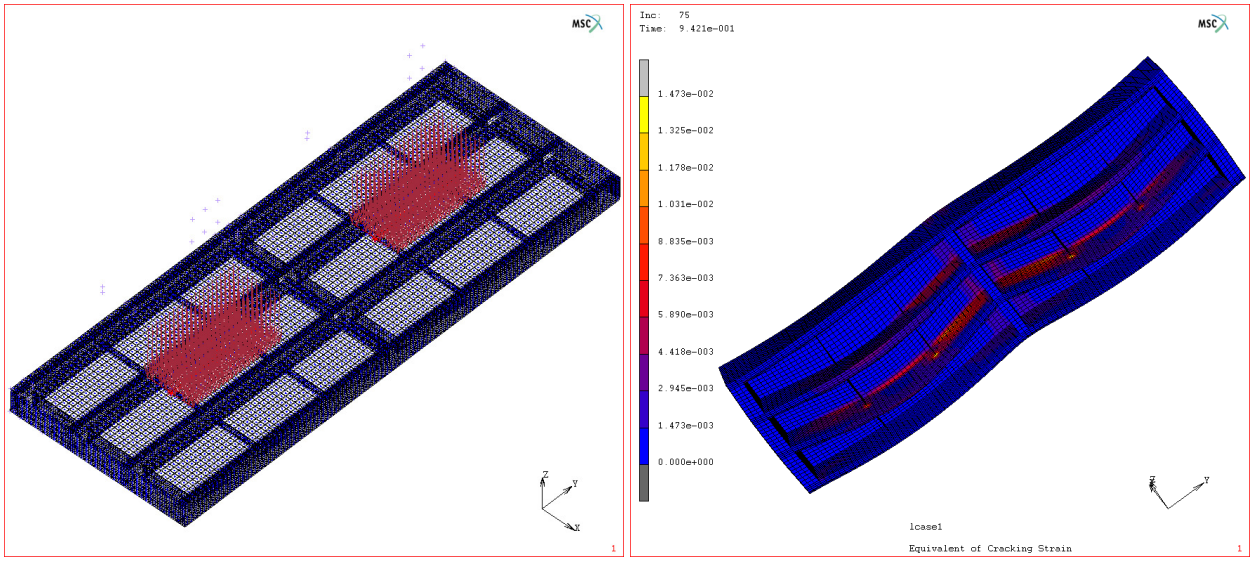

Figure 3.125 Discretized Model and Stress Distribution for Specimen 3T2S

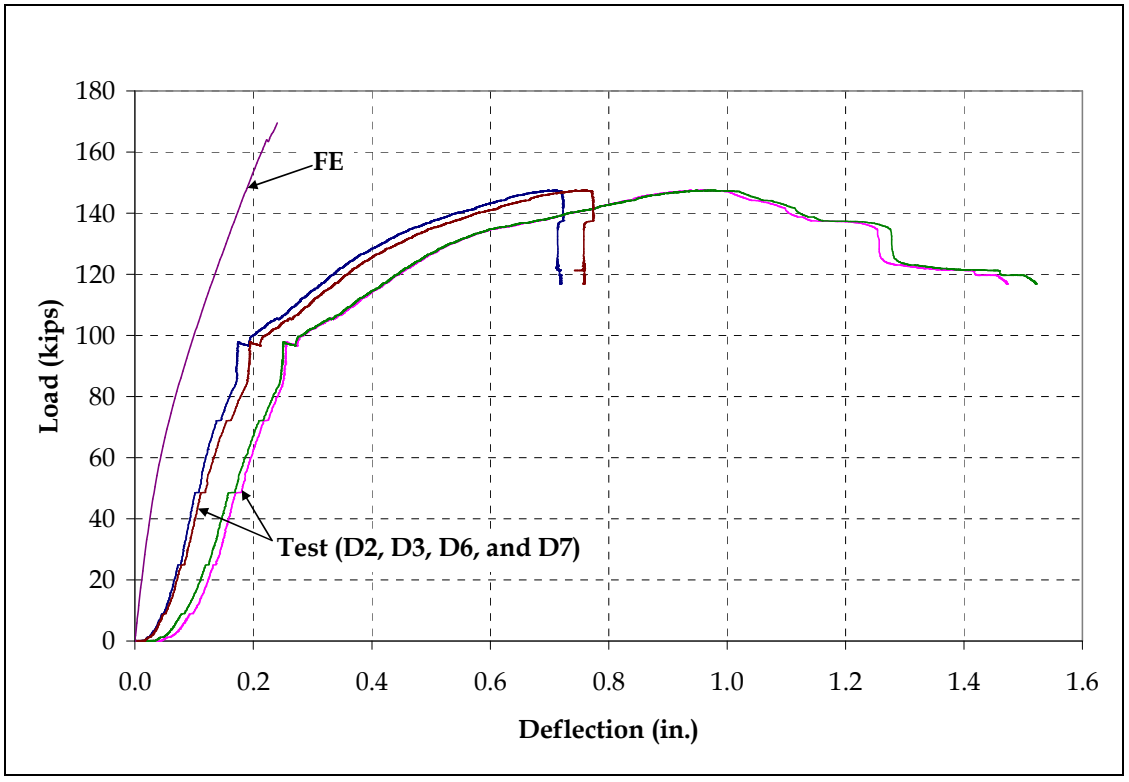

Figure 3.126 Comparison of Analytical and Experimental Load-Deflection Responses for Specimen 3T2S

3.6 Conclusions

A through experimental and analytical study was conducted to assess the performance of the Ductal®-MMFX steel deck, which led to the following conclusions:

1. The system has great potential to serve as an alternative to the open grid steel decks. The ultimate load capacity and behavior of the tested specimens make this system an appropriate choice to replace the conventional system.
2. The dominant mode of failure in most of the specimens was in shear, except for the first two specimens which suffered from shear-bond failure.
3. Use of standard 180^{o} hooks at both ends of flexural reinforcement helped effectively avoid bond failure.
4. Shear strengthening and reduced flexural steel did not change the failure mode from shear to flexure. The specimen with shear reinforcement, however, exhibited higher stiffness and a more distributed crack pattern than its counterparts.
5. For the multi-T simple-span and two-span specimens, most of the load was taken by the ribs present either under or near the loading pad, which ultimately led to punching through the slab.
6. Moment-curvature analysis provided a reasonably good estimate of the initial deflection. More elaborate finite element analysis did not provide much better estimate of either the stiffness or the ultimate load capacity.

3.7 Recommendations for Future Research

Based on the results of this study, the use of Ductal® for moveable bridge decks seems to be very promising, and requires development of only a few additional components before it is ready to be implemented. The following additional work is proposed:

1. Pull-out tests to determine the bond length and effectiveness of hooks and mechanical anchorages in Ductal®-MMFX steel deck.
2. Establishing the load distribution mechanism between the ribs for the design of deck panels.
3. Design of connection with supporting steel stringers.
4. Design of joints between adjacent deck panels.
5. Use of Ductal® materials as wearing surface.
6. Fatigue performance of the deck and its connections.
7. Potential for use of other types of high-strength steel, including stainless steel.

Chapter-4

SYSTEM 3-Ductal®-FRP Tubes Deck

4.1 Introduction

Ductal®-fiber reinforced polymer (FRP) tube hollow core deck is the third alternative to steel grid decks that was studied in this project. This is an entirely new concept. Prestressed hollow core slabs made of regular concrete are commonly used in building structures but are rarely used as bridge decks. As yet no design guidelines or literature is available for Ductal®-FRP tube hollow core decks. Researchers have worked on all-FRP bridge decks and concrete-filled FRP tubes, but none has combined Ductal® and FRP tubes for a bridge deck. This system has a potential to emerge as a very promising steel-free deck. The idea behind combing Ductal® with FRP tubes was to enhance the flexural capacity of Ductal®. FRP tubes serve as tensile reinforcement both in the positive and negative moment regions, and help reduce the self-weight of the deck. The FRP tubes used for this study were manufactured by Strongwell of Bristol, VA. Figure 4.1 shows the stress-strain behavior of glass FRP. Also, shown in the figure, are the geometric properties of the FRP tube.

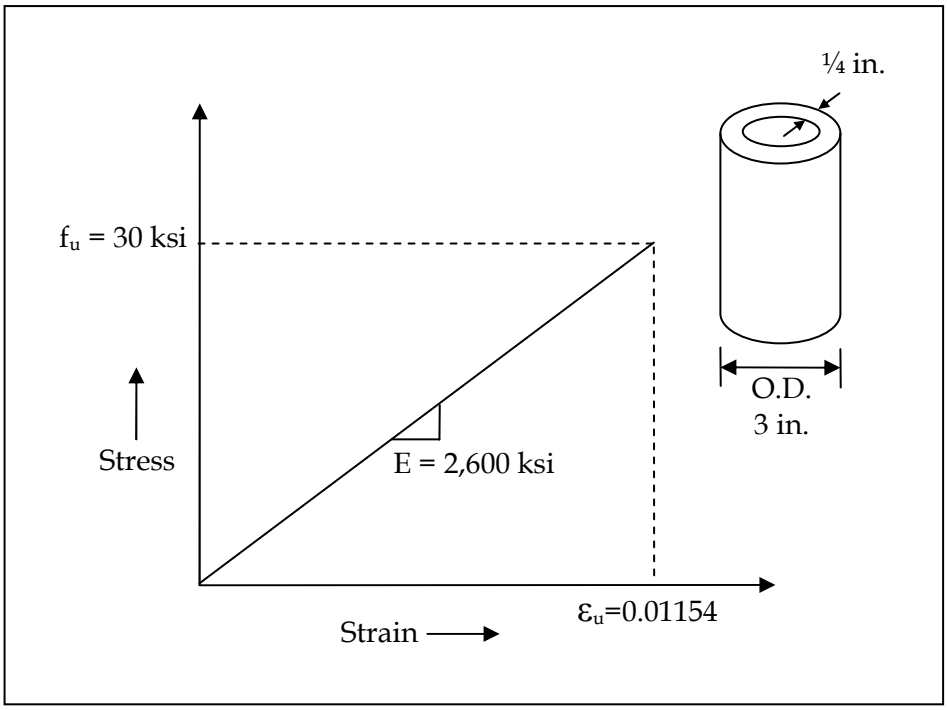

Figure 4.1 Stress-Strain Response of Glass FRP Tubes
Source: EXTREN Properties Guide

4.2 Literature Review

FRP composite materials have shown great potential as alternative construction materials, especially in the field of repair and rehabilitation of existing bridges, and to some extent in new bridge construction (Ehlen 1999). The acceptance of FRP composites in bridge industry is mainly due to their superior properties, such as high strength, long-term durability, and good corrosion and fatigue resistance (Zhang et al. 2006). Moreover, FRPs are well suited for mass production of structural shapes because of their light weight, which allows rapid installation of FRP modular decks on bridges (Plunkett 1997).

An FRP bridge deck weighs approximately 80% less than a concrete deck (Mu et al. 2006). The light-weight FRP deck could be especially beneficial for movable bridges, in which spans have to be lifted up for the passage of vessels.

In the past decade there have been numerous examples of new bridges using FRP decks, or old bridge decks replaced by new FRP decks. For example, an existing conventional concrete deck on a 60-year old Warren steel truss bridge was replaced by an FRP deck, which was funded by the New York Department of Transportation (Jerome et al. 2000). Currently, a total of nine states DOTs including Delaware, Illinois, Kansas, Maryland, New York, North Carolina, Ohio, Oregon, and Pennsylvania are using FRP bridge deck panels. In Oregon, FRP bridge deck panels have been used to replace an existing timber deck on a moveable bridge (Hong and Hastak 2006). Florida is also in the midst of installing an FRP bridge deck.

Several researchers including Robinson and Kosmatka (2008), Alagusundaramoorthy (2006), Prachasaree et al. (2006), Stiller et al. (2006), Aluri et al. (2005), and Hutcheson and Sheppard (2003) have conducted laboratory experiments on decks with different FRPs and connection types to characterize their static and dynamic behavior.

4.3 Preliminary Analytical Work

The self-weight of the FRP tube is 1.7 lb/ft according to the manufacturer's data sheet. If the Ductal®-FRP tube deck is designed with FRP tubes placed 4 in. apart and in perpendicular direction to the traffic, the maximum thickness of the Ductal® slab would be about 1.6 in., based on the limiting self-weight requirement of 25 lb/ft^2. Two different designs are proposed based on this weight limitation.

The first design has the entire tube section embedded in a 3½ in. thick Ductal® section. The estimated self-weight would then be 26.76 lb/ft^2. This design method will ensure the strongest bond between the tubes and concrete by using the ¼ in. cover on both the top and bottom sides. The concrete on the tension face is expected to crack at relatively low load levels. In order to maintain stability in the transverse direction as well as to accommodate the 10 in. wide loading pad, a 12 in. wide deck strip with three FRP tubes was selected as the first design configuration for the experiments.

For the second design configuration, concrete on the tension face of the deck was considered ineffective and therefore, was removed from the design. The resulting shape was tapered along the span. The section was designed based on the FE analysis of the first design configuration. If

it is assumed that the three encased tubes would share the load equally, the service load for each tube unit would be estimated as 16 kips/3 = 5.3 kips. The minimum thickness of the top Ductal® portion was designed as 1 in. to prevent punching shear failure based on previous results in the literature (Harris and Roberts 2005). The self-weight of the second design configuration was calculated as 25.8 lb/ft^2. Figure 4.2 shows the cross sections and schematics of the tapered Ductal®-FRP specimen.

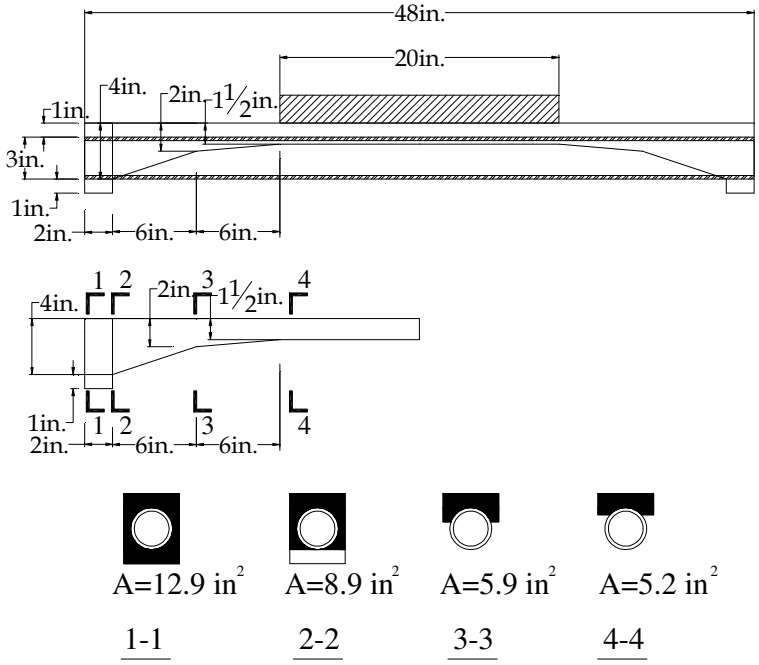

Figure 4.2 Cross Sections of Tapered Ductal®-FRP Deck Specimen

The UHPC material model used in the design is the same as the Ductal® used for System 2, with an elastic modulus of 6,000 ksi, a tensile strength of 1.125 ksi, a compressive strength of 28 ksi, and a Poisson's ratio of 0.17. The properties of FRP were obtained from the manufacturer's data sheet, as shown in Figure 4.1.

As both materials, Ductal® and FRP, behave linearly before cracking, the cracking load of the deck strip can be calculated using the sectional analysis and the flexural rigidity EI of 1.33 x 10^5 kip-in^2. Cracking moment would be 12.5 kip-in., which for a 48 in. span beam, is equivalent to a total load of 1.3 kips distributed evenly over the middle 20 in. of the span. Therefore, the cracking load for the 12 in. wide slab would be 3.9 kips.

Assuming perfect bond between the FRP tube and Ductal®, moment-curvature analysis of the composite system may provide an estimate of the moment capacity and the load-deflection response through integration over the span length. The section loses its moment capacity when Ductal® reaches its compressive strength or the FRP tube ruptures in tension. The load-deflection response for the 48 in. span deck strip is shown in Figure 4.3. The composite section was divided into 36 layers, as shown in the figure inset.

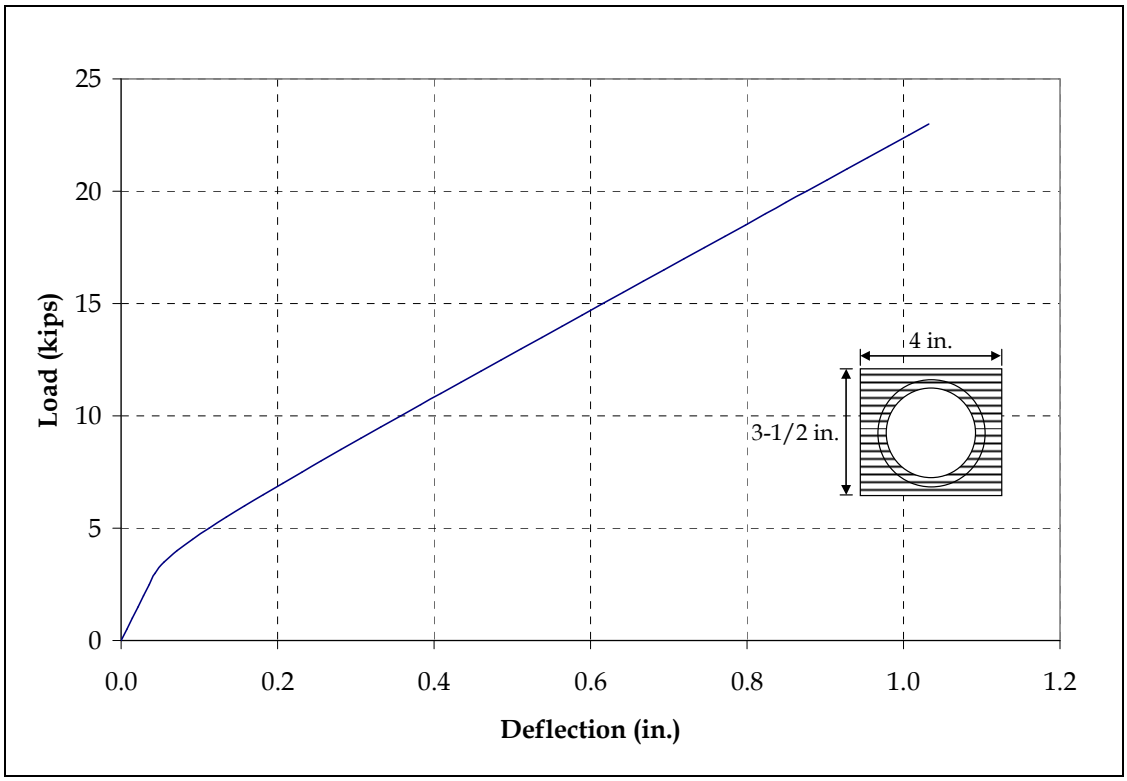

Figure 4.3 Load-Deflection Response for the 4 in. Wide Uniform Section Ductal®-FRP Deck

In order to investigate the cracked region in the uniform section deck, a 3D FE model was developed in MSC.Marc®. For reasons of simplicity, only one 4 in. unit was modeled, as shown in Figure 4.4. It was assumed that there would be no slippage between Ductal® and the FRP tube in the model.

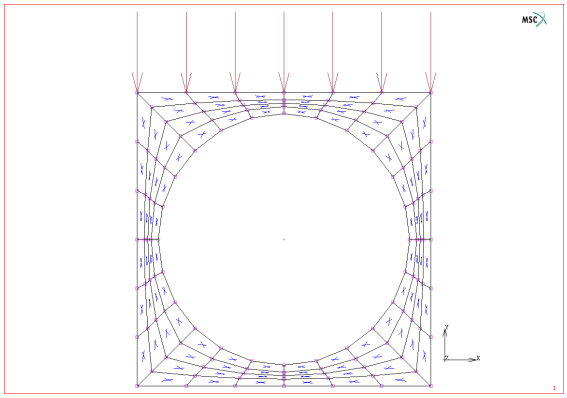

(a) Section Mesh

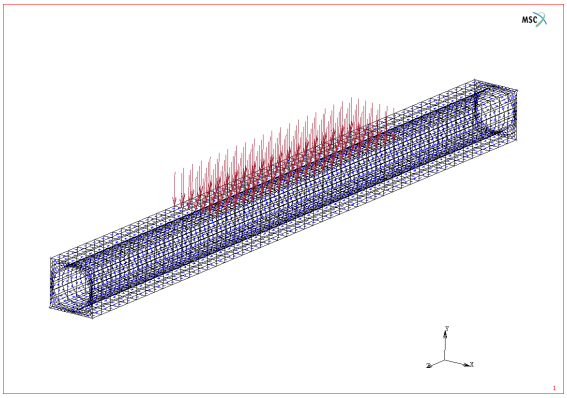

(b) 3D Mesh and Loading Configuration

Figure 4.4 FE Mesh of the Uniform Section Ductal®-FRP Deck

Figures 4.5 and 4.6 show the load-deflection and crack strain distribution in the FE model, respectively. The failure is expected to be by tensile rupture of FRP tubes.

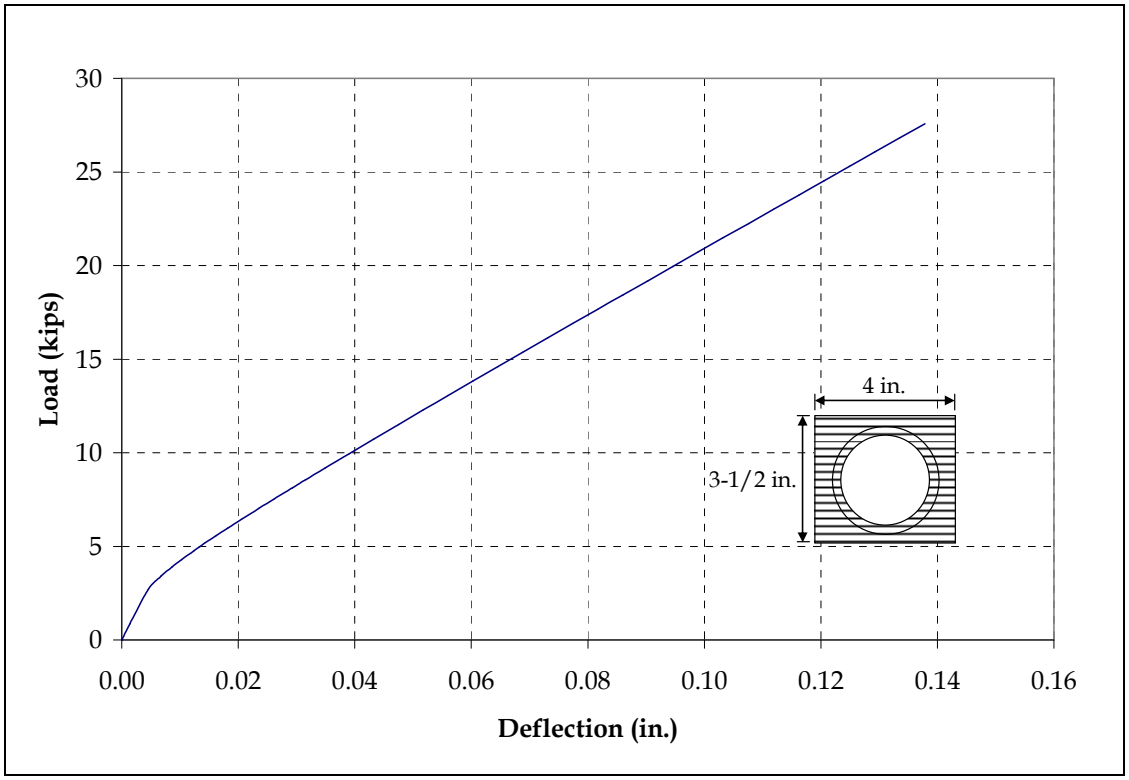

Figure 4.5 Load-Deflection Response from FE Analysis

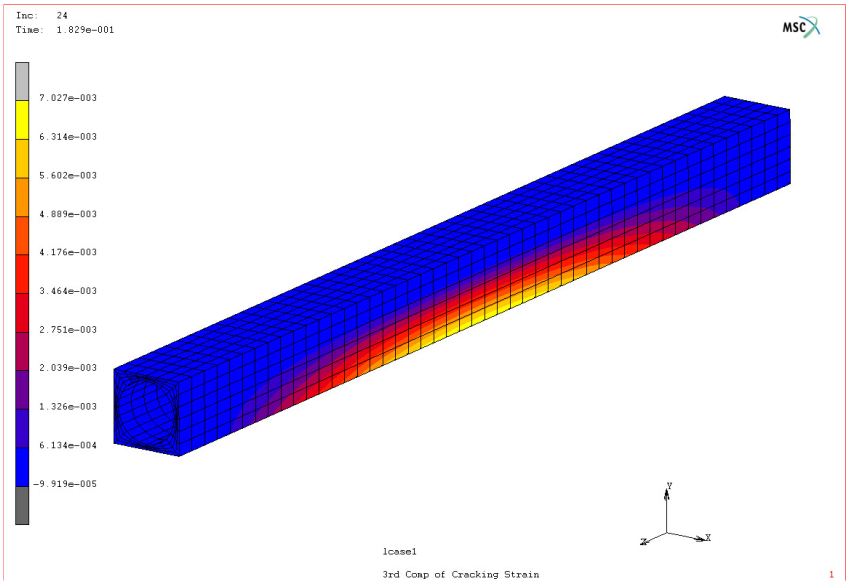

Figure 4.6 Cracking Strains at Service Load from FE Analysis

The cracking load of the tapered design was estimated based on the mid-span section, where the maximum moment occurs. The neutral axis was estimated to be at 1.573 in. above the center of the tube, as shown in Figure 4.7, hence, the section modulus EI would be 2.9×10^4 kip-in^2.

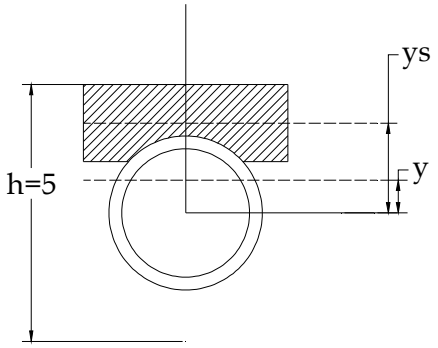

Figure 4.7 Tapered Section at Mid-Span

The moment capacity of the tapered section is estimated as 106 kip-in. based on the compressive strength of Ductal®, and 85.5 kip-in. based on the tensile strength of FRP. Therefore, it is the tensile strength of FRP that governs the failure of the deck. Using the 20 in. distributed load at mid-span, the ultimate load capacity is expected to be 27 kips for the 12 in. wide section.

4.4 Experimental Work

Preliminary experimental work was carried out to establish the behavior of Ductal®-FRP tube hollow core deck. Two simply-supported deck specimens were tested, one with uniform thickness cross-section and the other with tapered section. Figure 4.8 shows the geometry of the two deck specimens.

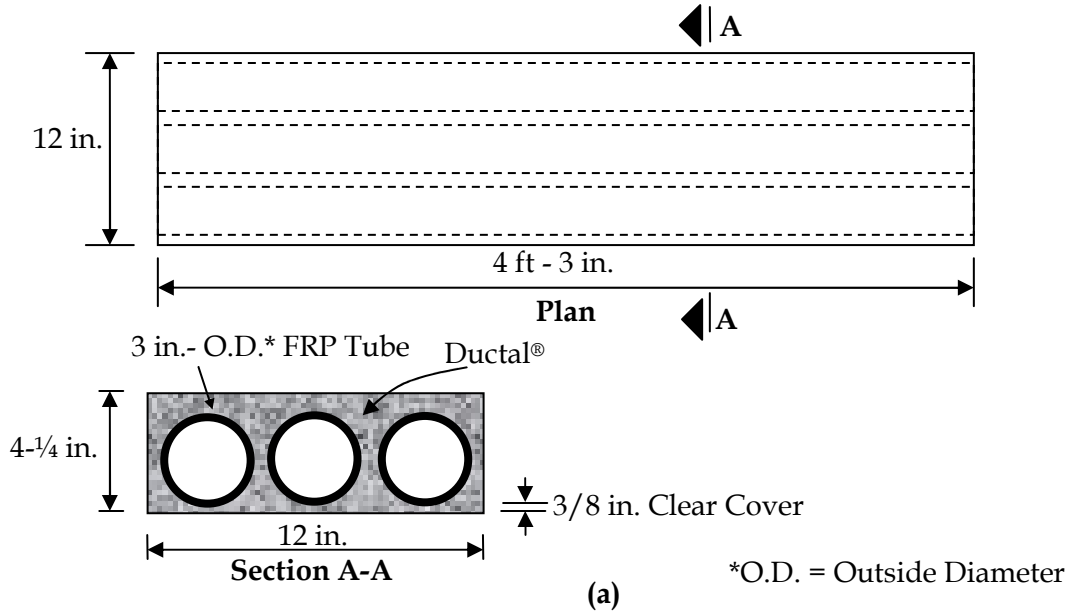

(a)

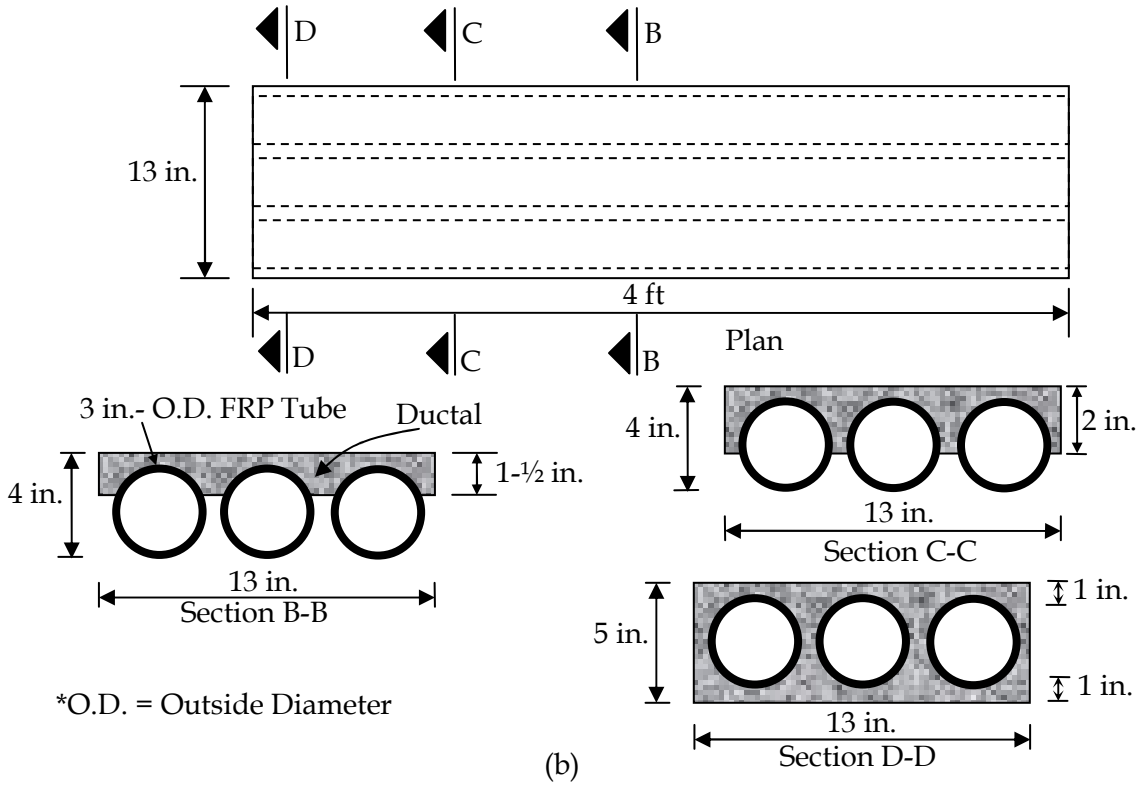

Figure 4.8 Geometry of Deck Sections: (a) Uniform Section, and (b) Tapered Section

Both specimens were subjected to a single load at the mid-span. Load was applied on a footprint of 20 in. x 10 in. Displacement control procedure was adopted with a displacement rate of 0.015 in./min. Surface-mounted strain gauges and string potentiometers were installed at strategic locations to gather strain and deflection data along with loading data from the actuator.

4.4.1 Test Results of Uniform Section Ductal®-FRP Deck Specimen

Figures 4.9 to 4.12 show the instrumentation plan, test setup, and failure pattern of the uniform section Ductal®-FRP tube deck specimen. Originally, the design depth of the section was 3-½ in. However, due to some problems in the formwork at the time of casting this height could not be maintained. The actual depth of the section turned out to be 4-¼ in. Increased depth affected the ultimate load as well as the self-weight. Figures 4.13 and 4.14 show the load-deflection and load-strain responses, respectively. Also shown in Figure 4.13 is the slippage of the center tube with respect to the Ductal® section. The first flexural crack appeared at 10.3 kips at the mid-span. The specimen failed at 37 kips. Two more flexural cracks appeared at the later stage, and kept on growing until failure. The three FRP tubes failed suddenly in compression one after the other. Figure 4.13 shows that there was no slippage in the tubes up to 20 kips, after which the tubes started slipping inwards because of the opening of flexural cracks at the mid-span. Figure 4.14 shows that the compressive strain of concrete was well above its crushing strain of 0.003.

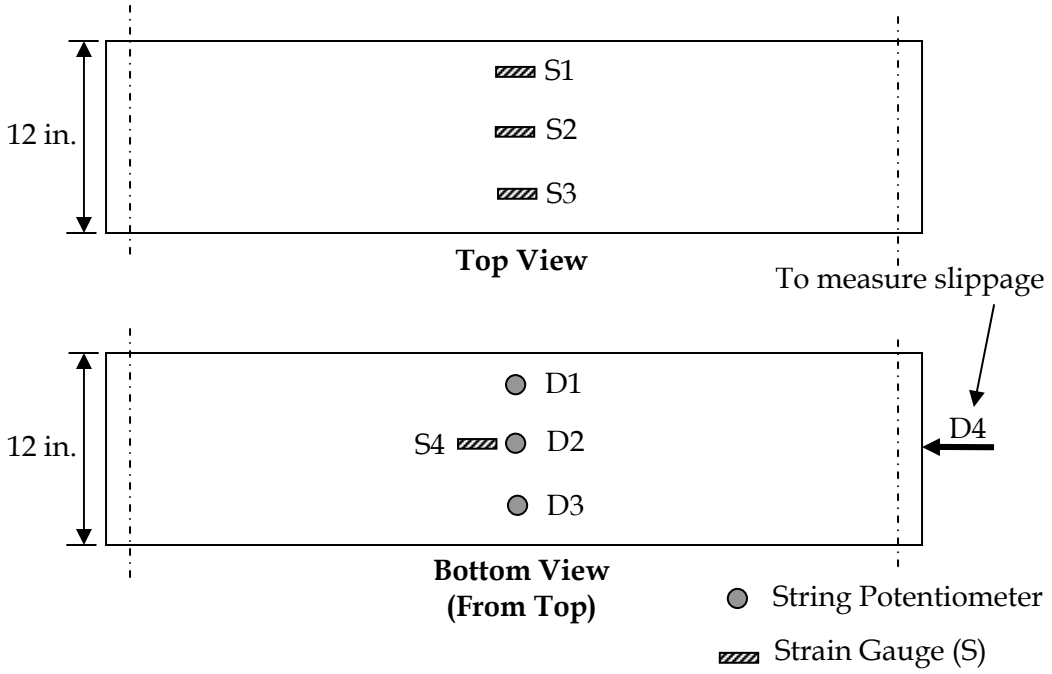

Figure 4.9 Instrumentation Plan for the Uniform Section Ductal®-FRP Deck Specimen

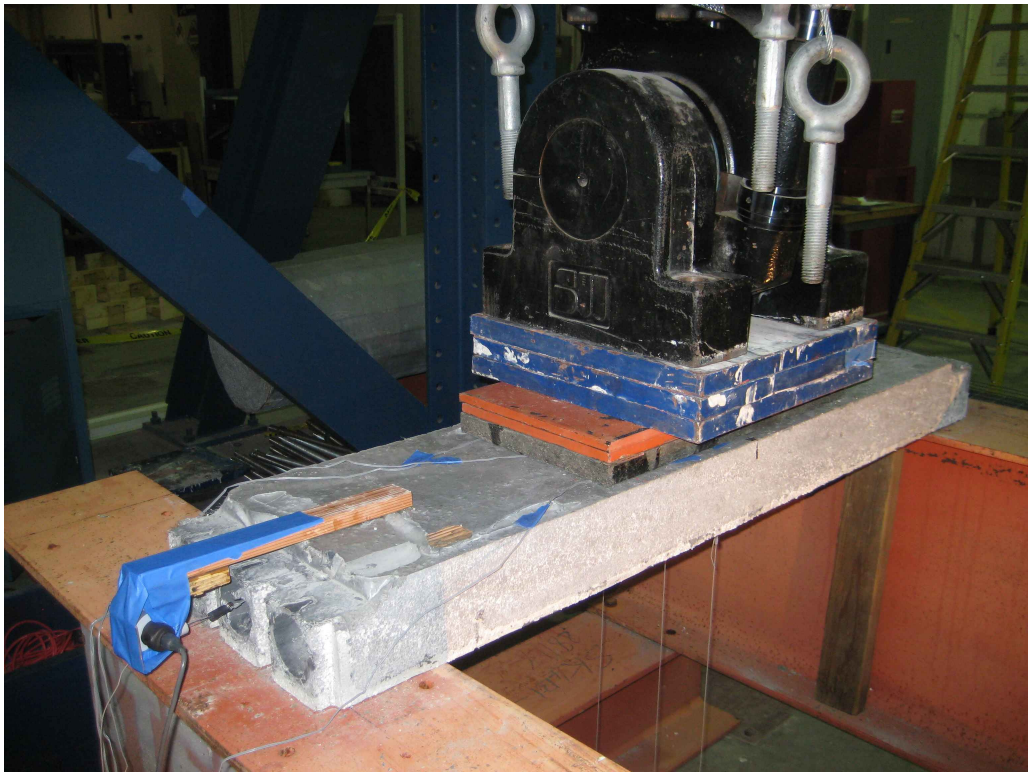

Figure 4.10 Test Setup for the Uniform Section Ductal®-FRP Deck Specimen

Figure 4.11 Flexural Cracks in the Uniform Section Ductal®-FRP Deck Specimen

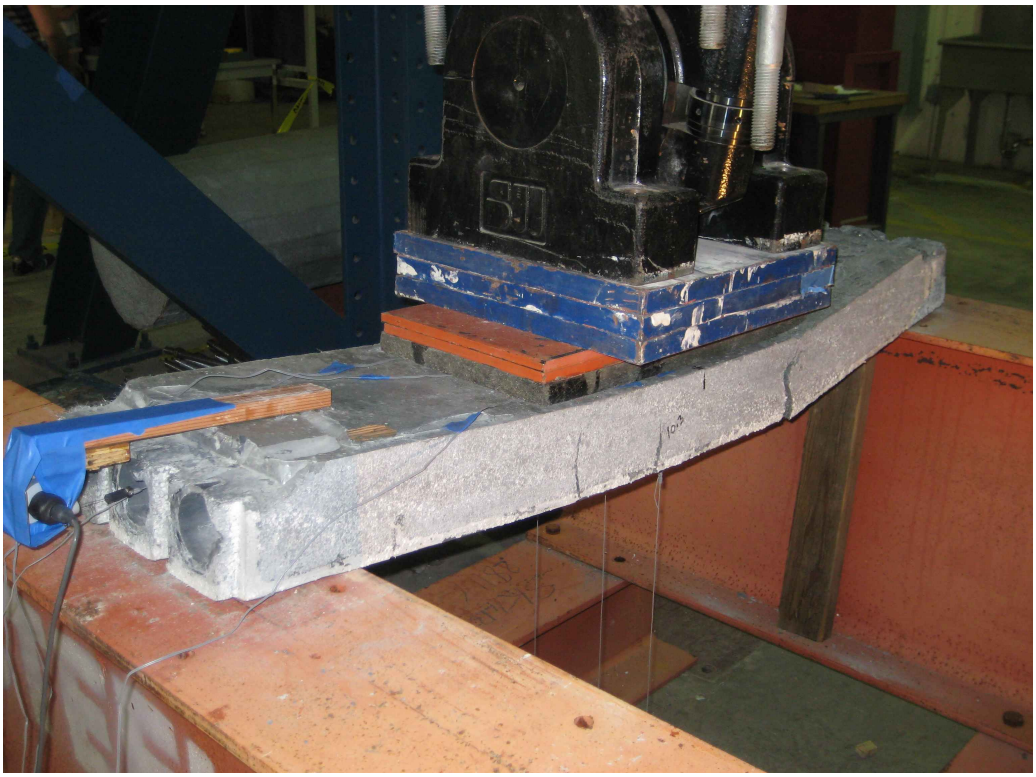

Figure 4.12 Uniform Section Ductal®-FRP Deck Specimen after Failure

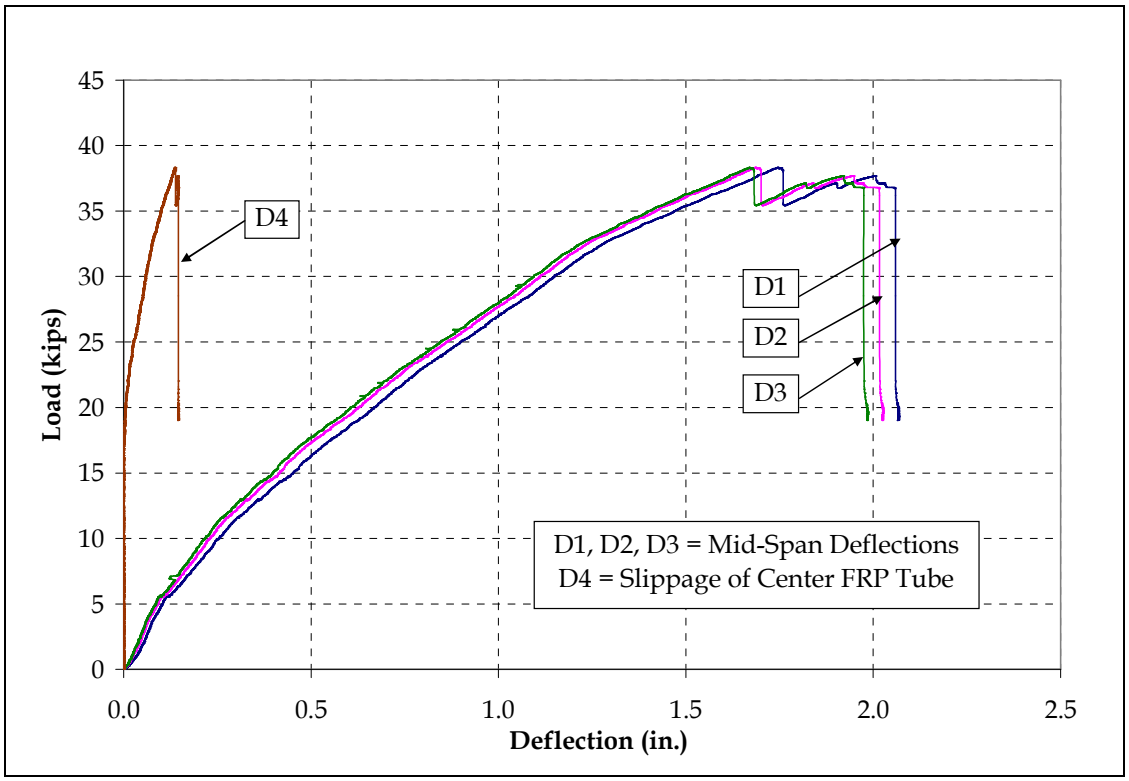

Figure 4.13 Load-Deflection and Load-Slippage Responses for the Uniform Section Ductal®-FRP Deck

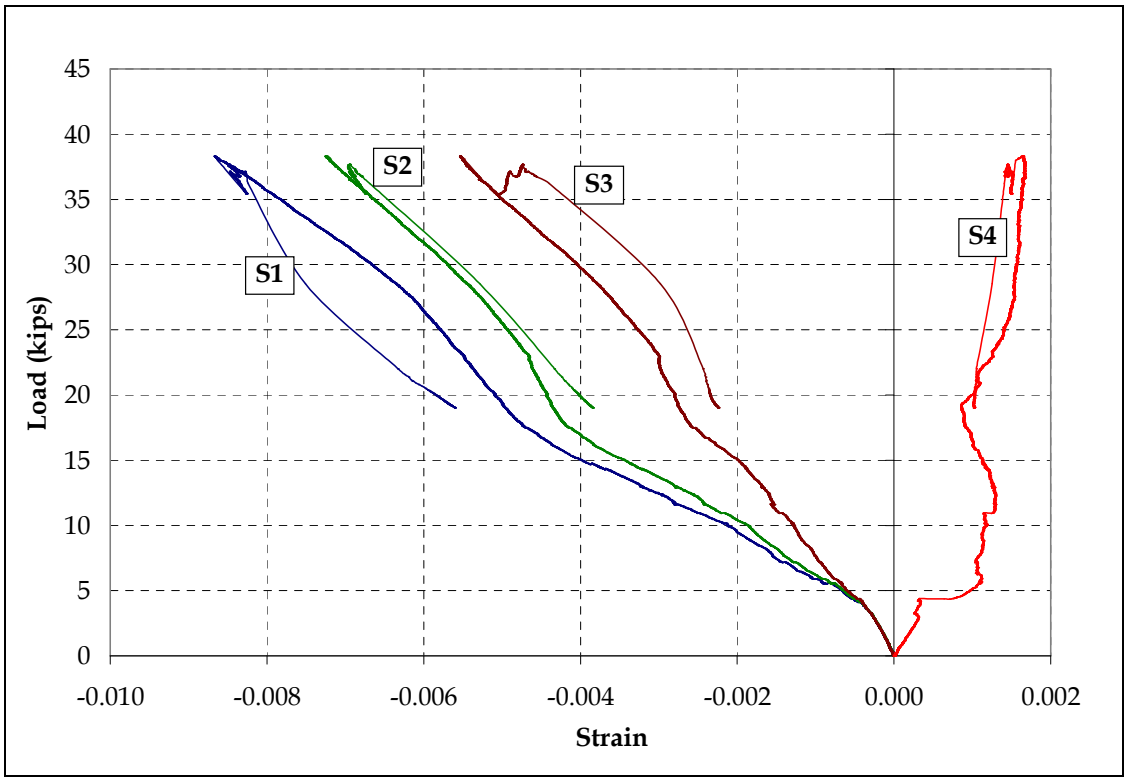

Figure 4.14 Load-Strain Responses for the Uniform Section Ductal®-FRP Deck

4.4.2 Test Results of Tapered Section Ductal®-FRP Deck Specimen

Figures 4.15 to 4.20 show the instrumentation plan, test setup, and failure pattern of the tapered section deck specimen. The deck failed suddenly in compression at 27 kips. Figures 4.21 to 4.24 show the load-deflection and load-strain responses. The failure initiated on the compression side of concrete, and then cracks penetrated into FRP tubes leading to a sudden compression burst failure. Figure 4.22 shows that the tension fibers of FRP tubes remained intact up to failure. The maximum tensile strain in FRP tubes at mid-span (see Figure 4.22) reached 0.032, which is 2.8 times the ultimate strain provided by the manufacturer. The maximum compressive strain in concrete at mid-span reached 0.0052, clearly indicating the crushing of concrete.

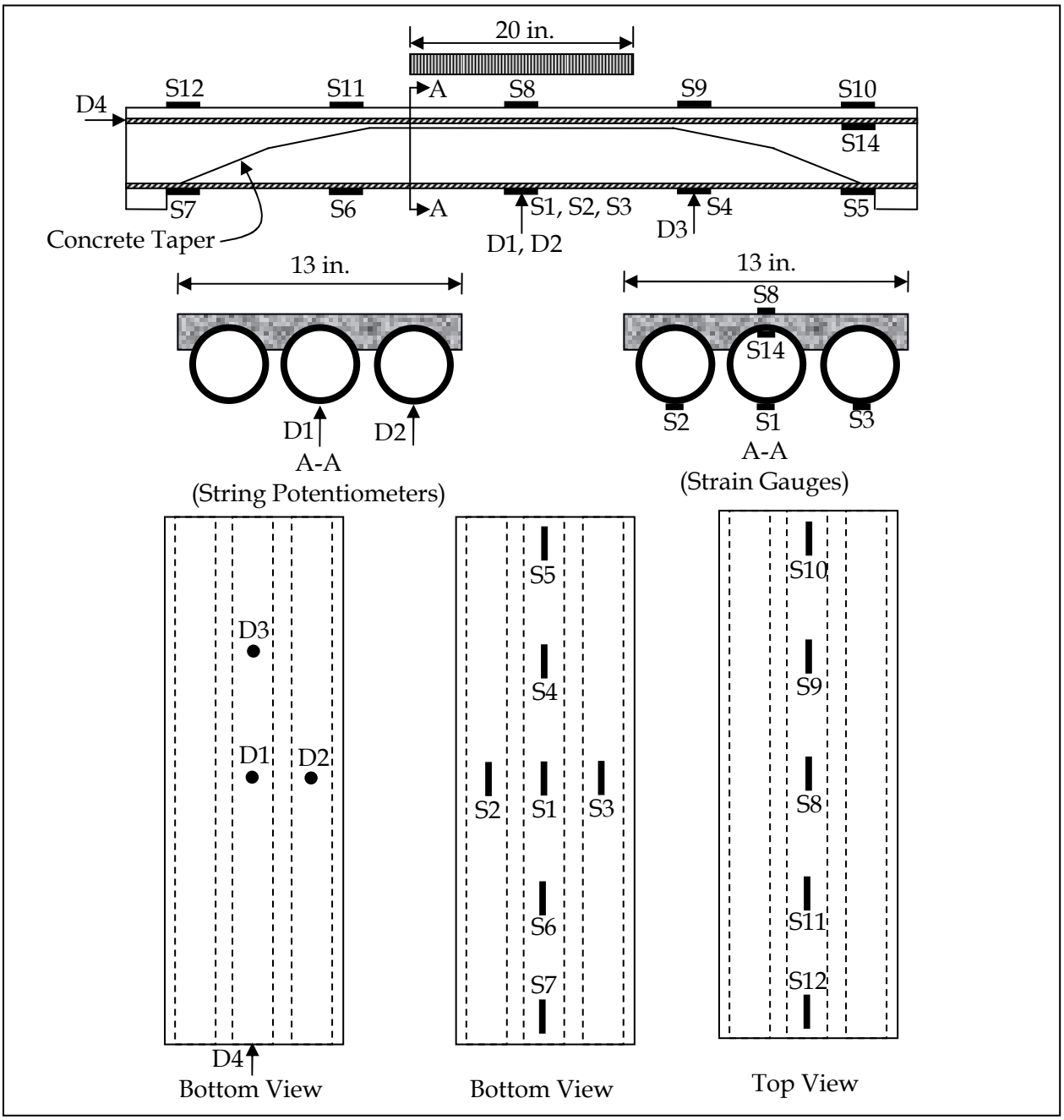

Figure 4.15 Instrumentation Plan for the Tapered Section Ductal®-FRP Deck Specimen

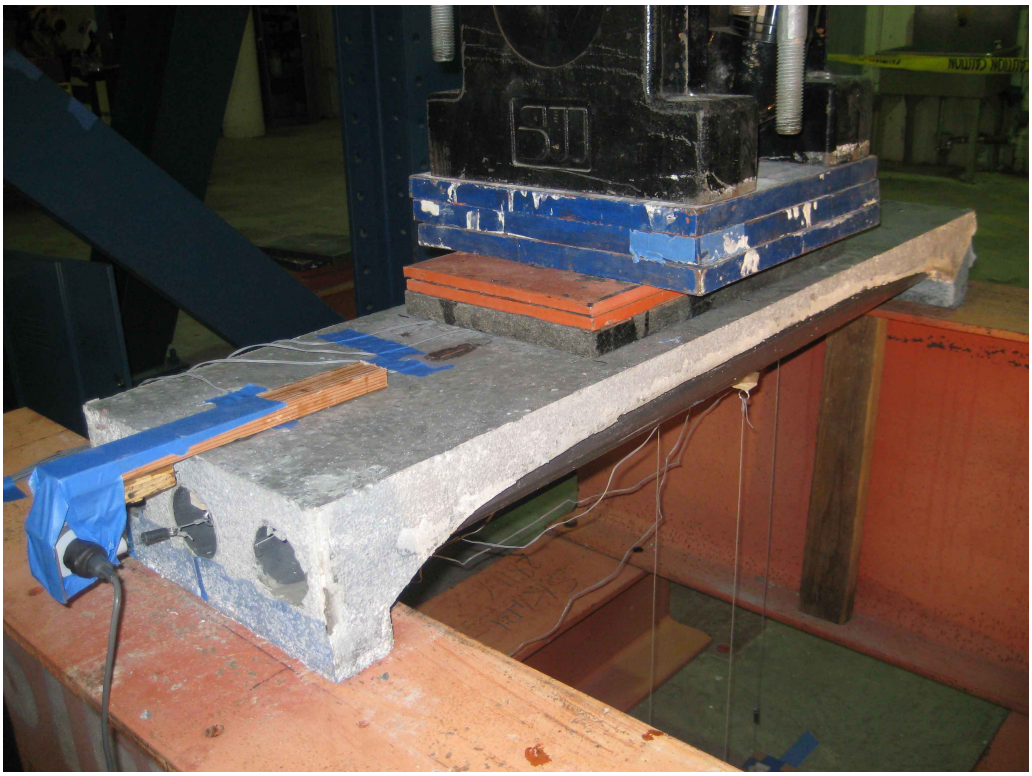

Figure 4.16 Test Setup for the Tapered Section Ductal®-FRP Deck Specimen

Figure 4.17 Failure Pattern of Tapered Section Ductal®-FRP Deck Specimen

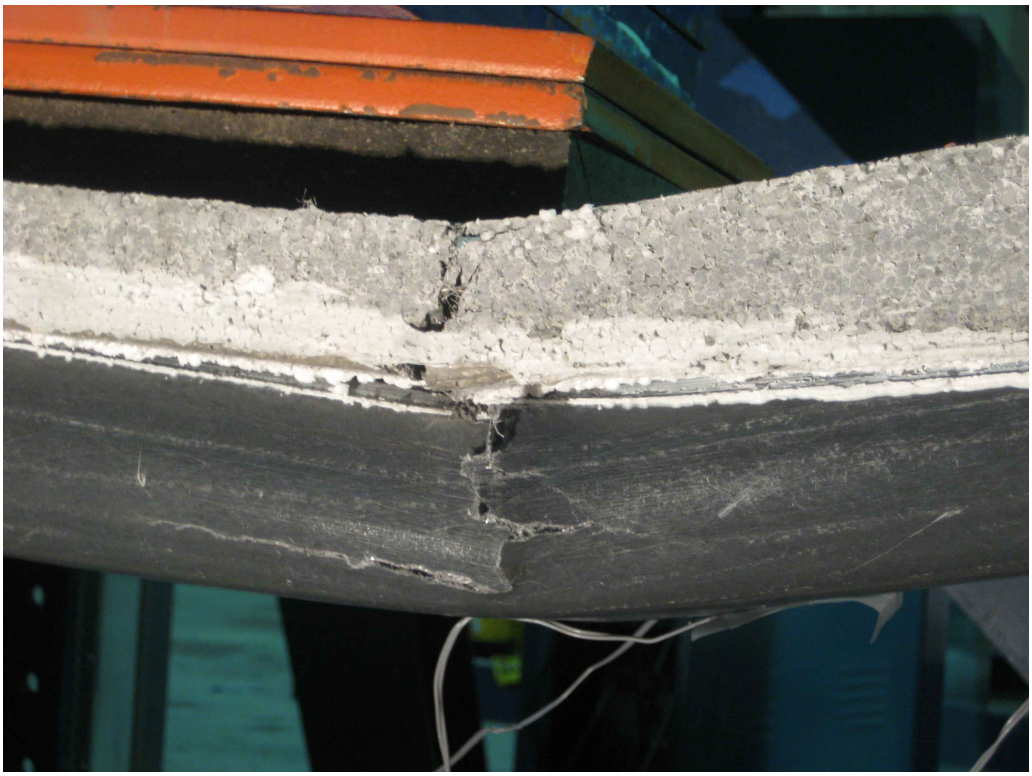

Figure 4.18 Compression Failure of Tapered Section Ductal®-FRP Deck Specimen

Figure 4.19 Un-cracked Tension Face of Tapered Section Ductal®-FRP Deck Specimen

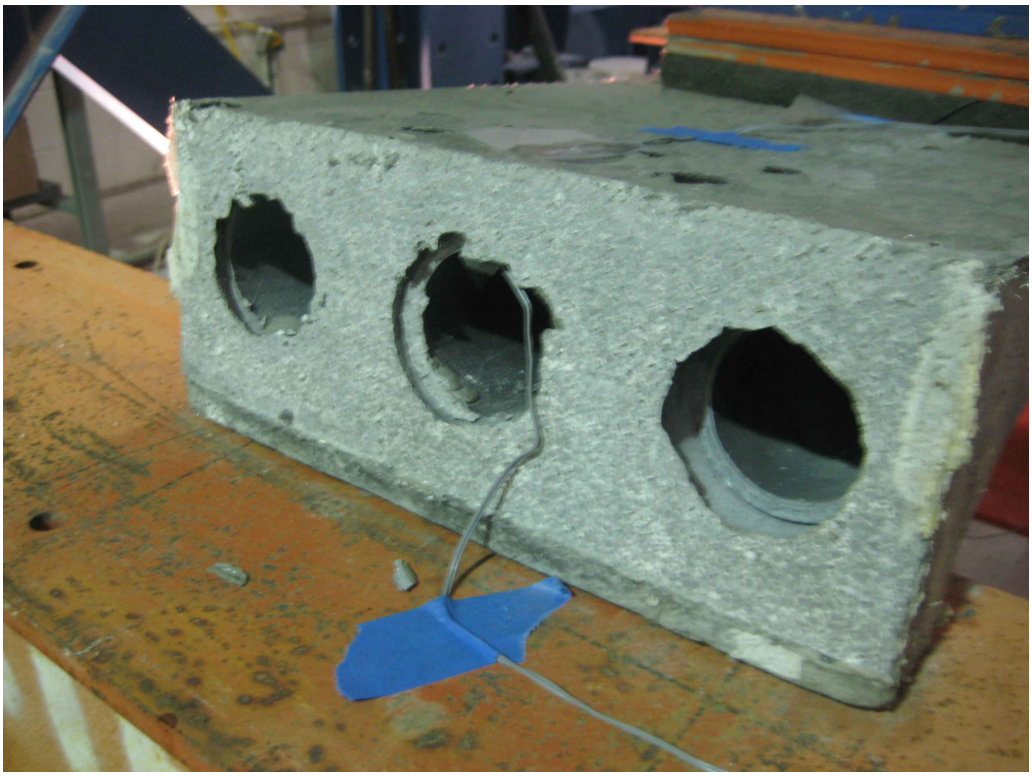

Figure 4.20 Slippage of FRP Tubes in Tapered Section Ductal®-FRP Deck Specimen

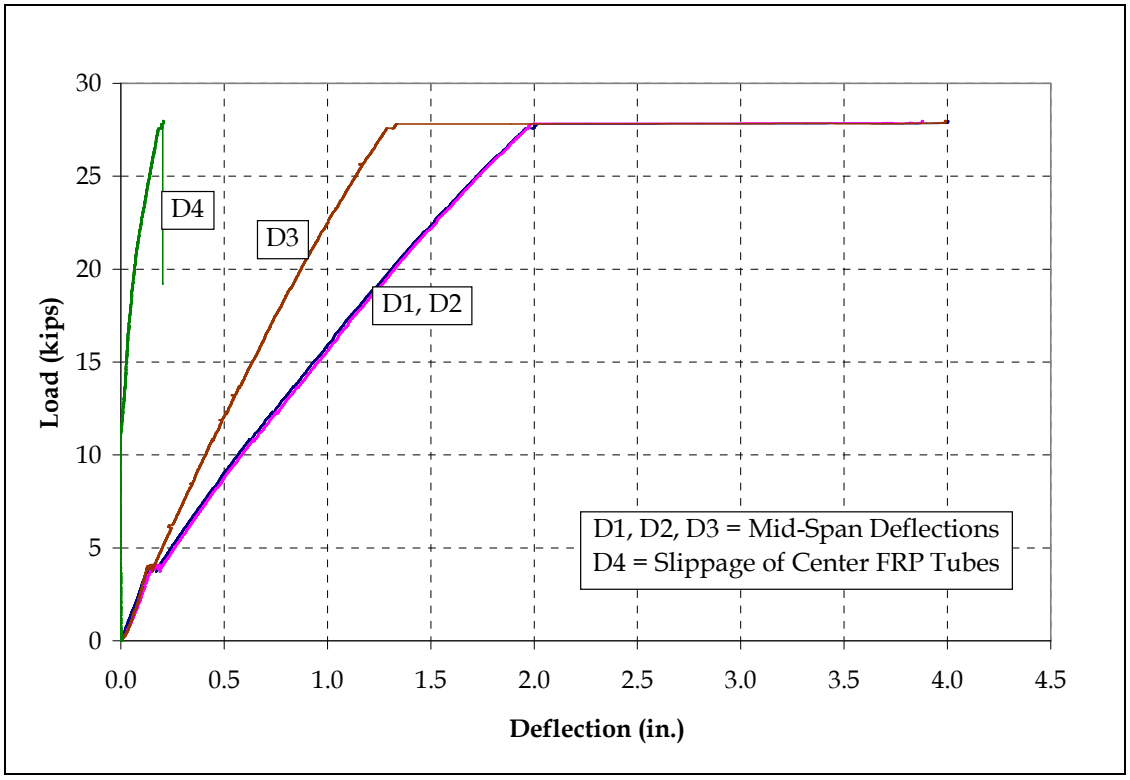

Figure 4.21 Load-Deflection and Load-Slippage Responses for the Tapered Section Ductal®-FRP Deck Specimen

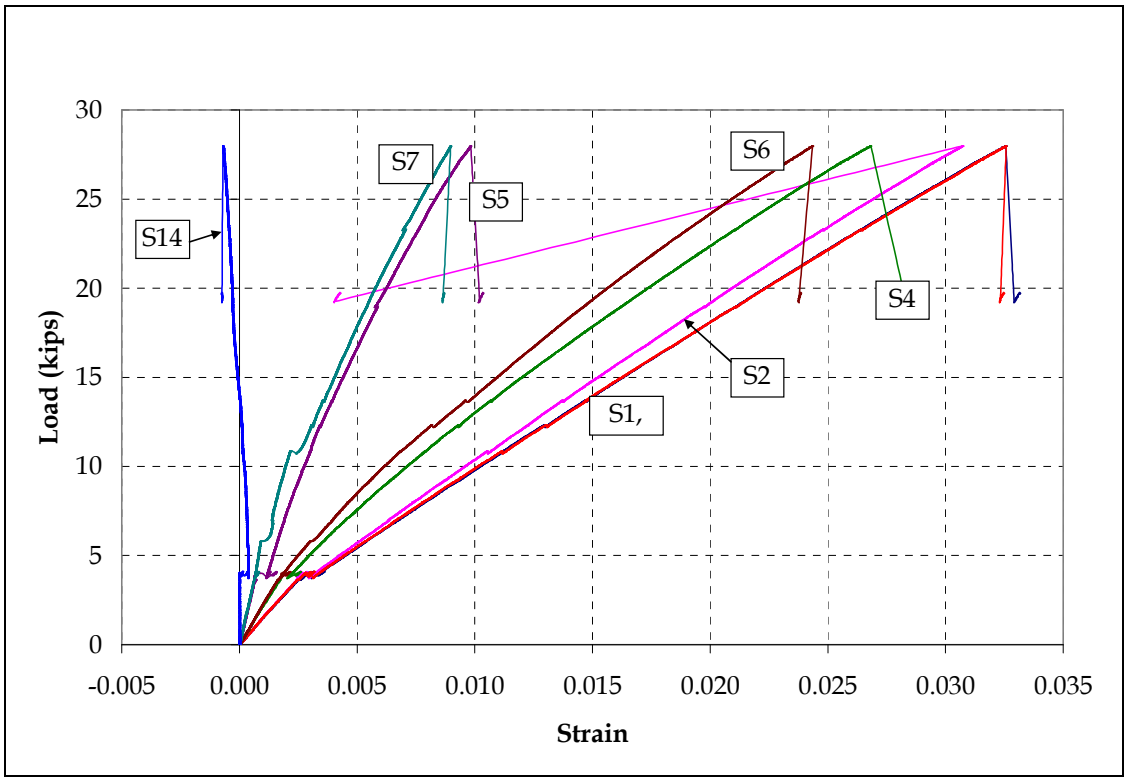

Figure 4.22 Load-Strain Responses for the Tapered Section Ductal®-FRP Deck Specimen

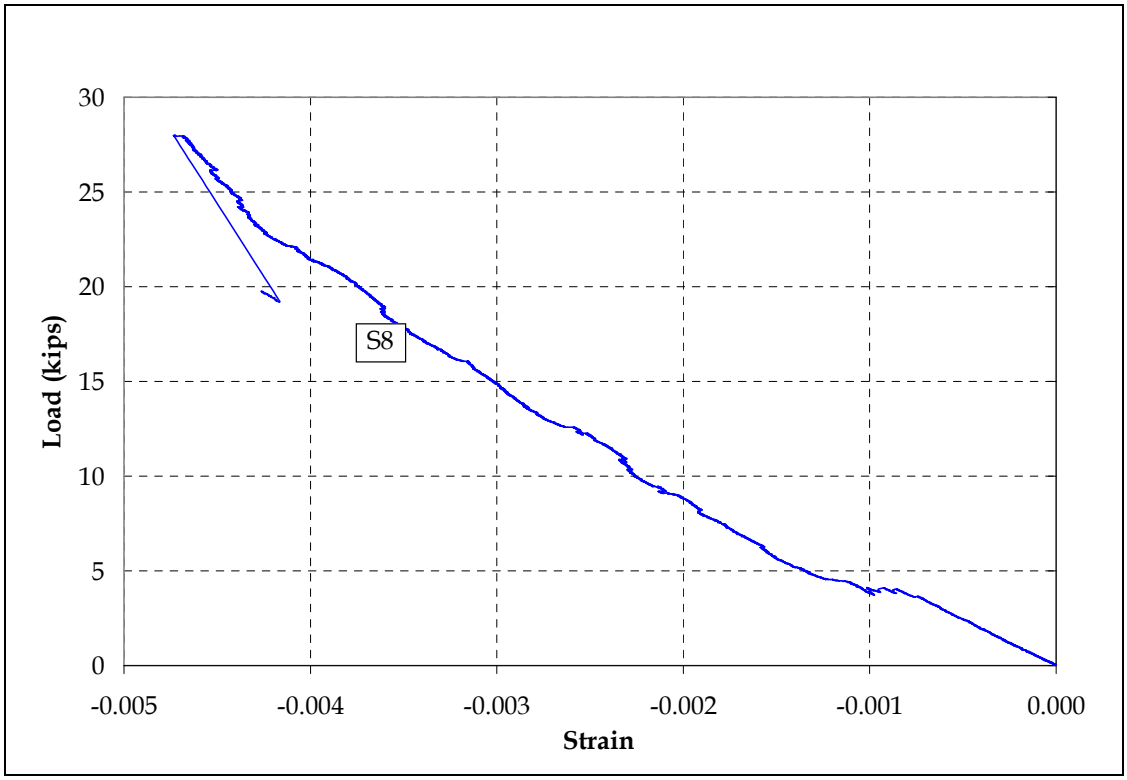

Figure 4.23 Load-Strain Response for the Tapered Section Ductal®-FRP Deck Specimen

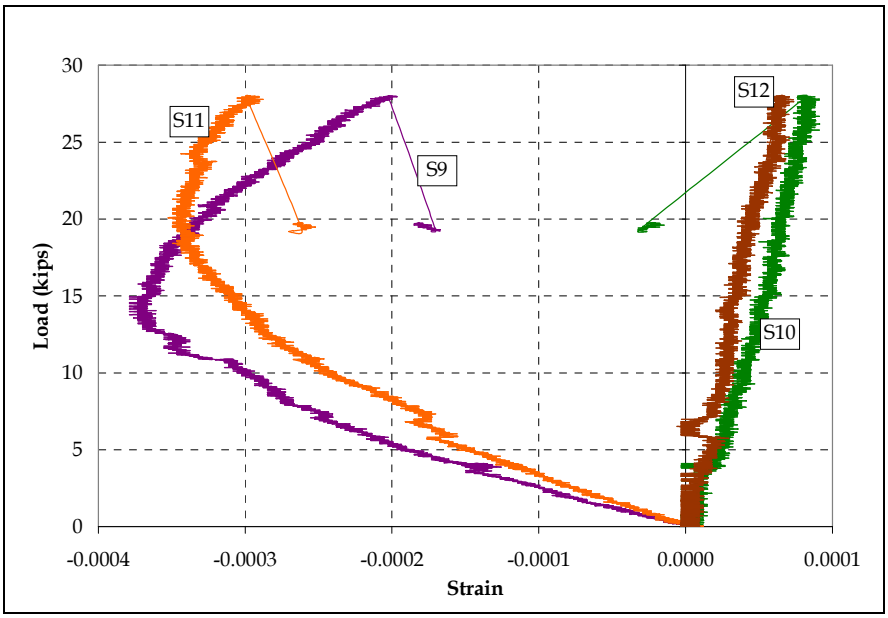

Figure 4.24 Load-Strain Responses for the Tapered Section Ductal®-FRP Deck Specimen

4.5 Comparison of Analytical and Experimental Results

Due to the difficulty encountered during construction of the uniform Ductal®-FRP specimen, the final dimensions of the specimen were slightly different from the preliminary design. Therefore, the analytical model was updated accordingly and compared with test results. The moment-curvature analysis for the 4¼ in. thick uniform Ductal®-FRP deck specimen was performed by dividing the section into 42 layers. Figure 4.25 compares the analytical and experimental results. The slight difference is attributed to the slippage of the tubes, which is not accounted for in the present analytical model.

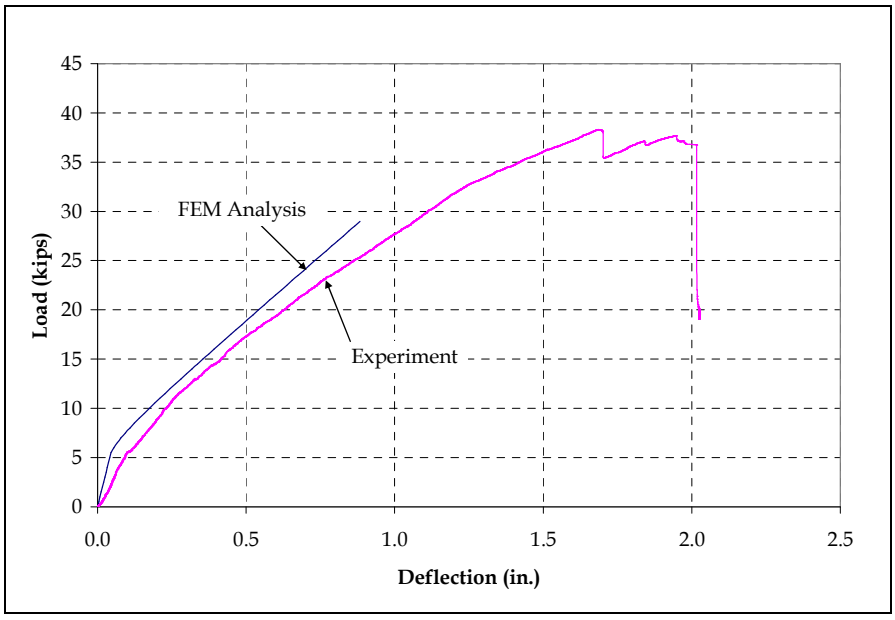

Figure 4.25 Comparison of Analytical and Experimental Load-Deflection Responses for the Uniform Section Ductal®-FRP Deck Specimen

A detailed finite element (FE) model was developed for the tapered section Ductal®-FRP deck specimen, as shown in Figure 4.26. The analytical and experimental load-deflection and load-strain responses for S1 and S8 are compared in Figures 4.27 to 4.29. Again, the difference may be attributed to the slippage of FRP tubes.

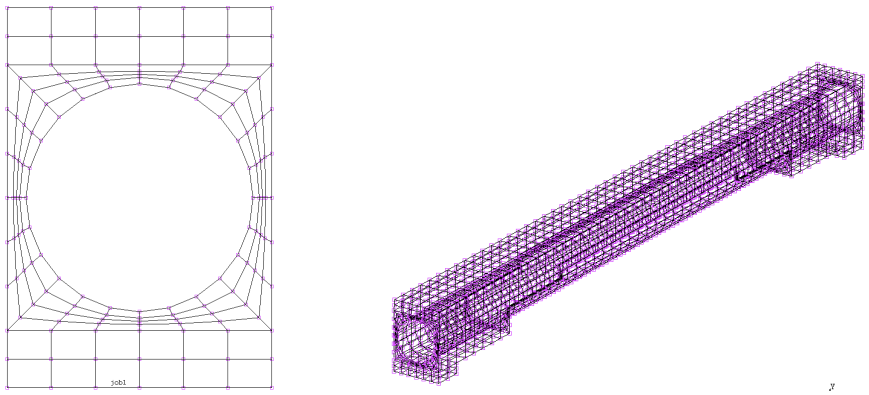

(a) Cross- Section (b) Perspective

Figure 4.26 FE Model for the Tapered Section Ductal®-FRP Deck Specimen

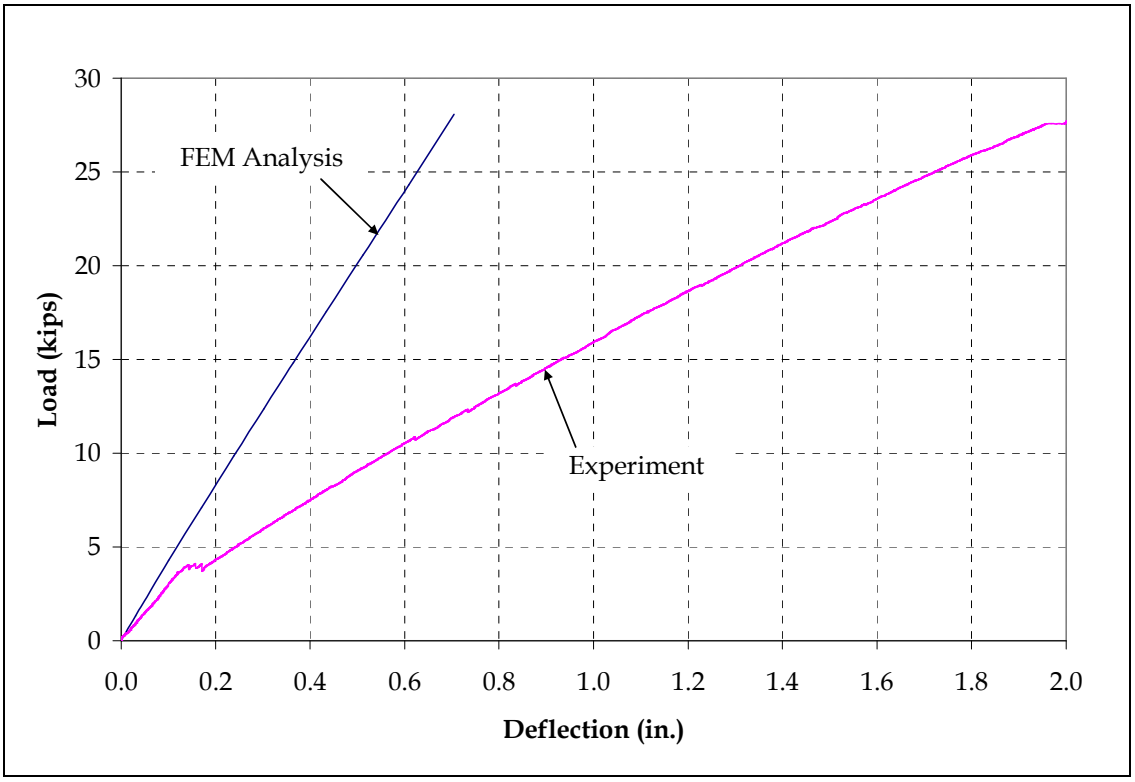

Figure 4.27 Comparison of Analytical and Experimental Load-Deflection Responses for the Tapered Section Ductal®-FRP Deck Specimen

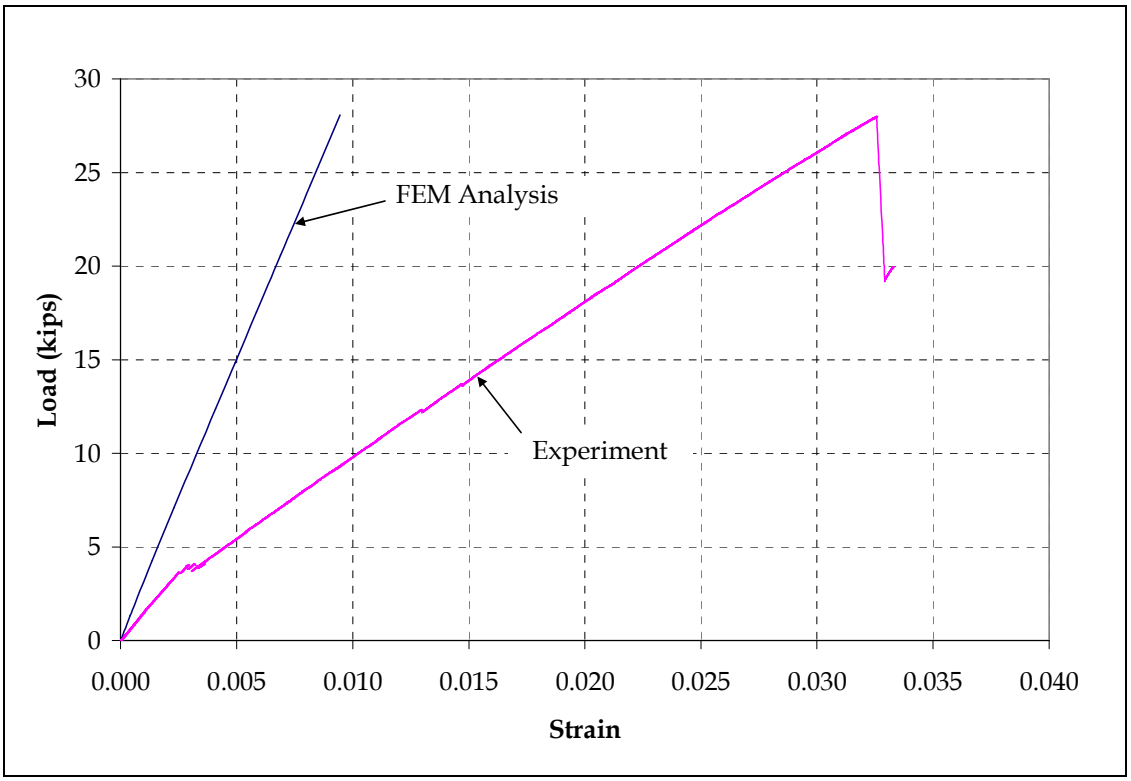

Figure 4.28 Comparison of Load-Strain Responses for Strain Gauge S1 in the Tapered Section Ductal®-FRP Deck Specimen

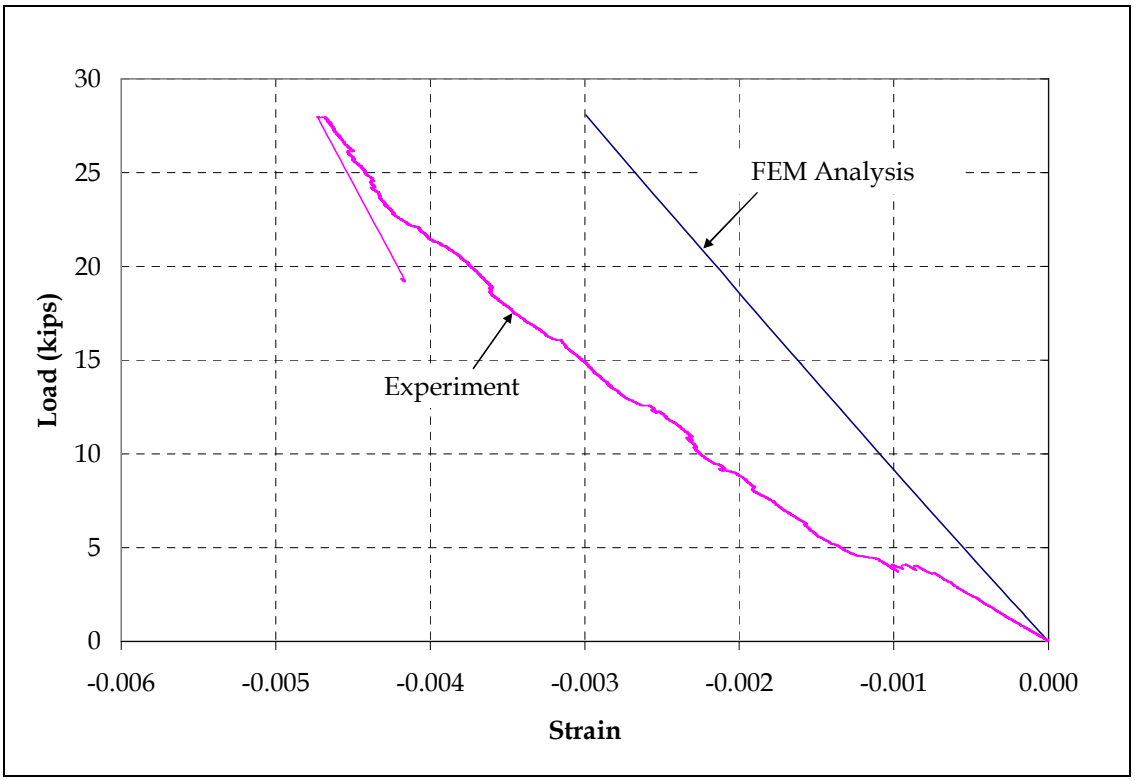

Figure 4.29 Comparison of Load-Strain Responses for Strain Gauge S8 in the Tapered Section Ductal®-FRP Deck Specimen

4.6 Conclusions

The preliminary experimental and analytical work on Ductal®-FRP tubes deck specimens has led to the following conclusions:

1. The system has shown good promise to replace the conventional open steel grid decks. Based on the ultimate loads of the two simple-span specimens, it can be inferred that the multi-unit system will achieve the target load.
2. Both specimens failed suddenly in compression. However, the uniform section deck specimen had significant tensile cracks, as opposed to the tapered section deck that developed no tensile cracks.
3. Greater composite behavior between Ductal® and FRP tubes was observed for the uniform section deck specimen, mainly because the FRP tubes were fully encased in Ductal® throughout the span length.

4.7 Recommendations for Future Research

Since the system has shown significant promise, the experimental work should be expanded to multi-unit two-span specimens. The connections between adjacent deck panels and as well with girders should be designed and tested. Detailed finite element analysis with provisions for slippage is recommended to predict the deck behavior for different load levels and configurations. Moreover, fatigue behavior of the deck needs to be evaluated.

Chapter-5

Summary and Conclusions

The major objective of this research was to develop three alternative deck systems to open grid steel deck. The alternative deck systems should address the rideability and environmental concerns while meeting the strict self-weight limit of 25 lb/ft^2. The three systems considered in this study included an aluminum deck by SAPA Group of Sweden, Ductal®-MMFX steel deck, and Ductal®-FRP tube deck. Detailed experimental and analytical evaluation of the three systems led to the conclusions and recommendations, as listed in the following sections.

5.1 System 1 – SAPA Aluminum Deck

SAPA aluminum deck system went through a rigorous set of component, system, and fatigue load testing, which led to the following conclusions:

1. SAPA aluminum bridge deck panel is a feasible alternative to the open grid steel decks from both the strength and serviceably points of view.

2. Two million cycles of AASHTO-specified fatigue loading on deck panels did not show any sign of global or local failure in the deck panels. Failure of a bolted connection during the fatigue testing was attributed to the fact that only half of the manufacturer-specified bolted clamps were used in the tests due to the narrow flanges of the stringers.

3. Even though deck panels were loaded up to 100 kips in the two residual strength tests, the extreme fiber stresses remained well within their elastic range.

4. Deck-to-girder connections proved adequate for the braking force and the uplift wind, although sudden failure of connections was observed in shear and uplift tests.

5. Elastic and simple plastic analyses may provide adequate estimates for the initial stiffness and ultimate load capacity of aluminum decks.

While the SAPA deck system appears quite ready for implementation, perhaps even as a test section on an existing bridge deck, the following issues still need to be further investigated:

1. Evaluation of available wearing surfaces, such as Acrydur®, poured mastic asphalt, or Ductal®.
2. Field monitoring of aluminum deck under ambient traffic and designated truck loading.

5.2 System 2-Ductal®-MMFX Steel Deck

Detailed component and ancillary tests on Ductal®-MMFX deck system led to the following conclusions:

1. The system has great potential to serve as an alternative to the open grid steel decks. The ultimate load capacity and behavior of the tested specimens make this system an appropriate choice to replace the conventional system.
2. The dominant mode of failure in most of the specimens was in shear, except for the first two specimens which suffered from shear-bond failure.
3. Use of standard 180^{o} hooks at both ends of flexural reinforcement helped effectively avoid bond failure.
4. Shear strengthening and reduced flexural steel did not change the failure mode from shear to flexure. The specimen with shear reinforcement, however, exhibited higher stiffness and a more distributed crack pattern than its counterparts.
5. For the multi-T simple-span and two-span specimens, most of the load was taken by the ribs present either under or near the loading pad, which ultimately led to punching through the slab.
6. Moment-curvature analysis provided a reasonably good estimate of the initial deflection. More elaborate finite element analysis did not provide much better estimate of either the stiffness or the ultimate load capacity.

Although the proposed Ductal®-MMFX deck system seems to be very promising, the following additional work is needed before implementation in the field:

1. Pull-out tests to determine the bond length and effectiveness of hooks and mechanical anchorages in Ductal®-MMFX steel deck.
2. Establishing the load distribution mechanism between the ribs for the design of deck panels.
3. Design of connection with supporting steel stringers.
4. Design of joints between adjacent deck panels.
5. Use of Ductal® materials as wearing surface.
6. Fatigue performance of the deck and its connections.
7. Potential for use of other types of high-strength steel, including stainless steel.

5.3 System 3-Ductal®-FRP Tube Deck

From a couple of preliminary experiments on the Ductal®-FRP tube deck system, one can make the following conclusions:

1. The system has shown good promise to replace the conventional open steel grid decks. Based on the ultimate loads of the two simple-span specimens, it can be inferred that the multi-unit system will achieve the target load.
2. Both specimens failed suddenly in compression. However, the uniform section deck specimen had significant tensile cracks, as opposed to the tapered section deck that developed no tensile cracks.

3. Greater composite behavior between Ductal® and FRP tubes was observed for the uniform section deck specimen, mainly because the FRP tubes were fully encased in Ductal® throughout the span length.

Since the system has shown significant promise, the experimental work should be expanded to multi-unit two-span specimens. The connections between adjacent deck panels and as well with girders should be designed and tested. Detailed finite element analysis with provisions for slippage is recommended to predict the deck behavior for different load levels and configurations. Moreover, fatigue behavior of the deck needs to be evaluated.

References

AASHTO LRFD Bridge Design Specifications, 2005 Interim Revisions, American Association of State Highway and Transportation Officials, Washington, D.C., 2005.

AASHTO LRFD Moveable Highway Bridge Design Specifications, 2008 Interim Revisions, American Association of State Highway and Transportation Officials, Washington, D.C., 2005.

ACI Committee 318, "Building Code Requirements for Structural Concrete (ACI 318-05)."American Concrete Institute, Farmington Hills, MI, 2005.

AFGC/SETRA Working Group, "Ultra High Performance Fiber-Reinforced Concretes, Interim Recommendations." Paris, France, 2002.

Alagusundaramoorthy, P., Harik, I., and Choo, C., "Structural Behavior of FRP Composite Bridge Deck Panels." *Journal of Bridge Engineering*, ASCE, Volume 11, Issue 4, 2006, pp. 384-393.

Aluri, S., Jinka, C., and GangaRao, H.V.S., "Dynamic Response of Three Fiber Reinforced Polymer Composite Bridge." *Journal of Bridge Engineering*, ASCE, Volume 11, Issue 6, November 2005, pp. 722-730.

Ansley, M. H., "Investigation into the Structural Performance of MMFX Reinforcing." *Final Report*, Florida Department of Transportation, 2002.

ASTM A 1035/A 1035M, "Standard Specification for Deformed and Plain, Low-Carbon, Chromium, Steel Bars for Concrete Reinforcement." ASTM International, West Conshohocken, PA., 2006.

ASTM A 615/A 615M, "Standard Specification for Deformed and Plain Carbon-Steel Bars for Concrete Reinforcement." ASTM International, West Conshohocken, PA., 2007.

ASTM C39, "Standard Specification for Flow Table for Use in Tests of Hydraulic Cement." ASTM International, West Conshohocken, PA., 2003.

Bridge Rail Guide, Federal Highway Administration, California Division, Caltrans, 2005.

Chajes, M. J., Mcnally, M., Richardson, D.R., Wenczel, G.C., and Liu, W., "MMFX Rebar Evaluation for I-95 Service Road Bridge 1-712-B." Delaware Center for Transportation, University of Delaware, 2005.

Chanvillard, G., and Rigaud, S., "Complete Characterization of Tensile Properties of Ductal® UHPFRC According to the French Recommendations." in press.

Clemeña, G. G., "Investigation of the Resistance of Several New Metallic Reinforcing Bars to Chloride-Induced Corrosion in Concrete." Virginia Transportation Research Council, 2003.

Communications with Mr. Ryan Fisher, Moveable Structures Project Manager, District 6.

Condition and Performance Report, "Status of the Nation's Highways, Bridges, and Transit." Federal Highway Administration, Washington D.C., 2004

Das, S.K., and Kaufman, J.G., "Aluminum Alloys for Bridges and Bridge Decks." The Minerals, Metals and Materials Society, Warrendale, PA., 2007.

Ductal® Mechanical Performances, Lafarge North America, Canada.

Ehlen, M.A., "Life-Cycle Costs of Fiber-Reinforced-Polymer Bridge Decks." *Journal of Materials in Civil Engineering*, ASCE, Volume 11, Issue 3, August 1999, pp. 224-230.

EXTREN Properties Guide, Strongwell Corporation, Bristol, VA.

Fehling, E., Bunje, K., "The Gartnerplatzbrucke Design of first Hybrid UHPC-Steel Bridge across the River Fulda in Kassel, Germany." Second International Symposium on Ultra High Performance Concrete, Germany, 2008, pp. 581-588.

Gowripalan, N., and Gilbert, R.I., "Design Guidelines for RPC Prestressed Concrete Beams." University of New South Wales, Australia, 2000.

Graybeal, B. A., "Analysis of an Ultra-High Performance Concrete Two-Way Ribbed Bridge Deck Slab." Federal Highway Administration, Washington D.C., 2007.

Graybeal, B. A., "Material Property Characterization of Ultra-High Performance Concrete." Federal Highway Administration, Washington D.C., 2006.

Harris, D.K., and Roberts, C.L., "Characterization of the Punching Shear Capacity of Thin Ultra-High Performance Concrete Slabs." Virginia Transportation Research Council, Charlottesville, VA, June 2005.

Hoglund, T., and Nilsson, L., "Aluminum in bridge decks and in a new military bridge in Sweden." Structural Engineering International, April 2006, pp. 248-351.

Hong, T., and Hastak, M., "Construction, Inspection, and Maintenance of FRP Deck Panels." *Journal of Composites for Construction*, ASCE, Volume 10, Issue 6, December 2006, pp. 561-572.

Hutcheson, D., and Sheppard, M., "Sandwich Panel Performance Optimizing with 3D Fiber Reinforcing Core Architecture." *SAMPE Journal*, Volume 39, Issue 6, 2003, pp. 68-75.

Jerome, S., Connor, O., Hoyos, H., Yannotti, A., and Wagh, V., "Installing an FRP Deck on a Truss Bridge." *Proceedings of the 17th Annual Meeting*, International Bridge Conference, Pittsburgh, PA., 2000.

JSCE Guidelines for Concrete No. 9, "Recommendations for Design and Construction of Ultra High Strength Fiber Reinforced Concrete Structures." Japan Society of Civil Engineering, 2006.

Kahl, S., "Corrosion Resistant Alloy Steel (MMFX) Reinforcing Bar in Bridge Decks." Michigan Department of Transportation, Construction and Technology Division, Lansing, MI., 2007.

Lataste, J. F., Behloul, M., and Breysse, D., "Characterization of Fibers Distribution in a Steel Fiber Reinforced Concrete with Electrical Resistivity Measurements." *NDT&E International*, Volume 41, Issue 8, December 2008, pp. 638-647.MSC Marc, "Theory and User Information, Volume A." MSC. Software Corporation, Santa Ana, CA., 2005.

Mu, B., Wu, H., Yan, A., Warnemuende, K., Fu, G., Gibson, R.F., and Kim, D., "FEA of Complex Bridge System with FRP Composite Deck." *Journal of Composite for Construction*, ASCE, Volume 10, Issue 1, 2006, pp. 79-86.

National Bridge Inventory, Federal Highway Administration, 2008.

Perry, V.H. "A Revolutionary New Material for New Solutions." Technical Forum Presentation, Lafarge North America, 2003.

Perry, V.H., "Innovative Field Cast UHPC Joints for Precast Deck Panel Bridge Superstructures - CN Overhead Bridge at Rainy Lake, Ontario." CSCE 2007 Annual General Meeting & Conference, Canada, 2007.

Perry, V.H., and Zakariasen, D., "Overview of UHPC Technology, Materials, Properties, Markets and Manufacturing." *Proceedings of the 2003 Concrete Bridge Conference*, Orlando, FL., 2003.

Plunkett, J.D., "Fiber-Reinforced Polymer Honeycomb Short Span Bridges for Rapid Installation." IDEA Project Final Report, Transportation Research Board, Washington, D.C., 1997.

Prachasaree, W., GangaRao, H.V.S., and Shekar, V., "Performance Evaluation of FRP Bridge Deck Component under Torsion." *Journal of Bridge Engineering*, ASCE, Volume 11, Issue 4, July 2006, pp. 430-442.

Product Guide on MMFX, MMFX Technologies Corporation, Irvine, CA.

Rizkalla, S., El-Hacha, R., and El-Agroudy, H., "Bond Characteristics of High-Strength Steel Reinforcement." *ACI Structural Journal*, Volume 103, Issue 6, November 2006, pp. 771-782.

Robinson, M.J., Kosmatka, J.B., "Light-Weight Fiber-Reinforced Polymer Composite Deck Panels for Extreme Applications." *Journal of Composites for Construction*, ASCE, Volume 12, Issue 3, June 2008, pp. 344-354.

SAP 2000, "CSI Analysis Reference Manual for SAP 2000, ETABS, and SAFE." Computers and Structures, Inc., Berkeley, CA., 2005

Seliem, H. M., Lucier, G., Rizkalla, S.H., and Zia, P., "Behavior of Concrete Bridge Decks Reinforced with High-Performance Steel." *ACI Structural Journal*, Volume 105, Issue 1, January 2008, pp. 78-86.

Siwowski, T., "Analytical and experimental evaluation of aluminum bridges deck." *Proceeding of European Bridge Engineering Conference*, Rotterdam, March 2003.

Soetens, F., and Straalen, V., "Aluminum bridges, Aluminum bridge decks." *Proceeding of European Bridge Engineering Conference*, Rotterdam, March 2003.

Stiller, W.B., Gergely, J., and Rochelle, R., "Testing, Analysis, and Evaluation of a GFRP Deck on Steel Girders." *Journal of Bridge Engineering*, ASCE, Volume 11, Issue 4, July 2006, pp. 394-400.

Takkasila, M., and Reddy, H. "Structural Modification of Bascule Bridges for Noise Mitigation." Florida Atlantic University, Boca Raton, Fl., April 1996.

Toutlemonde, F., "Fatigue Performance of UHPFRC Ribbed Slab Applied as a Road Bridge Deck Verified According to the Eurocodes." *Proceedings of 5th International Conference on Concrete under Severe Conditions*, France, 2007.

Toutlemonde, F., "Local Compression Tests and Analysis Validating Innovative Design of UHPFRC Anchor Blocks for Post-tensioning Tendons." *Proceedings of Fracture Mechanics of Concrete and Concrete Structures*, Italy, 2007.

Wright, W., "Building the bridge to the 21st century with Aluminum." *Public Roads Magazine*, Volume 60, Issue 4, Spring 1997.

www.aluminium.matter.org.uk, accessed on July 11, 2009

www.glasssteelandstone.com, accessed on May 12, 2009

www.heartlandconnection.com, accessed on June 26, 2009

www.idsi.org, accessed on April 12, 2009

Yotakhong, P., "Flexural Performance of MMFX Reinforcing Rebars in Concrete Structures." Department of Civil, Construction, and Environmental Engineering, North Carolina State University, 2003.

Zhang, Y., Cai, C.S., Shi, X., and Wang, C., "Vehicle-Induced Dynamic Performance of FRP versus Concrete Slab Bridge." *Journal of Bridge Engineering*, ASCE, Volume 11, Issue 4, July 2006, pp. 410-418.

Appendix A: Summary of SAPA Group Research Reports on Aluminum Decks

Report 1: On the Corrosion Resistance Point of View

In 1987, the Swedish corrosion institute conducted a corrosion assessment on the SAPA deck system made of Aluminum AA6063. The decks were placed on the steel girder with an isolation neoprene pad, along with an Acrydur® wearing surface. As the deck system is copper free, it is believed to be resistant to general corrosion. One possible form of corrosion is called inter-granular corrosion, which causes the formation of cracks, but these cracks have very little impact on the mechanical properties of the deck system. Another corrosion possibility is called stress corrosion, which only happens when the material is treated with high temperature or when it is aging for a long time. The report stated that the same material has been used under traffic for up to 20 years without any problem. Regarding the connecting bolts, several material choices are available; among them the stainless steel is the most corrosion-resistant choice.

In order to prevent corrosion problems, several suggestions are made in the report, among which is sealing the surface before assembling, and performing field inspections on a regular basis.

The report made the following conclusions:

- The experience to date suggests that the deck can normally be used in the urban, industrial, and marine environments.
- The risk of emergence of corrosion phenomenon (spanning corrosion or inter-crystalline corrosion) which can give rise to cracking is minute.
- Cracks that may occur under corrosion, if any, are relatively small, and do not affect the mechanical properties of the deck.
- The recommended bolt material is primarily stainless steel SS 2332, SS 2333 or SS 2343. Carbon steel bolts, hot zinc coated or treated with Sanbond-Z may also be recommended, but not in a marine environment.
- Regular bridge inspection can provide re-assurance on the health of structural members.

Report 2: On the Field Deformation Test

Report 2 is related to the field testing of aluminum deck on Tottnäs Bridge in 1990. The bridge links Toro with the mainland outside Launceston. This bridge is the first to use the 4 in. thick aluminum deck system. The bridge was 52.7 ft long with two fixed spans and an opening swing band. Deck width was 1.7 ft.

Both static and dynamic deflection readings were collected at 15 locations along the bridge. The maximum measured deflection on the bridge by a truck weighing 27.3 kips was 0.17 in. which corresponds to l/680 of the span length (wing-span 10 ft). During the crossing, four people were

present on the bridge near the loading point. None could say that the downward deflection in any way was disturbing.

Report 3: Lab Testing of the Clamps

This report covers the lab test on the clamps. Tensile force was applied to test the fatigue behavior of the connection under certain rotations. There was a 1.6 in. wide and 0.04 in. thick metal sheet between the clamps and the deck profile. Two clamps designated as clamp 50 and 100 were tested. For the screw fastening of the clamp 50, a torque of 41.3 kip-ft was applied. The fatigue load was 0-2 kips. After 2 million cycles the clamps were intact. For the screw fastening of the clamp 100 a torque of 53 kip-ft was applied. The fatigue load was 2.3-3.4 kips. After 1.59×10^6 cycles the lip of clamp broke, but this represents an extreme case in the field.

Report 4: Strength Test on Deck 100

Three bridge decks were assembled with the length 96 in. Wedge-shaped inserts (2 in. wide and 0.4 in. high) were used to simulate the concentrated loading on the edge of the beam. Loading was applied using two steel plates 8 in. x 12 in. each. The ultimate load was 90 kips, with the transverse load of 81 kips. The load-deflection response showed that as the load exceeded 72 kips, the deflection rose sharply.

Report 5: Fatigue, Railing, and Suspension Tests

In 1989, KTH (Kungl Tekniska Högskolan) performed the following three tests on the SAPA 100 bridge deck system:

1. Fatigue test of the aluminum profile with Z connections
2. Test of railing attachment
3. Test of suspension connection

Fatigue Test
The four-piece assembled deck was tested without joints and with the z profile joint and/or the splice plate. The loading ranged from 5.6 kips to 22.5 kips (or 28 kips). All three configurations went over 2 millions cycles, but the failure of the screw occurred on the specimen with the splice plate during the fatigue test largely due to its high stiffness. The residual strength test after fatigue loading showed the specimen with only Z profile provides a highest 105 kips ultimate load. The failure was localized in just one unit and thus the broken piece could be easily replaced.

Railing System
The test setup followed the exact dimensions from the real bridges. The rails on both sides were tested by applying a horizontal load to develop the 16 in. and 20 in. lateral displacement on the top of the 50 in. high rail rod. The ultimate moment capacity (around 18 kip-ft) of the rail system from the experiment exceeded the predicted value based on the material properties.

Suspension System
This test was aimed to get the suspension capacity of the deck system. A special connector installed between the deck units was used to provide the suspension connection using a hole for installing an M20 screw. The deck specimen was placed upside down and subjected to a tensile force on the edge of the deck as well as at a point 20 in. away from the edge. The two loading cases yielded similar results of the suspension load capacity as 55 kip/ft. The failure occurred because shear of the aluminum deck itself. The shear strength from the experiment was determined as 17,400 ksi compared to 16,675 ksi from the analysis.

Report 6: Bending and Twist of Deck Profile

Individual profiles were studied under bending, twist, and tension. Tensile test was carried out at different sections to determine tensile strength and elongation. Furthermore, bend and twist tests were carried out to study the impact of the surfacing on the bending and twist rigidity. The test consisted of five specimens. Three of the test cells used for bend test, one with surfacing and two without surfacing. For the twist test, one specimen was with surfacing and one without.

In the bending test, the flexural rigidity EI of the specimen with surfacing was compared with the unpaved specimen. These values were also compared with the theoretical bending stiffness. For the twist test, a similar analysis was performed. Torsional stiffness (GJ) was calculated theoretically and compared with the experimental.

Bending Test
The comparison of test 1 (with surfacing) and test 2 (without surfacing) showed that surfacing would increase the bending stiffness by 17%. The comparison of test 1 and test 3 (without surfacing) showed lesser difference in bending stiffness than between tests 1 and 2.

Torsion Test
Calculation of the torsional stiffness was made according to the elastic theory, as in the case of bending stiffness. Only St.Venant's torsion was taken into account. The analytical model had a simplified geometry, compared with the actual profile. In the four outer corners, the model had smaller cross-sectional area than the actual profile. Therefore, the theoretical stiffness was smaller than the experimental value.

Report 7: Testing of Acrydur® Coating on SAPA Bridge Deck

On behalf of SAPA Front and Ulfear the Division of the steel building at the Royal Institute of Technology conducted extensive tests on a bridge deck built of aluminum panels coated with Acrydur® coating. The purpose of the test was to study how the surface is affected by traffic load at different temperatures. In the past the cracking observed in some surfaces was believed to be due to embrittlement at low temperatures. The tests were carried out at room temperature and in the freezer as well.

For the test, a test machine was built by SAPA. The test machine was built to simulate a wheel from the rear axle of a truck running back and forth on a bridge deck. Bridge deck was constructed of two bridge elements with a total size of 8.9 ft x 11.8 ft.

Bridge deck used for the test was manufactured by two elements assembled in the factory. Each element consisted of six bridge planks with 4 in. height mounted on the Z-beams. Surface was laid in three stages, primer, the membrane layer and the tread surface.

At -32.8°F a crack in Acrydur® along the seal was observed. The crack was approximately 0.02 in. within the wheel width and 0.008 in. on both sides. The crack grew with lowering of the temperature to -40°F and was 0.04 in. at the wheel, and approximately 0.02 in. outside the wheel. No cracks or damage to the rest of the surface was observed during the test period.

Appendix B
(Drawings of SAPA Aluminum Deck and Connectors)

NUMMER F1-3121 BET 00

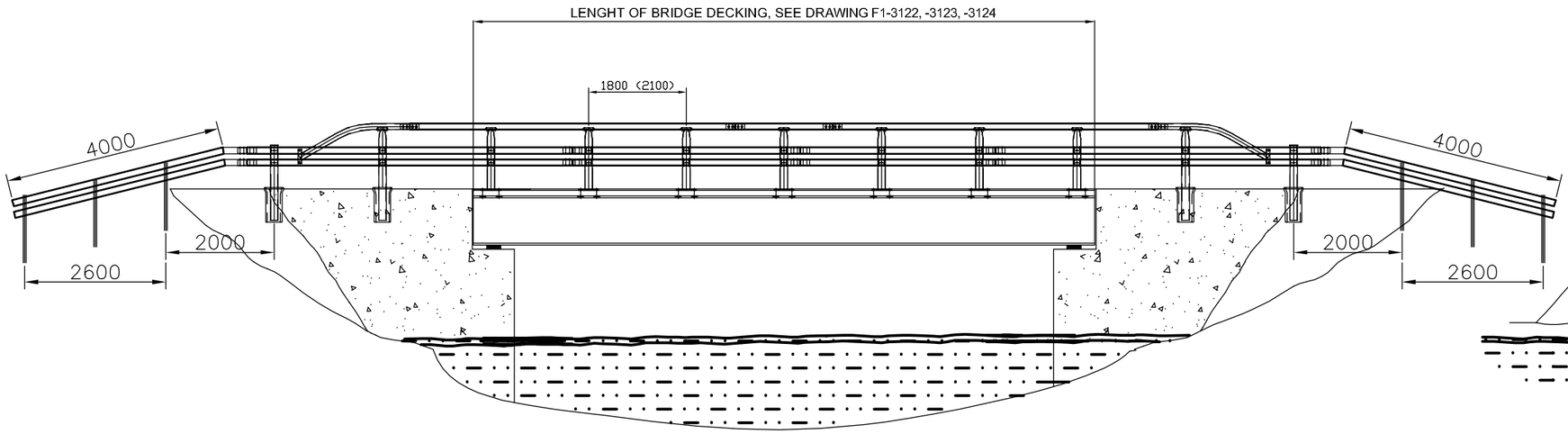

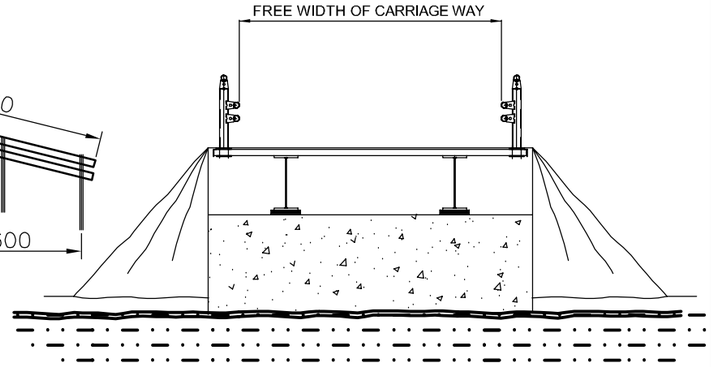

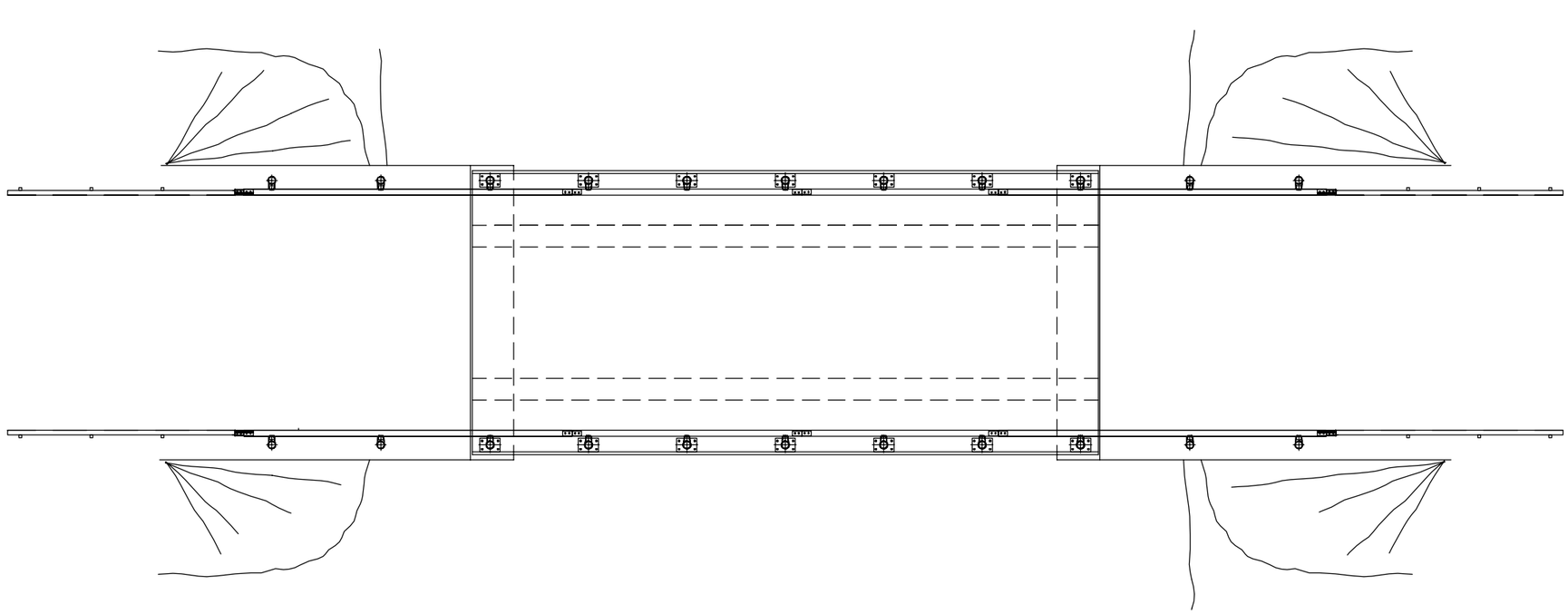

SCALE
1:100 1 0 1 2 3 4 5 6 7 8 9 10 M.
1:50 1 0 1 2 3 4 5 M.
1:20 1 0 1 2 M.

INSTRUCTIONS

LOADING REQUIREMENT
The bridge decking is designed for traffic loads according to Vägverket ATB Bro 2004, Publ 2004:56.

LOADING CAPACITY
The bridge decking is control calculated for traffic load EG A/B = 20/40 tons with axle weight A and bogie weight B according to Vägverket ATB Bro 2004, Publ 2004:56.

PAVEMENT
The bridge decking should be covered with either acrylic on poly-urethane to a thickness of 10 mm or poured asphalt to a thickness of 30 mm according to Vägverket ATB Bro 2004, Publ 2004:56.

GENERAL
The drawing shows the principal build up of the bridge decking with Sapa Bridge Decking System 100 according to Sapa System Description 2002-10-11.

Sapa Bridge Decking System 100 be suited for new constructions, reconstruction and repairing and can replace for example concrete bridge deckings.

Weight of Sapa Bridge Decking System 100 is 63 kgs/square metre.

DRAWING LIST

BET	ANT	ÄNDRINGEN AVSER	DATUM	UA SIGN	QA SIGN	VV DAT	VV SIGN
-		-	-	-			

SAPA BRIDGE DECKING SYSTEM

ALUMINIUM BRIDGE DECKING SYSTEM 100

Sapa Building System AB
SE-574 81 Vetlanda Sverige/Sweden
Telefon/Telephone +46 (0)383-942 00
Telefax/Telecopy +46 (0)383-76 19 80

UPPDRAG NR	RITAD	KONSTR	GRANSKAD
	MIL		RoS

PRINCIPAL ASSEMBLY DRAWING

DATUM	HANDLÄGGARE
050530	MIKAEL LINDQVIST

SKALA	GODKÄND	ERSÄTTER RITNING	NUMMER	BET
1:50		Nr	F1-3121	00

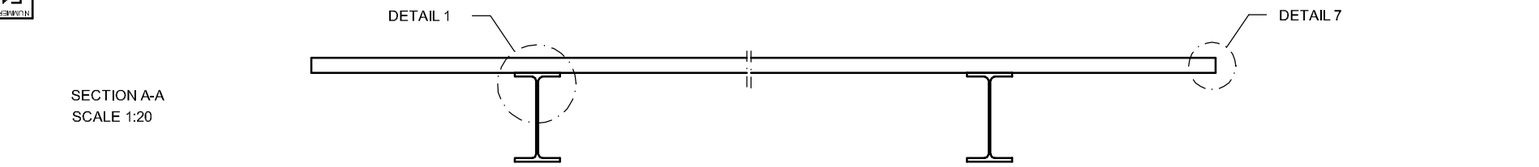

SECTION A-A
SCALE 1:20

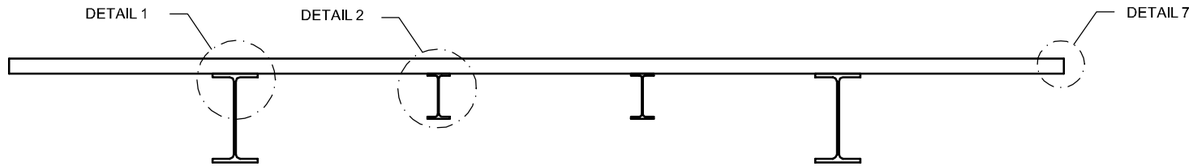

SECTION B-B
SCALE 1:20

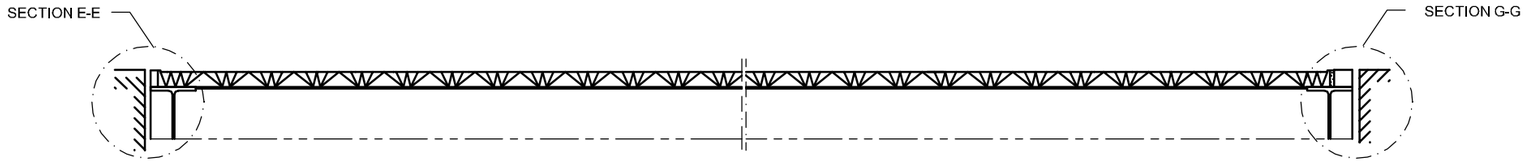

SECTION C-C
SCALE 1:20

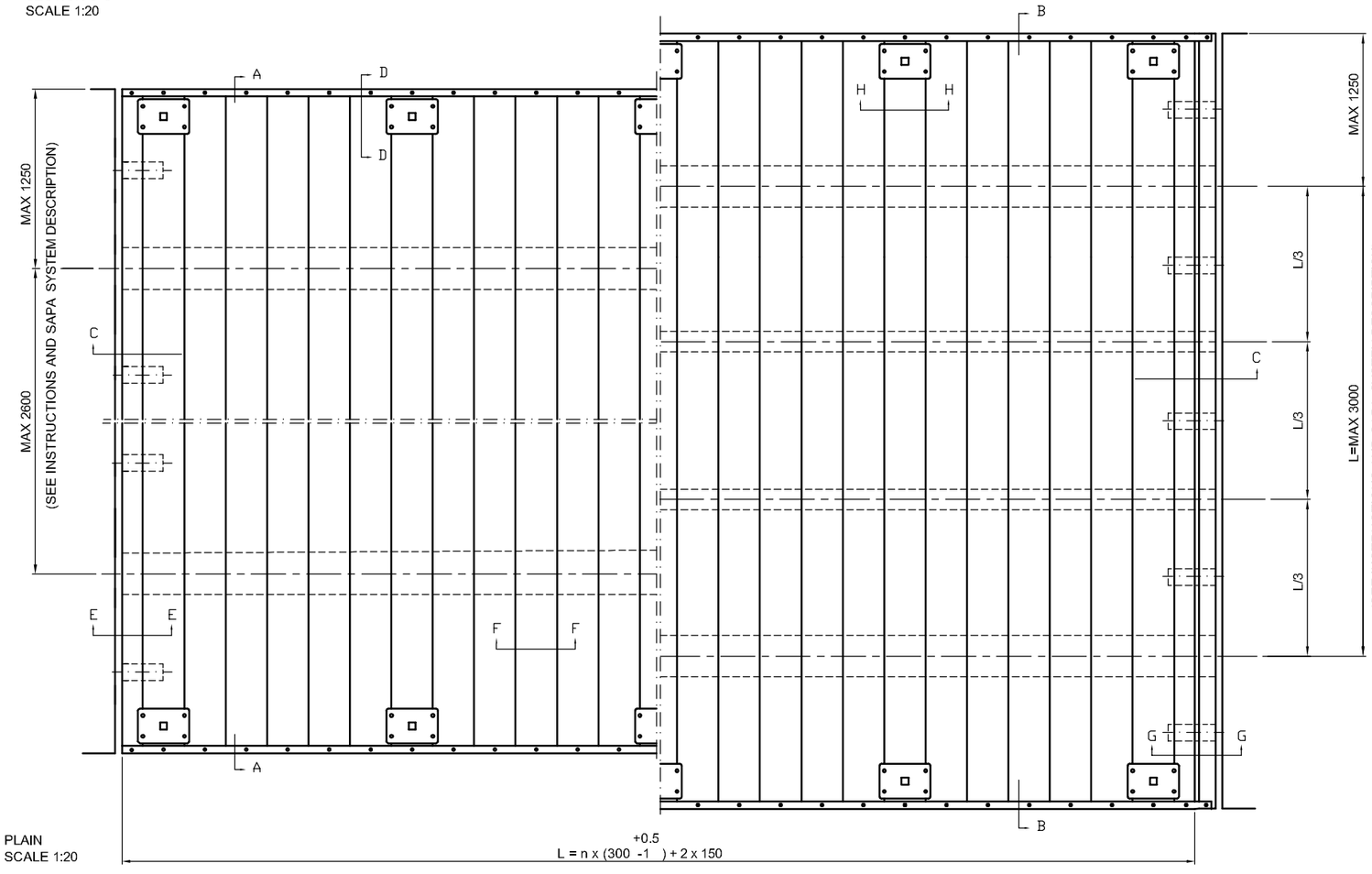

PLAIN
SCALE 1:20

SCALE
1:100 1 0 1 2 3 4 5 6 7 8 9 10 M.
1:50 1 0 1 2 3 4 5 M.
1:20 1 0 1 2 M.

INSTRUCTIONS

LOADING REQUIREMENT

The bridge decking is designed for traffic loads according to Vägverket ATB Bro 2004, Publ 2004:56.

LOADING CAPACITY

The bridge decking is control calculated for traffic load EG A/B = 20/40 tons with axle weight A and bogie weight B according to Vägverket ATB Bro 2004, Publ 2004:56.

PAVEMENT

The bridge decking should be covered with either acrylic on poly-urethane to a thickness of 10 mm or poured asphalt to a thickness of 30 mm according to Vägverket ATB Bro 2004, Publ 2004:56.

GENERAL

The drawing shows the principal build up of the bridge decking with Sapa Bridge Decking System 100 according to Sapa System Description 2002-10-11.

Sapa Bridge Decking System 100 be suited for new constructions, reconstruction and repairing and can replace for example concrete bridge deckings.

The end profiles 150/100 and the nearest first half of bridge decking profile 300/100 must be standing on a cross bar or bracket according to section E-E and G-G.

Stringers according to Detail 2 shall always be used in the ends of the bridge if a cross bar or brackets not can be used.

The total lenght L can be adjusted within using bridge decking profile 300/100 and 280/100 in combination. A combination of this profiles also is necassary to compensate possible building tolerance deviations. Two bridge decking profiles 280/100 NOT allowed to be placed side by side.

The base plate to the balusters for bridge railing placed on the decking shall be designed according to drawing F1-3128.

Possible water drain shall be designed according to drawing F1-3125.

Detail 1, 2 and 7 according to drawing F1-3125.

Section D-D to H-H according to drawing F1-3126.

BET	ANT	ÄNDRINGEN AVSER	DATUM	UA SIGN	QA SIGN	VV DAT	VV SIGN
-		-	-	-			

SAPA BRIDGE DECKING SYSTEM

ALUMINIUM BRIDGE DECKING SYSTEM 100

Sapa Building System AB
SE-574 81 Vetlanda
Sverige/Sweden
Telefon/Telephone +46 (0)383-942 00
Telefax/Telecopy +46 (0)383-76 19 80

UPPDRAG NR	RITAD	KONSTR	GRANSKAD
	MIL		RoS
DATUM	HANDLÄGGARE		
050531	MIKAEL LINDQVIST		
SKALA	GODKÄND		
1:20			

ASSEMBLY DRAWING

PLAIN BRIDGE DECKING

ERSÄTTER RITNING	NUMMER	BET
Nr	F1-3122	00

F1-3123 00
NUMMER BET

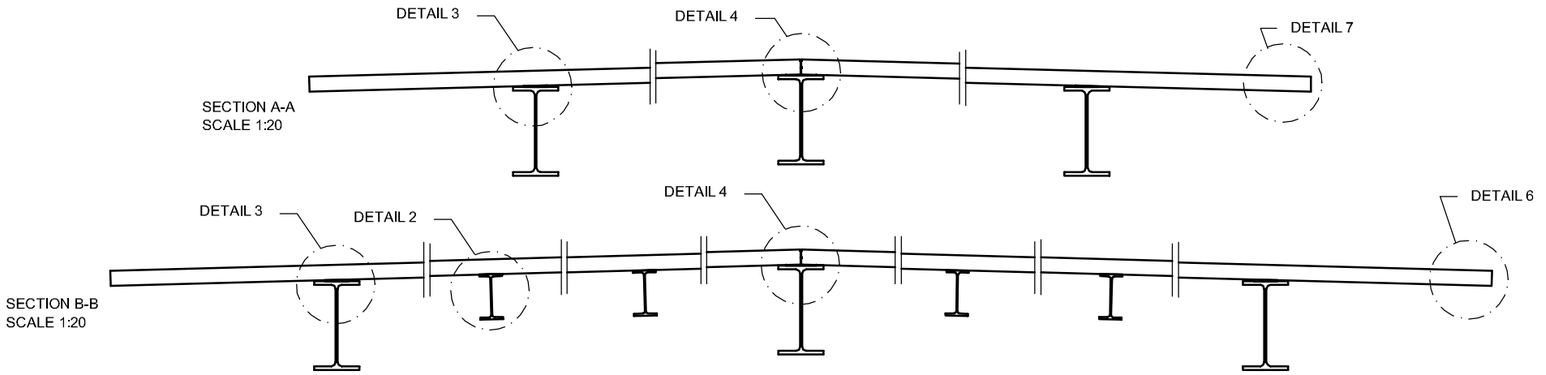

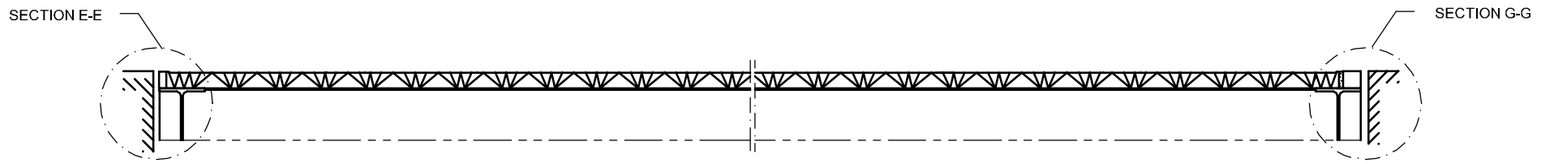

SECTION C-C
SCALE 1:20

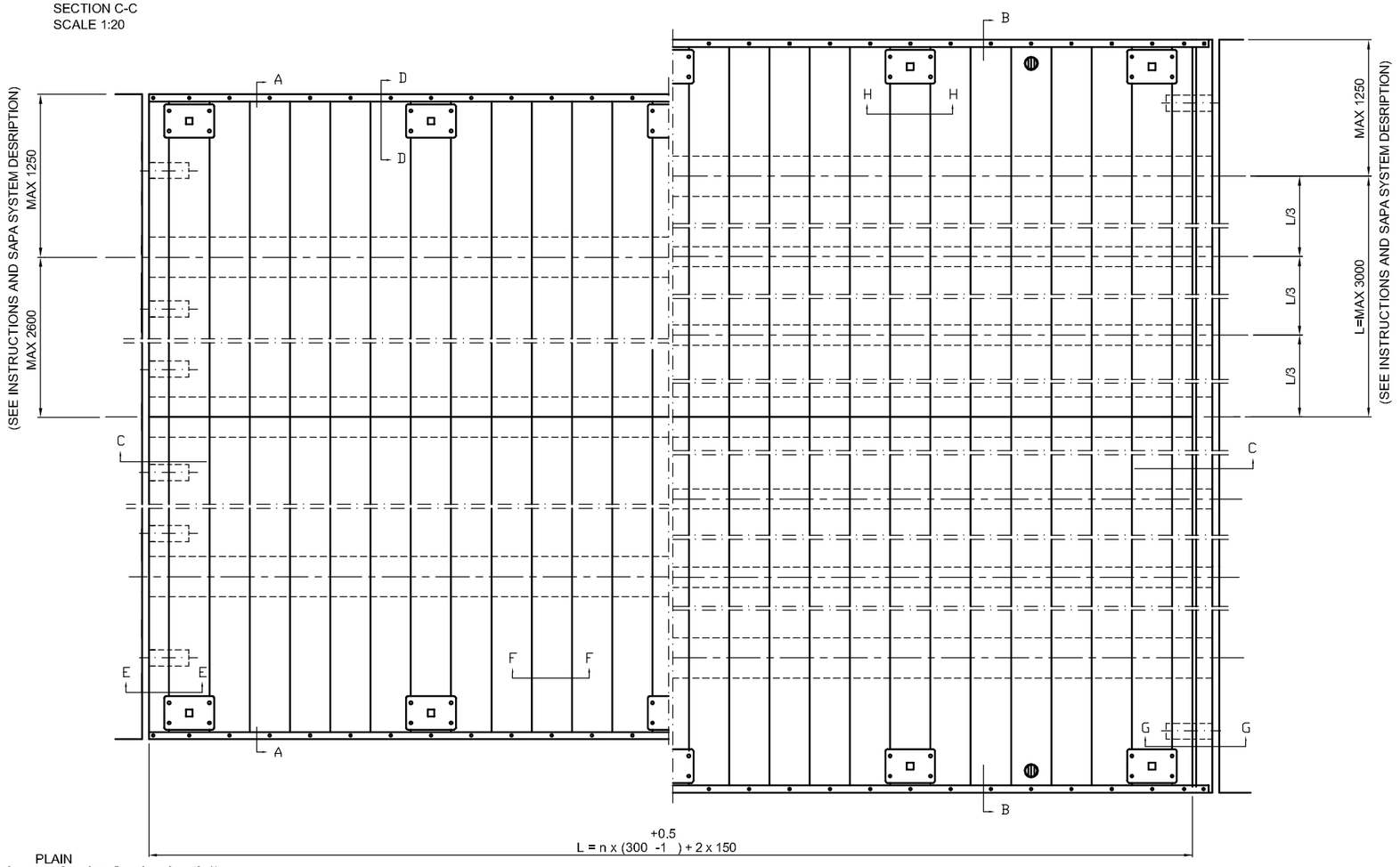

SCALE
1:100
1:50
1:20
PLAIN
SCALE 1:20

INSTRUCTIONS

LOADING REQUIREMENT

The bridge decking is designed for traffic loads according to Vägverket ATB Bro 2004, Publ 2004:56.

LOADING CAPACITY

The bridge decking is control calculated for traffic load EG A/B = 20/40 tons with axle weight A and bogie weight B according to Vägverket ATB Bro 2004, Publ 2004:56.

PAVEMENT

The bridge decking should be covered with either acrylic on poly-urethane to a thickness of 10 mm or poured asphalt to a thickness of 30 mm according to Vägverket ATB Bro 2004, Publ 2004:56.

GENERAL

The drawing shows the principal build up of the bridge decking with Sapa Bridge Decking System 100 according to Sapa System Description 2002-10-11.

Sapa Bridge Decking System 100 be suited for new constructions, reconstruction and repairing and can replace for example concrete bridge deckings.

The cambering profiles 50 and 100, detail 4, needs continuous support. This profiles only been used when the bridge decking is cambered. If poured asphalt been used as pavement we recommend to do the cambering in the asphalt.

The end profiles 150/100 and the nearest first half of bridge decking profile 300/100 must be standing on a cross bar or bracket according to section E-E and G-G.

Stringers according to Detail 2 shall always be used in the ends of the bridge if a cross bar or brackets not can be used.

The total lenght L can be adjusted within using bridge decking profile 300/100 and 280/100 in combination. A combination of this profiles also is necassary to compensate possible building tolerance deviations. Two bridge decking profiles 280/100 NOT allowed to be placed side by side.

The base plate to the balusters for bridge railing placed on the decking shall be designed according to drawing F1-3128.

Possible water drain shall be designed according to drawing F1-3125.

Detail 2, 3, 4, 6 and 7 according to drawing F1-3125.

Section D-D to H-H according to drawing F1-3126.

BET	ANT	ÄNDRINGEN AVSER	DATUM	UA SIGN	QA SIGN	VV DAT	VV SIGN
-	-	-	-				

SAPA BRIDGE DECKING SYSTEM

ALUMINIUM BRIDGE DECKING SYSTEM 100

Sapa Building System AB
SE-574 81 Vetlanda
Sverige/Sweden
Telefon/Telephone +46 (0)383-942 00
Telefax/Telecopy +46 (0)383-76 19 80

UPPDRAG NR	RITAD	KONSTR	GRANSKAD	
	MIL		RoS	ASSEMBLY DRAWING
DATUM	HANDLÄGGARE			CAMBERED BRIDGE DECKING
050531	MIKAEL LINDQVIST			
SKALA	GODKÄND	ERSÄTTER RITNING	NUMMER	BET
1:20		Nr	F1-3123	00

F1-3124 00

SECTION A-A
ALTERNATIVE WITH Z-PROFILE
SCALE 1:20

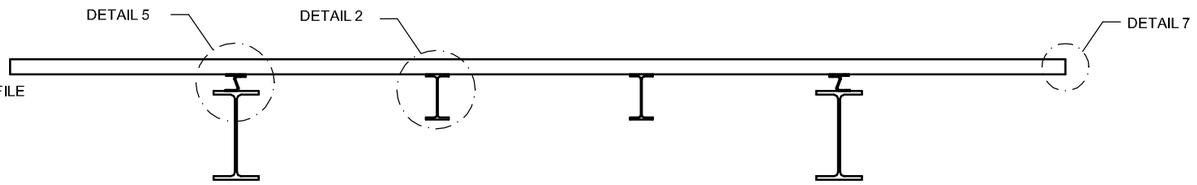

SECTION B-B
ALTERNATIVE WITH Z-PROFILE
SCALE 1:20

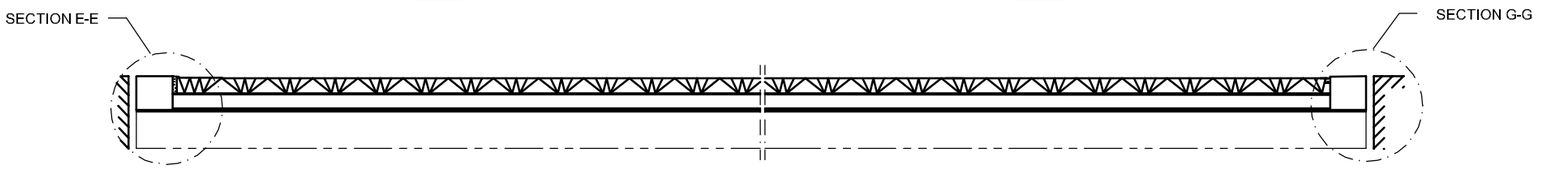

SEKTION C-C
SCALE 1:20

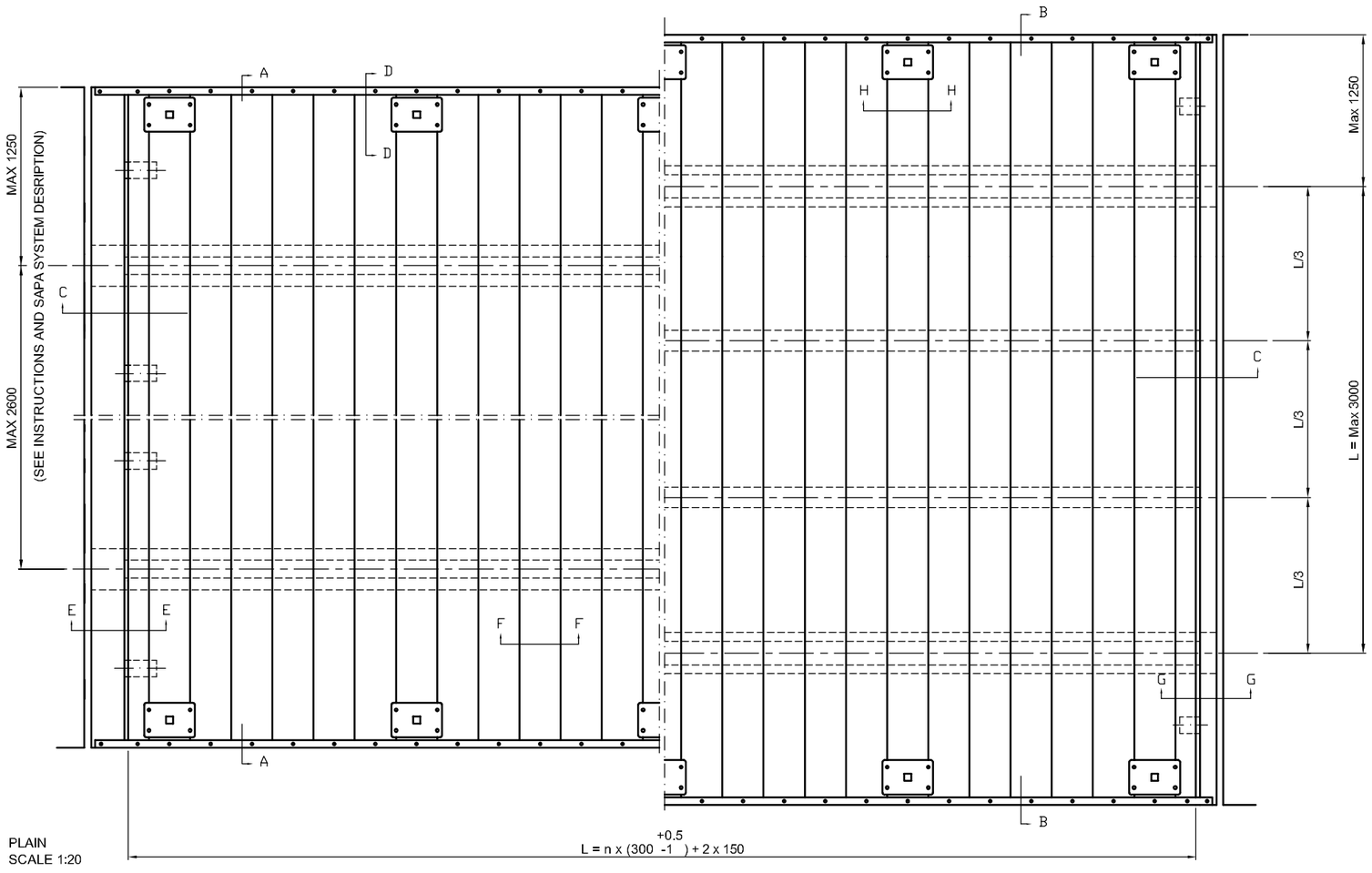

PLAIN
SCALE 1:20

$L = n \times (300\ ^{+0.5}_{-1}) + 2 \times 150$

SCALE
1:100 1 0 1 2 3 4 5 6 7 8 9 10 M.
1:50 1 0 2 3 4 5 M.
1:20 1 0 1 2 M.

INSTRUCTIONS

LOADING REQUIREMENT

The bridge decking is designed for traffic loads according to Vägverket ATB Bro 2004, Publ 2004:56.

LOADING CAPACITY

The bridge decking is control calculated for traffic load EG A/B = 20/40 tons with axle weight A and bogie weight B according to Vägverket ATB Bro 2004, Publ 2004:56.

PAVEMENT

The bridge decking should be covered with either acrylic on poly-urethane to a thickness of 10 mm or poured asphalt to a thickness of 30 mm according to Vägverket ATB Bro 2004, Publ 2004:56.

GENERAL

The drawing shows the principal build up of the bridge decking with Sapa Bridge Decking System 100 according to Sapa System Description 2002-10-11.

Sapa Bridge Decking System 100 be suited for new constructions, reconstruction and repairing and can replace for example concrete bridge deckings.

The Z-profile needs continuous support.

The end profiles 150/100 and the nearest first half of bridge decking profile 300/100 must be standing on a cross bar or bracket according to section E-E and G-G.

Stringers according to Detail 2 shall always be used in the ends of the bridge if a cross bar or brackets not can be used.

The total lenght L can be adjusted within using bridge decking profile 300/100 and 280/100 in combination. A combination of this profiles also is necassary to compensate possible building tolerance deviations. Two bridge decking profiles 280/100 NOT allowed to be placed side by side.

The base plate to the balusters for bridge railing placed on the decking shall be designed according to drawing F1-3128.

Possible water drain shall be designed according to drawing F1-3125.

Detail 2, 5 and 7 according to drawing F1-3125.

Section D-D to H-H according to drawing F1-3126.

BET	ANT	ÄNDRINGEN AVSER	DATUM	UA SIGN	QA SIGN	VV DAT	VV SIGN
-	-	-	-				

SAPA BRIDGE DECKING SYSTEM

ALUMINIUM BRIDGE DECKING SYSTEM 100

Sapa Building System AB
SE-574 81 Vetlanda
Sverige/Sweden
Telefon/Telephone +46 (0)383-942 00
Telefax/Telecopy +46 (0)383-76 19 80

UPPDRAG NR	RITAD	KONSTR	GRANSKAD	ASSEMBLY DRAWING
	MIL		RoS	
DATUM 050531	HANDLÄGGARE MIKAEL LINDQVIST			PLAIN BRIDGE DECKING ON Z-PROFILE
SKALA 1:20	GODKÄND	ERSÄTTER RITNING Nr	NUMMER F1-3124	BET 00

NUMMER F1-3125 BET 00

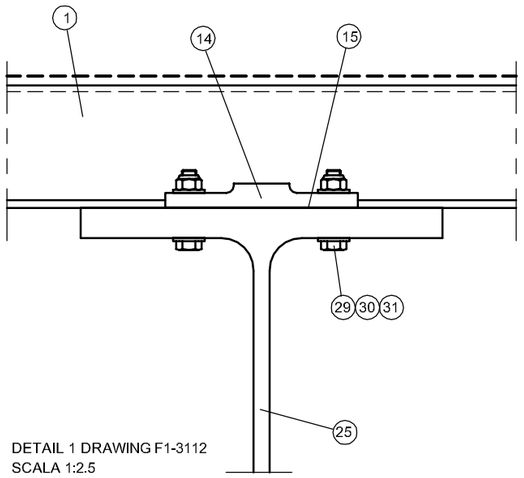

DETAIL 1 DRAWING F1-3112
SCALA 1:2.5

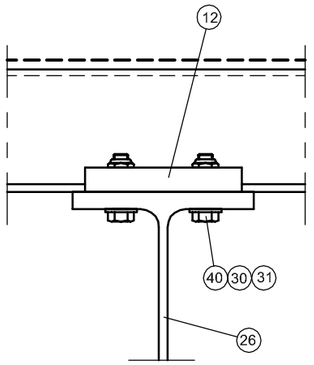

DETAIL 2 DRAWING F1-3112, F1-3113, F1-3114
SCALE 1:2.5

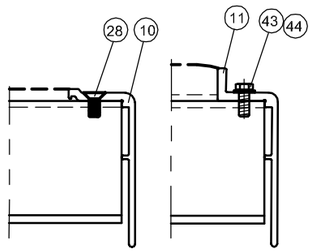

DETAIL 7 DRAWING F1-3112, F1-3114
SCALE 1:2.5

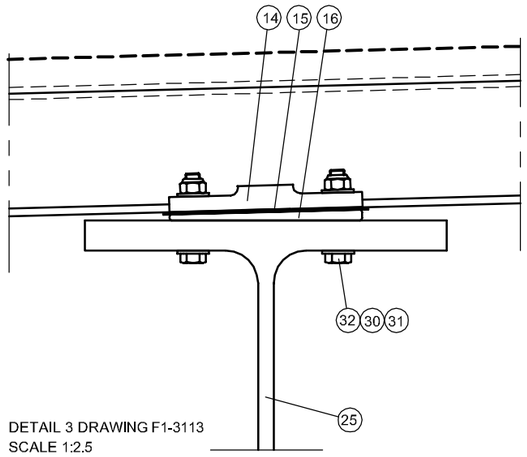

DETAIL 3 DRAWING F1-3113
SCALE 1:2.5

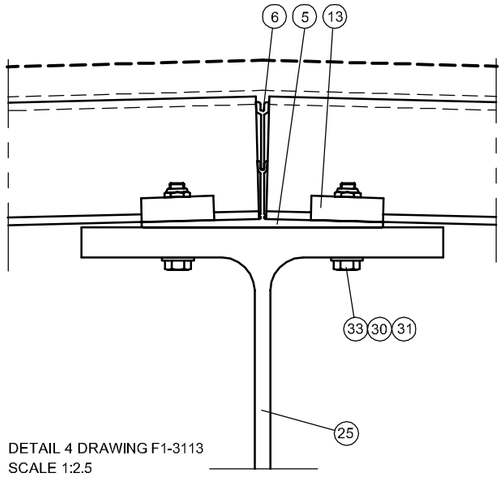

DETAIL 4 DRAWING F1-3113
SCALE 1:2.5

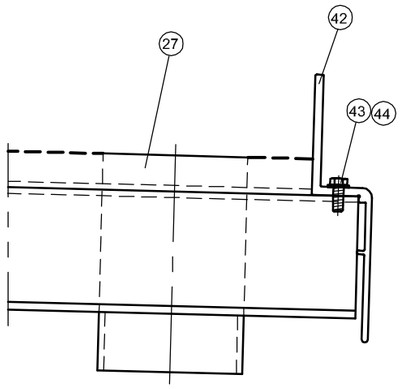

DETAIL 6 DRAWING F1-3113
SCALE 1:2.5

NR	ANT	BENÄMNING	MATERIAL	RITN.NR	ANM.
1		BRIDGE DECKING PROFILE 300/100	SAPA 6063F25-T6	F3-3012	
2		BRIDGE DECKING PROFILE 280/100	SAPA 6063F25-T6	F3-3018	
3		END PROFILE 150/100 A	SAPA 6063F25-T6	F4-3013	
4		END PROFILE 150/100 B	SAPA 6063F25-T6	F4-3014	
5		CAMBERING PROFILE 50	SS-EN 6063-T6	F3-3031	
6		CAMBERING PROFILE 100	SS-EN 6063-T6	F4-3032	
7		SHIMS 10x130	S235JRG2	F3-3151	GALVANIZED 4)
8		SUPPORT PROFILE (Z-PROFILE)	DOMEX 640XP 2)	F3-3152	SPRAY GALV.3)
10		EDGE PROFILE 100/10	SS-EN 6063-T6	??	
11		EDGE PROFILE 100/30	SS-EN 6063-T6	F3-3056	
12		FASTENER 100 Z	SS-EN 7021-T6	F4-3096	
13		FASTENER 100	SS-EN 7021-T6	F4-3027	
14		FASTENER 100 S	SS-EN 7021-T6	F4-3029	
15		SHIMS 100 S	SS 2343	F4-3030	
16		SPACER 100	SS-EN 7021-T6	F4-3033	
17		BRACKET 100 TO BALUSTER	SAPA 6063F25-T6	F4-3037	
18		FOOT PLATE TO BALUSTER	S235JRG2	F3-3090	
19		END PROFILE HEIGHTENER 100/10	SS-EN 6063-T6	??	
20		END PROFILE HEIGHTENER 100/30	SS-EN 6063-T6	F4-3016	
25		SUPPORT HEB	ACCORDING TO BRIDGE CONSTRUCTOR 1)		
26		STRINGER HEB	ACCORDING TO BRIDGE CONSTRUCTOR 1)		
27		WATER DRAINAGE 100	SS-EN 6063-T6	F3-3075	Ø100 ALT. Ø120
28		SCREW A4-MF6S 8x20	SS 2343		DIN 7991
29		SCREW A4-M6S 12x *	SS 2343		SS-ISO 4014
30		WASHER A4-HRB 13x24	SS 2343		ISO 7089
31		LOCKING NUT A4-M12	SS 2343		ISO 7040
32		SCREW A4-M6S 12x *	SS 2343		SS-ISO 4014
33		SCREW A4-M6S 12x *	SS 2343		SS-ISO 4014
34		SCREW A4-M6S 12x45	SS 2343		SS-ISO 4014
35		SCREW A4-M6S 12x50	SS 2343		SS-ISO 4014
36		SCREW A4-M6S 12x *	SS 2343		SS-ISO 4014
37		SCREW M6S 20x180 GALV.	8.8		SS-ISO 4014
38		WASHER HRB 21x36 GALV.			SS 3576
39		NUT M6M20 GALV.			SS-ISO 4032
40		SCREW A4-M6S 12x *	SS 2343		SS-ISO 4014
41		SCREW A4-M6S 12x *	SS 2343		–"–
42		EDGE PROFILE 100 Y	SS-EN 6063-T6	F3-3053	
43		SCREW A4-M6S 8x20	SS 2343		SS-ISO 4014
44		WASHER A4-RB 8.4	SS 2343		ISO 7089
45		SHIMS 100	SS 2343		
46		SHIMS 100 A-E	SS 2343		
47		FLEXIBLE JOINT COCON OR ILLMOD 2)			
48		FLEXIBLE JOINT SEALING			
49		BOTTOM SEALING			

1) STEEL QUALITY ACCORDING TO SS-EN 10025 +A1 (EU 25-72) OCH SS-EN 10113, EXCEPT Z-PROFILE IN QUALITY DOMEX 640
2) OR EQUIVAL
3) ACCORDING TO SS 2972
4) ACCORDING TO SS 3583, LOWEST CLASS B

*) THE LENGHT OF THE SCREW DEPEND ON THE FLANGE THICKNESS

INSTRUCTIONS SEE DRAWING F1-3121, F1-3122, F1-3123 och F1-3124

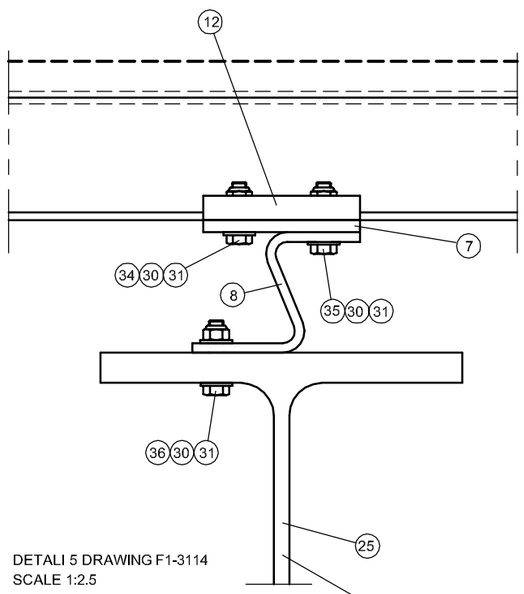

DETALI 5 DRAWING F1-3114
SCALE 1:2.5

NEW OR EXISTING STEEL CONSTRUCTION

SCALE
1:100 10 M.
1:50 5 M.
1:20 2 M.

BET	ANT	ÄNDRINGEN AVSER	DATUM	UA SIGN	QA SIGN	VV DAT	VV SIGN
-		-	-	-			

SAPA BRIDGE DECKING SYSTEM

ALUMINIUM BRIDGE DECKING SYSTEM 100

Sapa Building System AB
SE-574 81 Vetlanda Sverige/Sweden
Telefon/Telephone +46 (0)383-942 00
Telefax/Telecopy +46 (0)383-76 19 80

UPPDRAG NR	RITAD KONSTR GRANSKAD	ASSEMBLY DRAWING 1, DETAILS
	MIL RoS	
DATUM 050531	HANDLÄGGARE MIKAEL LINDQVIST	
SKALA 1:2,5	GODKÄND	ERSÄTTER RITNING Nr / NUMMER F1-3125 / BET 00

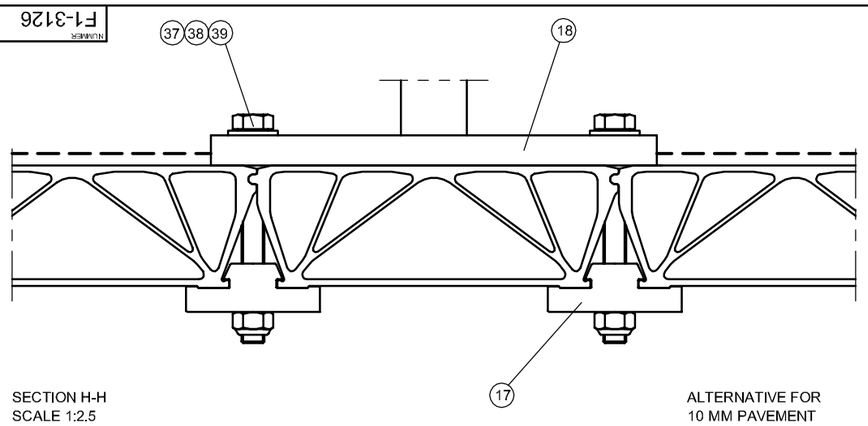

SECTION H-H
SCALE 1:2.5

ALTERNATIVE FOR
10 MM PAVEMENT

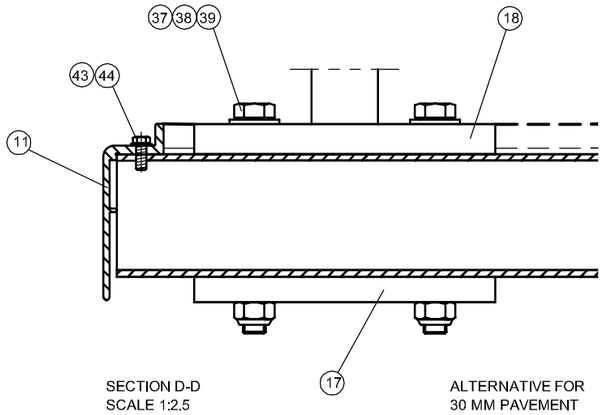

SECTION D-D
SCALE 1:2.5

ALTERNATIVE FOR
30 MM PAVEMENT

A		END CONSTRUCTION	ACCORDING TO BRIDGE CONSTRUCTOR 1)
B		END CONSTRUCTION	ACCORDING TO BRIDGE CONSTRUCTOR 1)
C		END CONSTRUCTION	ACCORDING TO BRIDGE CONSTRUCTOR 1)
D		SUPPORT	ACCORDING TO BRIDGE CONSTRUCTOR 1)
E		INTERMEDIATE SUPPORT	ACCORDING TO BRIDGE CONSTRUCTOR 1)

1) STEEL QUALITY ACCORDING TO SS-EN 10025 +A1 (EU 25-72) OCH SS-EN 10113, EXCEPT Z-PROFILE IN QUALITY DOMEX 640

DETAIL LIST SEE DRAWING F1-3115

INSTRUCTIONS SEE DRAWING F1-3111, F1-3112, F1-3113 och F1-3114

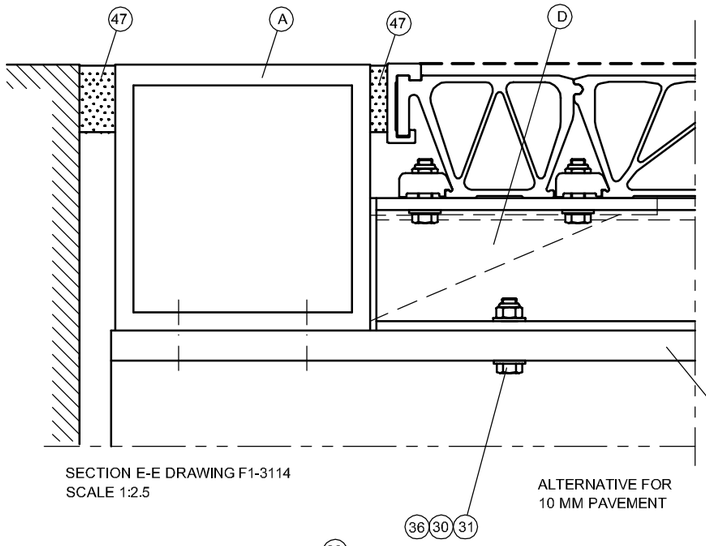

SECTION E-E DRAWING F1-3114
SCALE 1:2.5

ALTERNATIVE FOR
10 MM PAVEMENT

NEW OR EXISTING
CONSTRUCTION

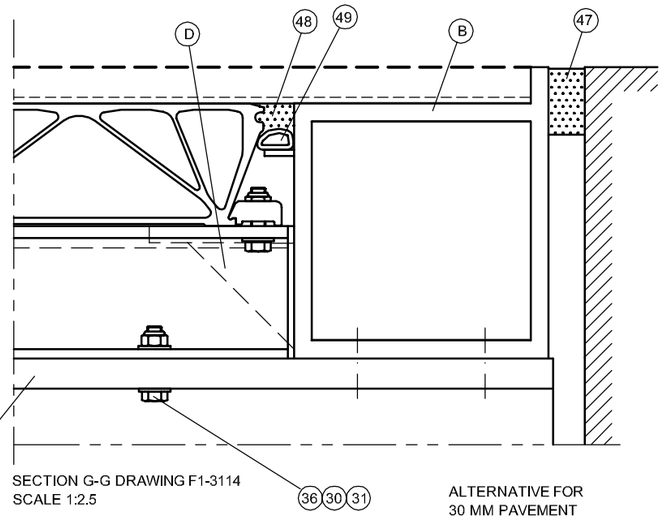

SECTION G-G DRAWING F1-3114
SCALE 1:2.5

ALTERNATIVE FOR
30 MM PAVEMENT

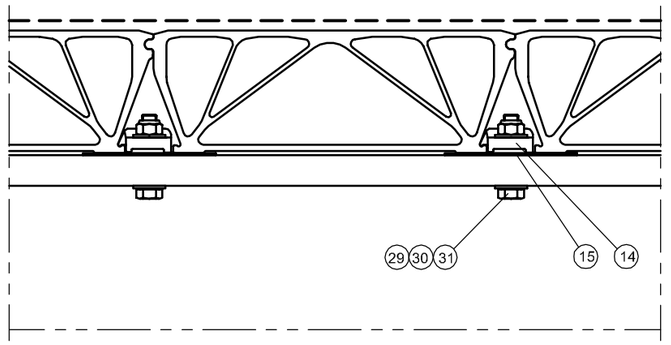

SECTION F-F DRAWING F1-3112, F1-3113
SCALE 1:2.5

ALTERNATIVE FOR
10 MM PAVEMENT

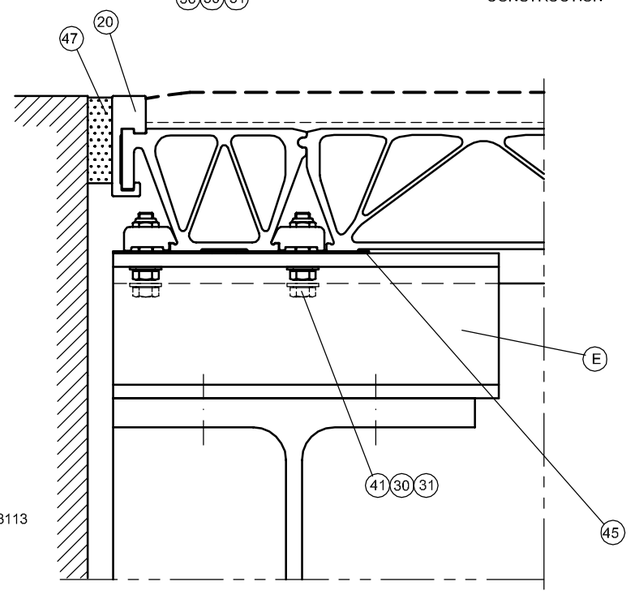

SECTION E-E DRAWING F1-3112, 3113
SCALE 1:2.5

ALTERNATIVE FOR
30 MM PAVEMENT

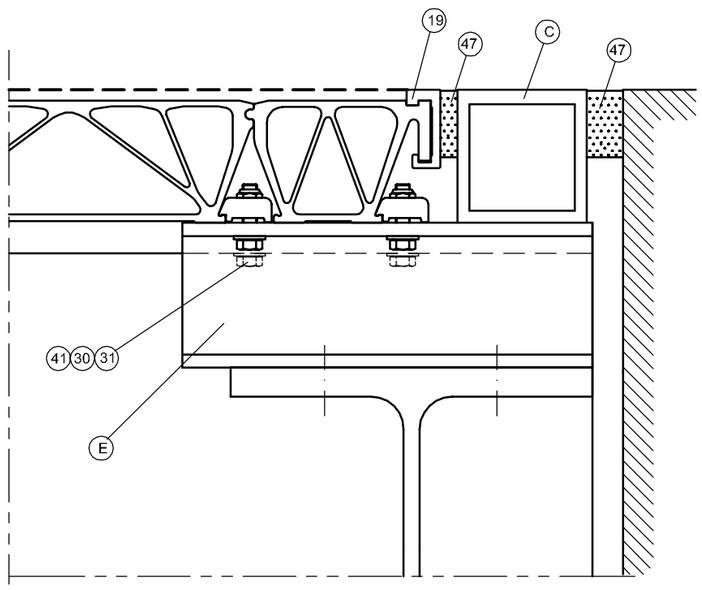

SECTION G-G DRAWING F1-3112, 3113
SCALE 1:2.5

ALTERNATIVE FOR
10 MM PAVEMENT

SCALE
1:100 1 0 1 2 3 4 5 6 7 8 9 10 M.
1:50 1 0 1 2 3 4 5 M.
1:20 1 0 1 2 M.

BET	ANT	ÄNDRINGEN AVSER	DATUM	UA SIGN	QA SIGN	VV DAT	VV SIGN
-		-	-	-			

SAPA BRIDGE DECKING SYSTEM

ALUMINIUM BRIDGE DECKING SYSTEM 100

sapa
Sapa Building System AB
SE-574 81 Vetlanda Telefon/Telephone Telefax/Telecopy
Sverige/Sweden +46 (0)383-942 00 +46 (0)383-76 19 80

UPPDRAG NR	RITAD	KONSTR	GRANSKAD
	MIL		RoS
DATUM	HANDLÄGGARE		
050601	MIKAEL LINDQVIST		
SKALA	GODKÄND	ERSÄTTER RITNING	NUMMER / BET
1:2,5		Nr	F1-3126 00

ASSEMBLY DRAWING 2, DETAILS

F1-3127 BET 00

NR	ANT	BENÄMNING	MATERIAL	RITN.NR	ANM.
1		BRIDGE DECKING PROFILE 300/100	SS-EN 6063F25-T6	F3-3012	
2		BRIDGE DECKING PROFILE 280/100	SS-EN 6063F25-T6	F3-3018	
3		END PROFILE 150/100 A	SS-EN 6063F25-T6	F4-3013	
4		END PROFILE 150/100 B	SS-EN 6063F25-T6	F4-3014	
5		CAMBERING PROFILE 50, DECL. 2,50%(1:40)	SS-EN 6063-T6	F3-3031	
6		CAMBERING PROFIL 100	SS-EN 6063-T6	F4-3032	
7		SHIMS 10x130	S235JRG2	F3-3151	GALVANIZED 3)
8		SUPPORT PROFILE (Z-PROFILE)	DOMEX 640XP 1)	F3-3152	SPRAY GALV. 2)
9		CAMBERING PROFILE 50, DECL. 1,67%(1:60)	SS-EN 6063-T6		

1) OR EQUIVAL
2) ACCORDING TO SS 2972
3) ACCORDING TO SS 3583 LOWEST CLASS B

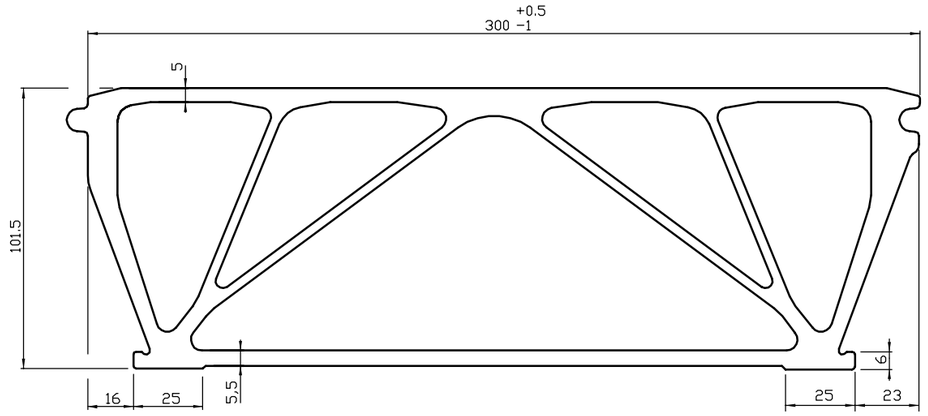

① BRIDGE DECKING PROFILE 300/100

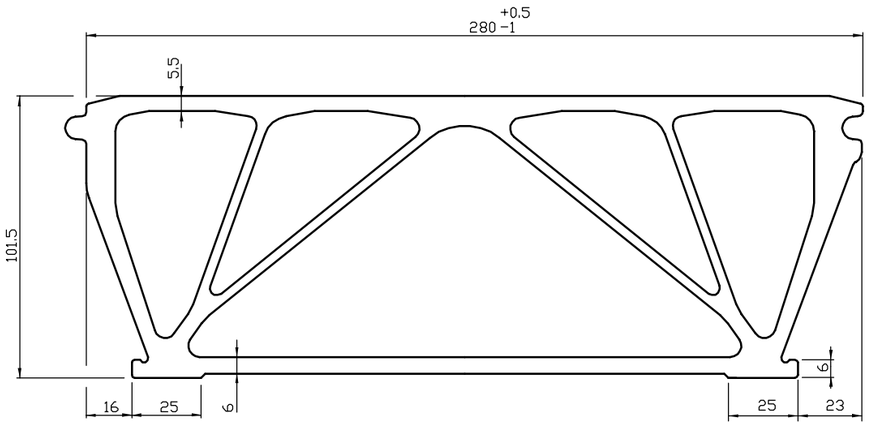

② BRIDGE DECKING PROFILE 280/100

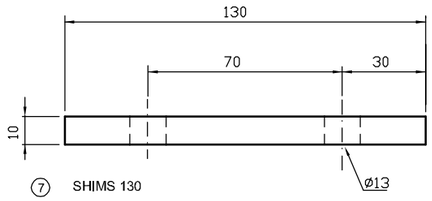

⑦ SHIMS 130

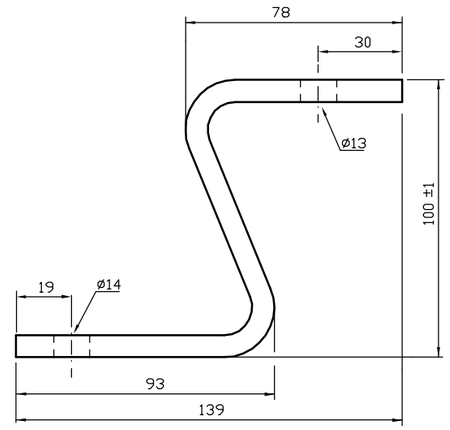

⑧ SUPPORT PROFILE (Z-PROFILE)

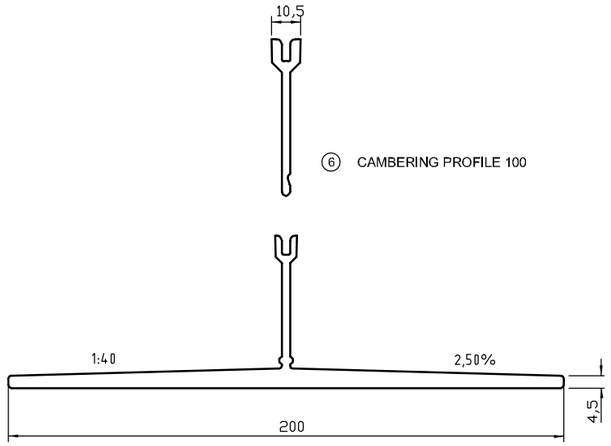

⑥ CAMBERING PROFILE 100

⑤ CAMBERING PROFILE 50

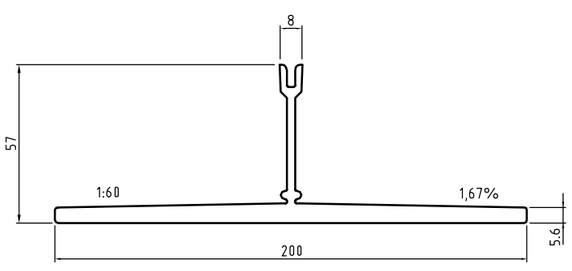

⑨ BOMBERINGSPROFIL 50

INSTRUCTIONS SEE DRAWING F1-3111, F1-3112, F1-3113 AND F1-3114

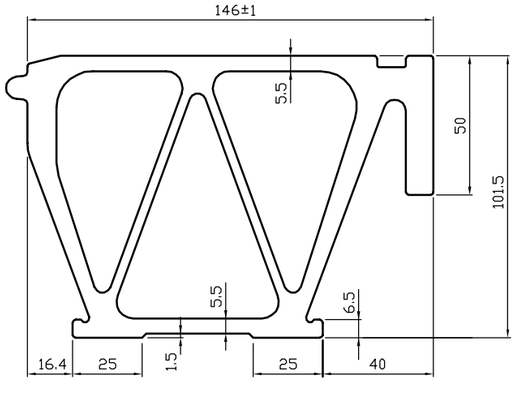

④ END PROFILE 150/100 B

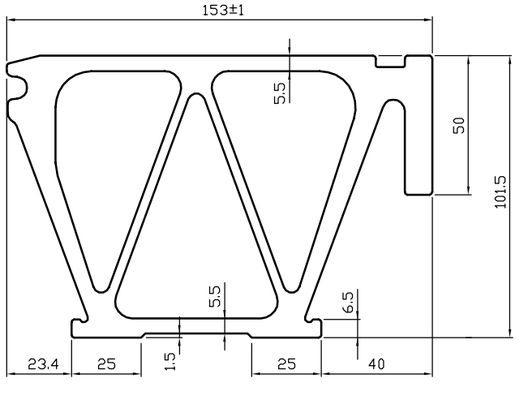

③ END PROFILE 150/100 A

SCALE
1:100 1 0 1 2 3 4 5 6 7 8 9 10 M.
1:50 1 0 1 2 3 4 5 M.
1:20 1 0 1 2 M.

BET	ANT	ÄNDRINGEN AVSER	DATUM	UA SIGN	QA SIGN	VV DAT	VV SIGN
-		-	-	-			

SAPA BRIDGE DECKING SYSTEM

ALUMINIUM BRIDGE DECKING SYSTEM 100

Sapa Building System AB
SE-574 81 Vetlanda Sverige/Sweden
Telefon/Telephone +46 (0)383-942 00
Telefax/Telecopy +46 (0)383-76 19 80

UPPDRAG NR	RITAD KONSTR GRANSKAD	DETAILS 1	
	MIL RoS		
DATUM 050601	HANDLÄGGARE MIKAEL LINDQVIST		
SKALA 1:1	GODKÄND	ERSÄTTER RITNING Nr	NUMMER F1-3127 BET 00

F1-3128 00

NR	ANT	BENÄMNING	MATERIAL	RITN.NR	ANM.
10		EDGE PROFILE 100/10	SS-EN 6063-T6	??	
11		EDGE PROFILE 100/30	SS-EN 6063-T6	F3-3056	
12		FASTENER 100 Z	SS-EN 7021-T6	F4-3096	
13		FASTENER 100	SS-EN 7021-T6	F4-3027	
14		FASTENER 100 S	SS-EN 7021-T6	F4-3029	
15		SHIMS 100 S	SS 2343	F4-3030	
16		SPACER 100	SS-EN 7021-T6	F4-3033	
17		MOTHÅLL 100 FÖR RÄCKESSTÄNDARE	SS-EN 6063F25-T6	F4-3037	
18		FOOT PLATE FOR BALUSTER	S235JRG2	F3-3090	
19		END PROFILE HEIGHTENER 100/10	SS-EN 6063-T6	??	
20		END PROFILE HEIGHTENER 100/30	SS-EN 6063-T6	F4-3016	
42		EDGE PROFILE 100 Y	SS-EN 6063-T6	F4-3053	
45		SHIMS 100	SS2343	F4-3034	
46		SHIMS 100 A-E	SS2343	F4-3035	

INSTRUCTIONS SEE DRAWING F1-3111, F1-3112, F1-3113 AND F1-3114

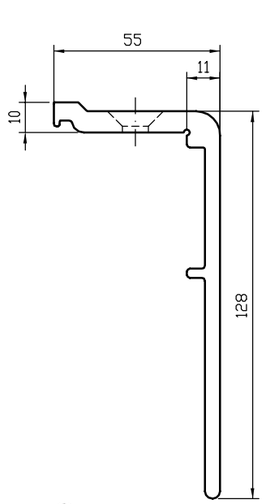

(10) EDGE PROFILE 100/10

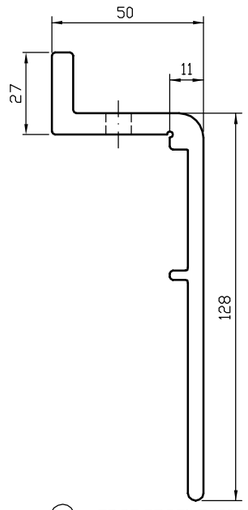

(11) EDGE PROFILE 100/30

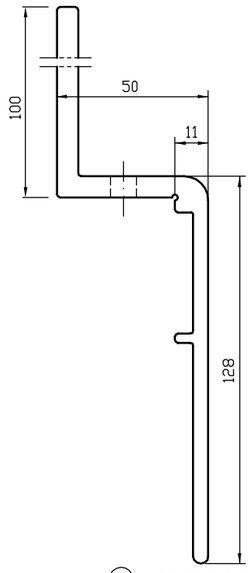

(42) EDGE PROFILE 100Y

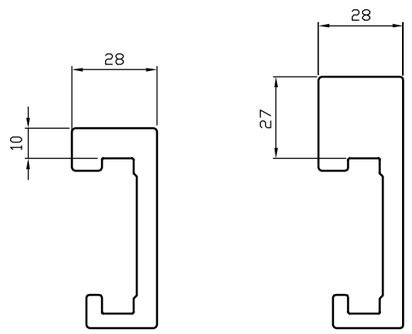

(19) END PROFILE HEIGHTENER 100/10

(20) END PROFILE HEIGHTENER 100/30

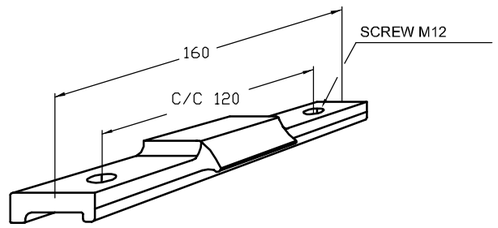

(14) FASTENER 100 S

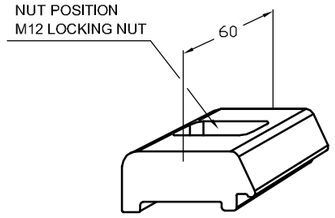

(13) FASTENER 100

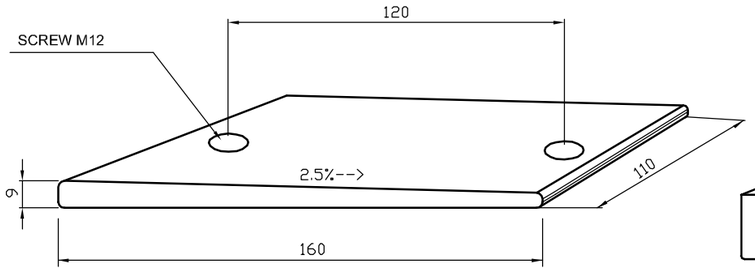

(16) SPACER 100

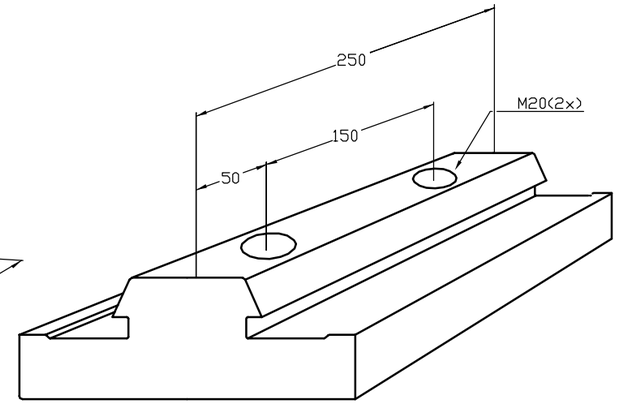

(17) BRACKET 100 TO BALUSTER

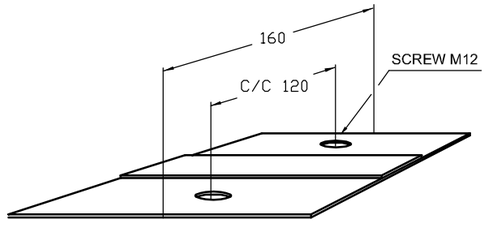

(15) SHIMS 100 S
THICKNESS 2 MM

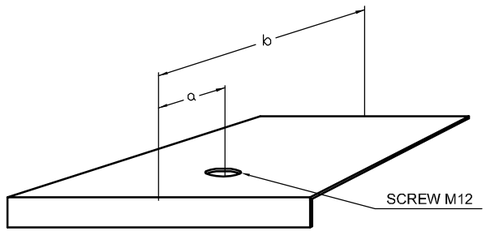

(46) SHIMS 100 A-E
THICKNESS 1 MM

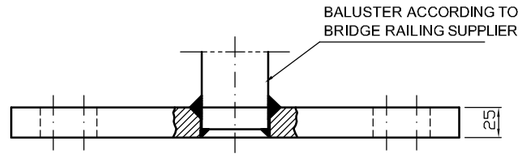

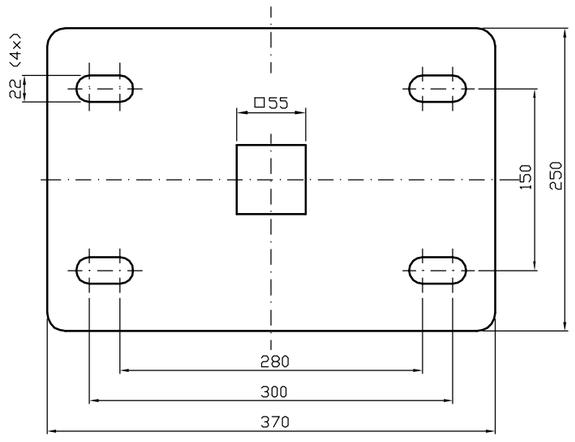

(18) FOOT PLATE TO BALUSTER
SCALE 1:2.5

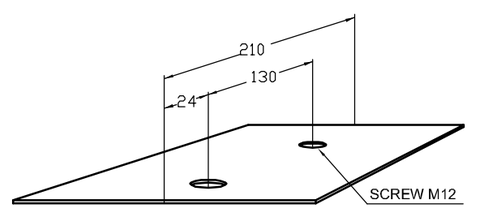

(45) MELLANLÄGGSPLÅT 100
TJOCKLEK 1 MM

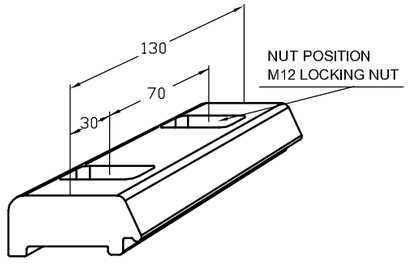

(12) FASTENER 100 Z

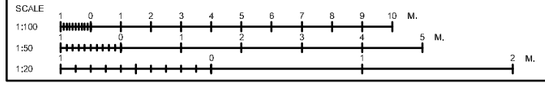

-		-	-	-			
BET	ANT	ÄNDRINGEN AVSER	DATUM	UA SIGN	QA SIGN	VV DAT	VV SIGN

SAPA BRIDGE DECKING SYSTEM

ALUMINIUM BRIDGE DECKING SYSTEM 100

sapa

Sapa Building System AB
SE-574 81 Vetlanda
Sverige/Sweden
Telefon/Telephone +46 (0)383-942 00
Telefax/Telecopy +46 (0)383-76 19 80

UPPDRAG NR	RITAD	KONSTR	GRANSKAD
	MIL		RoS
DATUM	HANDLÄGGARE		
050601	MIKAEL LINDQVIST		
SKALA	GODKÄND	ERSÄTTER RITNING	NUMMER
1:1; 1:2,5		Nr	F1-3128 00

DETAILS 2